DISCOVERY OF MECHANOSENSITIVE MICRORNA AND MESSENGER RNA IN MOUSE ARTERIAL ENDOTHELIUM AND IN CULTURED ENDOTHELIAL CELLS

A Dissertation
Presented to
The Academic Faculty

By

Chih-Wen Ni

In Partial Fulfillment
Of the Requirements for the Degree
Doctor of Philosophy in the
Wallace H. Coulter Department of Biomedical Engineering at the
Georgia Institute of Technology and Emory University

Georgia Institute of Technology

August 2010

DISCOVERY OF MECHANOSENSITIVE MICRORNA AND MESSENGER RNA IN MOUSE ARTERIAL ENDOTHELIUM AND IN CULTURED ENDOTHELIAL CELLS

Approved by:

Dr. Hanjoong Jo, Chair
Department of Biomedical Engineering
School of Medicine, Division of Cardiology
Georgia Institute of Technology and Emory University

Dr. Larry V. McIntire
Department of Biomedical Engineering
Georgia Institute of Technology

Dr. Kathy K. Griendling
School of Medicine, Division of Cardiology
Emory University

Dr. W. Robert Taylor
Department of Biomedical Engineering
Georgia Institute of Technology

Dr. David G. Harrison
School of Medicine, Division of Cardiology
Emory University

Date Approved: 4/21/2010

For my family

Especially my grandfather

Kao, Chin-Yuan
1933-2010

ACKNOWLEDGEMENTS

I would first like to thank my advisor, Dr. Hanjoong Jo, for giving me the opportunity to work in the Jo lab, guiding me the direction for the past five years, and supporting me like a family. I would also like to thank my thesis committee members, Drs. Kathy K. Griendling, David G. Harrison, Larry V. McIntire, and W. Robert Taylor for supporting this work and providing constructive and valuable comments. I am grateful to Johnafel Crowe and Deborah Martinson for offering their expertise in the core facilities, helping sort cells and assistance with confocal microscopy, as well as to the staff of the bioengineering and biomedical engineering departments, including Leita Young, Lisa Simmons, Sandra Wilson, Sally Gerrish and Chris Ruffin for their limitless help with financial and administrative matters. Furthermore, I would like to acknowledge Gregory Doho in the Emory biomarker center for all his assistance with the microarray study.

I have been privileged to work with the best team in the Jo lab. First I would like to acknowledge Deb Smith and Maria Aleman for providing me the training in animal work and their efficient running of the lab. I would also like to acknowledge our current lab manager, Dong Won Kang, for all his help in the lab. I am very appreciative to all previous lab members, Drs. Doug Nam, Won Jong Rhee, Seth Brodie, Kyung Hwa Chang, Manu Platt, Hannah Song, Hyuk Sang Kwon, Heonyong Park, and Michelle Sykes. Credit is also due to current members, Dr. Amir Rezvan, Noah Alberts-Grill, Dr. Dong Ju Son, Dr. Kiwhon Kwon, Dr. Wakako Takabe, Fanor Balderrama, and Dr. Chan Woo Kim. I would also like to thank Casey Holliday, Drs. Amy Mowbray, Sarah Tressel, and Mamta Patel for their assistance, support, and friendship. I am indebted to Haiwei Qiu for technical aid and scientific help. And lastly, I am especially grateful to Dr.

Randy Ankeny. Over the last five years, he has provided vast assistance in everything, and true friendship to last a lifetime.

Finally, I would like to thank my family, especially my parents and sisters for encouraging and supporting me in this endeavor. Special thank to my adorable little girl, Angel Ni for always giving me the most genuine smile whenever I felt frustrated. Importantly, I would not have been able to complete this venture without the infinite support of my wife, Li-Shan Hsu. I thank her for always being there as my best friend, my counselor, and my partner. The last but not the least, I extend my greatest appreciation to my recently deceased grandfather, Mr. Kao, Chin-Yuan for always having faith in me since I was a little boy.

TABLE OF CONTENTS

LIST OF TABLES

LIST OF FIGURES

LIST OF SYMBOLS AND ABBREVIATIONS

3’ UTR	3’ untranslated region
α-SMA	Smooth muscle cell α-actin
Angpt2	angiopoietin-2
ApoE	Apolipoprotein E
BMP	Bone morphogenic protein
BAEC	bovine aortic endothelial cells
CFD	computational fluid dynamics
DAVID	Database for Annotation, Visualization and Integrated Discovery
DHE	Dihydroethidium
Dhh	desert hedgehog
DiI-Ac-LDL	1,1’-dioctadecyl-3,3,3,3’-tetramethyl-indocarbocyanine perchlorate
DMEM	Dulbecco's Modified Eagle Medium
EC	Endothelial Cell
ECGS	Endothelial cell growth supplement
EMT	Epithelial-to-mesenchymal-transition
eNOS	Endothelial nitric oxide synthase
EGM2-MV	Endothelial growth medium 2- microvascular
FACS	fluorescence-activated cell sorting
FBS	fetal bovine serum
FDR	false discovery rate
GC	greater curvature
HAEC	human aortic endothelial cells

HBSS	Hank's buffered salt solution
HCAEC	human coronary artery endothelial cells
HUVEC	human umbilical vein cord endothelial cells
ICAM1	Inter-cellular adhesion molecule 1
IL-6	Interleukin -6
iMAEC	Immortalized mouse aortic endothelial cells
IPA	Ingenuity Pathway Analysis
Jam2	Junctional adhesion molecule 2
KLF2	Kruppel-like factor-2
KLF4	Kruppel-like factor-4
Klk10	Kallikrein-10
LC	lesser curvature
LCA	Left common carotid artery
LDL	Low density lipoprotein
LDLR	Low density lipoprotein receptor
LNA	Locked Nucleic Acid
Lmo4	LIM-only protein 4
LS	Laminar Shear
NO	Nitric oxide
MAEC	mouse aortic endothelial cells
MCP1	Monocyte chemoattractant protein 1
miRNA	microRNA
OS	Oscillatory Shear
PAEC	pig aortic endothelial cells
PBS	Phosphate buffered saline

PDGF	platelet-derived growth factor
PECAM-1	platelet endothelial cell adhesion molecule-1
PmT	Polymer middle T antigen
qPCR	Quantitative real time polymer chain reaction
RASM	rat aortic smooth muscle cells
RCA	Right common carotid artery
RISC	RNA-induced silencing complex
ROS	Reactive oxygen species
SAM	Significance Analysis of Microarrays
SDS-PAGE	sodium dodecyl sulfate polyacrylamide gel electrophoresis
SNP	sodium nitroprusside
TA	thoracic aorta
THP-1	Human acute monocytic leukemia cell line
TNFα	Tumor necrosis factor-α
VCAM1	Vascular cell adhesion molecule 1
vWF	von Willebrand facot
WSS	wall shear stress
WT	wildtype

SUMMARY

Cardiovascular disease is the leading cause of death among developed countries and is rapidly becoming the major cause of death in the developing world. Atherosclerosis is a major contributor to cardiovascular disease and accounts for an estimated one-third of deaths worldwide. In an effort to develop effective treatments for this pervasive pathology, research is now focused on the mechanisms of atherogenesis. In order to address the hemodynamic components of disease pathogenesis, researchers have focused on mechanotransduction of flow-dependent shear stress in the vascular endothelium as a source of novel pathological mechanisms. Understanding how unidirectional, laminar blood flow protects vessels from atherogenesis, while disturbed, oscillatory blood flow promotes it, stands to provide enormous insight into disease pathogenesis and may provide powerful, specific new therapies for cardiovascular disease intervention.

The overall *objective* of this dissertation was to determine which microRNAs and mRNAs are regulated by different flow conditions in vascular endothelial cells *in vitro* and in mouse carotid artery endothelium *in vivo*, and to identify which miRNAs mediate flow-dependent vascular inflammation. These results allow us to identify novel targets either for therapeutic intervention or for early clinical detection of atherosclerosis. The *overall hypothesis* of this project was that *oscillatory shear (OS) and laminar shear (LS) stress differentially alter the expression of mechanosensitive miRNAs each capable of regulating complex networks of gene expression, which in turn leads to inflammation in endothelial cells.* This hypothesis was tested according to three specific aims using both

in vitro and *in vivo* approaches via high throughput microarray analyses and functional validation of specific targets by PCR.

To achieve these specific aims, our lab first developed a mouse model which changes the flow pattern in the left common carotid artery by ligating three of the four caudal branches of the LCA - left external, left internal, and occipital arteries. We characterized the low and oscillatory shear stress acutely induced by the partial carotid ligation procedure which induces accelerated endothelial dysfunction in one week and advanced atherosclerotic plaques by 2 weeks in ApoE knockout mice fed a high fat diet. Using this model, I developed a simple method to isolate endothelial cell RNA from the partially ligated left common carotid as well as the contralateral right common carotid. This method was then fine-tuned to provide total RNA samples in sufficient quantity with little to no appreciable contamination from cells populating the underlying medial and adventitial layers of the artery. In addition, the time points (12hr and 48hr post-ligation) I selected for RNA samples collection are free of the infiltration of immune cells into intimal layer when exposed to disturbed flow. In addition, I also developed a method to generate iMAEC line for use *in vitro* for validation purpose. The methods used to develop iMAEC lines described in this dissertation can be applied to generate additional MAEC lines, using various knockout mouse lines, to provide a critical tool to investigate the vascular biology and pathobiology.

To investigate the mRNA expression profiles *in vivo*, I carried out genome-wide microarray assays using endothelial RNAs isolated from the flow-disturbed left and contralateral right common carotid arteries (LCA and RCA) in wildtype C57BL/6 mice. I found that 62 and 523 genes significantly changed in flow-disturbed LCA endothelium compared to the RCA by 12hr and 48hr post-ligation respectively. The array results for

44 out of 46 genes were validated by qPCR, including well-known shear-responsive genes, *Klf2*, *eNOS*, and *BMP4*, as well as numerous novel mechanosensitive genes such as *Klk10*, *Dhh*, *Jam2* and *Lmo4.* Lmo4 protein was specifically expressed in the flow disturbed mouse aortic arch endothelium and in human coronary endothelium in an asymmetric pattern. Comparison of *in vivo*, *ex vivo*, and *in vitro* endothelial gene expression patterns suggests that many mechanosensitive genes found *in vivo* appear to have been significantly dysregulated during culture. Gene ontology analyses revealed that disturbed flow induced cell proliferation and morphology by 12hr, followed by inflammatory and immune responses by 48hr.

To provide further insight into the possible mechanisms of observed mechanosensitive gene changes I performed microarrays looking at miRNA expression profiles using RNA samples isolated as described above. I found that 27 and 18 miRNAs were significantly either up- or down-regulated, respectively, in flow-disturbed LCA endothelium compared to the RCA 48 hours post-ligation. However, only 4 miRNAs showed significant differences between LCA and RCA as of 12 hours post-ligation. The array results were also validated by qPCR confirming several mechanosensitive miRNAs such as miR-23b, miR-29b, miR-30c, and miR-712, which have not been reported previously. Further analyses between mechanosensitive miRNAs and mRNAs reveal approximately 10 to 15% (25/295, and 31/228) of mechanosensitive mRNAs found to be potential targets of shear-sensitive miRNAs based on the sequence complementary prediction by TargetScan. This also suggests the significance of these mechanosensitive miRNAs and mRNAs identified in this dissertation and these targets could play an important role involving in the mechanisms underling the effect of shear stress on cardiovascular disease.

To further study the functional importance of mechanosensitive miRNAs, I examined the miRNAs expression profiles in cultured HUVEC exposed to OS or LS for 24hr. Given the difference between in vitro and in vivo system, the new data set were obtained and detailed functional validation were performed. After validation by PCR, we identified 10 OS-sensitive miRNAs. Of those, the most significant OS-induced miRNA, miR-663, was selected for determining its functional importance. miR-663 plays a specific role in endothelial inflammatory response, but not in apoptosis, in an ICAM-1 dependent manner. In order to identify potential target genes of miR663, we carried out an additional genome-wide DNA microarray, which uncovered 35 potential miR-663 targets, including a network of inflammatory genes and transcription factors such as *KLF4, ATF3, and FOSB*. Since these transcriptional factors have been known to serve as master regulators in several biological functions including inflammation, these results suggest that miR-663 is a shear-sensitive miRNA, regulating expression of many genes including the transcription factors, which in turn induce inflammatory response in ECs. Collectively, OS significantly altered the gene expression profiles including miRNA and mRNA compared to LS. These mechanosensitive genes regulated by miRNAs seem to involve in OS induced EC inflammation in the earliest stage of atherosclerosis development. In particular, miR-663, an OS-induced miRNA, is shown to mediate cellular inflammation by regulating a network of genes further support the notion that flow sensitive miRNAs and mRNA play important roles in disturbed flow induced cardiovascular diseases.

Overall, revealing the profiles of miRNAs and mRNAs regulated by hemodynamic flow provides a better understanding in vascular diseases and provide potential target for developing effective preventative therapeutic approaches in cardiovascular diseases.

CHAPTER 1

INTRODUCTION

Atherosclerosis is an inflammatory disease characterized by the development of lipid-filled plaques in arterial vessels[1]. It has been correlated to the dysfunction of endothelium exposed to disturbed flow in the defined regions of the vasculature[3-4]. In straight vessels, endothelial cells are exposed to high, unidirectional laminar shear stress (LS) and maintain an anti-atherogenic phenotype. In contrast, unstable shear flow including low and oscillatory shear stress (OS) occurs in curves and bifurcations of the arteries known as plaque-prone areas. Given that the endothelial cells respond differently to LS and OS, the cascade of altered gene expression induced by the shear response is likely modulated by different mechanisms at transcriptional or post-transcriptional level. Growing evidence indicates that microRNAs are a new category of molecules that regulate gene expression in a post-transcriptional manner and play diverse roles in fundamental biological processes, such as cell proliferation, migration, and inflammation[5-7]. Thus, this dissertation will address the protective and pathological effects of arterial hemodynamics with respect to microRNA and gene regulation using *in vitro* (cell culture) and *in vivo* (mouse model) experimental systems. In particular, we will present the discovery of novel shear-sensitive genes including microRNAs and mRNAs in endothelial cells. The focus of these genes will concentrate on the functions related to inflammation which leads to atherosclerosis subsequently.

Atherosclerosis and inflammation

Atherosclerotic cardiovascular disease is one of the leading causes of death in the western world[8]. In the United States alone, nearly 2400 people die of cardiovascular

disease each day, an average of 1 death every 36 seconds[8]. The increased prevalence of cardiovascular disease suggests a need for further research exploring the mechanisms of disease pathogenesis and therapies that address early detection and prevention.

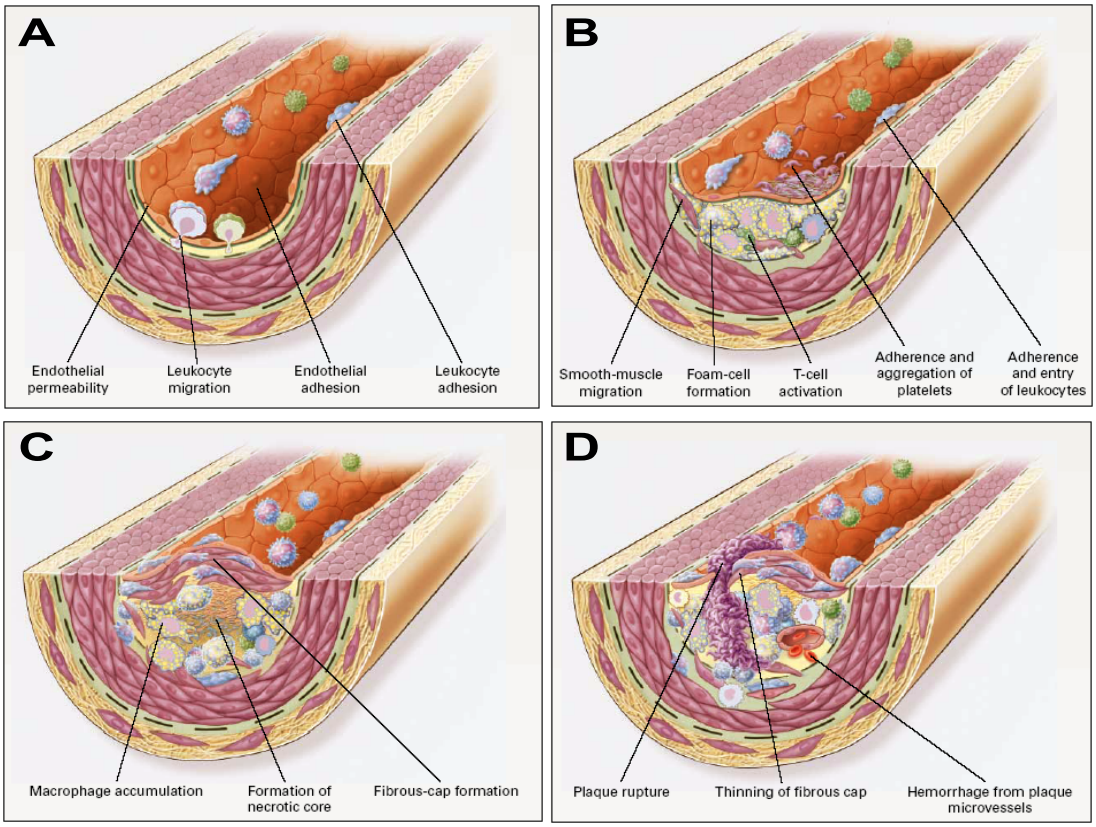

Figure 1.1 Atherosclerosis is an inflammatory disease. *Endothelium dysfunction (A) results in fatty streak formation (B), advanced plaque development (C), and rupture (D). Figure reprinted with permission[1]. Copyright © 1999 Massachusetts Medical Society.*

Atherosclerosis is an inflammatory disease of the large arteries and is characterized by the development of lipid-filled plaques that obstruct the vessel lumen (Figure. 1.1)[1]. In the vasculature, atherosclerosis is initiated by a "response-to-injury." This causes functional changes in endothelial cells known as endothelial dysfunction[9]. Globally,

endothelial dysfunction can be induced by hypercholesterolemia, smoking, hypertension, diabetes mellitus, genetic diseases, and elevated plasma homocysteine levels[9].

The endothelial dysfunction that results from one or a combination of these risk factors or "injuries" leads to compensatory responses that alter the normal homeostatic properties of the endothelium. The different forms of injury elevate the expression of inflammatory adhesion molecules, secrete cytokines and growth factors, and increase endothelial permeability to lipoproteins and other plasma constituents[1]. The first stage of atherosclerosis is marked by the development of deposits of oxidized cholesterol and macrophages known as fatty streaks. As the inflammatory response continues, endothelial cells express more adhesion molecules, including VCAM-1 and MCP-1, which recruit more circulating monocytes. Monocytes differentiate into macrophages, digest oxidized LDL and become foam cells. Foam cells burst and die releasing modified lipids, DNA, and other inflammatory molecules, further propagating the inflammatory process in the developing lesion. Smooth muscle cells also proliferate and migrate from the medial layer into the intima in response to cytokines secreted by damaged endothelial cells. This causes the formation of a fibrous capsule covering the fatty streak[1, 9]. Continued inflammatory cell infiltration can cause the plaque to become unstable and rupture, leading to thrombosis and embolism resulting in heart attack or stroke.

Atherosclerosis and Hemodynamics

Despite the global nature of many risk factors, it has been established that pockets of sustained inflammation and atherosclerosis develop in hemodynamically-defined regions of the vasculature[3-4]. Development of atherosclerotic lesions is largely restricted to bifurcations or sharp curves in the arterial tree. Vascular regions such as the carotid

bifurcation, the coronary vessels, the lesser curvature of the ascending aorta, and the abdominal aorta are clinically prone to plaque formation[3-4]. Studies have shown that these areas of the vasculature coincide with regions of disturbed blood flow where endothelial cells are exposed to low and oscillatory shear stress (OS) [3, 10]. In contrast, straight vessels exposed to high, unidirectional laminar shear stress (LS) resist both spontaneous clinical disease and experimentally induced disease[11]. These local mechanical forces have been correlated to the action of the exposed endothelium. In addition, a developing atherosclerotic lesion can itself alter the local shear stress pattern on the endothelium. An increased velocity of flow through the narrowed luminal space can create disturbed flow in the region immediately downstream to a substantial stenosis. The disturbed flow created by lesion has similar characteristics to those seen in prelesional sites, and may contribute to the growth of the lesion over time[12]. Furthermore, vein grafts transferred to the high pressure coronary artery circulation frequently develop stenoses, particularly at the artery-vein attachment sites[13]. In this local area, complex vascular geometry can contribute to flow separation and could be responsible for endothelial dysfunction[12-13]. Collectively, these phenomena suggest that blood flow and the forces it imparts on vessels, directly influence the local inflammatory environment of the vascular wall, thus playing a critical role in cellular function and vascular wall physiology during health and disease.

Shear Stress and Endothelial Cell Biology

Shear stress

Endothelial cells lining the vascular wall are under the constant influence of hemodynamic forces generated by blood flow from the heart. These forces are described in terms of flow-induced shear stress and pressure-induced cyclic strain (Figure. 1.2) [14].

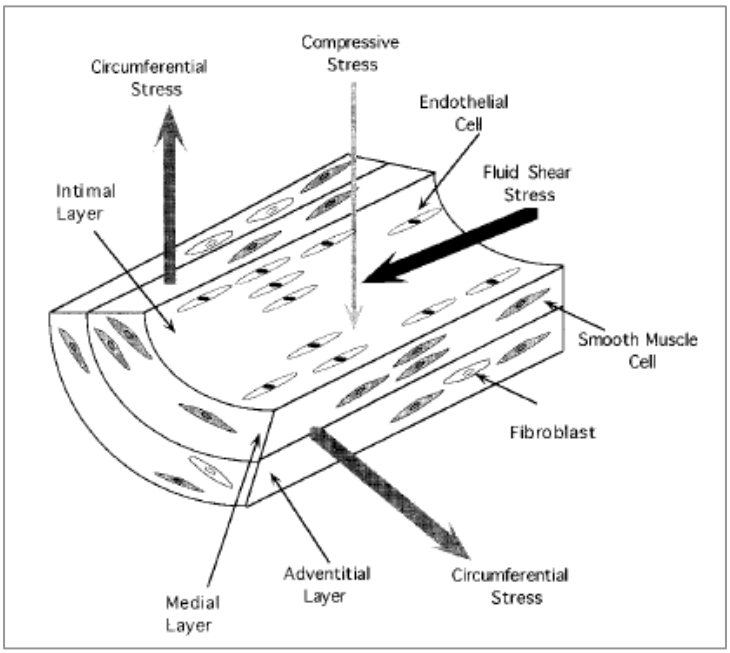

Figure 1.2 Blood flow acts on the arterial wall via three hemodynamic forces. *Figure reprinted with permission[14]. Copyright © 1997 American Chemical Society and American Institute of Chemical Engineers.*

The frictional wall shear stress acting tangentially as a result of blood flow over the vessel wall[14] has been identified as the critical force mediating flow-dependent atherosusceptibility. Disturbed, or oscillatory blood flow at vessel branches correlates with low, bidirectional shear stress, yielding atheroprone vessel regions, while unidirectional laminar flow results in high unidirectional shear stress, which is atheroprotective[10, 15-16].

Mechanotransduction

It is well established that endothelial cells experience dramatic morphological changes when exposed to different flow patterns. Endothelial cells are known to align and elongate parallel to the plane of unidirectional laminar blood flow. This alignment disappears under oscillatory or static flow conditions with cells orienting randomly or assuming a distinctive polygonal morphology.[17] The morphological sensitivity of

endothelial cells to different flow conditions is mediated by cell surface "mechanoreceptors". Shear stress mechanotransduction in the endothelium requires several sequential steps including: 1) physical deformation of the cell surface, 2) intracellular transmission of stress, 3) conversion of mechanical force to chemical activity, and 4) downstream biochemical signaling with feedback[12, 18]. The mechanotransduction is through these mechanoreceptors either by the direct transmission of shear forces to intracellular organelles via networks of cytoskeletal filaments, junctional complexes, and focal adhesions, or by activating biomolecular pathways that lead to altered gene expression[19]. As shear stress acts at the luminal cell surface, local membrane structures can participate in mechanotransduction. Examples include activation of ion channels and G proteins, and changes in phospholipid metabolism and membrane fluidity[12, 18]. This combination of biochemical and biomechanical signal transduction leads to both outside-in and inside-out signaling phenomena. For instance, the integrin can activate intracellular signaling pathway through conformational change by shear stress (outside-in) or can receive signals from other shear regulated-receptors activating intracellular signaling pathways that impingent on integrin cytoplasmic domains and make extracellular domain competent for ligand binding (inside-out) [19-20]. The diversity of endothelial functions is reflected in the variety of mechanotransduction mechanisms.

Microarray study in shear stress regulated EC gene expression

The differential mechanisms by which disturbed and stable flow promotes and inhibits atherogenesis, respectively, have been a subject of intense study, mostly using cultured endothelial cells [21-24]. To define molecular mechanisms responsible for these changes, investigators have carried out DNA microarray studies using endothelial cells [25-33] and have subsequently identified numerous shear sensitive genes such as kruppel-like factor

2 and 4 (*Klf2, Klf4*), endothelial nitric oxide synthase (*eNOS*), vascular cell adhesion molecule-1 (*VCAM-1*), intercellular adhesion molecule-1 (*ICAM-1*), bone morphogenic protein 4 (*BMP-4*), cathepsins and angiopoietin-2 (*Angpt2*) [27, 30, 34-42] Functional studies based on these shear-sensitive genes and their protein products have revealed the critical roles that they play in regulation of inflammation, thrombosis, vascular remodeling, angiogenesis and arteriogenesis[27, 35-38, 42-43]. While these *in vitro* studies have provided critical insights regarding shear sensitive mechanisms in cultured endothelial cells using modeled flow conditions, it cannot be assumed whether identical mechanosensitive genes and pathways are involved *in vivo* regulating flow-dependent vascular responses and diseases. In addition, given the exquisite sensitivity of endothelial gene expression to various flow conditions, it is quite plausible that many genes could be dysregulated (lost, overexpressed or modified) during cell culture which is carried out under no-flow condition for extended period. Recently, Davies and colleagues have conducted *in vivo* DNA microarray studies using endothelial RNAs obtained directly from the flow-disturbed inner aortic arch and undisturbed flow region of normal pig aorta [44-46]. Since pig aortic arch is exposed to chronic changes including flow-disturbance for many months from birth, the observed gene profile changes may be complex and may not be solely attributed to flow-disturbance. Therefore, it is critical to study how arterial endothelium responds to acute flow disturbance *in vivo*. However, the adequate pathophysiological animal models enabling acute and reproducible modulation of flow conditions that rapidly lead to atherosclerosis have been lacking.

Signal transduction and gene regulation

Steady laminar shear stress promotes the release of factors from endothelial cells that inhibit coagulation, leukocyte transmigration, and smooth muscle cell proliferation, while

simultaneously promoting endothelial cell survival (Figure 1.3)[2].

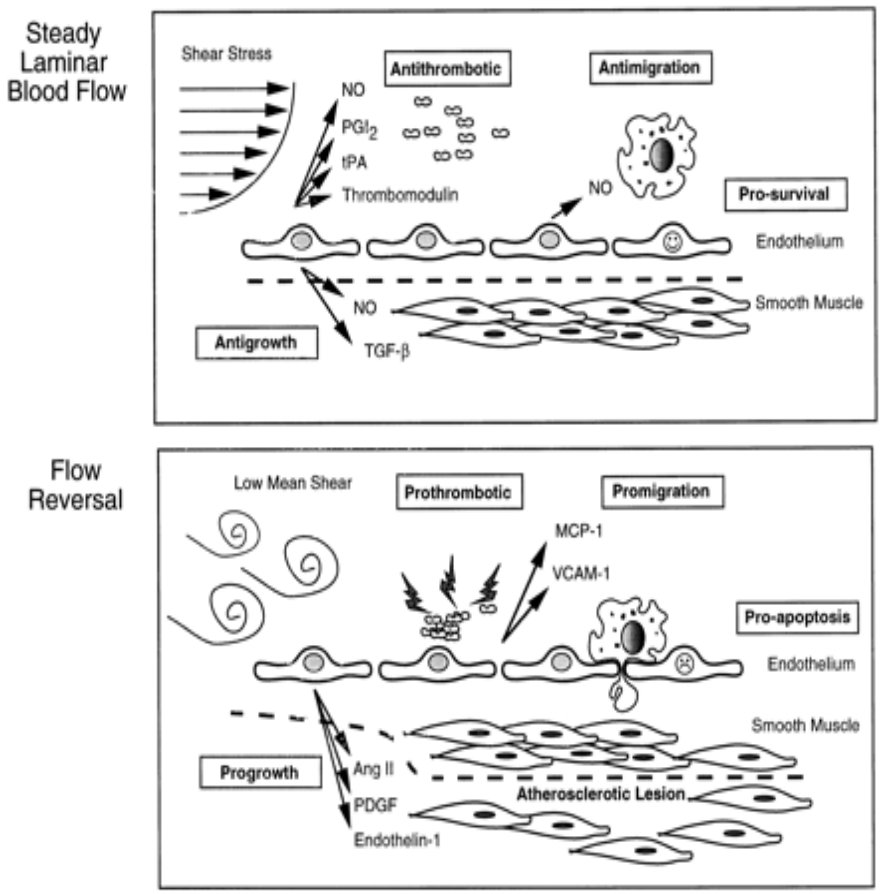

Figure 1.3 Mechanoresponses in endothelial cells exposed to different flow patterns. *Figure reprinted with permission[2]. Copyright © 1998 American Heart Association, Inc.*

For instance, vasoactive molecules, including nitric oxide (NO) and prostacyclin, promote vessel dilation and increased blood flow[2, 15, 47]. It is well known that exposure of endothelial cells to laminar shear stress stimulates the production of NO from eNOS in cultured cells[48-53]. Studies have shown that laminar shear stress stimulates serine/threonine kinase Akt phosphorylation on serine-473 in a vascular endothelial growth factor (VEGF) receptor dependent manner. Activation of Akt in turn phosphorylates eNOS at Ser-1177, leading to eNOS activation and NO production[50, 54-

[55]. Bioavailable NO production by laminar shear stress inhibits several key early events in the development of atherosclerosis. However, low shear stress and flow reversal induce a pro-inflammatory profile of gene and protein expression, contributing to the early development of atherosclerosis[2]. NO inhibits the expression of monocyte chemoattractant peptide-1 (MCP-1) and monocyte adhesion induced by cytokines and oxidized LDL, reduces vascular cell adhesion molecule-1 (VCAM-1) expression, prevents propagation of lipid oxidation, inhibits vascular smooth muscle cell proliferation, decreases platelet aggregation, and prevents cell death[56-60] . In contrast, the expression of VCAM-1, ICAM-1, and MCP-1 induced by oscillatory shear stress promotes monocyte adhesion[2, 47] which is a early marker for cellular inflammation. Endothelial cells exposed to disturbed flow also secrete pro-inflammatory, vasoactive factors such as platelet-derived growth factor (PDGF), endothelin-1, and angiotensin II, which encourages vasoconstriction, vascular smooth muscle cell proliferation, and reactive oxygen species production[2, 47, 61].

Given the range and scope of endothelial responses to LS and OS, it is likely that shear-induced response programs are mediated by several different mechanisms. Classical signal transduction and mechanotransduction of shear-induced signals can explain certain specific changes in gene expression and cell morphology, but microarray studies have noted hundreds to thousands of changes in gene expression between endothelial cells exposed to different shear conditions[26, 28-29]. In order to achieve such large-magnitude changes in gene expression, master regulator switches, namely microRNAs, which can regulate the expression levels of hundreds of genes each, must be directly influenced by shear-dependent stimuli.

microRNAs

microRNAs (miRNAs) are a large class of evolutionarily conserved, noncoding, small RNAs, typically 18 to 22 nucleotides in length that primarily function post-transcriptionally by interacting with the 3' untranslated region (3' UTR) of specific target mRNAs in a sequence-specific manner[62]. More than 800 miRNAs are encoded in the human genome, and each is thought to target multiple mRNAs (over hundreds), resulting in mRNA degradation or translational inhibition. miRNAs are transcribed by RNA polymerase II and can be derived from individual miRNA genes, from introns of protein-coding genes, or from polycistronic transcripts that often encode multiple, closely related miRNAs[63] (Figure 1.4). Pri-miRNAs are processed in the nucleus by the RNase Drosha into 70–100 nucleotides, hairpin-shaped precursors, called pre-miRNAs. Following transport to the cytoplasm, the pre-miRNA is further processed by the RNA endonuclease Dicer to produce a double-stranded miRNA. The fully processed miRNA duplex is then incorporated into a multicomponent protein complex known as RNA-induced silencing complex (RISC)[64-66] . During this process, one strand of the miRNA duplex is selected as a mature miRNA while the other strand, known as miRNA*, is in general rapidly removed and degraded. As part of the RISC, miRNAs negatively regulate gene expression through translational repression and mRNA cleavage, which depend on the extent of complementarity between the miRNA and its mRNA target and other criteria that are still being defined (Figure 1.4). Despite advances in miRNA discovery, the role of miRNAs in various physiological and pathophysiological processes is just emerging. In endothelial cells, it has become clear that miRNAs play diverse roles in fundamental biological processes, such as cell proliferation, migration, and inflammation[67-68]. Furthermore, miRNAs are considered as critical regulators in cardiovascular development and different aspects of the angiogenic process.

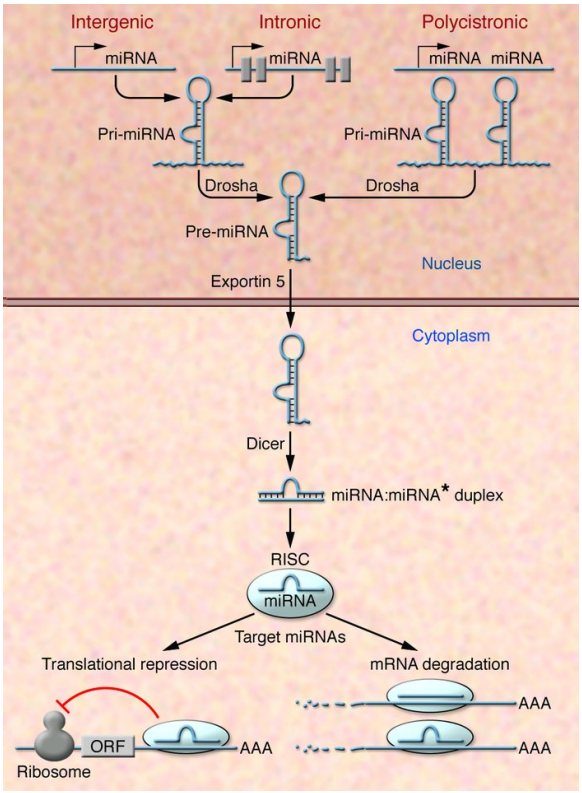

Figure 1.4 miRNA biogenesis and function. *Figure reprinted with permission*[63]*. Copyright © 2007, American Society for Clinical Investigation.*

miRNAs and Angiogenesis

Several studies have been aimed at elucidating the role of individual miRNAs in the regulation of angiogenesis. Specifically in endothelial cells, let-7f and miR-27b have been shown to exert pro-angiogenic effects as evidenced by the blockade of *in vitro* angiogenesis with 2'-*O*-methyl oligonucleotide antisenses specific to let-7f and miR-27b.[69]. Their gene targets in endothelial cells, however, have yet to be identified. Overexpression of miR-221/222 in HUVEC inhibits tube formation, migration, and wound healing in response to stem cell factor[70], suggesting that it exerts an anti-angiogenic effect. In hematopoietic progenitor cells, miR221/222 was also shown to control the growth of erythropoietic and erythroleukeic cells through the regulation of *c-kit* expression at the translational level[71]. miR-221 and miR-222 overexpression also

indirectly reduces the expression of endothelial nitric oxide synthase (eNOS) in dicer siRNA-transfected cells[72]. Nitric oxide (NO) is not only a key regulator for endothelial cell growth, migration, vascular remodeling, and angiogenesis; its impaired bioavailability is also a hallmark of patients with atherosclerosis and ischemic cardiomyopathy. miRNAs targeting eNOS might not only regulate angiogenesis as it has been shown for miR-221/222, but may also be involved in vasculogenesis.

miRNAs and Inflammation.

The role of miRNAs in vascular inflammation, particularly in leukocyte activation and infiltration into the vascular wall, has been recently reported. The first evidence that miRNAs control vascular inflammation identified miR-126 as an inhibitor of vascular cell adhesion molecule 1 (VCAM-1) expression, which mediates leukocyte adhesion to endothelial cells[73]. Thus, decreasing miR-126 in endothelial cells increases TNF-stimulated VCAM-1 expression, enhancing leukocyte adhesion to endothelial cells. Recently, it has been shown that miR-21 is a regulator of neointimal lesion formation[74]. Downregulation of aberrantly expressed miR-21 decreased neointimal lesion formation in rat carotid artery following angioplasty. Although only a few studies have directly assessed the role of miRNAs in vascular inflammation and diseases, several studies have looked at the contribution of miRNAs in the differentiation and function of hematopoietic cells involved in inflammation. While it is now clear that inflammation is a key event in atherosclerosis that is at least spatially linked to arterial regions of disturbed flow regions, it is not known whether flow conditions regulate miRNA expression profiles in the vessel wall and the subsequent pro-inflammatory and atherogenic responses that follow. This is the major issue that will be addressed in this dissertation.

In Vitro Models of Shear Stress

To investigate how local hemodynamic conditions regulate endothelial cell function in *vivo*, several *in vitro* systems have been developed to examine endothelial function and structure under conditions simulating certain aspects of *in vivo* conditions[75]. Devices such as the parallel plate flow chamber, vertical step flow chamber, cone-and-plate viscometer, modified cone-and-plate shear apparatus, and microfluidics device have allowed for controlled experiments on cultured endothelial cells[17, 33, 35, 75-76]. Cone-and-plate and parallel plate flow chamber are two of the most popular *in vitro* shear devices. Here, we will discuss each model. In the parallel plate system, cells are cultured on glass slides and positioned within a rectangular flow chamber. A roller pump is used to circulate medium through the chamber to provide uniform levels of shear stress. The dimensions of the chamber and the pressure drop across it dictate the fluid flow rate and result in specific shear stress conditions[47]. In the cone-and-plate shear system, a Teflon cone is used to generate shear stress. The cone is placed in a circular culture dish containing adherent endothelial cells and medium.

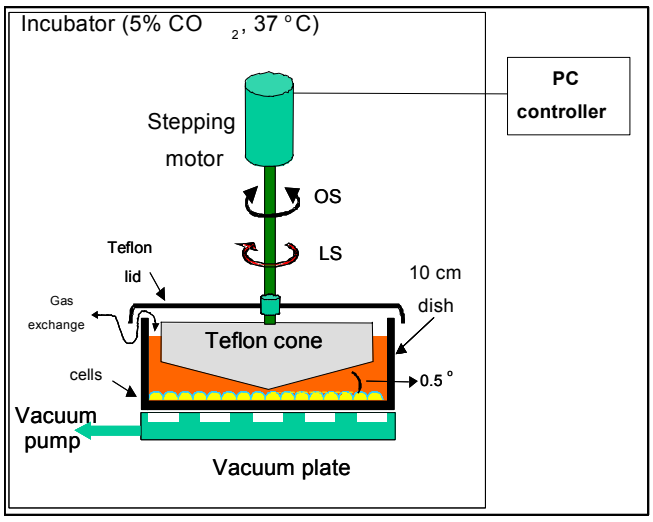

Figure 1.5 Schematic of the cone-and-plate shear stress system

As illustrated in Figure 1.5, the angle of the cone is 0.5^0. Rotation of the cone forces the fluid between the cone and plate to flow azimuthally and produce a shear stress on the stationary endothelial cell monolayer[77]. The Navier-Stokes equations can be used to accurately calculate the magnitude and direction of this shear stress and to determine the limits to which this system can produce laminar arterial flow profiles[77]. When compared to the parallel plate system, the cone-and-plate shear apparatus exhibits several advantages and disadvantages. For example, the low volume of media used in the cone-and-plate viscometer may permit secreted growth factors and cytokines to accumulate over time and produce non-physiological effects on cultured cells. In addition, this system results in a gradient of shear stress, and cells at the center of the culture dish, near the cone apex, may experience lower shear stress than those at the perimeter. Alternatively, the cone-and-plate viscometer can expose a greater number of cells to shear stress when compared to the parallel plate system using small glass coverslips. This is critical for RNA and protein analyses of cells. The system can also be used to simulate reversal of flow by rotating the cone back and forth. Although secondary flow can occur at high rotational speeds, this is generally negligible to achieve physiologically relevant shear stresses[78]. As a result the cone-and-plate viscometer can expose cultured endothelial cells to both atherogenic oscillatory shear stress (OS) and atheroprotective unidirectional laminar shear stress (LS).

In Vivo Models of Shear Stress

Atherosclerosis is a local disease, occurring mostly in areas of low and oscillatory shear stress, key features of disturbed flow. Many researchers have focused on studying the areas of naturally occurring disturbed flow in animal models while others have attempted to create areas of disturbed flow to mimic the shear stress profile experienced in areas of naturally occurring atherosclerosis. With respect to animal models, shear stress levels

not only vary in different regions of the arterial tree within individuals of a species, they also vary greatly between different species, with higher shear stress values generally seen in smaller animals[79]. Change in vessel diameter in response to shear stress alterations is not only species- but also strain-dependent[80].

For many years, atherosclerosis research in animal models was performed mostly by studying spontaneous atherosclerosis in animals susceptible to atheroma formation [81]. A disturbed pattern of flow can be found in many different areas of the arterial tree including, but not limited to, the aortic sinus, the lesser curvature of the aortic arch, the root of the innominate artery, the carotid bifurcation, the branching of the celiac artery from the abdominal aorta and regions in the coronary system [82-91]. The predilection of these sites to develop spontaneous lesions experimentally is what brought the relationship of mechanical forces and atherosclerosis to the attention of investigators. These areas can be used to study the effects of disturbed flow on endothelial biology including gene and protein expression. The widely used mouse model is to examine the plaque development in aortic arch or aortic sinus using $ApoE^{-/-}$ or $LDLR^{-/-}$ mice fed a high cholesterol diet for several months[92]. The major advantage of using these areas of naturally occurring disturbed flow is their pathophysiological relevance, as these are atheroprone regions in humans as well. These areas are chronically exposed to disturbed flow patterns, making them appropriate models for long term atheroma formation. However, naturally occurring regions of disturbed flow cannot adequately model the effects of acute changes in shear stress *in vivo*.

Our lab recently characterized a mouse model in which disturbed flow is acutely produced within the common carotid artery by ligating the internal carotid, occipital, and external carotid arteries distal to the branching of the superior thyroid artery, restricting

common carotid blood flow solely to the superior thyroid artery. This results in a significant reduction in blood flow within the common carotid that, importantly, is accompanied by flow reversal during diastole giving rise to a combined low and oscillatory shear stress pattern characteristic of naturally occurring areas of disturbed flow in the arterial tree [93]. In this dissertation, the mouse partial carotid ligation model will be used to discover novel mechanosensitive genes and miRNAs. A detailed description of this mouse model will be presented in Chapter 4.

Mouse Aortic Endothelial Cell line

In vitro systems using cultured endothelial cells serve as important tools to study vascular physiology and disease pathology. Endothelial cells from different origins and species have been successfully cultured for several decades[94-95]. Popular human primary endothelial cell lines include human umbilical vein cord endothelial cells (HUVECs)[96], human aortic endothelial cells (HAECs)[97], human coronary artery endothelial cells (HCAEC)[98], and microvascular endothelial cells[99-100]. In addition, endothelial cell lines have also been developed from other species, such as bovine aortic endothelial cells (BAECs)[101], pig aortic endothelial cells (PAECs)[102] and endothelial cells from the mouse[103-117]. In particular, murine ECs allow the use of the powerful tool of mouse genetics in identifying genetic and molecular mechanisms in endothelial cell function. While several studies have developed different methods for the isolation of primary mouse aortic endothelial cells (MAECs)[107-108, 112-117], the isolation and maintenance of primary MAECs still remain a formidable challenge: they are time-, cost-, and labor-intensive. The main obstacle to primary MAEC culture is the almost prohibitively low number of cells yielded by a single animal, which is compounded by the limited proliferative potential of these cells. Contamination of cultures by other cell types that out-proliferate MAECs is common. Moreover, it seems that MAECs have a tendency

to trans-differentiate to mesenchymal cells during culture[118-119]. As such, the development of pure and stable immortalized MAEC lines presents significant technical challenges, in spite of their obvious promise as an *in vitro* model system. In this dissertation, the method for generating immortalized MAEC lines will be described in Chapter 3 and iMAEC lines will be used to validate the expression of miRNAs and mRNA based on the results obtained *in vivo*.

References

1. Ross R. Atherosclerosis--an inflammatory disease. *N Engl J Med*. 1999;340:115-126

2. Traub O, Berk BC. Laminar shear stress: Mechanisms by which endothelial cells transduce an atheroprotective force. *Arterioscler Thromb Vasc Biol*. 1998;18:677-685

3. Ku DN, Giddens DP, Zarins CK, Glagov S. Pulsatile flow and atherosclerosis in the human carotid bifurcation. Positive correlation between plaque location and low oscillating shear stress. *Arteriosclerosis*. 1985;5:293-302

4. VanderLaan PA, Reardon CA, Getz GS. Site specificity of atherosclerosis: Site-selective responses to atherosclerotic modulators. *Arterioscler Thromb Vasc Biol*. 2004;24:12-22

5. Chen CZ, Li L, Lodish HF, Bartel DP. Micrornas modulate hematopoietic lineage differentiation. *Science*. 2004;303:83-86

6. Xu P, Guo M, Hay BA. Micrornas and the regulation of cell death. *Trends Genet*. 2004;20:617-624

7. Mendell JT. Miriad roles for the mir-17-92 cluster in development and disease. *Cell*. 2008;133:217-222

8. Association AH. Heart disease and stroke statistics — 2008 update. 2008

9. Ross R. The pathogenesis of atherosclerosis: A perspective for the 1990s. *Nature*. 1993;362:801-809

10. Zarins CK, Giddens DP, Bharadvaj BK, Sottiurai VS, Mabon RF, Glagov S. Carotid bifurcation atherosclerosis. Quantitative correlation of plaque localization with flow velocity profiles and wall shear stress. *Circ Res*. 1983;53:502-514

11. Davies PF, Shi C, Depaola N, Helmke BP, Polacek DC. Hemodynamics and the focal origin of atherosclerosis: A spatial approach to endothelial structure, gene expression, and function. *Ann N Y Acad Sci*. 2001;947:7-16; discussion 16-17

12. Davies PF. Hemodynamic shear stress and the endothelium in cardiovascular pathophysiology. *Nat Clin Pract Cardiovasc Med*. 2009;6:16-26

13. Loth F, Fischer PF, Arslan N, Bertram CD, Lee SE, Royston TJ, Shaalan WE, Bassiouny HS. Transitional flow at the venous anastomosis of an arteriovenous graft: Potential activation of the erk1/2 mechanotransduction pathway. *J Biomech Eng*. 2003;125:49-61

14. Papadaki M, Eskin SG. Effects of fluid shear stress on gene regulation of vascular cells. *Biotechnol. Prog.* 1997;13:209-221

15. Nerem RM, Harrison DG, Taylor WR, Alexander RW. Hemodynamics and vascular endothelial biology. *J Cardiovasc Pharmacol*. 1993;21 Suppl 1:S6-10

16. Caro CG, Fitz-Gerald JM, Schroter RC. Arterial wall shear and distribution of early atheroma in man. *Nature*. 1969;223:1159-1160

17. Helmlinger G, Geiger RV, Schreck S, Nerem RM. Effects of pulsatile flow on cultured vascular endothelial cell morphology. *J Biomech Eng*. 1991;113:123-131

18. Davies PF. Flow-mediated endothelial mechanotransduction. *Physiol Rev*. 1995;75:519-560

19. Papadaki M, Eskin SG. Effects of fluid shear stress on gene regulation of vascular cells. *Biotechnol Prog*. 1997;13:209-221

20. Takagi J, Petre BM, Walz T, Springer TA. Global conformational rearrangements in integrin extracellular domains in outside-in and inside-out signaling. *Cell*. 2002;110:599-511

21. Berk BC. Atheroprotective signaling mechanisms activated by steady laminar flow in endothelial cells. *Circulation*. 2008;117:1082-1089

22. Davies PF, Mundel T, Barbee KA. A mechanism for heterogeneous endothelial responses to flow in vivo and in vitro. *J Biomech*. 1995;28:1553-1560

23. Jo H, Song H, Mowbray A. Role of nadph oxidases in disturbed flow- and bmp4-induced inflammation and atherosclerosis. *Antioxid Redox Signal*. 2006;8:1609-1619

24. Chien S. Effects of disturbed flow on endothelial cells. *Ann Biomed Eng*. 2008;36:554-562

25. Garcia-Cardena G, Comander JI, Blackman BR, Anderson KR, Gimbrone MA. Mechanosensitive endothelial gene expression profiles: Scripts for the role of hemodynamics in atherogenesis? *Ann N Y Acad Sci*. 2001;947:1-6

26. Zhao Y, Chen BP, Miao H, Yuan S, Li YS, Hu Y, Rocke DM, Chien S. Improved significance test for DNA microarray data: Temporal effects of shear stress on endothelial genes. *Physiol Genomics*. 2002;12:1-11

27. Dekker RJ, van Soest S, Fontijn RD, Salamanca S, de Groot PG, VanBavel E, Pannekoek H, Horrevoets AJ. Prolonged fluid shear stress induces a distinct set of endothelial cell genes, most specifically lung kruppel-like factor (klf2). *Blood*. 2002;100:1689-1698

28. Chen BP, Li YS, Zhao Y, Chen KD, Li S, Lao J, Yuan S, Shyy JY, Chien S. DNA microarray analysis of gene expression in endothelial cells in response to 24-h shear stress. *Physiol Genomics*. 2001;7:55-63

29. McCormick SM, Eskin SG, McIntire LV, Teng CL, Lu CM, Russell CG, Chittur KK. DNA microarray reveals changes in gene expression of shear stressed human umbilical vein endothelial cells. *Proc Natl Acad Sci U S A*. 2001;98:8955-8960

30. Conway DE, Williams MR, Eskin SG, McIntire LV. Endothelial cell responses to atheroprone flow are driven by two separate flow components: Low time-average shear stress and fluid flow reversal. *American journal of physiology*. 2010;298:H367-374

31. Himburg HA, Dowd SE, Friedman MH. Frequency-dependent response of the vascular endothelium to pulsatile shear stress. *American journal of physiology*. 2007;293:H645-653

32. Chu TJ, Peters DG. Serial analysis of the vascular endothelial transcriptome under static and shear stress conditions. *Physiol Genomics*. 2008;34:185-192

33. Dai G, Kaazempur-Mofrad MR, Natarajan S, Zhang Y, Vaughn S, Blackman BR, Kamm RD, Garcia-Cardena G, Gimbrone MA, Jr. Distinct endothelial phenotypes evoked by arterial waveforms derived from atherosclerosis-susceptible and -resistant regions of human vasculature. *Proc Natl Acad Sci U S A*. 2004;101:14871-14876

34. Chang K, Weiss D, Suo J, Vega JD, Giddens D, Taylor WR, Jo H. Bone morphogenic protein antagonists are coexpressed with bone morphogenic protein 4 in endothelial cells exposed to unstable flow in vitro in mouse aortas and in human coronary arteries: Role of bone morphogenic protein antagonists in inflammation and atherosclerosis. *Circulation*. 2007;116:1258-1266

35. Sorescu GP, Sykes M, Weiss D, Platt MO, Saha A, Hwang J, Boyd N, Boo YC, Vega JD, Taylor WR, Jo H. Bone morphogenic protein 4 produced in endothelial cells by oscillatory shear stress stimulates an inflammatory response. *J Biol Chem*. 2003;278:31128-31135

36. SenBanerjee S, Lin Z, Atkins GB, Greif DM, Rao RM, Kumar A, Feinberg MW, Chen Z, Simon DI, Luscinskas FW, Michel TM, Gimbrone MA, Jr., Garcia-Cardena G, Jain MK. Klf2 is a novel transcriptional regulator of endothelial proinflammatory activation. *J Exp Med*. 2004;199:1305-1315

37. Tressel SL, Kim H, Ni CW, Chang K, Velasquez-Castano JC, Taylor WR, Yoon YS, Jo H. Angiopoietin-2 stimulates blood flow recovery after femoral artery occlusion by inducing inflammation and arteriogenesis. *Arterioscler Thromb Vasc Biol*. 2008;28:1989-1995

38. Tressel SL, Huang RP, Tomsen N, Jo H. Laminar shear inhibits tubule formation and migration of endothelial cells by an angiopoietin-2 dependent mechanism. *Arterioscler Thromb Vasc Biol*. 2007;27:2150-2156

39. Platt MO, Ankeny RF, Shi GP, Weiss D, Vega JD, Taylor WR, Jo H. Expression of cathepsin k is regulated by shear stress in cultured endothelial cells and is increased in endothelium in human atherosclerosis. *American journal of physiology*. 2007;292:H1479-1486

40. Platt MO, Ankeny RF, Jo H. Laminar shear stress inhibits cathepsin l activity in endothelial cells. *Arterioscler Thromb Vasc Biol*. 2006;26:1784-1790

41. Won D, Zhu SN, Chen M, Teichert AM, Fish JE, Matouk CC, Bonert M, Ojha M, Marsden PA, Cybulsky MI. Relative reduction of endothelial nitric-oxide synthase expression and transcription in atherosclerosis-prone regions of the mouse aorta and in an in vitro model of disturbed flow. *Am J Pathol*. 2007;171:1691-1704

42. Villarreal G, Jr., Zhang Y, Larman HB, Gracia-Sancho J, Koo A, Garcia-Cardena G. Defining the regulation of klf4 expression and its downstream transcriptional targets in vascular endothelial cells. *Biochem Biophys Res Commun*. 2009

43. Sorescu GP, Song H, Tressel SL, Hwang J, Dikalov S, Smith DA, Boyd NL, Platt MO, Lassegue B, Griendling KK, Jo H. Bone morphogenic protein 4 produced in endothelial cells by oscillatory shear stress induces monocyte adhesion by stimulating reactive oxygen species production from a nox1-based nadph oxidase. *Circ Res*. 2004;95:773-779

44. Civelek M, Manduchi E, Riley RJ, Stoeckert CJ, Jr., Davies PF. Chronic endoplasmic reticulum stress activates unfolded protein response in arterial endothelium in regions of susceptibility to atherosclerosis. *Circ Res*. 2009;105:453-461

45. Passerini AG, Polacek DC, Shi C, Francesco NM, Manduchi E, Grant GR, Pritchard WF, Powell S, Chang GY, Stoeckert CJ, Jr., Davies PF. Coexisting proinflammatory and antioxidative endothelial transcription profiles in a disturbed flow region of the adult porcine aorta. *Proc Natl Acad Sci U S A*. 2004;101:2482-2487

46. Passerini AG, Shi C, Francesco NM, Chuan P, Manduchi E, Grant GR, Stoeckert CJ, Jr., Karanian JW, Wray-Cahen D, Pritchard WF, Davies PF. Regional determinants of arterial endothelial phenotype dominate the impact of gender or short-term exposure to a high-fat diet. *Biochem Biophys Res Commun*. 2005;332:142-148

47. Nerem RM, Alexander RW, Chappell DC, Medford RM, Varner SE, Taylor WR. The study of the influence of flow on vascular endothelial biology. *Am J Med Sci*. 1998;316:169-175

48. Boo YC, Hwang J, Sykes M, Michell BJ, Kemp BE, Lum H, Jo H. Shear stress stimulates phosphorylation of enos at ser(635) by a protein kinase a-dependent mechanism. *Am J Physiol Heart Circ Physiol*. 2002;283:H1819-1828

49. Boo YC, Sorescu G, Boyd N, Shiojima I, Walsh K, Du J, Jo H. Shear stress stimulates phosphorylation of endothelial nitric-oxide synthase at ser1179 by akt-independent mechanisms: Role of protein kinase a. *J Biol Chem*. 2002;277:3388-3396

50. Gallis B, Corthals GL, Goodlett DR, Ueba H, Kim F, Presnell SR, Figeys D, Harrison DG, Berk BC, Aebersold R, Corson MA. Identification of flow-dependent endothelial nitric-oxide synthase phosphorylation sites by mass spectrometry and regulation of phosphorylation and nitric oxide production by the phosphatidylinositol 3-kinase inhibitor ly294002. *J Biol Chem*. 1999;274:30101-30108

51. Jin ZG, Wong C, Wu J, Berk BC. Flow shear stress stimulates gab1 tyrosine phosphorylation to mediate protein kinase b and endothelial nitric-oxide synthase activation in endothelial cells. *J Biol Chem*. 2005;280:12305-12309

52. Mata-Greenwood E, Jenkins C, Farrow KN, Konduri GG, Russell JA, Lakshminrusimha S, Black SM, Steinhorn RH. Enos function is developmentally regulated: Uncoupling of enos occurs postnatally. *Am J Physiol Lung Cell Mol Physiol*. 2006;290:L232-241

53. Moore JP, Weber M, Searles CD. Laminar shear stress modulates phosphorylation and localization of rna polymerase ii on the endothelial nitric oxide synthase gene. *Arterioscler Thromb Vasc Biol*. 2010;30:561-567

54. Dimmeler S, Fleming I, Fisslthaler B, Hermann C, Busse R, Zeiher AM. Activation of nitric oxide synthase in endothelial cells by akt-dependent phosphorylation. *Nature*. 1999;399:601-605

55. Fulton D, Gratton JP, McCabe TJ, Fontana J, Fujio Y, Walsh K, Franke TF, Papapetropoulos A, Sessa WC. Regulation of endothelium-derived nitric oxide production by the protein kinase akt. *Nature*. 1999;399:597-601

56. Cai H, Harrison DG. Endothelial dysfunction in cardiovascular diseases: The role of oxidant stress. *Circ Res*. 2000;87:840-844

57. Cardona-Sanclemente LE, Born GV. Effect of inhibition of nitric oxide synthesis on the uptake of ldl and fibrinogen by arterial walls and other organs of the rat. *Br J Pharmacol*. 1995;114:1490-1494

58. Dimmeler S, Hermann C, Galle J, Zeiher AM. Upregulation of superoxide dismutase and nitric oxide synthase mediates the apoptosis-suppressive effects of shear stress on endothelial cells. *Arterioscler Thromb Vasc Biol*. 1999;19:656-664

59. Harrison DG, Widder J, Grumbach I, Chen W, Weber M, Searles C. Endothelial mechanotransduction, nitric oxide and vascular inflammation. *J Intern Med*. 2006;259:351-363

60. Tsao PS, Buitrago R, Chan JR, Cooke JP. Fluid flow inhibits endothelial adhesiveness. Nitric oxide and transcriptional regulation of vcam-1. *Circulation*. 1996;94:1682-1689

61. Harrison D, Griendling KK, Landmesser U, Hornig B, Drexler H. Role of oxidative stress in atherosclerosis. *Am J Cardiol*. 2003;91:7A-11A

62. Zhao Y, Srivastava D. A developmental view of microrna function. *Trends Biochem Sci*. 2007;32:189-197

63. van Rooij E, Olson EN. Micrornas: Powerful new regulators of heart disease and provocative therapeutic targets. *J Clin Invest*. 2007;117:2369-2376

64. Lee Y, Ahn C, Han J, Choi H, Kim J, Yim J, Lee J, Provost P, Radmark O, Kim S, Kim VN. The nuclear rnase iii drosha initiates microrna processing. *Nature*. 2003;425:415-419

65. Gregory RI, Yan KP, Amuthan G, Chendrimada T, Doratotaj B, Cooch N, Shiekhattar R. The microprocessor complex mediates the genesis of micrornas. *Nature*. 2004;432:235-240

66. Denli AM, Tops BB, Plasterk RH, Ketting RF, Hannon GJ. Processing of primary micrornas by the microprocessor complex. *Nature*. 2004;432:231-235

67. Cordes KR, Srivastava D. Microrna regulation of cardiovascular development. *Circ Res*. 2009;104:724-732

68. Suarez Y, Sessa WC. Micrornas as novel regulators of angiogenesis. *Circ Res*. 2009;104:442-454

69. Kuehbacher A, Urbich C, Zeiher AM, Dimmeler S. Role of dicer and drosha for endothelial microrna expression and angiogenesis. *Circ Res*. 2007;101:59-68

70. Poliseno L, Tuccoli A, Mariani L, Evangelista M, Citti L, Woods K, Mercatanti A, Hammond S, Rainaldi G. Micrornas modulate the angiogenic properties of huvecs. *Blood*. 2006;108:3068-3071

71. Felli N, Fontana L, Pelosi E, Botta R, Bonci D, Facchiano F, Liuzzi F, Lulli V, Morsilli O, Santoro S, Valtieri M, Calin GA, Liu CG, Sorrentino A, Croce CM, Peschle C. Micrornas 221 and 222 inhibit normal erythropoiesis and erythroleukemic cell growth via kit receptor down-modulation. *Proc Natl Acad Sci U S A*. 2005;102:18081-18086

72. Suarez Y, Fernandez-Hernando C, Pober JS, Sessa WC. Dicer dependent micrornas regulate gene expression and functions in human endothelial cells. *Circ Res*. 2007;100:1164-1173

73. Harris TA, Yamakuchi M, Ferlito M, Mendell JT, Lowenstein CJ. Microrna-126 regulates endothelial expression of vascular cell adhesion molecule 1. *Proc Natl Acad Sci U S A*. 2008;105:1516-1521

74. Ji R, Cheng Y, Yue J, Yang J, Liu X, Chen H, Dean DB, Zhang C. Microrna expression signature and antisense-mediated depletion reveal an essential role of microrna in vascular neointimal lesion formation. *Circ Res*. 2007;100:1579-1588

75. Resnick N, Gimbrone MA, Jr. Hemodynamic forces are complex regulators of endothelial gene expression. *Faseb J*. 1995;9:874-882

76. Chiu JJ, Chen LJ, Lee PL, Lee CI, Lo LW, Usami S, Chien S. Shear stress inhibits adhesion molecule expression in vascular endothelial cells induced by coculture with smooth muscle cells. *Blood*. 2003;101:2667-2674

77. Dewey CJ, Bussolari S, Gimbrone MJ, Davies P. The dynamic response of vascular endothelial cells to fluid shear stress. *J Biomech Eng*. 1981;103:177-185

78. Sdougos HP, Bussolari SR, Dewey CF. Secondary flow and turbulence in a cone-and-plate device. *J Fluid Mech*. 1984;138:379-404

79. Cheng C, Helderman F, Tempel D, Segers D, Hierck B, Poelmann R, van Tol A, Duncker DJ, Robbers-Visser D, Ursem NT, van Haperen R, Wentzel JJ, Gijsen F, van der Steen AF, de Crom R, Krams R. Large variations in absolute wall shear stress levels within one species and between species. *Atherosclerosis*. 2007;195:225-235

80. Ibrahim J, Miyashiro JK, Berk BC. Shear stress is differentially regulated among inbred rat strains. *Circ Res*. 2003;92:1001-1009

81. Jokinen MP, Clarkson TB, Prichard RW. Animal models in atherosclerosis research. *Exp Mol Pathol*. 1985;42:1-28

82. Farmakis TM, Soulis JV, Giannoglou GD, Zioupos GJ, Louridas GE. Wall shear stress gradient topography in the normal left coronary arterial tree: Possible implications for atherogenesis. *Curr Med Res Opin*. 2004;20:587-596

83. Asakura T, Karino T. Flow patterns and spatial distribution of atherosclerotic lesions in human coronary arteries. *Circ Res*. 1990;66:1045-1066

84. Del Gaudio C, Morbiducci U, Grigioni M. Time dependent non-newtonian numerical study of the flow field in a realistic model of aortic arch. *Int J Artif Organs*. 2006;29:709-718

85. Suo J, Ferrara DE, Sorescu D, Guldberg RE, Taylor WR, Giddens DP. Hemodynamic shear stresses in mouse aortas: Implications for atherogenesis. *Arterioscler Thromb Vasc Biol*. 2007;27:346-351

86. Lutz RJ, Cannon JN, Bischoff KB, Dedrick RL, Stiles RK, Fry DL. Wall shear stress distribution in a model canine artery during steady flow. *Circ Res*. 1977;41:391-399

87. Lei M, Kleinstreuer C, Truskey GA. Numerical investigation and prediction of atherogenic sites in branching arteries. *J Biomech Eng*. 1995;117:350-357

88. Kleinstreuer C, Hyun S, Buchanan JR, Jr., Longest PW, Archie JP, Jr., Truskey GA. Hemodynamic parameters and early intimal thickening in branching blood vessels. *Crit Rev Biomed Eng*. 2001;29:1-64

89. Cheng CP, Parker D, Taylor CA. Quantification of wall shear stress in large blood vessels using lagrangian interpolation functions with cine phase-contrast magnetic resonance imaging. *Ann Biomed Eng*. 2002;30:1020-1032

90. Tang BT, Cheng CP, Draney MT, Wilson NM, Tsao PS, Herfkens RJ, Taylor CA. Abdominal aortic hemodynamics in young healthy adults at rest and during lower limb exercise: Quantification using image-based computer modeling. *Am J Physiol Heart Circ Physiol*. 2006;291:H668-676

91. Buchanan JR, Jr., Kleinstreuer C, Truskey GA, Lei M. Relation between non-uniform hemodynamics and sites of altered permeability and lesion growth at the rabbit aorto-celiac junction. *Atherosclerosis*. 1999;143:27-40

92. Zadelaar S, Kleemann R, Verschuren L, de Vries-Van der Weij J, van der Hoorn J, Princen HM, Kooistra T. Mouse models for atherosclerosis and pharmaceutical modifiers. *Arterioscler Thromb Vasc Biol*. 2007;27:1706-1721

93. Nam D, Ni CW, Rezvan A, Suo J, Budzyn K, Llanos A, Harrison D, Giddens D, Jo H. Partial carotid ligation is a model of acutely induced disturbed flow, leading

to rapid endothelial dysfunction and atherosclerosis. *Am J Physiol Heart Circ Physiol*. 2009;297:H1535-1543

94. Jaffe EA, Nachman RL, Becker CG, Minick CR. Culture of human endothelial cells derived from umbilical veins. Identification by morphologic and immunologic criteria. *J Clin Invest*. 1973;52:2745-2756

95. Jaffe EA, Hoyer LW, Nachman RL. Synthesis of antihemophilic factor antigen by cultured human endothelial cells. *J Clin Invest*. 1973;52:2757-2764

96. Baudin B, Bruneel A, Bosselut N, Vaubourdolle M. A protocol for isolation and culture of human umbilical vein endothelial cells. *Nat Protoc*. 2007;2:481-485

97. Akeson AL, Mosher LB, Woods CW, Schroeder KK, Bowlin TL. Human aortic endothelial cells express the type i but not the type ii receptor for interleukin-1 (il-1). *J Cell Physiol*. 1992;153:583-588

98. Yu SY, Song YM, Li AM, Yu XJ, Zhao G, Song MB, Lin CM, Tao CR, Huang L. Isolation and characterization of human coronary artery-derived endothelial cells in vivo from patients undergoing percutaneous coronary interventions. *J Vasc Res*. 2009;46:487-494

99. Marks RM, Czerniecki M, Penny R. Human dermal microvascular endothelial cells: An improved method for tissue culture and a description of some singular properties in culture. *In Vitro Cell Dev Biol*. 1985;21:627-635

100. Gargett CE, Bucak K, Rogers PA. Isolation, characterization and long-term culture of human myometrial microvascular endothelial cells. *Hum Reprod*. 2000;15:293-301

101. Booyse FM, Sedlak BJ, Rafelson ME, Jr. Culture of arterial endothelial cells: Characterization and growth of bovine aortic cells. *Thromb Diath Haemorrh*. 1975;34:825-839

102. Merrilees MJ, Scott L. Interaction of aortic endothelial and smooth muscle cells in culture. Effect on glycosaminoglycan levels. *Atherosclerosis*. 1981;39:147-161

103. Nishiyama T, Mishima K, Ide F, Yamada K, Obara K, Sato A, Hitosugi N, Inoue H, Tsubota K, Saito I. Functional analysis of an established mouse vascular endothelial cell line. *J Vasc Res*. 2007;44:138-148

104. Canault M, Peiretti F, Mueller C, Deprez P, Bonardo B, Bernot D, Juhan-Vague I, Nalbone G. Proinflammatory properties of murine aortic endothelial cells exclusively expressing a non cleavable form of tnfalpha. Effect on tumor necrosis factor alpha receptor type 2. *Thromb Haemost*. 2004;92:1428-1437

105. Kevil CG, Pruitt H, Kavanagh TJ, Wilkerson J, Farin F, Moellering D, Darley-Usmar VM, Bullard DC, Patel RP. Regulation of endothelial glutathione by icam-1: Implications for inflammation. *FASEB J*. 2004;18:1321-1323

106. Seol GH, Ahn SC, Kim JA, Nilius B, Suh SH. Inhibition of endothelium-dependent vasorelaxation by extracellular k(+): A novel controlling signal for vascular contractility. *Am J Physiol Heart Circ Physiol*. 2004;286:H329-339

107. Huang H, McIntosh J, Hoyt DG. An efficient, nonenzymatic method for isolation and culture of murine aortic endothelial cells and their response to inflammatory stimuli. *In Vitro Cell Dev Biol Anim*. 2003;39:43-50

108. Kevil CG, Bullard DC. In vitro culture and characterization of gene targeted mouse endothelium. *Acta Physiol Scand*. 2001;173:151-157

109. Kevil CG, Patel RP, Bullard DC. Essential role of icam-1 in mediating monocyte adhesion to aortic endothelial cells. *Am J Physiol Cell Physiol*. 2001;281:C1442-1447

110. Wei L, Freichel M, Jaspers M, Cuppens H, Cassiman JJ, Droogmans G, Flockerzi V, Nilius B. Functional interaction between trp4 and cftr in mouse aorta endothelial cells. *BMC Physiol*. 2001;1:3

111. Hwang J, Saha A, Boo YC, Sorescu GP, McNally JS, Holland SM, Dikalov S, Giddens DP, Griendling KK, Harrison DG, Jo H. Oscillatory shear stress stimulates endothelial production of o2- from p47phox-dependent nad(p)h oxidases, leading to monocyte adhesion. *J Biol Chem*. 2003;278:47291-47298

112. Magid R, Martinson D, Hwang J, Jo H, Galis ZS. Optimization of isolation and functional characterization of primary murine aortic endothelial cells. *Endothelium*. 2003;10:103-109

113. Suh SH, Vennekens R, Manolopoulos VG, Freichel M, Schweig U, Prenen J, Flockerzi V, Droogmans G, Nilius B. Characterisation of explanted endothelial cells from mouse aorta: Electrophysiology and ca2+ signalling. *Pflugers Arch*. 1999;438:612-620

114. Kreisel D, Krupnick AS, Szeto WY, Popma SH, Sankaran D, Krasinskas AM, Amin KM, Rosengard BR. A simple method for culturing mouse vascular endothelium. *J Immunol Methods*. 2001;254:31-45

115. Lincoln DW, 2nd, Larsen AM, Phillips PG, Bove K. Isolation of murine aortic endothelial cells in culture and the effects of sex steroids on their growth. *In Vitro Cell Dev Biol Anim*. 2003;39:140-145

116. Chen S, Sega M, Agarwal A. "Lumen digestion" Technique for isolation of aortic endothelial cells from heme oxygenase-1 knockout mice. *Biotechniques*. 2004;37:84-86, 88-89

117. Kobayashi M, Inoue K, Warabi E, Minami T, Kodama T. A simple method of isolating mouse aortic endothelial cells. *J Atheroscler Thromb*. 2005;12:138-142

118. Zeisberg EM, Potenta S, Xie L, Zeisberg M, Kalluri R. Discovery of endothelial to mesenchymal transition as a source for carcinoma-associated fibroblasts. *Cancer Res*. 2007;67:10123-10128

119. Zeisberg EM, Tarnavski O, Zeisberg M, Dorfman AL, McMullen JR, Gustafsson E, Chandraker A, Yuan X, Pu WT, Roberts AB, Neilson EG, Sayegh MH, Izumo S, Kalluri R. Endothelial-to-mesenchymal transition contributes to cardiac fibrosis. *Nat Med*. 2007;13:952-961

CHAPTER 2

SPECIFIC AIMS

Project Significance

Atherosclerosis preferentially occurs in the lesion-prone areas exposed to disturbed flow conditions in branched or curved arteries, while the arterial regions exposed to unidirectional laminar flow are relatively lesion-free[1-2]. It is now well accepted that atherosclerosis is an inflammatory disease and the characteristic of the earliest stage of atherogenesis is the recruitment of innate cells such as monocytes and dendritic cells in the lesion prone areas subsequent to the expression of adhesion molecules[3]. In addition, disturbed flow conditions such as oscillatory shear (OS) alter gene expression in the vessel wall in a pro-inflammatory manner[4-5]. This includes the upregulation of adhesion molecules (ICAM-1, VCAM-1, and E-Selectin), overexpression of pro-inflammatory cytokine or chemokine (IL-6 and MCP-1), and induction of prothrombotic phenotype in endothelial cells (ECs). All of these disturbed flow induced responses in ECs are all considered as earliest stage of inflammation leading to the late development of atherosclerotic plaque. However, the precise mechanisms by which shear stress regulates gene expression and in turn governs inflammation and the development of atherosclerosis remain unclear.

MicroRNAs (miRNAs) are short noncoding RNAs, typically 18 to 22 nucleotides in length, and can regulate the expression of multiple genes at the post-transcriptional level. It is believed that miRNAs primarily function by interacting with 3' untranslated region (3' UTR) of specific target mRNAs in a sequence-specific manner[6]. Previous studies have shown the important role of miRNAs in the regulation of a multitude of

physiological functions, such as stem cell differentiation, neurogenesis, hematopoiesis, immune response, and skeletal and cardiac muscle development and stress[7-13] Furthermore, a variety of diseases, such as cancer, diabetes, and heart hypertrophy and failure, have been related to aberrant expression of miRNAs. Although several miRNAs have been shown to play roles in cardiovascular development, angiogenesis, and vascular inflammation[12, 14], it has not been reported whether miRNAs are involved in the development of atherosclerosis. In this study, we investigate several mechanosensitive-sensitive mRNAs and miRNAs *in vitro* and *in vivo* in response to different shear conditions and study their functional relevance in inflammatory responses.

Project Objective

The goals of this project were 1) to determine which microRNAs and mRNAs are regulated by different flow conditions in vascular endothelial cells *in vitro* and in mouse carotid artery endothelium *in vivo*, and 2) to identify which miRNAs are responsible for vascular inflammation by disturbed flow. These results will help to identify novel targets as biomarkers of early disease or as therapeutic targets.

Overall Hypothesis

Oscillatory shear (OS) and laminar shear (LS) stress differentially alter the expression of mechanosensitive miRNAs that regulate networks of gene expression, *which in turn* leads to inflammation in endothelial cells. This hypothesis was tested according to three specific aims using both *in vitro* and *in vivo* approaches via high throughput microarray analyses and functional validation of specific targets by qPCR:

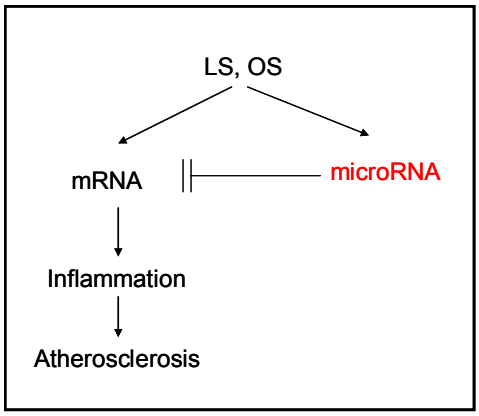

Figure 2.1 Overall Hypothesis. *Oscillatory and laminar shear stress differentially regulate miRNAs and mRNA, which in turn leads to inflammation in endothelial cells.*

Specific Aim 1

Develop a novel mouse model of experimentally inducible disturbed flow and a method for isolating endothelial cell RNA with intensive validation of minimal contamination, to examine the expression profiles of miRNA and mRNA *in vivo*.

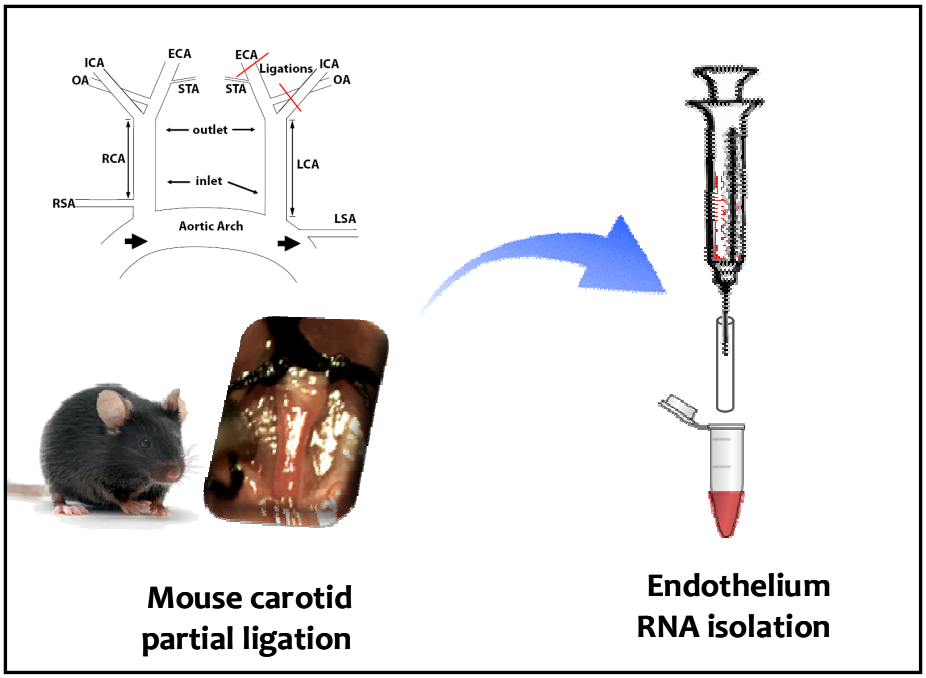

Figure 2.2 Experimental layout for Specific Aim 1

To determine the effect of different hemodynamic profiles on miRNAs and mRNAs *in vivo*, we developed a novel mouse model of shear stress which creates low and oscillatory flow through partial ligation of the left common carotid artery (Figure 2.2). We also developed a simple method for endothelial RNA isolation from the flow-disturbed left and the contralateral right common carotid arteries. This mouse model is well characterized and the purity and quantity of isolated RNA is qualified for high throughput microarray applications. iMAEC lines were also developed for use *in vitro* to validate the novel miRNAs and mRNAs.

Specific Aim 2

Identify flow-sensitive miRNAs and mRNAs in partially ligated murine carotid endothelium and cultured HUVEC.

Hypothesis: Oscillatory shear stress (OS) alters expression profiles of miRNA and mRNA both *in vivo* and *in vitro* as compared to laminar shear stress (LS).

Using the mouse model and RNA isolation method developed in specific aim 1, the screening of miRNA and mRNA expressions in response to LS or OS was performed by high throughput microarray analyses using RNA samples from partially ligated carotid endothelium or cultured HUVEC. All microarray data was verified by real-time quantitative PCR (Figure 2.3). The *in vivo* mouse data was also validated using iMAEC lines.

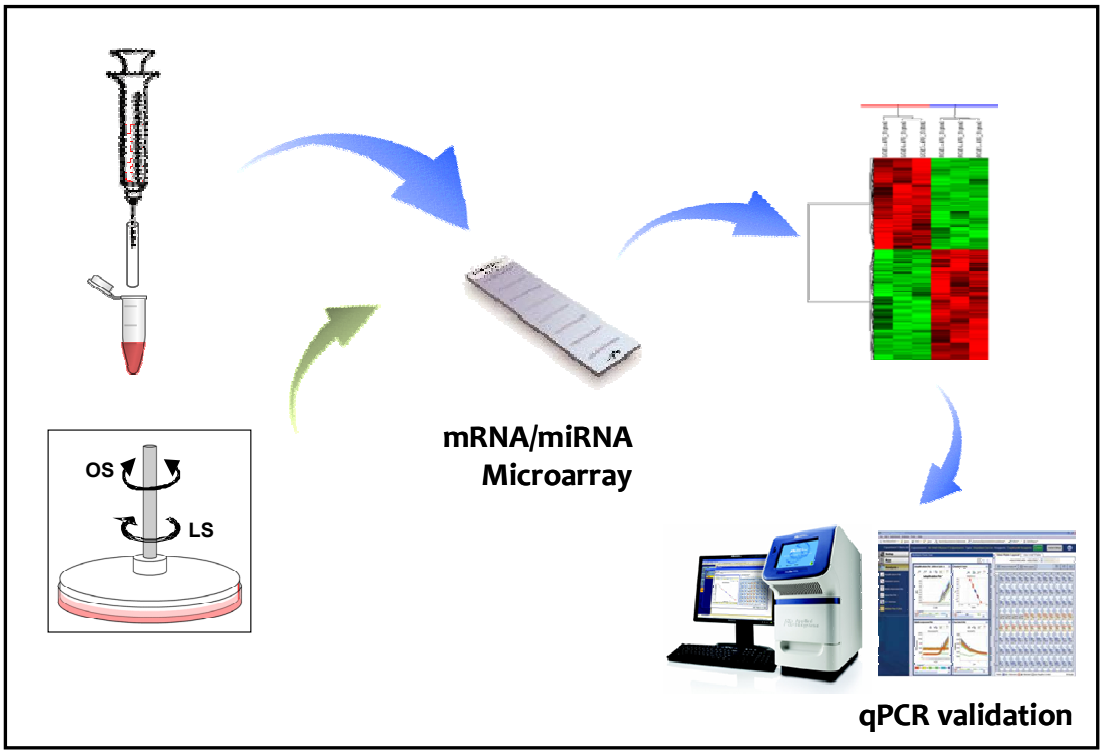

Figure 2.3 Experimental layout for Specific Aim 2

Specific Aim 3

Investigate the role of mechanosensitive miRNA-663 in OS induced cellular inflammation in HUVEC.

Hypothesis: The novel mechanosensitive miRNA, miR-663, mediates OS-induced inflammation in HUVEC.

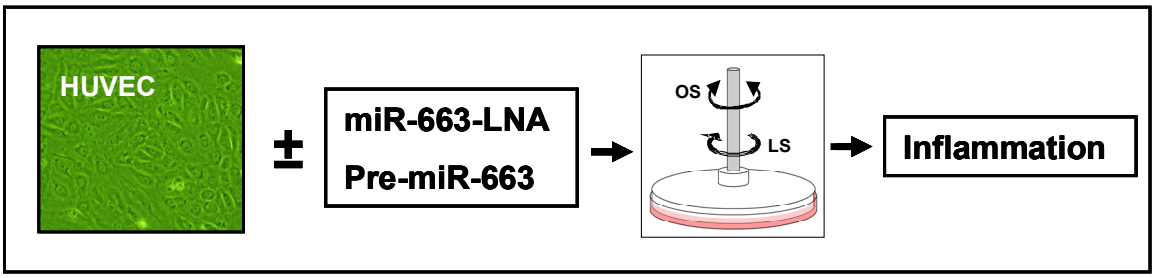

Figure 2.4 Experimental layout for Specific Aim 3

In Specific Aim 2, miR-663 was found to be a novel mechanosensitive miRNA in HUVEC. To identify the role of OS-induced miR-663, we investigated the functional importance of the miR-663 (Figure 2.4). The depletion or elevation of miR-663 from cellular systems provided a useful tool to study the functional role of miR-663. In these studies, specific miRNA inhibitor (miR-663-LNA) or miRNA precursor (pre-miR-663) was used to knockdown or overexpress miR-663 expression respectively in HUVEC. Subsequently, the OS-induced inflammatory response was assessed via a monocyte binding assay.

References

1. Ku DN, Giddens DP, Zarins CK, Glagov S. Pulsatile flow and atherosclerosis in the human carotid bifurcation. Positive correlation between plaque location and low oscillating shear stress. *Arteriosclerosis*. 1985;5:293-302

2. VanderLaan PA, Reardon CA, Getz GS. Site specificity of atherosclerosis: Site-selective responses to atherosclerotic modulators. *Arterioscler Thromb Vasc Biol*. 2004;24:12-22

3. Ross R. Atherosclerosis--an inflammatory disease. *N Engl J Med*. 1999;340:115-126

4. Sorescu GP, Song H, Tressel SL, Hwang J, Dikalov S, Smith DA, Boyd NL, Platt MO, Lassegue B, Griendling KK, Jo H. Bone morphogenic protein 4 produced in endothelial cells by oscillatory shear stress induces monocyte adhesion by stimulating reactive oxygen species production from a nox1-based nadph oxidase. *Circ Res*. 2004;95:773-779

5. Sorescu GP, Sykes M, Weiss D, Platt MO, Saha A, Hwang J, Boyd N, Boo YC, Vega JD, Taylor WR, Jo H. Bone morphogenic protein 4 produced in endothelial cells by oscillatory shear stress stimulates an inflammatory response. *J Biol Chem*. 2003;278:31128-31135

6. Zhao Y, Srivastava D. A developmental view of microrna function. *Trends Biochem Sci*. 2007;32:189-197

7. Krichevsky AM, Sonntag KC, Isacson O, Kosik KS. Specific micrornas modulate embryonic stem cell-derived neurogenesis. *Stem Cells*. 2006;24:857-864

8. Chen JF, Mandel EM, Thomson JM, Wu Q, Callis TE, Hammond SM, Conlon FL, Wang DZ. The role of microrna-1 and microrna-133 in skeletal muscle proliferation and differentiation. *Nat Genet*. 2006;38:228-233

9. Zhao Y, Samal E, Srivastava D. Serum response factor regulates a muscle-specific microrna that targets hand2 during cardiogenesis. *Nature*. 2005;436:214-220

10. Pedersen IM, Cheng G, Wieland S, Volinia S, Croce CM, Chisari FV, David M. Interferon modulation of cellular microrna as an antiviral mechanism. *Nature*. 2007;449:919-922

11. Kloosterman WP, Lagendijk AK, Ketting RF, Moulton JD, Plasterk RH. Targeted inhibition of mirna maturation with morpholinos reveals a role for mir-375 in pancreatic islet development. *PLoS Biol*. 2007;5:e203

12. Felli N, Fontana L, Pelosi E, Botta R, Bonci D, Facchiano F, Liuzzi F, Lulli V, Morsilli O, Santoro S, Valtieri M, Calin GA, Liu CG, Sorrentino A, Croce CM, Peschle C. Microrna 221 and 222 inhibit normal erythropoiesis and erythroleukemic cell growth via kit receptor down-modulation. *Proc Natl Acad Sci U S A*. 2005;102:18081-18086

13. Tay YM, Tam WL, Ang YS, Gaughwin PM, Yang H, Wang W, Liu R, George J, Ng HH, Perera RJ, Lufkin T, Rigoutsos I, Thomson AM, Lim B. Microrna-134 modulates the differentiation of mouse embryonic stem cells, where it causes post-transcriptional attenuation of nanog and lrh1. *Stem Cells*. 2008;26:17-29

14. Harris TA, Yamakuchi M, Ferlito M, Mendell JT, Lowenstein CJ. Microrna-126 regulates endothelial expression of vascular cell adhesion molecule 1. *Proc Natl Acad Sci U S A*. 2008;105:1516-1521

CHAPTER 3

DEVELOPMENT OF IMMORTALIZED MOUSE AORTIC ENDOTHELIAL CELL (IMAEC) LINES

Summary

Our understanding of endothelial cell biology has increased during the past decades, largely due to the availability of primary endothelial cell cultures from various species and vascular beds. Given the availability of numerous transgenic mouse lines, we and others have attempted to isolate and culture primary mouse aortic endothelial cells (MAEC). Yet, isolation and maintenance of primary MAEC remain a formidable challenge: They are time-, cost-, and labor-intensive. Moreover, MAEC have limited proliferative potential and high tendency to trans-differentiate to mesenchymal cells during culture. Therefore, we developed immortalized MAEC (iMAEC) lines from aortas obtained from C57BL/6 mice including wild type and several transgenics such as p47 KO, eNOS KO, and caveolin-1 KO. Primary MAEC were first isolated from mouse cultured aortic explants on collagen gels, and were immortalized by using retrovirus expressing polyoma middle T antigen. Immortalized cells were selected by G418 antibiotics. iMAEC's were further selected by FACS using DiI-Ac-LDL, and were analyzed for their expression of endothelial markers including PECAM1, eNOS, VE-cadherin, and von Willebrand factor. These cell lines were characterized for their functional responses to laminar shear stress. iMAEC aligned in the direction of flow, increased the expression and phosphorylation of eNOS, and induced KLF2 expression. The methods used to develop iMAEC lines described here can be applied to generate

additional MAEC lines, using various knockout mouse lines, to provide a critical tool to investigate the vascular biology and pathobiology.

Introduction

Endothelial cells (ECs) play critical roles in cardiovascular system. As the inner lining of the blood vessel, ECs are barriers which control the transportation of molecules between blood and tissues. Not only do ECs act as a passive barrier inside the vessel, it is hypothesized that ECs also play an active role in maintaining physiological homeostasis in response to stimuli[1]. Endothelial dysfunction is thought to be one of the earliest stages in the onset of atherosclerosis[2]. This dysfunction is characterized by gene dysregulation and inflammatory responses[2-3]. Therefore, cultured ECs are an important tool to study vascular physiology and disease pathology.

ECs from different origins and species have been successfully cultured for several decades[4-5]. The most common human primary ECs used in culture includes human umbilical vein cord endothelial cells (HUVECs)[6], human aortic endothelial cells (HAECs)[7], human coronary artery endothelial cells (HCAEC)[8], and microvascular ECs[9-10]. In addition, ECs culture is also available from other species, such as bovine aortic endothelial cells (BAECs)[11], pig aortic endothelial cells (PAECs)[12] and mouse ECs[13-27]. Due to the numerous transgenic mouse lines, the isolation and culture of mouse ECs is of particular interest. Several studies have developed methods for isolation primary mouse aortic endothelial cells (MAECs) which have been used for experiments[17-18, 22-27]. However, the isolation and maintenance of primary MAECs remain a formidable challenge: They are time-, cost-, and labor-intensive. The main obstacle in primary

MAECs isolation is the low cell number in a single anima, the limited proliferative potential, and contamination of other cell types. Moreover, studies have shown MAECs have high tendency to trans-differentiate to mesenchymal cells during culture[28-29]. Therefore, development of immortalized MAECs lines could provide tremendous benefits and provide critical tools for functional studies.

In this study, we have developed several iMAEC lines including iMAEC-WT, iMAEC-eNOSKO, iMAEC-cavKO, and iMAEC-p47KO. We carried out detailed characteristic studies to show that these iMAEC lines maintain endothelial phenotype. All the cells expressed endothelial specific markers such as PECAM-1, VE-Cadherin, and von Willebrand factor (vWF) but not smooth cell marker (α-SMA). Importantly, iMAEC-WT possesses typical endothelial responses to shear stress. The cells aligned in the direction of flow, increased the expression and phosphorylation of eNOS, and elevated KLF2 expression. In addition, the expression of VCAM-1 showed significant increase in iMAEC-eNOSKO compared to iMAEC-WT, demonstrating the use of knockout cell lines to address the function of specific genes. Collectively, these results validate our method for development iMAEC lines which can be used to generate more iMAEC-KO lines. This method, used to develop endothelial cell lines, provides a critical tool to investigate the vascular biology and pathophysiology.

Methods

Mice

Mouse aortic endothelial cells were isolated from several different transgenic (and wildtype) mouse lines. Wildtype C57Bl/6 and $p47^{phox}$ knockout mice were purchased

from Jackson Laboratories (Bar Harbor, Maine). Caveolin-1 knockout mice were kindly provided by Dr. Marek Drab (Max Planck Institute for Molecular Cell Biology and Genetics, Dresden, Germany); eNOS knockout mice were kindly provided by Dr. Mark C. Fishman and Dr. Paul Huang (Cardiovascular Research Center, Harvard Medical School, Charlestown, MA).

Primary MAEC Isolation

Mice used for MAEC isolation were 4 weeks old. Each mouse was sacrificed by CO_2 asphyxiation and doused in 70% ethanol. The abdominal and thoracic cavity was opened and the mouse was perfused, via the left ventricle, with 3-4 mL of sterile heparinized (10U/mL) 1X Hank's buffered salt solution (HBSS, Cellgro). All organs were removed except for the thoracic/abdominal aorta, which was left intact. Perivascular fat tissue and adventitia were removed from the ventral side of the aorta. To lyse the cells surrounding the artery while preserving the lumen, the aorta was incubated with HBSS containing 0.5% TritonX-100 for 5 minutes. It is important to note the Triton solution was not allowed to contact the endothelium. The clean aorta was removed after 5 rinses with fresh HBSS and placed in a sterile dish of cold HBSS. The aorta was cut into small rings (1 mm long) using a sterile scalpel and each aorta ring was cut open with a small scissors. The aorta section was carefully transferred (lumen side down) to a bead of collagen gel. The composition of collagen gel is a mixture of type I collagen (BioRad) and EGM2-MV (Lnoza) to the final concentration of 1.75mg/ml. Note that each piece should lay flat on the surface of collagen gel and the collagen gel bead submerged with EGM2-MV without disturbing aorta piece. The explants were observed daily and cultured in incubator in 37^{o}C and 5% CO_2. The key steps of primary MAEC isolation are summarized in Figure 3.1.

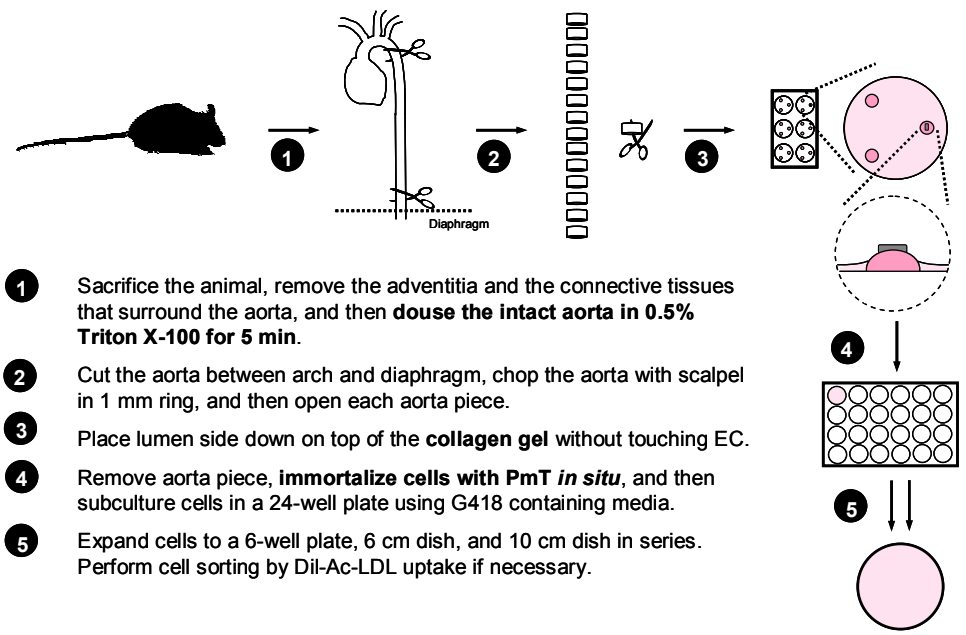

Figure 3.1 Scheme of mouse aortic endothelial cell isolation and immortalization.

Immortalization

Cells were immortalized by infection with a polyoma middle-sized T-antigen (PmT) as previously described by Balconi et. al[30]. PmT-producing packaging cell line was kindly provided by Dr. Elisabetta Dejana (Institute of Pharmacological Research, Milan, Italy). Briefly, PmT conditioned medium was collected, 0.22μm-sterile-filtered, and stored at -80°C until use. After MAECs have proliferated on the collagen gel, the aorta piece was removed followed by addition of complete growth media (DMEM with 10% FBS, crude extract of ECGS, 1% penicillin and streptomycin). After culture for one day, cells were treated with the PmT conditioned medium, along with 8 μg/ml polybrene (Sigma) for 4 hours at 37 °C. After the incubation with PmT, media was removed and replaced with complete growth medium. Forty-eight hours later, cells were passaged into a 48-well plate and grown in selective growth medium containing G418 (800 μg/ml). Cells were

observed and passaged for several weeks (4 to 8 weeks) before complete cell selection was observed (summarized in Figure 3.1).

FACS cell sorting

Cells were stained with 1,1'-dioctadecyl-3,3,3,3'-tetramethyl-indocarbocyanine perchlorate (DiI-Ac-LDL) and then sorted by fluorescence-activated cell sorting (FACS). Briefly, cells were incubated with 10μg/mL DiI-Ac-LDL (Biomedical Technologies) for 4 hours at 37°C. Cells were then washed three times with fresh growth medium, trypsinized with 0.05% trypsin-EDTA, pelleted for 3 minutes at 2,300 RPM, and re-suspended in 0.5-1.0 mL of sorting buffer (1% FBS in 1X calcium- and magnesium-free HBSS). Cells were then sorted using a FACS VantageSE (Becton Dickinson, San Jose, CA) based on relative fluorescence intensity of DiI using common gates for morphology (FSC-H vs SSC-H), singlets (FSC-W vs SSC-H), and separation gates for DiI staining. Positive cells were collected in complete growth media and seeded to a gelatin-coated (0.1%) culture dish. Cells were then observed and passaged at a ratio of 1 to 2 until characterization experiments.

Immunocytochemistry

Primary antibodies against PECAM-1 (Santa Cruz), VE-Cadherin (Cayman Chemical), Von Willebrand factor (Dako) and smooth muscle cell α-actin (Sigma) were used for immunocytochemical staining of the iMAEC and control cells such as HUVEC, 3T3 fibroblast and rat aortic smooth muscle cells (RASM). Cells were fixed with 4% paraformaldehyde and permeabilized in 0.2% Triton X-100. Primary antibody in 3% bovine serum albumin was applied overnight at 4°C, followed by incubation with secondary antibody conjugated rhodamine red-X (Molecular Probes) for 1 hour at room temperature. Nuclei were labeled with Hoechst #33258 in 3% bovine serum albumin for

15 min at room temperature. All cells were mounted using Dako mounting media (Dako), and fluorescence images were collected via fluorescence microscope (Zeiss epi-fluorescent microscope).

Shear Stress Studies

iMAEC were grown to confluent monolayers in 100-mm tissue culture dishes (Falcon) and were subsequently exposed to laminar shear (LS, 15 dynes/cm^2) or oscillatory shear (OS, ±5 dynes/cm^2) via cone-and-plate shear apparatus as previously described by us [ref]. All shear stress studies were performed in growth medium for 24 h.

Western Blotting

Following experimental treatment, cells were washed three times with ice-cold phosphate-buffered saline (PBS) and lysed with RIPA as described previously[31].The lysate was further homogenized by sonication. The protein content of each sample was determined by Bio-Rad DC assay. Aliquots of cell lysate (20μg of protein) were resolved by size on 10% SDS-polyacrylamide gels and subsequently transferred to a polyvinylidene difluoride membrane (Millipore). The membrane was incubated with a primary antibody overnight at 4 °C, followed by incubation with an alkaline phosphatase-conjugated secondary antibody for 1 h at room temperature. Protein expression was detected by a chemiluminescence method, and the intensities of immunoreactive bands were determined via densitometry using the NIH Image program[32]. Primary antibodies specific for KLF2, eNOS (BD Biosciences), phoso-eNOS (Ser1177) (Cellsignaling), actin (Santa Cruz), VCAM-1 (Santa Cruz), Flk-1 (Santa Cruz), Caviolin-1 (Santa Cruz) were used.

Quantitative real time PCR (qPCR)

Total RNA of each sample was reverse transcribed into cDNA using SuperScript III and random primers (Invitrogen) as previously described[33]. Briefly, qPCR was performed on selected genes using Brilliant II SYBR Green QPCR Master Mix (Stratagene) with custom designed primers on a Real-Time PCR System (ABI StepOne Plus). All qPCR results were normalized based on 18S RNA expression in each sample.

Dihydroethidium (DHE) staining

iMAEC were stained in 2 μM DHE in phosphate buffered saline for 30 minutes at 37°C. Cells were then fixed with 4% paraformaldehyde and mounted with DAKO mounting media and immediately imaged with fluorescence microscope (Zeiss epi-fluorescent microscope).

Results

The morphology of cultured mouse aortic endothelial cells.

The summary of MAEC isolation and immortalization is shown in Figure 3.1. During explant culture on the collagen gel, the endothelial cells migrated out of the explants from the edge and gradually covered the gel within an average of 3-4 days (Figure 3.2A). However, a portion of ECs attached to the collagen gel, did not migrate, and seemed to keep their original flow elongated morphology as seen *in vivo* (Figure 3.2B). Because of the immortalization and subculture in gelatin-coating dishes, the EC morphology looks different from primary isolated (Figure 3.2C). During the selection process, the contaminating cells (fibroblasts and smooth muscle cells etc.) competed with ECs for

growth space as indicated in Figure 3.2C. However, through cell selection and limited subculture, ECs eventually dominated cell populations. In addition, FACS helped to purify the iMAEC.

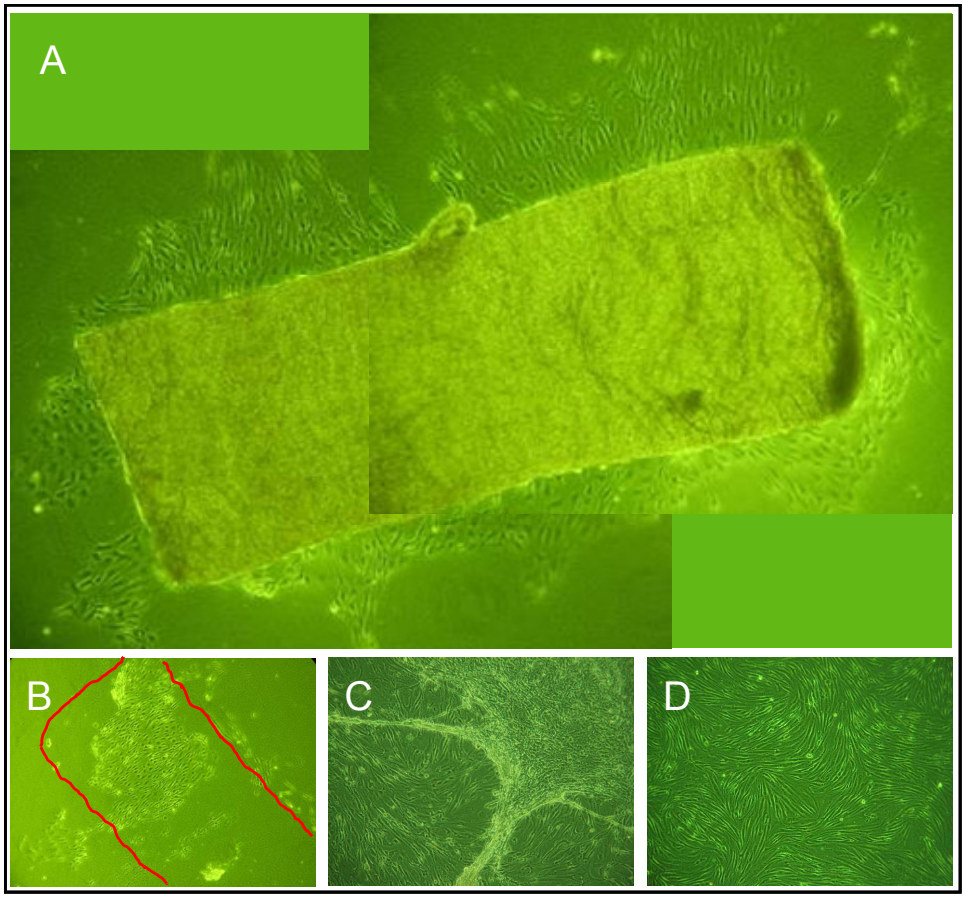

Figure 3.2 Morphology of mouse aortic endothelial cells. ***A,*** *Aorta explant was cultured on top of collagen gel for 4 days. ECs grew and migrated out of the aorta piece.* ***B,*** *ECs grown on collagen gel without migration seems to keep their original elongated morphology.* ***C****, ECs Morphology changed after immortalization and subculture in gelatin-coating dishes. The contaminating cells competed growth space with ECs as indicated with an arrow.* ***D****. Pure cell population of iMAEC after cell sorting.*

Characterization of iMAEC

Since we have developed several iMAEC cell lines including wildtype (iMAEC-WT), caveolin-1 knockout (iMAEC-cavKO), eNOS knockout (iMAEC-eNOSKO), and $p47^{phox}$ knockout (iMAEC-p47KO), the phenotype of these immortalized cells were carefully examined. First, we performed Western blot to confirm the lack of protein expression in knockout cell lines. As expected, we did not detect of cav-1 in iMAEC-cavKO and eNOS in iMAEC-eNOSKO (Figure 3.3).

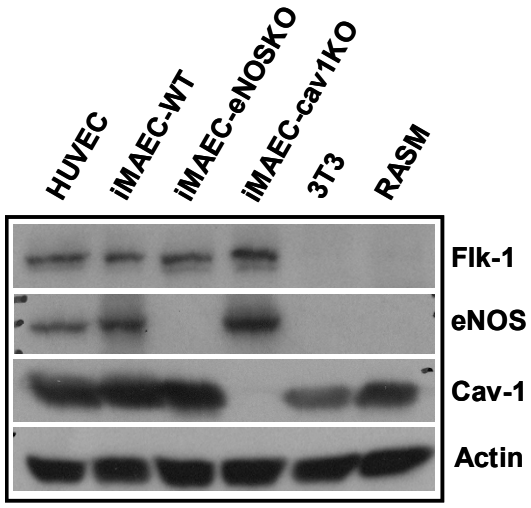

Figure 3.3 Validation of knockout iMAEC lines. *Total cell lysates were collected from iMAEC lines or control cells such as HUVEC, 3T3, and RASM. Western blot were performed to measure the protein expression using specific antibodies against Flk-1, eNOS and Cav-1. Actin blot is the internal loading control.*

We then incubated cells with Dil-Ac-LDL to confirm the cell lines were endothelial cells. As shown in Figure. 3.4, iMAEC showed homogeneous Dil-Ac-LDL uptake similar to primary HUVEC. As expected, other cell types such as fibroblasts (3T3) and smooth muscle cells (RASM) failed to uptake Dil-Ac-LDL, suggesting the staining specificity of Dil-Ac-LDL to ECs. Next, several endothelial specific protein markers were examined by

immunocytochemistry. PECAM-1, VE-Cadherin, and von Willebriand factor (vWF) are well-known endothelial markers with specific staining patterns. PECAM-1 and VE-Cadherin stained positive at the cell border in iMAEC and HUVEC but not in 3T3 and RASM (Figure 3.5). vWF also exhibited positive cytosolic staining patterns in iMAEC and HUVEC. In addition, the Western blot, shown in Figure 3.3, further supported the endothelial phenotype in iMAEC by expression of Flk-1, a VEGF receptor, which specific to endothelial cells. In contrast, smooth muscle cell specific maker (α-SMA) was used to further confirm iMAEC lines were free contaminating cell types. As expected, positive staining was only seen in RASM, demonstrating that iMAEC lines kept their endothelial phenotype without other cell population contamination.

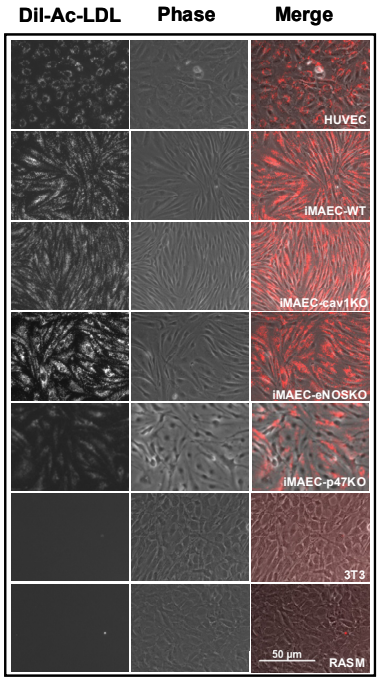

Figure 3.4 Characterization of iMAEC lines by DiI-Ac-LDL staining. *iMAEC lines including wildtype (iMAEC-WT), caveolin-1 knockout (iMAEC-cavKO), eNOS knockout (iMAEC-eNOSKO), and p47^{phox} knockout (iMAEC-p47KO), were incubated with DiI-Ac-LDL (10µg/mL) for 4 hr, and images were taken by with fluorescence microscope. HUVEC was served as positive control while 3T3 and RASM were negative control.*

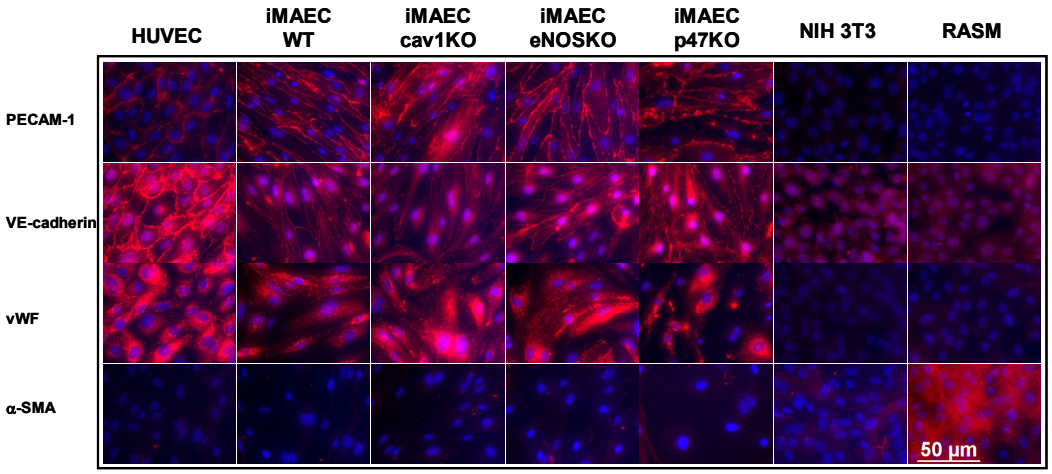

Figure 3.5 Characterization of iMAEC lines by immunostaining against PECAM-1, VE-Cadherin, von Willebrand factor, and smooth muscle cell α-actin. *iMAEC lines including wildtype (iMAEC-WT), caveolin-1 knockout (iMAEC-cavKO), eNOS knockout (iMAEC-eNOSKO), and p47^{phox} knockout (iMAEC-p47KO), were used for immunostaining using endothelial markers PECAM-1, VE-Cadherin, and von Willenbrand factor (vWF). Smooth muscle cell α-actin (α-SMA) was also used as negative marker for ECs. HUVEC was served as positive control while 3T3 and RASM were negative control.*

Shear responses in iMAEC

To demonstrate the similarities between iMAEC and primary human ECs, we tested the gene expression response when iMAEC were exposed to shear stress. Numerous reports have shown laminar shear stress (LS) induces KLF2 and eNOS mRNA and protein expression compared to static culture or oscillatory shear (OS)[34-35]. In addition, LS also elevates eNOS phosphorylation which, in turn, increases eNOS enzyme activity and nitric oxide production[36]. We performed shear studies using iMAEC-WT and examined the expression of KLF2 and eNOS. Consistent with previous reports, after 24hr shear stress, iMAEC-WT aligned with flow direction in LS but not OS (Figure 3.6A)[37]. We found that LS significantly increases KLF2 and eNOS expression both at mRNA (Figure 3.6B) and protein (Figure 3.6C) levels. Furthermore, eNOS

phosphorylation was also elevated in iMAEC-WT exposed to LS when compared to OS. These results demonstrate that iMAEC reacted in a similar manner to other cultured endothelial cells.

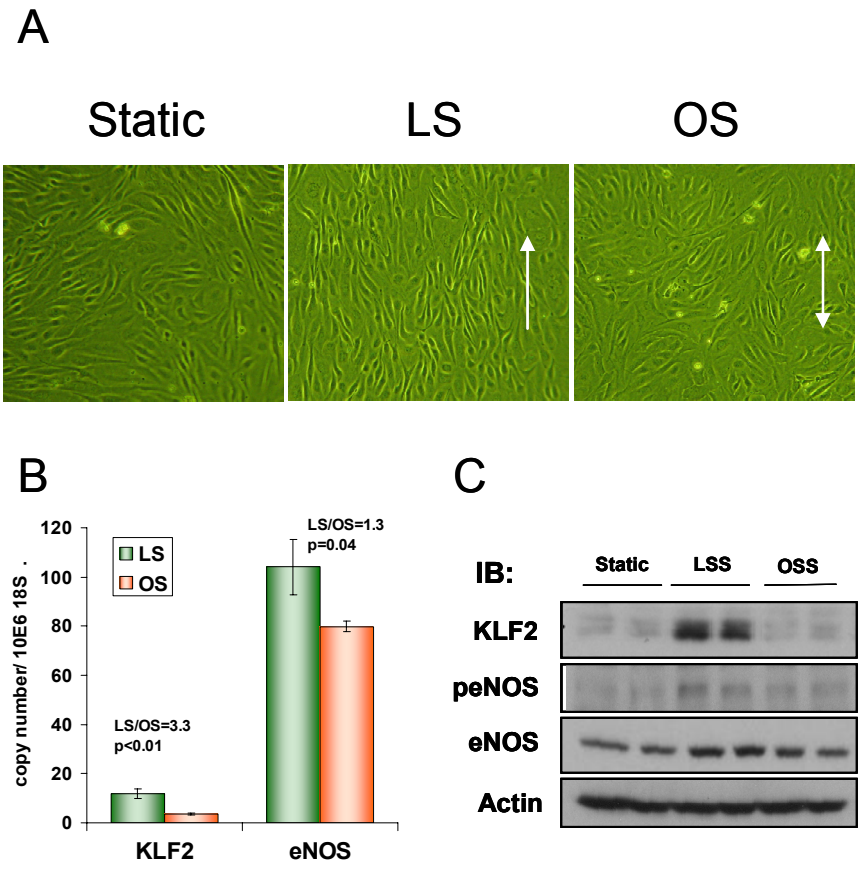

Figure 3.6 iMAEC-WT maintained endothelial phenotype in response to shear stress. *iMAEC-WT were exposed to LS or OS or kept for static for 24hr.* ***A****, iMAEC-WT aligned with the flow direction when exposed to LS but not OS or static control.* ***B****, Total RNA were collected and qPCR were performed to measure mRNA expression of KLF2 and eNOS.* ***C****, Total cell lysates were collected and protein level of KLF2 and eNOS were measured by Western blot. Phosphorylation of eNOS was also measured. Data were shown as mean±SEM, n=3.*

Functional analysis of iMAEC lines

To further demonstrate that iMAEC lines are a useful tool to study the gene function, we tested the functional differences between wildtype and knockout cell lines. Since it has been shown that nitric oxide treatment in cultured HUVEC decreases VCAM-1 expression[38], we first examined the protein expression of VCAM-1 between iMAEC-WT and iMAEC-eNOSKO under different shear conditions. VCAM-1 protein expression significantly decreased in iMAEC-WT exposed to LS compared to OS; however, no difference of VCAM-1 expression between LS and OS was detected in iMAEC-eNOSKO cells (Figure 3.7). Interestingly, VCAM-1 expression in iMAEC-eNOSKO was significantly higher compared to iMAEC-WT (Figure 3.7). These results support the notion that nitric oxide, which is produced by LS stimulated-eNOS, inhibits the expression of VCAM-1.

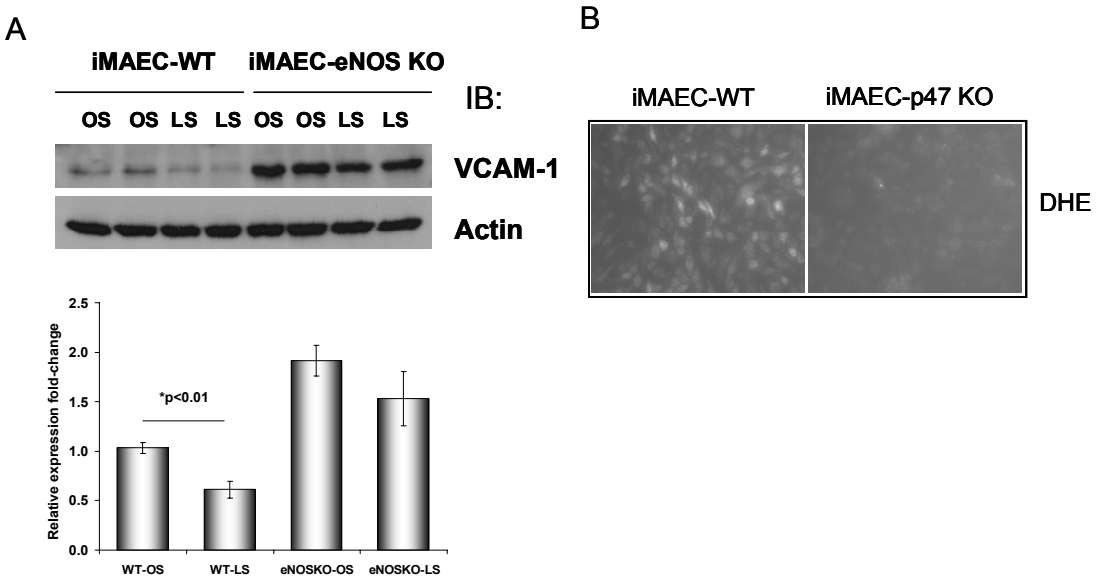

Figure. 3.7 VCAM-1 expression is elevated in iMAEC-eNOSKO while superoxide production is diminished in iMAEC-p47KO. ***A****, iMAEC-WT and iMAEC-eNOSKO were exposed to LS or OS for 24 hr. Total cell lysates were collected and VCAM-1 protein expression was measured by Western blot.* ***B****, iMAEC-WT and iMAEC-p47KO were incubated with DHE (2 μM) for 30 min. Images were taken using fluorescence microscopy.*

Finally, we also examined the superoxide expression in iMAEC-p47KO cells. Given p47 is an important component of NADPH oxidases which produce superoxide, lack of p47 in EC may reduce the production of superoxide[21]. As shown in Figure. 3.7B, the measurement of superoxide production by DHE staining in lower in iMAEC-p47KO cells compared to iMAEC-WT cells.

Discussion

In this study, we developed a method to generate iMAEC lines which maintain endothelial phenotype and respond to shear stress. We also demonstrated functional differences between knockout and wildtype iMAEC lines in a gene specific manner. For example, iMAEC-p47KO showed diminished production of superoxide while iMAEC-eNOSKO exhibited elevated VCAM-1 protein expression. These results validate our method and provide a useful tool to study vascular biology. Given the vast array of transgenic mice, using our method, iMAEC lines can be generated, expanded, and shared within research communities to provide a valuable tool for researchers.

Over the years, several groups have suggested different methods for the isolation and culture of primary MAEC[17-18, 22-27]. However, the major issue of most protocols is the failure to address the purity and expansion of primary MAEC. Cell culture experiments performed *in vitro* requires a pure cell population due to the diversity among different cell types. The impurity of primary MAEC comes from contaminating cells such as fibroblasts and SMCs or from the re-differentiation of MAEC. The characterization of endothelial cells should be conducted on regular basis to confirm the lack of

contamination and re-differentiation. This is especially important for primary MAEC because of the small cell number obtained from a signal mouse. Previous reports have shown the phenotypic change of cultured endothelial cells during passaging[39]. It is difficult to maintain the phenotype of primary MAEC in sufficient amounts for a series of experiments without excessive time and effort. In contrast, immortalized cells are easily expandable and maintain an EC phenotype that lasts several months. However, it should be noted that iMAEC lines only provide a model for studying the vascular biology or disease *in vitro*, and may provide different responses when compared to primary culture or *in vivo* studies. Because the cells were immortalized and cultured, the phenotype has been altered and is different from that *in vivo*, but our results showed that iMAEC still maintain some of the EC phenotypes, while losing others such as cell proliferation. Therefore, researchers should be cautious when interpreting iMAEC derived data.

The explants culture of aorta has been reported previously[17, 23, 25]. Most of the protocol used matrix gel as the base matrix for MAEC to grow and migrate[17, 23, 25]. Matrix gel has been widely used in angiogenesis assay that provides ECs an angiogenic environment and induces tube formation. This property of matrix gel causes a dilemma between stimulating cell proliferation/migration and changing the phenotype of the primary cells. Our method modified the explants culture by using a collagen gel with growth media. The results indicated that MAEC still maintain their original morphology while not stimulating tube formation (Figure 3.2). Our modified method also provided a high yield of primary MAECs and they could be easily identified by their morphology which is helpfully when evaluating potential contamination of other cell types.

Immortalized mouse endothelial cells isolated from embryo or brain in different transgenic mice have been reported in several studies[30]. These studies demonstrated the need of transgenic iMAEC lines to address questions about functions of specific genes. In our knowledge, this is the first report showing a method for generating immortalized MAEC. Because the origins of an EC (from artery, vein, or microvessels) show different responses to stimuli, our method provides another option to study arterial ECs in vascular biology.

In summary, we provide a simple method to generate iMAEC lines which maintain EC phenotype and respond to shear stress in a similar way as primary ECs. This method can be applied to generate various knockout MAEC lines to be used as critical tools in vascular biology and pathobiology.

References

1. Tedgui A, Mallat Z. Anti-inflammatory mechanisms in the vascular wall. *Circ Res*. 2001;88:877-887

2. d'Uscio LV, Baker TA, Mantilla CB, Smith L, Weiler D, Sieck GC, Katusic ZS. Mechanism of endothelial dysfunction in apolipoprotein e-deficient mice. *Arterioscler Thromb Vasc Biol*. 2001;21:1017-1022

3. Rao RM, Yang L, Garcia-Cardena G, Luscinskas FW. Endothelial-dependent mechanisms of leukocyte recruitment to the vascular wall. *Circ Res*. 2007;101:234-247

4. Jaffe EA, Nachman RL, Becker CG, Minick CR. Culture of human endothelial cells derived from umbilical veins. Identification by morphologic and immunologic criteria. *J Clin Invest*. 1973;52:2745-2756

5. Jaffe EA, Hoyer LW, Nachman RL. Synthesis of antihemophilic factor antigen by cultured human endothelial cells. *J Clin Invest*. 1973;52:2757-2764

6. Baudin B, Bruneel A, Bosselut N, Vaubourdolle M. A protocol for isolation and culture of human umbilical vein endothelial cells. *Nat Protoc*. 2007;2:481-485

7. Akeson AL, Mosher LB, Woods CW, Schroeder KK, Bowlin TL. Human aortic endothelial cells express the type i but not the type ii receptor for interleukin-1 (il-1). *J Cell Physiol*. 1992;153:583-588

8. Yu SY, Song YM, Li AM, Yu XJ, Zhao G, Song MB, Lin CM, Tao CR, Huang L. Isolation and characterization of human coronary artery-derived endothelial cells in vivo from patients undergoing percutaneous coronary interventions. *J Vasc Res*. 2009;46:487-494

9. Marks RM, Czerniecki M, Penny R. Human dermal microvascular endothelial cells: An improved method for tissue culture and a description of some singular properties in culture. *In Vitro Cell Dev Biol*. 1985;21:627-635

10. Gargett CE, Bucak K, Rogers PA. Isolation, characterization and long-term culture of human myometrial microvascular endothelial cells. *Hum Reprod*. 2000;15:293-301

11. Booyse FM, Sedlak BJ, Rafelson ME, Jr. Culture of arterial endothelial cells: Characterization and growth of bovine aortic cells. *Thromb Diath Haemorrh*. 1975;34:825-839

12. Merrilees MJ, Scott L. Interaction of aortic endothelial and smooth muscle cells in culture. Effect on glycosaminoglycan levels. *Atherosclerosis*. 1981;39:147-161

13. Nishiyama T, Mishima K, Ide F, Yamada K, Obara K, Sato A, Hitosugi N, Inoue H, Tsubota K, Saito I. Functional analysis of an established mouse vascular endothelial cell line. *J Vasc Res*. 2007;44:138-148

14. Canault M, Peiretti F, Mueller C, Deprez P, Bonardo B, Bernot D, Juhan-Vague I, Nalbone G. Proinflammatory properties of murine aortic endothelial cells exclusively expressing a non cleavable form of tnfalpha. Effect on tumor necrosis factor alpha receptor type 2. *Thromb Haemost*. 2004;92:1428-1437

15. Kevil CG, Pruitt H, Kavanagh TJ, Wilkerson J, Farin F, Moellering D, Darley-Usmar VM, Bullard DC, Patel RP. Regulation of endothelial glutathione by icam-1: Implications for inflammation. *FASEB J*. 2004;18:1321-1323

16. Seol GH, Ahn SC, Kim JA, Nilius B, Suh SH. Inhibition of endothelium-dependent vasorelaxation by extracellular k(+): A novel controlling signal for vascular contractility. *Am J Physiol Heart Circ Physiol*. 2004;286:H329-339

17. Huang H, McIntosh J, Hoyt DG. An efficient, nonenzymatic method for isolation and culture of murine aortic endothelial cells and their response to inflammatory stimuli. *In Vitro Cell Dev Biol Anim*. 2003;39:43-50

18. Kevil CG, Bullard DC. In vitro culture and characterization of gene targeted mouse endothelium. *Acta Physiol Scand*. 2001;173:151-157

19. Kevil CG, Patel RP, Bullard DC. Essential role of icam-1 in mediating monocyte adhesion to aortic endothelial cells. *Am J Physiol Cell Physiol*. 2001;281:C1442-1447

20. Wei L, Freichel M, Jaspers M, Cuppens H, Cassiman JJ, Droogmans G, Flockerzi V, Nilius B. Functional interaction between trp4 and cftr in mouse aorta endothelial cells. *BMC Physiol*. 2001;1:3

21. Hwang J, Saha A, Boo YC, Sorescu GP, McNally JS, Holland SM, Dikalov S, Giddens DP, Griendling KK, Harrison DG, Jo H. Oscillatory shear stress

stimulates endothelial production of o2- from p47phox-dependent nad(p)h oxidases, leading to monocyte adhesion. *J Biol Chem*. 2003;278:47291-47298

22. Magid R, Martinson D, Hwang J, Jo H, Galis ZS. Optimization of isolation and functional characterization of primary murine aortic endothelial cells. *Endothelium*. 2003;10:103-109

23. Suh SH, Vennekens R, Manolopoulos VG, Freichel M, Schweig U, Prenen J, Flockerzi V, Droogmans G, Nilius B. Characterisation of explanted endothelial cells from mouse aorta: Electrophysiology and ca2+ signalling. *Pflugers Arch*. 1999;438:612-620

24. Kreisel D, Krupnick AS, Szeto WY, Popma SH, Sankaran D, Krasinskas AM, Amin KM, Rosengard BR. A simple method for culturing mouse vascular endothelium. *J Immunol Methods*. 2001;254:31-45

25. Lincoln DW, 2nd, Larsen AM, Phillips PG, Bove K. Isolation of murine aortic endothelial cells in culture and the effects of sex steroids on their growth. *In Vitro Cell Dev Biol Anim*. 2003;39:140-145

26. Chen S, Sega M, Agarwal A. "Lumen digestion" Technique for isolation of aortic endothelial cells from heme oxygenase-1 knockout mice. *Biotechniques*. 2004;37:84-86, 88-89

27. Kobayashi M, Inoue K, Warabi E, Minami T, Kodama T. A simple method of isolating mouse aortic endothelial cells. *J Atheroscler Thromb*. 2005;12:138-142

28. Zeisberg EM, Potenta S, Xie L, Zeisberg M, Kalluri R. Discovery of endothelial to mesenchymal transition as a source for carcinoma-associated fibroblasts. *Cancer Res*. 2007;67:10123-10128

29. Zeisberg EM, Tarnavski O, Zeisberg M, Dorfman AL, McMullen JR, Gustafsson E, Chandraker A, Yuan X, Pu WT, Roberts AB, Neilson EG, Sayegh MH, Izumo S, Kalluri R. Endothelial-to-mesenchymal transition contributes to cardiac fibrosis. *Nat Med*. 2007;13:952-961

30. Balconi G, Spagnuolo R, Dejana E. Development of endothelial cell lines from embryonic stem cells: A tool for studying genetically manipulated endothelial cells in vitro. *Arterioscler Thromb Vasc Biol*. 2000;20:1443-1451

31. Mowbray AL, Kang DH, Rhee SG, Kang SW, Jo H. Laminar shear stress up-regulates peroxiredoxins (prx) in endothelial cells: Prx 1 as a mechanosensitive antioxidant. *J Biol Chem*. 2008;283:1622-1627

32. Boo YC, Sorescu G, Boyd N, Shiojima I, Walsh K, Du J, Jo H. Shear stress stimulates phosphorylation of endothelial nitric-oxide synthase at ser1179 by akt-independent mechanisms: Role of protein kinase a. *J Biol Chem*. 2002;277:3388-3396

33. Nam D, Ni CW, Rezvan A, Suo J, Budzyn K, Llanos A, Harrison D, Giddens D, Jo H. Partial carotid ligation is a model of acutely induced disturbed flow, leading to rapid endothelial dysfunction and atherosclerosis. *Am J Physiol Heart Circ Physiol*. 2009;297:H1535-1543

34. Fledderus JO, van Thienen JV, Boon RA, Dekker RJ, Rohlena J, Volger OL, Bijnens AP, Daemen MJ, Kuiper J, van Berkel TJ, Pannekoek H, Horrevoets AJ. Prolonged shear stress and klf2 suppress constitutive proinflammatory transcription through inhibition of atf2. *Blood*. 2007;109:4249-4257

35. van Thienen JV, Fledderus JO, Dekker RJ, Rohlena J, van Ijzendoorn GA, Kootstra NA, Pannekoek H, Horrevoets AJ. Shear stress sustains atheroprotective endothelial klf2 expression more potently than statins through mrna stabilization. *Cardiovasc Res*. 2006;72:231-240

36. Jin ZG, Wong C, Wu J, Berk BC. Flow shear stress stimulates gab1 tyrosine phosphorylation to mediate protein kinase b and endothelial nitric-oxide synthase activation in endothelial cells. *J Biol Chem*. 2005;280:12305-12309

37. Sorescu GP, Sykes M, Weiss D, Platt MO, Saha A, Hwang J, Boyd N, Boo YC, Vega JD, Taylor WR, Jo H. Bone morphogenic protein 4 produced in endothelial cells by oscillatory shear stress stimulates an inflammatory response. *J Biol Chem*. 2003;278:31128-31135

38. De Caterina R, Libby P, Peng HB, Thannickal VJ, Rajavashisth TB, Gimbrone MA, Jr., Shin WS, Liao JK. Nitric oxide decreases cytokine-induced endothelial activation. Nitric oxide selectively reduces endothelial expression of adhesion molecules and proinflammatory cytokines. *J Clin Invest*. 1995;96:60-68

39. Gagnon E, Cattaruzzi P, Griffith M, Muzakare L, LeFlao K, Faure R, Beliveau R, Hussain SN, Koutsilieris M, Doillon CJ. Human vascular endothelial cells with extended life spans: In vitro cell response, protein expression, and angiogenesis. *Angiogenesis*. 2002;5:21-33

CHAPTER 4

DEVELOPMENT OF A MOUSE MODEL OF PARTIAL CAROTID LIGATION WHICH ACUTELY INDUCES DISTURBED FLOW AND A METHOD TO ISOLATE INTIMAL EMDOTHELIUM RNA

Summary

Atherosclerosis is closely associated with disturbed flow characterized by low and oscillatory shear stress, but studies directly linking it to atherogenesis is lacking. The major reason for this has been a lack of an animal model in which disturbed flow can be acutely induced and cause atherosclerosis. Here, we characterize partial carotid ligation as a model of disturbed flow with characteristics of low and oscillatory wall shear stress. We also describe a method of isolating intimal RNA in sufficient quantity from mouse carotid arteries. Using this model and method, we found that partial ligation causes upregulation of pro-atherogenic genes, downregulation of anti-atherogenic genes, endothelial dysfunction, and rapid atherosclerosis in 2 weeks and advanced lesions by 4 weeks. Partial ligation results in endothelial dysfunction, rapid atherosclerosis and advanced lesion development in a physiologically relevant model of disturbed flow. It also allows for easy and rapid intimal RNA isolation. This novel model and method could be used for genome-wide studies to determine molecular mechanisms underlying flow-dependent regulation of vascular biology and diseases.

Introduction

Atherosclerosis is a leading cause of morbidity and mortality in developed countries and is shown to be an inflammatory disease[1-2]. While multiple systemic factors such as hypercholesterolemia, diabetes, hypertension and smoking are well-known risk factors, atherosclerosis occurs preferentially at particular areas of disturbed flow characterized by low and oscillatory wall shear stress in branched or curved arteries [3-4]. In contrast, straight arterial regions are exposed to high and stable shear stress and are well protected from atherosclerosis[4]. Despite the close association between the two, evidence directly linking disturbed flow conditions to atherosclerosis has been lacking and the mechanisms responsible for pro- and anti-atherogenic effects of shear stress are still incompletely understood.

Shear stress is the tangential force imparted by viscous fluid flowing over endothelial cells[5-6]. Endothelial cells sense changes in shear stress and trigger mechanosensitive cell signaling events [7-8]. This in turn regulates endothelial function and structure, which affects vascular wall biology and pathophysiology[5]. Endothelial cells in straight part of the arteries experience unidirectional, high time-averaged wall shear stress (laminar shear). Laminar shear induces acute and chronic changes in endothelial cells leading to cell alignment, vasodilation, inhibition of inflammation and coagulation - atheroprotective responses. In contrast, disturbed flow stimulates pro-atherogenic responses including cell turnover, inflammation, thrombosis, and oxidative stress [5-8].

The differential mechanisms by which disturbed and stable flow promotes and inhibits atherogenesis, respectively, have been a subject of intense study, mostly using cultured endothelial cells [6-8]. To define molecular mechanisms responsible for these changes, investigators have carried out DNA micro-array studies using endothelial cells and have

identified shear sensitive genes such as kruppel-like factor 2 (*klf-2*), endothelial nitric oxide synthase (*eNOS*), vascular cell adhesion molecule-1 (*VCAM-1*), intercellular adhesion molecule-1 (*ICAM-1*), and bone morphogenic protein 4 (*BMP-4*) [9-16]. While these in vitro studies have provided critical insights regarding shear sensitive mechanisms in cultured endothelial cells using modeled flow conditions, it cannot be assumed whether identical mechanisms are responsible for flow-dependent changes in vessels *in vivo* and vascular diseases such as atherosclerosis.

Several mouse models have been used to examine the role of shear sensitive genes and proteins in atherogenesis. These models include 1) naturally occurring athero-prone regions of arterial tree, 2) complete ligation of common carotid artery, and 3) peri-vascular shear modifier cuff placed around common carotid artery in mice deficient in Apolipoprotein-E (ApoE KO) or Low-density-lipoprotein receptor (LDLR KO). Naturally occurring athero-prone regions, such as lesser curvature of the aortic arch and root of innominate artery, are exposed to disturbed flow[17]. These flow disturbed areas in ApoE KO and LDLR KO mice develop measurable atherosclerotic lesions upon feeding atherogenic diets for at least 2 to 3 months[18]. While these studies show that flow disturbance is associated with atherogenesis, they do not provide evidence directly linking disturbed flow to atherogenesis as the flow disturbance is chronic from the early developmental stage and not due to an acute flow alteration. Other difficulties include small sample area of atherosclerosis, making reproducible endothelial RNA isolation from these areas in sufficient quantity and purity difficult[18]. Complete ligation of common carotid artery has also been used to study atherosclerosis [19-20]. This model results in no flow through the LCA and may be associated with endothelial denudation and thrombosis. It may not be a physiologically relevant model in the study of shear-mediated atherosclerosis. [21]. Peri-vascular shear modifier cuff model was recently

reported and applied to the study of shear-mediated vascular inflammation and atherogenesis. It was shown to create three distinct regions of shear stress via application of a peri-vascular cuff around LCA - lower shear (proximal to the cuff), high shear (inside the cuff) or oscillatory shear (distal to the cuff) [22]. It is important to note thatlow and oscillatory shear stress, two characteristics of disturbed flow, were predicted to be in two separate regions. The region of oscillatory shear stress (distal to cuff) had high average shear stress, and the region of low average shear stress (proximal to cuff) did not have oscillatory shear stress component [22]. This dissociation of oscillatory shear from low shear stress is a unique characteristic of the cuff model and it is different from typical disturbed flow conditions displaying co-localized low and oscillatory shear stress.

Partial carotid ligation has previously been described as a model of flow reduction and has been used in the study of vascular remodeling[23-24]. In this model, three of the four caudal branches of left common carotid artery (LCA) were ligated, resulting in a substantial flow reduction in LCA with inward remodeling of LCA [24]. Changes in shear stress levels were not reported, and changes in flow were only described as flow reduction. Moreover, partial ligation has not previously been applied to the study of atherosclerosis. We hypothesized that partial carotid ligation causes low and oscillatory shear stresses– two major characteristics of disturbed flow which has been closely associated with atherogenesis[5]. We further hypothesized that this disturbed flow would cause atherosclerosis in hyperlipidemic conditions. To test these hypotheses, we first measured flow velocity and direction as well as vessel dimensions by a high resolution ultrasound system before and after partially ligating LCA. These measurements were used for computational fluid dynamics (CFD) modeling to estimate shear stress magnitudes and directions. Next, ApoE KO mice were partially ligated and fed a high fat diet to determine if this would result in atherosclerosis in LCA. In addition, we used a

simple method of isolating intimal RNA in significant quantity and purity from carotid arteries for mechanistic studies. Here, we report that partial ligation causes disturbed flow, induces atherosclerosis rapidly within two weeks upon feeding a high-fat diet and that the additional simple RNA isolation method is extremely useful to determine gene expression changes occurring in carotid intima in response to changes in shear stress.

Methods

Animal studies with partial ligation

All animal studies were carried out by procedures approved by Emory University IACUC. Male and female mice were ligated between 6 to 8 weeks of age. C57Bl/6 and ApoE KO mice were obtained from Jackson Laboratories. All mice were fed a chow diet and water *ad libitum* until partial ligation. Partial ligation of LCA was carried out as previously described[23] with minor modifications. Briefly, anesthesia was induced by intra-peritoneal injection of Xylazine (10mg/kg) and Ketamine (80mg/kg) mixture. Dehaired area was disinfected with Betadine and a ventral mid-line incision (4 to 5mm) was made in the neck. LCA was exposed by blunt dissection. Three of four caudal branches of LCA - left external artery, left internal artery, and occipital artery - were ligated with 6-0 silk suture (Figure. 4.1) while superior thyroid artery was left intact. The incision was then closed with Tissue-Mend (Veterinary Product Laboratories). Mice were monitored until recovery in a chamber on a heating pad following surgery. A single subcutaneous injection of Buprenorphine (0.1 mg/kg) was given 12 hours after partial ligation for additional pain relief. For atherosclerosis studies, ApoE KO mice were fed the Paigen's high fat diet [18] (Science Diets) immediately following partial ligation until sacrificed, from 2 days up to 6 weeks. C57Bl/6 mice were continued on chow diet post-ligation.

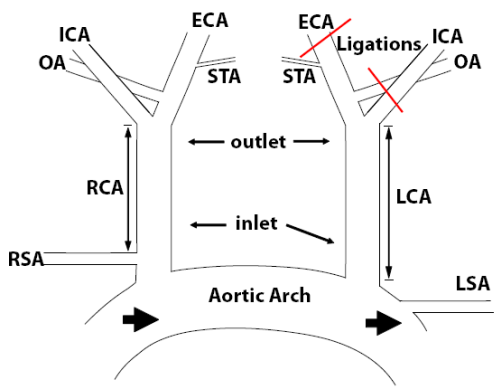

Figure 4.1. Scheme of partial carotid ligation. *Three branches of the LCA, ECA, ICA and OA were ligated in the left common carotid artery while leaving STA open.*

High Resolution Ultrasound Measurements

All ultrasound measurements were taken using VEVO 770 High-resolution *in vivo* micro-imaging ultrasound system with a 30 MHz mouse probe (Visualsonics). Mice were anesthetized with inhaled isoflurane and body temperature was maintained on a heated stage for the duration of studies. Levels of anesthesia, heart rate, temperature, and respirations were continuously monitored. Pulse wave Doppler mode was used at the inlet, mid-point and outlet of the common carotid arteries (see Figure. 4.1) for measuring flow velocity, M-mode for vessel dimensions, and B-mode for vessel length. All measurements were gated to ECG and respiration.

CFD

The CFD models incorporated the geometry of mouse carotid arteries as determined by the ultrasound system. Left and right common carotid arteries of mouse are similar in geometry to a straight tube with different diameters at two ends (inlet and outlet, Figure.

4.1), which made a moving mesh CFD model simple. The geometric resolution of ultrasound images was 10μm. After segmentation and measuring, the diameter waveforms, sequential diameters, at three sections over one cardiac cycle were obtained and included the inlet diameters, outlet diameters and middle diameters. A 3D model was reconstructed based on the diameters at end diastole, and then a moving mesh was designed for the model according to individual diameter waveform[17]. The moving model replicated the geometry and compliance characteristics of the mouse carotid artery. Computations were performed using the commercial CFD-ACE code based on a finite volume method for solving the Navier-Stokes equations as previously described[17]. The velocity waveforms at three sections (inlet, outlet and mid-point, Figure 4.1) were acquired from Doppler measurements. Two end velocity waveforms were transformed to correspond with flow waveforms according to the diameter waveform. The flow waveforms were the inflow and outflow boundary conditions for CFD modeling. The mid-point velocity waveform was used later to compare with the CFD results at the same section. The blood was assumed to be a Newtonian and incompressible fluid, and the flowing state was assumed to be laminar flow.

Intimal RNA isolation from carotid arteries

Mice were euthanized by CO_2 inhalation according to Emory University's IACUC protocol and pressure perfused with saline containing heparin (10 units/mL) via left ventricle after severing inferior vena cava (IVC). LCA and RCA were then isolated and carefully cleaned of peri-adventitial fat. Tthe carotid lumen was quickly flushed (few seconds) with 150 □l of QIAzol lysis reagent (QIAGEN) using 29G insulin syringe into a microfuge tube. The eluate was then used for intimal RNA isolation using miRNeasy mini kit (QIAGEN) according to manufacturer's instructions. The carotid artery leftover after flushing with QIAzol was used to prepare RNA from media and adventitia (m+a). m+a

was snap frozen in liquid nitrogen, pulverized by mortar and pestle, lysed in QIAzol lysis reagent (700μl per carotid) and RNA was isolated using miRNeasy mini kit.

Immunohistochemical staining studies (IHC)

Mice were euthanized and pressure perfused with saline containing heparin as described above. LCA and RCA were collected *en block* with the trachea and esophagus. For frozen sections, tissue was embedded in Tissue-Tek OCT, frozen on dry ice and stored at –80°C until used. Frozen sections (7μm) were fixed in acetone for 8 mintues, blocked with 10% goat serum for 1 hour at room temperature and incubated with primary antibodies overnight at 4°C[9]. To visualize primary antibodies, rhodamine-conjugated secondary antibody was used for one hour at room temperature. Nuclei were counter stained with Hoechst #33258. Oil-red-o staining was carried out using frozen sections as described[25]. For pentachrome staining, fixed tissue was paraffin embedded and sectioned at 5 μm and stained with Russell-Movat pentachrome stain kit (American Master Tech Scientific, Inc.). Micrographs were taken with Zeiss (Jena, Germany) epifluorescent microscope. Images were analyzed with NIH Image J software to quantify lesion size in each animal as described[26].

Vascular relaxation study

Vascular relaxation study was carried out using carotid rings obtained from LCA and RCA of partially ligation ApoE KO mice as previously described[27].

Statistical analysis

Data are presented as mean±SEM. Student's t-test for two groups and ANOVA with Games-Howell post-hoc tests for comparing multiple groups were carried out using the SPSS program. $P<0.05$ was considered statistically significant.

Results

Partial ligation results in low and oscillatory shear stress

To determine whether partial ligation caused changes in shear stress levels and direction, we ligated the external carotid, internal carotid and occipital arteries of LCA, while leaving the superior thyroid artery intact in C57Bl/7 and ApoE KO mice (Figure 4.1). Next, flow velocity and direction and vessel dimensions of LCA and RCA were determined by high resolution ultrasonography. This showed a reduction in flow velocity during systole in LCA 1 and 7 days after ligation as expected (Figure 4.2). Moreover, flow direction was reversed during diastole in LCA 1 and 7 days after ligation (arrows in Figure 4.2). Similar flow profiles were observed at both the pre-defined inlet and outlet. Flow profiles as shown in Figure 4.2 were obtained from inlet. Blood flow in LCA decreased by 90% 1 and 7 days after ligation but blood flow in RCA did not change significantly compared to that of pre-ligation (Figure 4.3).

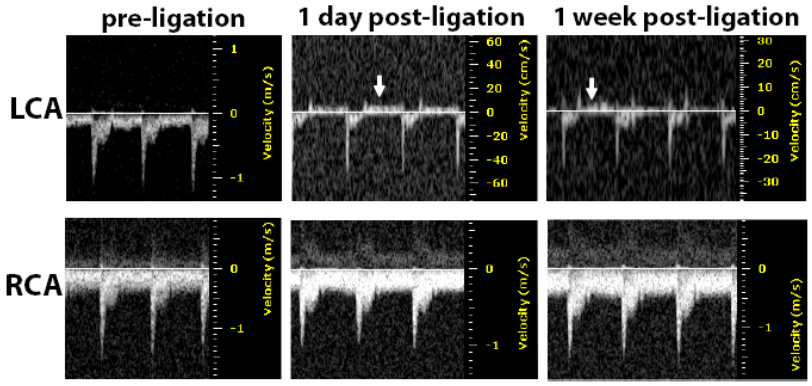

Figure 4.2 The echocardiograms of partial carotid ligation. *The echocardiograms show flow velocity profiles and reveals that partial ligation induces flow reversal (indicated by arrows) in LCA during diastole. Flow in RCA remains unchanged after ligation. Images shown were obtained from an ApoE KO mouse and are representative of at least 10 ApoE KO mice. Partial ligation in C57BL/6 mice results in similar flow reversal profiles.*

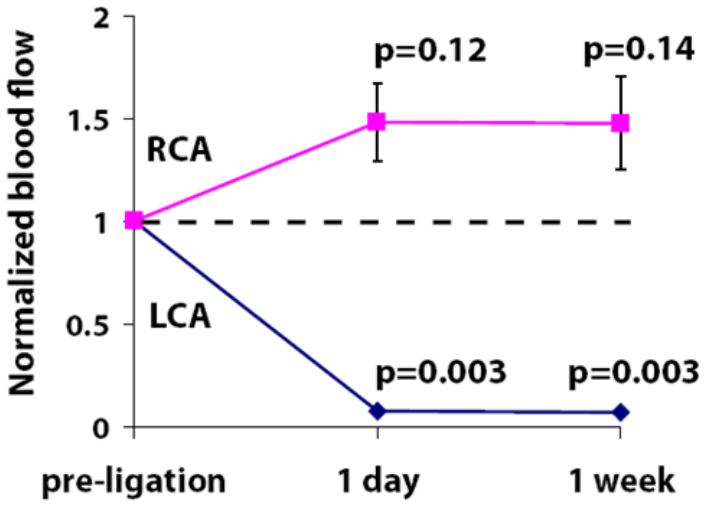

Figure 4.3 Partial ligation reduces blood flow through the LCA, without significantly raising flow in RCA. *The dotted line indicates pre-ligation flow level. Shown are mean ± SEM, n=4.*

Using values of flow velocity, direction and vessel dimensions, we performed CFD modeling of LCA and RCA pre and 1 day post-ligation. This showed wall shear stress (WSS) value remained positive without any significant difference in RCA in both before and after ligation of LCA during the entire cardiac cycle (Figure 4.4). In contrast, WSS level was reduced during systole compared to that of RCA and became negative (due to flow reversal) during diastole in ligated LCA (Figure 4.4). Time-averaged WSS was reduced from approximately 110 dynes/cm^2 pre-ligation to 30 dynes/cm^2 post-ligation (Figure 4.4). These results show that partial ligation causes low and oscillatory shear stress in LCA, characteristic of disturbed flow.

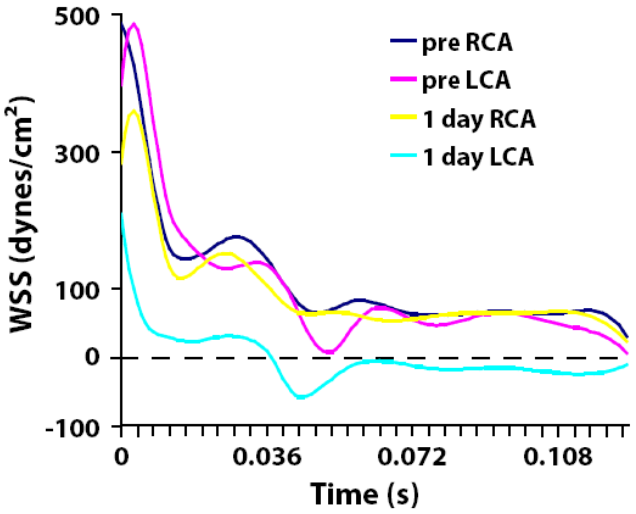

Figure 4.4 CFD study: Partial ligation results in low and oscillatory shear stress. *CFD was carried out using the values shown in Figure 4.3 (ligated ApoE KO mice). Figure shows WSS over a cardiac cycle. in LCA and RCA before and 1 day after partial ligation.*

Method of isolating intimal RNA from carotid arteries

Lumens of LCA and RCA from sham-ligated C57 mice were flushed once with Qiazol (Qiagen). The leftover LCA and RCA after collecting intimal RNA were also saved for analysis. RNA was then isolated with miRNeasy kit (Qiagen), resulting in 10 to 20 ng total RNA from each eluate (intima), while each leftover vessel (media + adventitia) resulted in approximately 800 ng to 1 □g of total RNA. To test for endothelial purity of intimal RNA, we performed qPCR for *PECAM-1* and *α-SMA* (Figure. 4.5A). Intimal eluate showed endothelial marker *PECAM-1* without any evidence of smooth muscle specific *α-SMA*. Conversely, media+adventitial RNA contained *α-SMA* without any evidence of *PECAM-1*. Quantitative real-time PCR (qPCR) and en face protein staining

further confirmed the results (Figure. 4.5B,C). This shows that intimal RNA can be obtained from carotid arteries by our simple and reproducible method in sufficient quantity and purity without significant smooth muscle RNA contamination. In addition, media+adventitial RNA can also be isolated from the arteries without significant endothelial contamination.

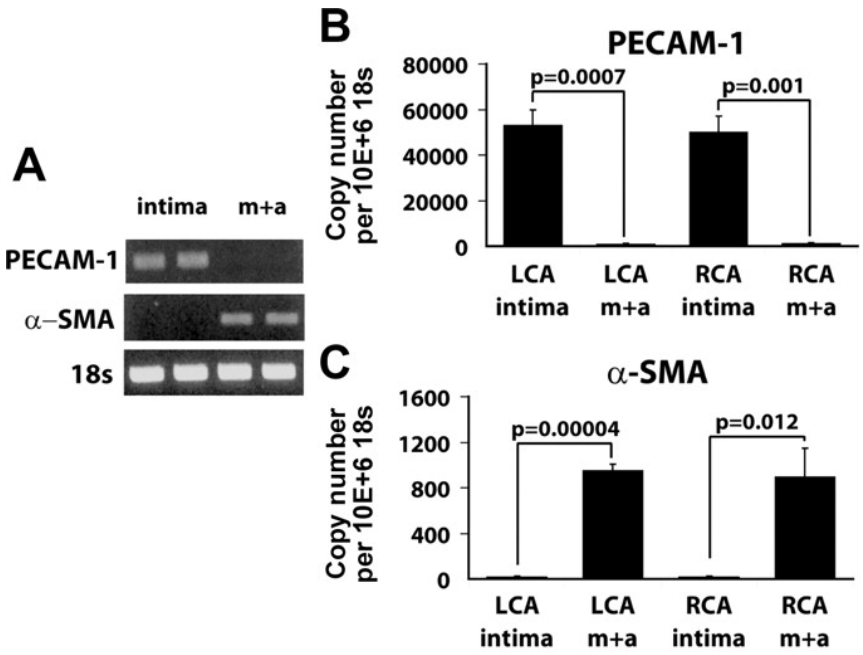

Figure 4.5 Validation of the method of intimal RNA preparation. *Intimal RNA and medial+adventitial (m+a) RNA were obtained from sham-operated RCA and LCA in C57BL/6 mice. RNA's were analyzed by semi-quantitative RT-PCR (A) and qPCR (B, C) for PECAM-1 and □-SMA using 18s as an internal control. Bar graphs are mean ± SEM, n=3.*

Partial ligation down-regulates Klf-2 and eNOS while up-regulating ICAM-1, VCAM-1, and BMP4

We tested whether intimal RNA obtained from LCA and RCA by our method could be used to study regulation of mechanosensitive genes in endothelial cells. Intimal RNA

from sham and partially ligated C57BL/6 mice were collected 2 days after surgery and analyzed by qPCR. We chose this 2 day time point because we did not observe measurable accumulation of Cd11b+ leukocytes in the intima in either LCA or RCA in these mice (Figure 4.6), while this seems to be a sufficient duration to ensure robust gene expression changes following the partial ligation.

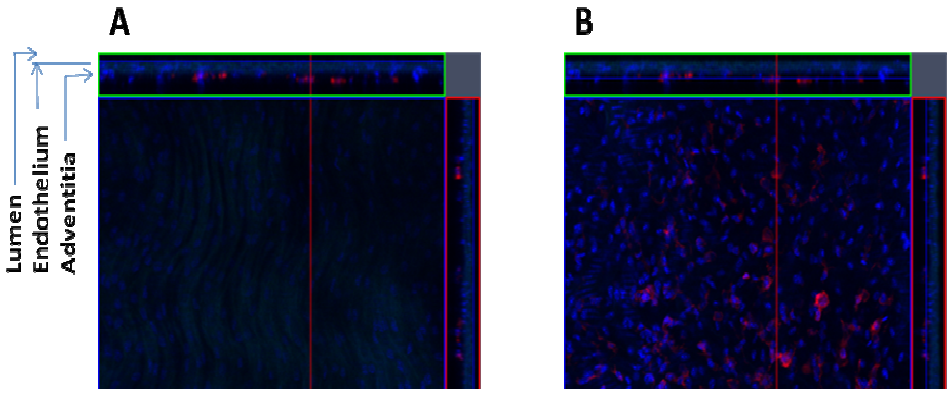

Figure 4.6 Partial ligation does not cause detectable accumulation of Cd11b+ leukocytes in lumen of LCA 2 days post-ligation in c57Bl/6 mice. *C57Bl/6 mice underwent partial ligation. En face staining was done 2 days post-ligation for both LCA and RCA with cd11b (red). Nuclei were counterstained with DAPI (blue). No Cd11b+ cells were seen in carotid lumen (orthogonal view from confocal z-stack imaging with main picture showing endothelial layer, A). However, some Cd11b+ cells were observed in the adventitia (orthogonal view from confocal z-stack with main picture showing adventitia, B).*

Klf-2 and *eNOS* were significantly down-regulated in LCA by 80% and 50%, respectively, whereas *BMP4*, *ICAM-1* and *VCAM-1* were significantly up-regulated in LCA by approximately two-fold compared to RCA (Figure 4.7). In sham-operated mice, mRNA levels of these genes did not differ between LCA and RCA. Protein levels for ICAM-1 and VCAM-1 were verified by immunohistochemical staining (Figure 4.8). These results are consistent with previous observations *in vitro* and *in vivo* that KLF-2 and eNOS are down-regulated in areas of disturbed flow while BMP4, ICAM-1 and VCAM-1 are up-regulated in areas of disturbed flow [9-14, 17, 28-29].

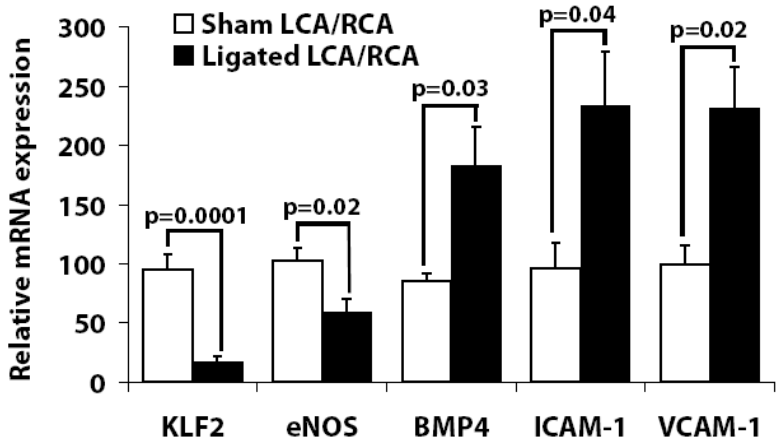

Figure 4.7 Partial ligation results in decreases in KLF2 and eNOS while increasing BMP4, ICAM-1, and VCAM-1. *Intimal RNA from sham and partially ligated C57BL/6 mice were collected from LCA and RCA, respectively, two days after surgery and analyzed by qPCR using 18s as internal control. Data shown as percent ratio of mRNA expressed in LCA over RCA of sham and partially ligated mice. Mean ± SEM, n=3 sham, n=5 ligated.*

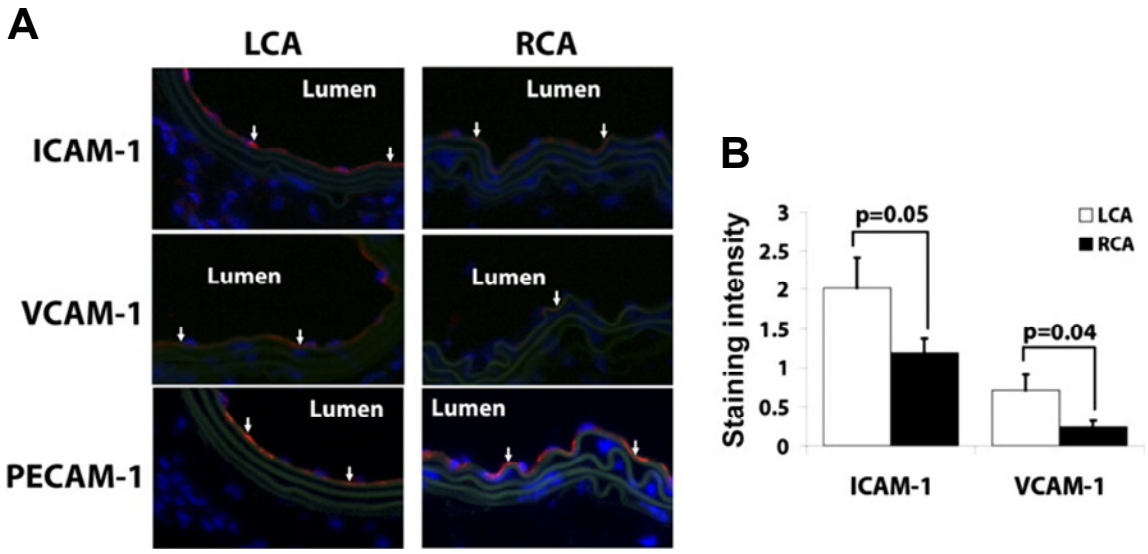

Figure 4.8 Partial ligation increases ICAM-1 and VCAM-1 protein expression in LCA. *C57BL/6 mice underwent partial ligation, and LCA and RCA were collected 2 days postligation. Frozen sections were stained for ICAM-1, VCAM-1, and PECAM-1 (red). Nuclei were counterstained with Hoechst (blue). Images are representative of n = 4 (A). Average staining intensity per stained area for each was quantified and shown as the mean ± SE (B).*

Partial ligation in ApoE KO mice impairs endothelium-dependent vasorelaxation

To determine if disturbed flow causes endothelial dysfunction, we examined vasorelaxation response to acetylcholine. Carotid artery rings were obtained from LCA and RCA of partially ligated ApoE KO mice fed a high fat diet for 2 or 7 days. In 2 days post-ligation, LCA and RCA showed normal relaxation response to acetylcholine, exceeding 90% of precontracted tone (Figure 4.9). In 7 days, however, relaxation of LCA by acetylcholine was significantly inhibited, reaching only 50% of precontracted tone, while RCA vasorelaxtion response remained unchanged (Figure 4.9). To determine whether the impaired response was due to endothelial defect, endothelium-independent vasodilator sodium nitroprusside (SNP) was studied. At 2 and 7 days post-ligation, both LCA and RCA relaxed to similar degrees in response to SNP (Figure 4.9), suggesting that disturbed flow induces endothelial dysfunction in ApoE KO mice in 7 days.

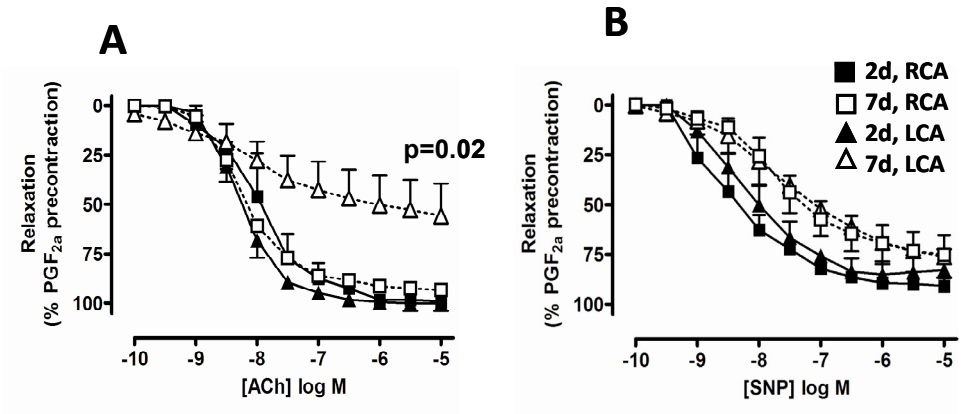

Figure 4.9 Partial ligation induces endothelial dysfunction. *Arterial rings were obtained from LCA and RCA that were partially ligated and fed high-fat diet for 2 and 7 days in ApoE KO mice. Rings pre-constricted with PGF2α were dilated with increasing concentrations of acetylcholine (A) or SNP (B) for endothelial-independent relaxation. Shown are mean $\pm$ SEM, n=2 for 2 days, and n=6 for 7 days.*

Partial ligation in ApoE-null mice causes accelerated

To examine whether partial ligation causes accelerated atherosclerosis, ApoE KO mice were partially ligated, and fed the high fat diet for one, two or three weeks. At one week, LCA did not show any evidence of atherosclerotic lesion as determined by Oil-Red-O staining (Figure 4.10). By two weeks, LCA developed robust lipid lesion that increased dramatically by three weeks after ligation (Figure 4.10). However, RCA did not show any lesions for as long as 6 weeks post-ligation.

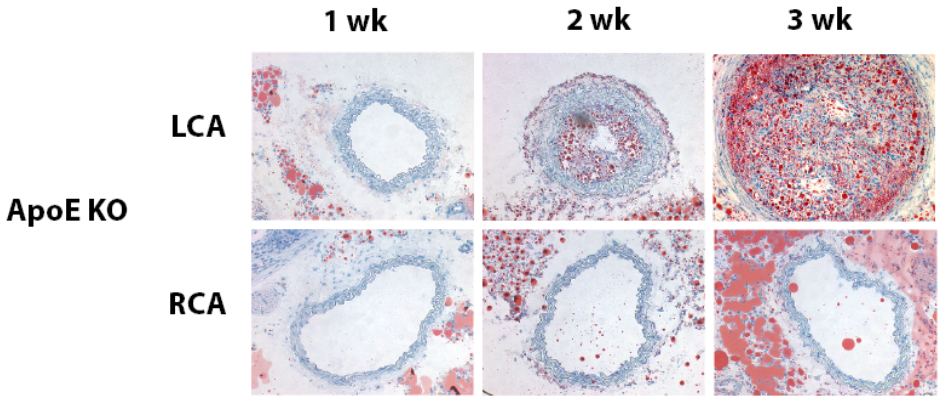

Figure 4.10 Partial ligation and high-fat diet rapidly induces atherosclerosis in LCA of ApoE KO mice. *ApoE KO mice were partially ligated and fed the high-fat diet for 1 to 3 weeks. Shown are representative images of at least n=6 (A). Frozen sections from LCA were stained with Oil-Red-O*

Partial ligation in ApoE KO mice develops complex lesion

Next we examined whether partial ligation can induce advanced atherosclerotic lesion. Pentachrome staining of LCA of ApoE KO mice 4 to 6 weeks post-partial ligation and high fat diet showed robust cholesterol clefts and several remarkable intra-plaque neovessels (Fig. 4.11). These results show that at least some features of advanced lesions develop quickly within 4 to 6 weeks following partial ligation, providing additional unique advantage of our model in the study of atherosclerosis.

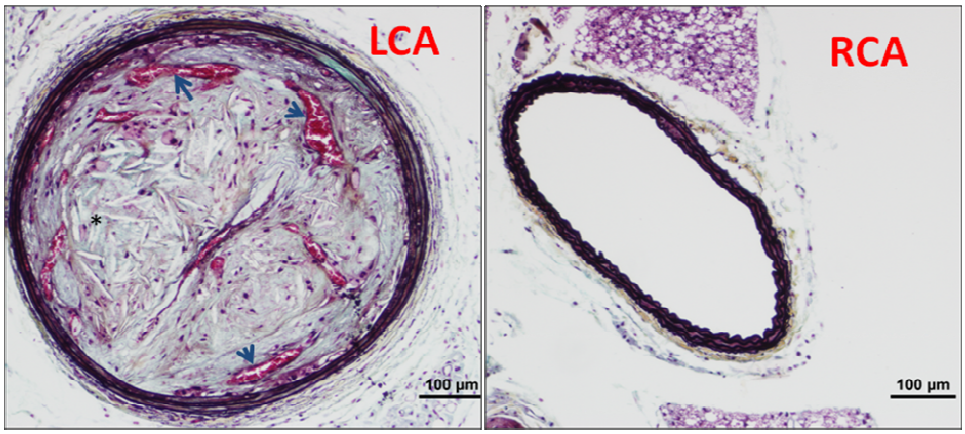

Figure 4.11 Partial ligation and high-fat diet induces features of advanced atherosclerosis in LCA. *ApoE KO mice were partially ligated and fed high-fat diet for 4 weeks. Paraffin sections obtained from LCA and RCA were stained with Pentachrome. Note needle-shaped cholesterol clefts (*) and intraplaque neovessels (arrows) containing red blood cells.*

Discussion

Here, we characterized partial carotid ligation as a model of disturbed flow with low and oscillatory shear stress which causes endothelial dysfunction and accelerated atherosclerosis. We also describe a simple method of isolating intimal RNA from mouse carotid arteries. In this mouse model, we found that partial ligation of LCA causes 1) low and oscillatory shear, 2) upregulation of pro-atherogenic genes, 3) downregulation of anti-atherogenic genes, 4) endothelial dysfunction in ApoE KO mice in 1 week, 5) rapid atherosclerosis within 2 weeks in ApoE KO mice, and 6) advanced lesions by 4 weeks.

Partial ligation causes not only low shear stress but also oscillatory shear stress - two characteristics of patho-physiologically relevant disturbed flow associated with atherogenesis (3). Previously, Cheng et al. used peri-vascular cuff model to create 3

distinct regions of shear stress: lower shear (100 dynes/cm^2), higher shear (250 dynes/cm^2), or oscillatory shear (140 dynes/cm^2)[22]. Using 15-20 week old ApoE KO mice fed an atherogenic diet for minimum of 8 weeks; they demonstrated that lower shear was more atherogenic than oscillatory shear, although flow oscillation was not directly demonstrated in their mouse model[22]. It should be noted, however, that typical athero-prone regions in carotid bifurcations and aortic arches are exposed to disturbed flow characterized by co localization of both low and oscillatory shear stress[4-5, 17]. Perhaps one reason that our partial ligation induced atherosclerosis much faster than the peri-vascular cuff model is that LCA is exposed to both low and oscillatory shear in our partial ligated artery while peri-vascular cuff exposes LCA to either low or oscillatory shear, but not both. Complete ligation of carotid artery [20] has also been used to induce rapid atherosclerosis [19]. However, its patho-physiologic relevance is debated as it is a model of no flow and likely does not mimic disturbed flow with low and oscillatory shear[21]. We propose that partial ligation model provides a physiologically relevant model well-suited for the study of atherosclerosis induced by disturbed flow.

Intra-plaque neo-vessel formation and cholesterol clefts are important features of advanced atherosclerotic lesions[30]. In our model, Pentachrome staining revealed numerous large vascular structures containing red blood cells within the plaque. It is interesting to note that many of these intra-plaque neo-vessels were found near internal elastic lamina, consistent with a previous report showing that intra-plaque hemorrhage in innominate artery of 60 week old ApoE KO mice occurred in similar region[31]. In addition, we observed abundant needle-like cholesterol clefts within the plaque, providing further evidence of advanced lesions. This could serve as a very useful model to study the mechanisms underlying intra-plaque neo-vascularization and its importance in atherosclerosis.

Here we describe a simple method of isolating intimal RNA from carotid arteries in sufficient quantity with virtually no appreciable contamination from underlying media and adventitia. Intimal RNA obtained by this method is nearly free of medial smooth muscle RNA contamination. Previous efforts to isolate intimal RNA from athero-prone and athero-protected areas of vasculature have been reported using a scrapping method [32]. However, we found our method of simply flushing the carotid artery with lysis reagent easier and highly reproducible. Having our partial ligation model, which exposes the entire length of the common carotid artery to disturbed flow, enabled us to apply this easy method of endothelial RNA isolation. This method could easily be applied to obtain sufficient quantities of RNA for high through-put genome wide studies including DNA microarray and microRNA array.

We applied this method to study mechanisms by which disturbed flow induces endothelial dysfunction and atherosclerosis. By comparing endothelial RNA from LCA and RCA, we found that partial ligation downregulated expression of anti-atherogenic genes such as *eNOS* and *Klf-2* while upregulating pro-atherogenic genes such as *ICAM-1, VCAM-1* and *BMP4*. These gene expression changes are consistent with known endothelial responses to disturbed flow *in vitro* and *in vivo* [9-14]

We believe that this is the first report demonstrating that acute induction of disturbed flow *in vivo* causes endothelial dysfunction. It was reported previously that endothelial dysfunction could be induced in carotid arteries of ApoE KO mice by feeding a Western diet for more than 26 weeks[33]. By comparison, our model impairs vasorelaxation response within one week, providing a rapid and useful model to study flow-dependent endothelial dysfunction.

In conclusion, we characterized partial carotid ligation as a model acutely induced disturbed flow which results in accelerated endothelial dysfunction and atherosclerosis and allows for simple method of intimal RNA isolation. These could be used in ApoE, LDL receptor KO, or other transgenic mice to further study molecular mechanisms underlying flow-dependent regulation of vascular biology and disease, such as neo-vascularization and atherosclerosis. Moreover, this *in vivo* model could be used to test various therapeutic interventions targeting endothelial dysfunction and atherosclerosis in considerably reduced study duration.

References

1. Ross R. Atherosclerosis--an inflammatory disease. *N Engl J Med*. 1999;340:115-126

2. Libby P. Inflammation in atherosclerosis. *Nature*. 2002;420:868-874

3. Ku DN, Giddens DP, Zarins CK, Glagov S. Pulsatile flow and atherosclerosis in the human carotid bifurcation. Positive correlation between plaque location and low oscillating shear stress. *Arteriosclerosis*. 1985;5:293-302

4. VanderLaan PA, Reardon CA, Getz GS. Site specificity of atherosclerosis: Site-selective responses to atherosclerotic modulators. *Arterioscler Thromb Vasc Biol*. 2004;24:12-22

5. Chatzizisis YS, Coskun AU, Jonas M, Edelman ER, Feldman CL, Stone PH. Role of endothelial shear stress in the natural history of coronary atherosclerosis and vascular remodeling: Molecular, cellular, and vascular behavior. *J Am Coll Cardiol*. 2007;49:2379-2393

6. Jo H, Song H, Mowbray A. Role of nadph oxidases in disturbed flow- and bmp4-induced inflammation and atherosclerosis. *Antioxidants & redox signaling*. 2006;8:1609-1619

7. Berk BC. Atheroprotective signaling mechanisms activated by steady laminar flow in endothelial cells. *Circulation*. 2008;117:1082-1089

8. Davies PF. Flow-mediated endothelial mechanotransduction. *Physiological reviews*. 1995;75:519-560

9. Chang K, Weiss D, Suo J, Vega JD, Giddens D, Taylor WR, Jo H. Bone morphogenic protein antagonists are coexpressed with bone morphogenic protein 4 in endothelial cells exposed to unstable flow in vitro in mouse aortas and in human coronary arteries: Role of bone morphogenic protein antagonists in inflammation and atherosclerosis. *Circulation*. 2007;116:1258-1266

10. Cheng C, van Haperen R, de Waard M, van Damme LC, Tempel D, Hanemaaijer L, van Capellen GW, Bos J, Slager CJ, Duncker DJ, van der Steen AF, de Crom R, Krams R. Shear stress affects the intracellular distribution of enos: Direct demonstration by a novel in vivo technique. *Blood*. 2005

11. Davis ME, Cai H, Drummond GR, Harrison DG. Shear stress regulates endothelial nitric oxide synthase expression through c-src by divergent signaling pathways. *Circ Res*. 2001;89:1073-1080

12. SenBanerjee S, Lin Z, Atkins GB, Greif DM, Rao RM, Kumar A, Feinberg MW, Chen Z, Simon DI, Luscinskas FW, Michel TM, Gimbrone MA, Jr., Garcia-Cardena G, Jain MK. Klf2 is a novel transcriptional regulator of endothelial proinflammatory activation. *The Journal of experimental medicine*. 2004;199:1305-1315

13. Sorescu GP, Sykes M, Weiss D, Platt MO, Saha A, Hwang J, Boyd N, Boo YC, Vega JD, Taylor WR, Jo H. Bone morphogenic protein 4 produced in endothelial cells by oscillatory shear stress stimulates an inflammatory response. *J Biol Chem*. 2003;278:31128-31135

14. Dekker RJ, van Soest S, Fontijn RD, Salamanca S, de Groot PG, VanBavel E, Pannekoek H, Horrevoets AJ. Prolonged fluid shear stress induces a distinct set of endothelial cell genes, most specifically lung kruppel-like factor (klf2). *Blood*. 2002;100:1689-1698

15. Dai G, Kaazempur-Mofrad MR, Natarajan S, Zhang Y, Vaughn S, Blackman BR, Kamm RD, Garcia-Cardena G, Gimbrone MA, Jr. Distinct endothelial phenotypes evoked by arterial waveforms derived from atherosclerosis-susceptible and -resistant regions of human vasculature. *Proc Natl Acad Sci U S A*. 2004;101:14871-14876

16. McCormick SM, Eskin SG, McIntire LV, Teng CL, Lu CM, Russell CG, Chittur KK. DNA microarray reveals changes in gene expression of shear stressed human umbilical vein endothelial cells. *Proc Natl Acad Sci U S A*. 2001;98:8955-8960

17. Suo J, Ferrara DE, Sorescu D, Guldberg RE, Taylor WR, Giddens DP. Hemodynamic shear stresses in mouse aortas: Implications for atherogenesis. *Arterioscler Thromb Vasc Biol*. 2007;27:346-351

18. Paigen B, Morrow A, Holmes PA, Mitchell D, Williams RA. Quantitative assessment of atherosclerotic lesions in mice. *Atherosclerosis*. 1987;68:231-240

19. Khatri JJ, Johnson C, Magid R, Lessner SM, Laude KM, Dikalov SI, Harrison DG, Sung HJ, Rong Y, Galis ZS. Vascular oxidant stress enhances progression and angiogenesis of experimental atheroma. *Circulation*. 2004;109:520-525

20. Kumar A, Lindner V. Remodeling with neointima formation in the mouse carotid artery after cessation of blood flow. *Arterioscler Thromb Vasc Biol*. 1997;17:2238-2244

21. Xu Q. Mouse models of arteriosclerosis: From arterial injuries to vascular grafts. *Am J Pathol*. 2004;165:1-10

22. Cheng C, Tempel D, van Haperen R, van der Baan A, Grosveld F, Daemen MJ, Krams R, de Crom R. Atherosclerotic lesion size and vulnerability are determined by patterns of fluid shear stress. *Circulation*. 2006;113:2744-2753

23. Sullivan CJ, Hoying JB. Flow-dependent remodeling in the carotid artery of fibroblast growth factor-2 knockout mice. *Arterioscler Thromb Vasc Biol*. 2002;22:1100-1105

24. Korshunov VA, Berk BC. Flow-induced vascular remodeling in the mouse: A model for carotid intima-media thickening. *Arterioscler Thromb Vasc Biol*. 2003;23:2185-2191

25. Zhou J, Lhotak S, Hilditch BA, Austin RC. Activation of the unfolded protein response occurs at all stages of atherosclerotic lesion development in apolipoprotein e-deficient mice. *Circulation*. 2005;111:1814-1821

26. Lessner SM, Prado HL, Waller EK, Galis ZS. Atherosclerotic lesions grow through recruitment and proliferation of circulating monocytes in a murine model. *Am J Pathol*. 2002;160:2145-2155

27. Miriyala S, Gongora Nieto MC, Mingone C, Smith D, Dikalov S, Harrison DG, Jo H. Bone morphogenic protein-4 induces hypertension in mice: Role of noggin, vascular nadph oxidases, and impaired vasorelaxation. *Circulation*. 2006;113:2818-2825

28. Ziegler T, Bouzourene K, Harrison VJ, Brunner HR, Hayoz D. Influence of oscillatory and unidirectional flow environments on the expression of endothelin and nitric oxide synthase in cultured endothelial cells. *Arterioscler Thromb Vasc Biol*. 1998;18:686-692

29. Chappell DC, Varner SE, Nerem RM, Medford RM, Alexander RW. Oscillatory shear stress stimulates adhesion molecule expression in cultured human endothelium. *Circ Res*. 1998;82:532-539

30. Doyle B, Caplice N. Plaque neovascularization and antiangiogenic therapy for atherosclerosis. *J Am Coll Cardiol*. 2007;49:2073-2080

31. Rosenfeld ME, Polinsky P, Virmani R, Kauser K, Rubanyi G, Schwartz SM. Advanced atherosclerotic lesions in the innominate artery of the apoe knockout mouse. *Arterioscler Thromb Vasc Biol*. 2000;20:2587-2592

32. Won D, Zhu SN, Chen M, Teichert AM, Fish JE, Matouk CC, Bonert M, Ojha M, Marsden PA, Cybulsky MI. Relative reduction of endothelial nitric-oxide synthase expression and transcription in atherosclerosis-prone regions of the mouse aorta and in an in vitro model of disturbed flow. *The American journal of pathology*. 2007;171:1691-1704

33. d'Uscio LV, Baker TA, Mantilla CB, Smith L, Weiler D, Sieck GC, Katusic ZS. Mechanism of endothelial dysfunction in apolipoprotein e-deficient mice. *Arterioscler Thromb Vasc Biol*. 2001;21:1017-1022

CHAPTER 5

DISCOVERY OF NOVEL MECHANOSENSITIVE GENES USING IN VIVO MODEL OF MOSUE CAROTID ENDOTHELIUM EPXOSED TO DISTURBED FLOW

Summary

We have shown in Chapter 4 that disturbed flow caused by partial ligation of mouse carotid artery rapidly induces endothelial dysfunction and atherosclerosis in one and two weeks, respectively. Using this acute *in vivo* model, we identified mechanosensitive genes in partially ligated mouse arterial endothelium to understand the mechanism by which disturbed flow induces atherosclerosis. Genome-wide microarray study was carried out using endothelial RNAs isolated from the flow-disturbed left and the undisturbed right common carotid artery (LCA and RCA) in C57BL/6 mice. We found 62 and 523 genes that changed significantly in LCA endothelium compared to the RCA by 12hr and 48hr post-ligation. The array results for 44 genes of 46 were validated by qPCR including well-known shear-responsive genes, *Klf2*, *eNOS*, and *BMP4*, and numerous novel mechanosensitive genes including *Lmo4, klk10* and *dhh.* Lmo4 protein was specifically expressed in the flow-disturbed mouse aortic arch and in human coronary endothelium in an asymmetric pattern. Comparison of *in vivo*, *ex vivo*, and *in vitro* endothelial gene expression profiles indicates that numerous *in vivo* mechanosensitive genes appear to be lost or dysregulated during culture. Gene ontology analyses show that disturbed flow regulates genes involved in cell proliferation and morphology by 12hr, followed by inflammatory and immune responses by 48hr. *In*

vivo genome-wide array study using mouse aortic endothelium reveals numerous novel mechanosensitive genes, while confirming previously well-characterized ones. Determining functional importance of these novel mechanosensitive genes may provide important insights into understanding vascular biology and atherosclerosis.

Introduction

Atherosclerosis is an inflammatory disease [1-2] preferentially occurring in arterial regions exposed to disturbed flow characterized by low and oscillatory shear stress, whereas straight arterial regions exposed to stable flow are protected from atherosclerosis[3-4]. Despite the close association between the two, *in vivo* evidence directly linking disturbed flow conditions to atherosclerosis has been scarce.

The differential mechanisms by which disturbed and stable flow promotes and inhibits atherogenesis, respectively, have been a subject of intense study, mostly using cultured endothelial cells [5-8]. To define molecular mechanisms responsible for these changes, investigators have carried out DNA microarray studies using endothelial cells [9-17] and have subsequently identified numerous shear sensitive genes such as kruppel-like factor 2 and 4 (*Klf2, Klf4*), endothelial nitric oxide synthase (*eNOS*), vascular cell adhesion molecule-1 (*VCAM-1*), intercellular adhesion molecule-1 (*ICAM-1*), bone morphogenic protein 4 (*BMP-4*), cathepsins and angiopoietin-2 (*Angpt2*) [11, 14, 18-26] Functional studies based on these shear-sensitive genes and their protein products have revealed the critical roles that they play in regulation of inflammation, thrombosis, vascular remodeling, angiogenesis and arteriogenesis[11, 19-22, 26-27]. While these *in vitro* studies have provided critical insights regarding shear sensitive mechanisms in cultured endothelial cells using modeled flow conditions, it cannot be assumed whether identical mechanosensitive

genes and pathways are involved *in vivo* regulating flow-dependent vascular responses and diseases. In addition, given the exquisite sensitivity of endothelial gene expression to various flow conditions, it is quite plausible that many genes could be dysregulated (lost, overexpressed, or modified) during cell culture which is carried out under no-flow condition for extended period. Therefore, it is critical to study how arterial endothelium responds to different flow conditions *in vivo*. However, the adequate pathophysiological animal models enabling acute and reproducible modulation of flow conditions that rapidly lead to atherosclerosis have been lacking.

Recently, we characterized partial carotid ligation as a model of disturbed flow with characteristics of low and oscillatory wall shear stress. Using this model, we showed that disturbed flow caused by carotid partial ligation rapidly induces endothelial dysfunction (by 1 week), robust atheroma formation (by two weeks), and features of advanced lesions such as intraplaque neovascularization (by 4 weeks) in hyperlipidemic mice, directly demonstrating the causal relationship between disturbed flow and atherosclerosis [28] In addition, using carotid arteries of the same mouse model, we developed a novel method of obtaining endothelial RNA samples that are nearly free of contamination of smooth muscle cells and leukocytes [28]. Using this method and the partially ligated mouse carotid arteries, we have shown by qPCR studies that disturbed flow induces pro-inflammatory genes, *ICAM1*, *VCAM1*, and *BMP4*, while significantly down-regulating pro-atherogenic genes *Klf2* and *eNOS* within two days [28]. These findings not only provided the proof-of-concept that disturbed flow rapidly regulates mechanosensitive gene expression, but also demonstrated that sufficient quantity of endothelial RNA could be obtained for genome-wide microarray studies.

Here, we indeed carried out DNA microarray studies using endothelial RNAs obtained from flow-disturbed left common carotid arterial (LCA) and contralateral, undisturbed

right CA (RCA) after 12 or 48hr partial ligation in mice. These results were validated by qPCR and immunostaining. Gene ontology analyses were further carried out demonstrating that disturbed flow initially regulates genes involved in cell proliferation and morphogenesis, followed by regulation of genes controlling inflammation and immune responses at a later time point. Based on the number of genes we confirmed (42 genes), our results predict approximately 55% of the mechanosensitive genes found in our *in vivo* studies are also found in various *in vitro* studies, but the remaining 45% seems to be dysregulated. While the similarity between the *in vitro* and *in vivo* results demonstrate the validity and complementary nature of both systems, the significant difference between them, especially the dysregulated or lost genes in cultured endothelial cells, highlights the critical importance of *in vivo* models in studying flow-dependent vascular biology and atherosclerosis.

Methods

Partial carotid ligation and flow characterization by ultrasound study

All animal studies were performed with Male C57Bl/6 mice according to the approved IACUC protocol by Emory University. Mice (Jackson Laboratories) were partially ligated between 6 to 8 weeks of age as we recently described [28]. Briefly, three of four caudal branches of left common carotid artery (LCA) - left external carotid, internal carotid, and occipital artery - were ligated with 6-0 silk suture while the superior thyroid artery was left intact in anesthetized mice. Six hours post-surgery, each animal was examined by VEVO 770 High-resolution *in vivo* micro-imaging ultrasound system whether the ligation induced low and oscillatory shear stress in LCA with the contralateral RCA as a control [28].

Intimal RNA isolation from carotid arteries

Total RNA from intima were separately obtained from LCA and RCA at 12, 24 and 48 hr post-ligation as we described previously [28]. Briefly, LCA and RCA were quickly flushed (few seconds) with 150 □l of QIAzol lysis reagent (QIAGEN) using 29G insulin syringe into a microfuge tube. The eluate was then used for total intimal RNA isolation using miRNeasy mini kit (QIAGEN).

Microarray Procedures

Total intimal RNAs were obtained from LCA and RCA at 12hr and 48hr post-ligation. Intimal RNAs from three LCAs or RCAs were pooled to obtain ~30 ng total RNA. All RNA samples used for the microarray study passed a quality control test using Agilent BioAnalyze NanoChip. Each sample was linearly amplified by WT-Ovation RNA amplification system (NuGEN) and used for the microarray study using MouseWG-6 v2 Expression BeadChip array with 45,281 probes (Illumina) at the Emory Biomarker Service Center. After hybridization, BeadChips are scanned on the Illumina BeadArray Reader to determine the probe fluorescence intensity. The raw probe intensities were then normalized by the quantile normalization algorithm[29] using the GenomeStudio software from Illumina.

Microarray Data Analysis and Bioinformatics

The microarray data was statistically analyzed by Significance Analysis of Microarrays software (SAM) [30]. The differentially expressed genes between LCA and RCA were identified for those which showed more than 1.5 fold-changes at <10% false discovery rate. The lists of differentially expressed genes were interrogated for statistically significant overrepresented cellular functions and disorders using DAVID analysis and Ingenuity Pathway (IPA) Analysis (Ingenuity Systems).

Quantitative real time PCR (qPCR) validation

Total RNA of each sample was reverse transcribed into cDNA using SuperScript III and random primers (Invitrogen) as we described [28]. Briefly, qPCR was performed on selected genes using Brilliant II SYBR Green QPCR Master Mix (Stratagene) with custom designed primers on a Real-Time PCR System (ABI StepOne Plus). Predesigned TaqMan Gene Expression Assay probes (Applied Biosystems) were also used for some selected genes. All qPCR results were normalized based on 18S RNA expression in each sample. Fold changes between LCA and RCA were determined using the $\Delta\Delta$Ct method [31].

Immunohistochemical staining

Paraffin section immunostaining – Mice were euthanized by CO_2 inhalation and then were pressure-perfused at 100 mmHg with normal saline followed by pressure fixation with a 10% formalin solution. LCA and RCA were collected *en block* with the trachea and esophagus. Paraffin sections (5 μm) were then microwaved for 20 min in citrate buffer (0.1 M, pH 6.0) for BMP4 and Lmo4 staining or in Tris buffer (0.1 M, pH 9.0) for Angpt2 and Jam2 staining. Sections were blocked with 10% donkey serum for 1 hour at room temperature and incubated with primary antibodies specific to BMP4 (5 μg/ml, Biovision), Lmo4 (5 μg/ml, [32-34]), Jam2 (2 μg/ml, R&D System), and Angpt2 (0.4 μg/ml, Santa Cruz) overnight at 4°C in a humidified chamber [18]. To visualize primary antibodies, rhodamine-conjugated secondary antibodies (donkey anti-goat, anti-rat IgG, Jackson) were used for one hour at room temperature. Nuclei were counter stained with Hoechst #33258. All photographs were taken using a Zeiss epi-fluorescent microscope. Paraffin sections of human coronary arteries from patients undergoing heart transplants were obtained with

the patients' consent according to the IRB protocol approved at Emory as described previously[18]. The same staining method used for mouse carotids as described above was used for Lmo4 staining.

En Face staining – Mice were euthanized by CO_2 inhalation and the aortas were pressure-perfused at 100 mmHg with normal saline followed by pressure fixation with a 10% formalin solution. The aortas were carefully dissected *in situ* and the aortic arches and thoracic aortas were dissected and stained with Lmo4 antibody [32-34], followed by rhodamine-conjugated secondary antibodies for 2 hours at room temperature. The aortas were then mounted on glass slides using Vectashield containing DAPI (Vector Laboratories). They were then opened and lesser curvature and the greater curvature of the arch were separated. *En face* images were obtained using a Zeiss LSM 510 META confocal microscope.

Ex vivo tissue culture

Mice were euthanized by CO_2 inhalation and then pressure-perfused with heparinized normal saline. Under sterile conditions, common carotid arteries were harvested and carefully cleaned of perivascular fat. Carotid artery rings (~3 mm) and incubated for 3 to 5 days at 37 °C and 5% CO2 in Dulbecco's Modified Eagle Medium (DMEM) supplemented with 100 U/mL of penicillin and 100 μg/mL of streptomycin and 10% of heat-inactivated fetal bovine serum.

Statistical analysis

Data are presented as mean±SEM. Paired Student's t-test was carried out for all qPCR results of each gene to compare LCA vs. RCA and $p<0.05$ (n=3-5) was considered statistically significant.

Results

Discovery of mechanosensitive genes regulated by disturbed flow in mouse carotid endothelium in vivo.

We carried out a DNA microarray study using Illumina BeadChip array containing 45,281 mouse gene probes and endothelial RNAs obtained from the flow-disturbed LCA and

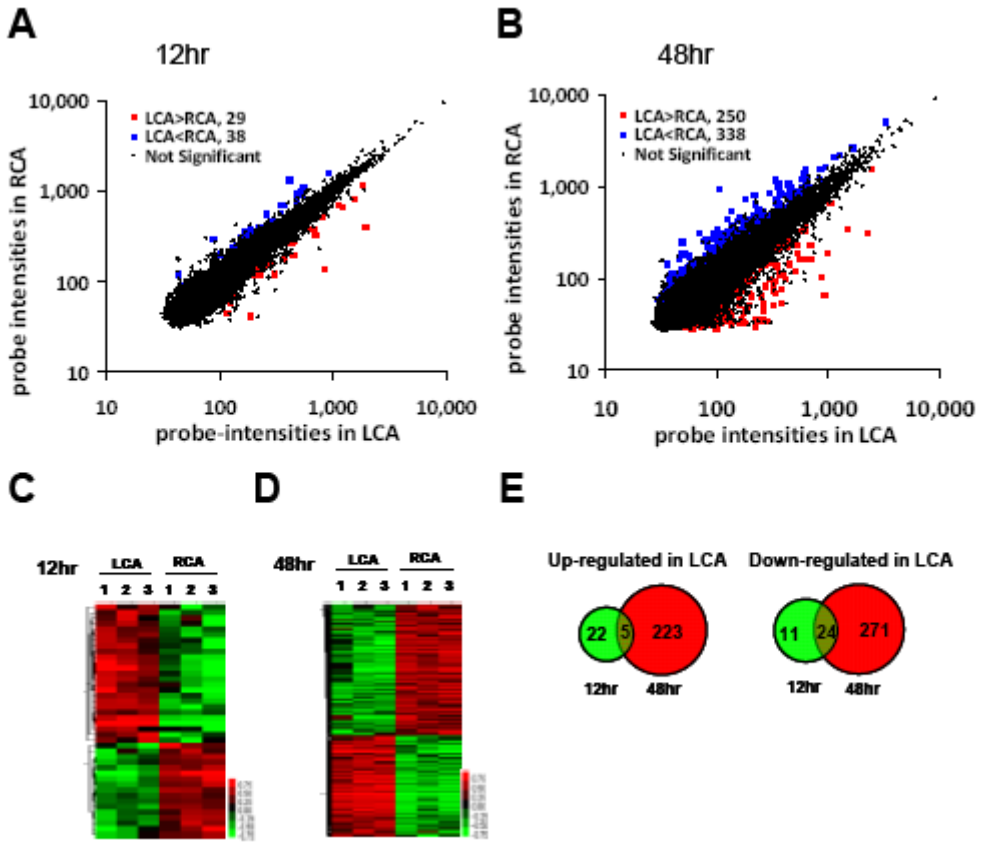

Figure 5.1 Global gene expression profiles in response to disturbed flow in mouse carotid artery endothelium in vivo. *Total RNAs were obtained from intima of mouse left carotid (flow-disturbed LCA) and right carotid (contralateral control, RCA) 12 and 48 hrs post-ligation. Illumina BeadsChips containing 45,281 mouse genome-wide probes were used for the array study. Scatter plots show normalized intensities of each probe under two experimental conditions: LCA vs. RCA at 12hr (**A**) and 48hr (**B**) post-ligation. Genes that were up- (red) or down-regulated (Blue) (≥ 1.5-fold) at the false discovery rate (FDR) (≤ 10%) in LCA compared to RCA are shown. Hierarchical clustering analyses of mechanosensitive genes found in LCA endothelium compared to that of RCA are shown as heat maps (**C** and **D**). Each column represents a single sample pooled from 3 different LCAs or RCAs, and each row represents a single gene probe. Venn diagrams show the temporal effects of disturbed flow on the number of up or down-regulated mechanosensitive genes (**E**).*

contralateral RCA at 12 and 48 hrs following the partial ligation of LCA of C57BL/6 mice. The array results of detected probes were analyzed by the SAM analysis. We found that 67 (29 up- and 38 down-regulated) out of 45,281 gene probes were significantly altered by more than 50% in flow-disturbed LCA endothelium compared to the RCA by 12 hr post-surgery at 10% FDR (Figure 5.1A). By 48 hrs, 588 gene probes (250 up- and 338 down-) were regulated in LCA endothelium compared to the RCA at 10% FDR (Figure. 5.1B). The array data were deposited to Gene Expression Omnibus (GSE 20741). Next, the significantly altered gene probes in individual samples were analyzed by hierarchical clustering to examine the intra- and inter-group variations. As shown in the heat maps (Figure 5.1C and D), the results showed remarkably low variations within each group in both time points, demonstrating the reproducibility of the data. Since a single gene can be represented by multiple gene probes, the number of mechanosensitive genes is smaller than the number of detected probes. By 12 hrs, 27 genes were up- while 35 genes were down-regulated in LCA endothelium (Figure 5.1E). In contrast, by 48 hrs, 228 genes were up- and 295 genes were down-regulated in LCA endothelium (Figure 5.1E). As the Venn diagrams show (Figure 5.1E), 5 of the 27 genes that were upregulated in the LCA endothelium at the early time point (12 hr) continued to be upregulated in the later time point (48 hr). These 5 genes are *Ctgf, Ctps, Fosl2, Got2* and *Lmo4*. In contrast, 24 of 35 genes that were down-regulated at the early time point continued to be down-regulated at the later time point. These genes (Table S2) include some of the well-known shear sensitive genes such as *Klf2* and *Klf4*, while the majority of them have never been reported previously as mechanosensitive genes [11, 20, 26]. These results demonstrated that *in vivo* microarray study not only confirmed some of the well-known shear-sensitive genes reported previously, but also discovered numerous novel mechanosensitive genes.

Validation of mechanosensitive genes by qPCR

We validated the microarray results by two different methods of qPCR. We selected 46 genes (10 up-, 30 down-regulated genes plus 6 additional genes of interests although they were not significantly changed at 48 hr post-ligation) and tested by qPCR assay with either Taqman (28 genes) or SYBR Green (18 genes) method using total endothelial RNAs obtained from LCAs or RCAs collected at three different time points (12hr, 24hr, and 48hr post-ligation). These RNAs used for qPCR validation were entirely independent from those used in the microarray study. First, our qPCR results validated the microarray results for the 48 hr time point for the 10 up- and 30-down regulated genes (Figure 5.2 A vs. B and C vs. D). For 12 hr time point, 3 significantly upregulated genes (*Ctgf*, *Ctps*, and *Lmo4*) were all confirmed by qPCR assays (Figure. 5.2 A,B). In addition, 13 genes that were significantly down-regulated at 12 hr in the microarray study were also validated by the qPCR analysis (Figure. 5.2 C, D). These results demonstrate the superb accuracy of microarray results with few false positives. There were, however, some genes at 12 hr time point that were not shown to be significantly changed according to the array results, but qPCR results showed that they were significantly changed. These include *Hdc*, *Coro1a*, and *Tyrobp* (Figure 5.2B) and those marked with * including *Col4a3*, *Pthlh, Ramp2* (Figure 5.2D). This suggests that our microarray result using 10% FDR underestimated the number of mechanosensitive genes that changed significantly. Therefore, we selected 6 additional genes of interests which did not change significantly according to the microarray result. For example, *Angpt2*, *BMP4*, and *ICAM1* were previously identified as mechanosensitive genes [19, 21-22, 27], but were not included in the list of the significantly changed genes by the microarray (Figure 5.2E). qPCR results showed that *Angpt2*, *BMP4* and *ICAM1* were all significantly upregulated at 24 hr post-ligation and showed similar trend at 48 hr (Figure 5.2E). Overall, to our

complete but pleasant surprise, we were able to validate 16 out of 16 genes at 12 hr and 40 out of 40 genes at 48hr.

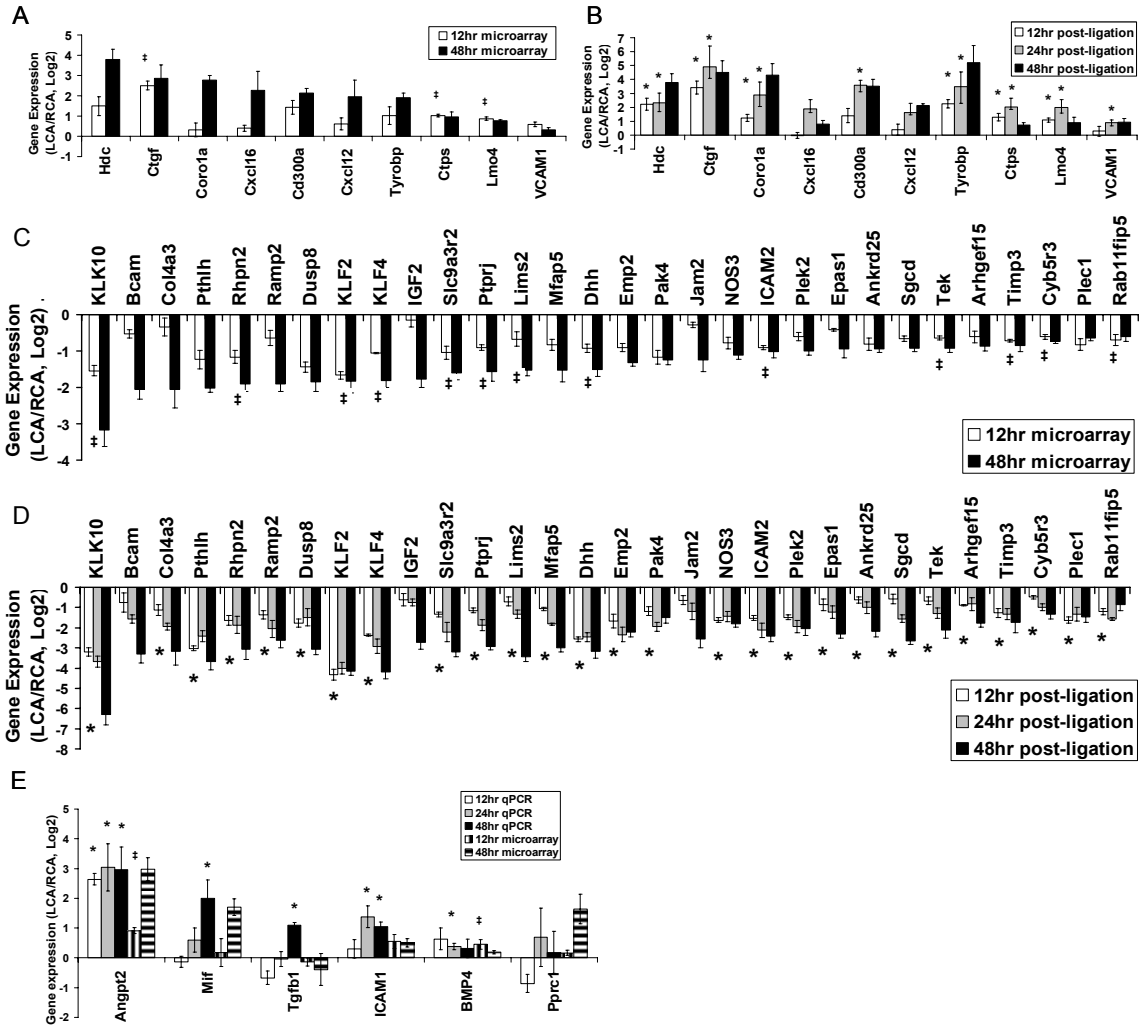

Figure 5.2 Validation of mechanosensitive genes by qPCR. *Total RNAs from intima of LCA or RCA at different time points (12hr, 24hr, and 48hr) after ligation were collected. Differentially expressed genes were selected for qPCR analyses based on 48hr microarray results. Each RNA sample at each time was pooled from 3 different mouse carotid, representing total of 9 (n=3) to 15 (n=5) mice. Microarray results for 12 and 48hr time points are shown as fold-increase (**A**) or fold-decrease (**C**) of genes expressed in LCA over RCA in log2 scale are shown as mean± SEM (n=3). All genes shown in the graphs were significant at FDR <10% at 48hr, while those genes marked with ‡ were also statistically significant (FDR <10%) at 12hr. qPCR validation results for 12, 24, and 48hr time points are shown as fold-increase (**B**) or fold-decrease (**D**) of genes expressed in LCA over RCA in log2 scale are shown as mean± SEM (n=3-5). All genes shown in the graphs were significant (p<0.05) at 48hr, while those genes marked with * were also statistically significant (p<0.05) at 12 and 48 hrs. In **E**, 6 genes of interests that did not reach statistical significance (>10% FDR) were examined by qPCR. Shown are mean± SEM (n=3), ‡ < 10% FDR (LCA vs. RCA) and *< 0.05 (LCA vs.RCA).*

Functional annotation and categorization of mechanosensitive genes

To understand the potential functional importance of the mechanosensitive genes that changed in response to disturbed flow in mouse carotid endothelium, we used the list of the significantly changed genes at 12 and 48 hr groups from the microarray result for functional annotation analysis. Ingenuity Pathway analysis showed that disturbed flow for 12 hrs regulated genes that are involved in the disease processes such as developmental disorder, cancer, immunological and cardiovascular diseases that are mediated through changes in cell growth, proliferation, development, and morphology (Table 5.1). By 48 hrs, disturbed flow induced genes that are involved in inflammatory and immunological diseases while regulating cellular responses such as antigen presentation, cellular movement, and cell-cell signaling (Table 5.1).

Table 5.1. Overrepresented Gene Ontology categories regulated by flow-disturbance in mouse carotid endothelium

12hr post-ligation	*No. of Genes*	*48hr post-ligation*	*No. of Genes*
Diseases and Disorders		**Diseases and Disorders**	
Developmental Disorder	10	Immunological Disease	40
Cancer	9	Inflammatory Response	75
Immunological Disease	4	Connective Tissue Disorders	22
Cardiovascular Disease	6	Inflammatory Disease	36
Respiratory Disease	4	Skeletal and Muscular Disorders	34
Molecular and Cellular Functions		**Molecular and Cellular Functions**	
Cellular Growth and Proliferation	12	Cellular Movement	70
Cellular Development	20	Cell-To-Cell Signaling and Interaction	76
Cell Morphology	12	Antigen Presentation	30
Cellular Function and Maintenance	6	Cellular Function and Maintenance	44
Cell Cycle	4	Cellular Growth and Proliferation	73

Top mechanosensitive genes that are involved in inflammation and cell growth and proliferation are listed in Table 5.2. These include inflammatory cytokines (*Ccl11, Ccl4, Cxcl12, and Cxcl16*), adhesion molecules (*SELL* and *VCAM1*), and transcription factors (*Klf2, Klf4, and Fosl2*) and morphogens (*Id1 and BMP4*). These results suggested that disturbed flow initially induces genes that regulate cell morphogenesis and proliferation, followed by those that regulate inflammatory and immune responses in the later time point.

Table 5.2 Flow-regulated genes involved in inflammation and cell growth and proliferation in mouse carotid endothelium

Gene Symbol	*12hr (LCA/RCA)*	*FDR*	*48hr (LCA/RCA)*	*FDR*	*Gene Symbol*	*12hr (LCA/RCA)*	*FDR*	*48hr (LCA/RCA)*	*FDR*
Inflammation					**Cell growth and proliferation**				
downregulated					***downregulated***				
Col4a3	0.71	>10	0.22	8.1	KLF2	0.30	0.0	0.27	9.1
CCl11	1.41	>10	0.64	8.4	ELN	0.56	0.0	0.57	6.0
CD40	0.88	>10	0.43	8.4	Id1	0.59	0.0	0.45	0.0
CD59a	0.93	>10	0.45	9.9	GNAQ	0.66	0.0	0.76	>10
					PDGFA	0.54	4.8	0.87	>10
upregualted					KLF4	0.48	7.2	0.28	8.1
					KRAS	0.54	7.2	0.63	8.6
Tyrobp	2.93	>10	3.64	0.0	CDKN1A	0.54	7.2	1.31	>10
CCl4	1.78	>10	2.41	3.1	F2RL1	0.56	7.2	0.60	6.9
SELL	1.47	>10	2.82	3.4	Pthlh	0.42	>10	0.24	0.0
Coro1a	2.03	>10	6.70	7.5	IGF2	0.85	>10	0.29	9.1
CD74	1.41	>10	3.80	8.6	MAP3K1	1.03	>10	0.60	8.1
CD300a	2.98	>10	4.31	9.5					
IL17RA	2.01	>10	3.69	9.5	***upregualted***				
Cxcl12	0.96	>10	3.43	9.5					
Cxcl16	1.32	>10	2.20	9.5	BMP4	1.54	0.0	1.37	>10
SPP1	ND	NA	2.11	9.5	FOSL2	1.79	9.6	1.71	3.4
ITGB2	1.15	>10	1.89	9.5	BCL2L11	1.44	>10	1.84	9.5
TNFRSF1B	1.46	>10	1.75	9.5					
IL1RN	ND	NA	1.67	9.5					
VCAM1	1.47	>10	1.53	9.5					

Comparison of microarray data between the in vivo mouse carotid endothelium and in vitro cultured endothelial cells

We next determined whether the 42 validated mechanosensitive genes from mouse carotid endothelium *in vivo* behaved similarly in cultured endothelium *in vitro*. For this study, we compared the *in vivo* mouse microarray and qPCR results to the microarray results of HUVEC exposed to oscillatory shear as opposed to laminar shear for 1 day. Since it is well-known that microarray results obtained by different laboratories significantly vary [35], we first compared our mouse array result obtained by using the mouse Illumina BeadChip array to that of HUVEC microarray using the human Illumina BeadChip array as we recently reported (GSE20739). As shown in Table 5.3, several mechanosensitive genes (e.g. *Klf2, Klf4, NOS3, VCAM1, Ctgf, Angpt2 and BMP4*) in mouse carotid endothelium were also found in the HUVEC microarray results. Of 42 mechanosensitive genes compared here, 23 genes (55%) showed similar responses between the mouse LCA endothelium and OS-exposed HUVEC. Of the remaining 19, 6 genes (14%) were not detected in cultured HUVEC while 13 genes (31%) showed either no change or opposite trends. We hypothesized that those 6 undetectable genes in HUVEC were lost during culture under static condition. To test this hypothesis, we incubated mouse carotid arteries *ex vivo* for 0, 3 and 5 days under sterile conditions, and examined endothelial mRNA levels by qPCR. *Klk10* (down-regulated gene in LCA) became undetectable by 3 days of culture. In contrast, Lmo4 (up-regulated in LCA) levels did not change significantly in the same samples, while *Klf2* and *Dhh* (down-regulated in LCA) were decreased but still detectable at 3 and 5 days during culture (Figure 5.3).

Table 5.3. Comparison of flow-sensitive genes found in vivo mouse carotid endothelium to cultured HUVEC

Gene Symbol	Gene Name	Carotid 48hr (LCA/RCA) microarray	Carotid 48hr (LCA/RCA) qPCR	HUVEC 24hr (OS/LS) microarray	Congruency
Downregulated (LCA/RCA)					
KLK10	kallikrein related-peptidase 10	0.10	0.01	ND	N
Col4a3	collagen, type IV, alpha 3	0.22	0.11	ND	N
Bcam	basal cell adhesion molecule	0.23	0.10	0.81	Y
Pthlh	parathyroid hormone-like peptide	0.24	0.08	0.06	Y
Rhpn2	rhophilin, Rho GTPase binding protein 2	0.26	0.12	1.52	N
KLF2	kruppel-like factor 2	0.27	0.06	0.37	Y
Dusp8	dual specificity phosphatase 8	0.27	0.12	0.70	Y
KLF4	kruppel-like factor 4	0.28	0.06	0.12	Y
IGF2	insulin-like growth factor 2	0.29	0.15	0.78	Y
Slc9a3r2	solute carrier family 9 (sodium/hydrogen exchanger), member 3 regulator 2	0.32	0.11	0.22	Y
Ptprj	protein tyrosine phosphatase, receptor type, J	0.33	0.13	ND	N
Mfap5	microfibrillar associated protein 5	0.33	0.13	0.94	N
Dhh	desert hedgehog	0.36	0.11	0.16	Y
Emp2	epithelial membrane protein 2	0.40	0.22	1.09	N
Lims2	LIM and senescent cell antigen like domains 2	0.40	0.09	0.45	Y
Jam2	junction adhesion molecule 2	0.40	0.17	0.45	Y
Pak4	p21 (CDKN1A)-activated kinase 4	0.42	0.36	0.78	Y
Ramp2	receptor (calcitonin) activity modifying protein 2	0.44	0.16	0.33	Y
NOS3	nitric oxide synthase 3	0.46	0.28	0.25	Y
ICAM2	intercellular adhesion molecule 2	0.48	0.19	1.04	N
Plek2	pleckstrin 2	0.50	0.24	0.52	Y
Epas1	endothelial PAS domain protein 1	0.50	0.20	0.59	Y
Ankrd25	ankyrin repeat domain 25	0.52	0.22	ND	N
Sgcd	sarcoglycan, delta	0.52	0.16	0.97	N
Tek	endothelial-specific receptor tyrosine kinase	0.53	0.23	0.30	Y
Timp3	tissue inhibitor of metalloproteinase 3	0.55	0.30	1.26	N
Arhgef15	Rho guanine nucleotide exchange factor (GEF) 15	0.60	0.29	1.12	N
Cyb5r3	cytochrome b5 reductase 3	0.61	0.40	0.71	Y
Plec1	plectin 1	0.62	0.36	0.50	Y
Rab11fip5	RAB11 family interacting protein 5 (class I) (Rab11fip5), transcript variant 1	0.65	0.56	0.73	Y
Upregulated (LCA/RCA)					
Angpt2	angiopoietin 2	8.44	7.81	4.53	Y
Ctgf	connective tissue growth factor	6.00	22.88	3.87	Y
Cd300a	CD300A antigen	4.31	11.36	ND	N
Tyrobp	TYRO protein tyrosine kinase binding protein	3.64	37.05	ND	N
Cxcl12	chemokine (C-X-C motif) ligand 12	3.43	4.33	1.14	N
Cxcl16	chemokine (C-X-C motif) ligand 16	2.20	1.74	0.56	N
Ctps	cytidine 5'-triphosphate synthase 2	1.98	1.64	1.63	Y
Lmo4	LIM domain only 4	1.70	1.87	1.18	N
VCAM1	vascular cell adhesion molecule 1	1.53	1.90	0.87	N
BMP4	Bone morphogenetic protein 4	1.37	1.25	4.57	Y
					23/42

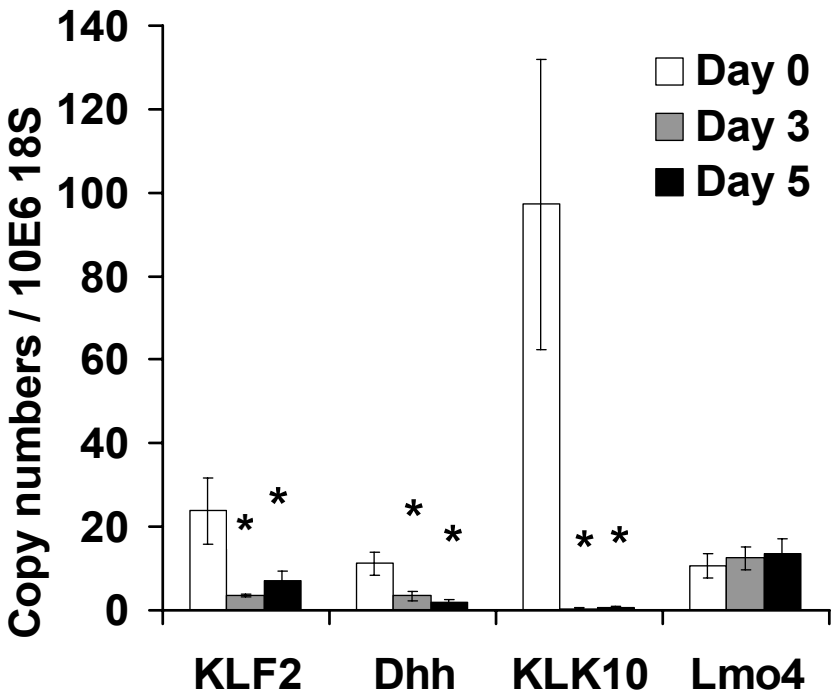

Figure 5.3 Endothelial expression of KLF2, Dhh, and KLK10, but not Lmo4, decreased during ex vivo tissue culture. *Mouse carotid rings were incubated ex vivo in a growth medium. Intimal RNAs were collected after 0, 3, and 5 days during culture. qPCR analyses were carried out to examine the mRNA levels of KLF2, Dhh, KLK10 and Lmo4. mRNA copy numbers were normalized against 18S and were shown as mean± SEM (n=3), * p<0.05 (vs. Day 0).*

Additional qPCR results using cultured HUVEC and iMAEC-WT further confirmed that *Klk10 and Col4a3* genes were not detectable even under shear conditions (Figure 5.4, Figure 5.5). These results are consistent with the notion that expression of some mechanosensitive genes became low or undetectable in cultured endothelial cells, due at least in part, to their no-flow culture conditions.

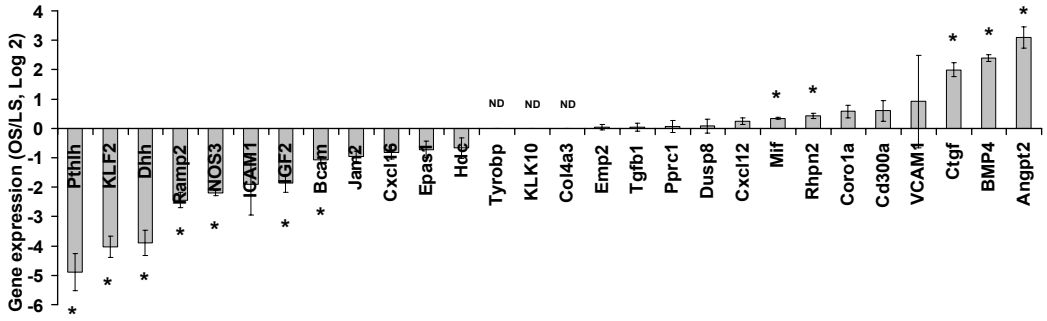

Figure 5.4 Validation of shear-sensitive mRNAs in HUVEC by qPCR. *Total RNAs were collected from HUVECs exposed to OS or LS for 24hr. qPCR analysis was then performed using SYBR green with custom designed primers. mRNA copy numbers were normalized against 18S and are shown as mean± SEM (n=4). p*< 0.05 (OS vs, LS). ND is not detectable in qPCR.*

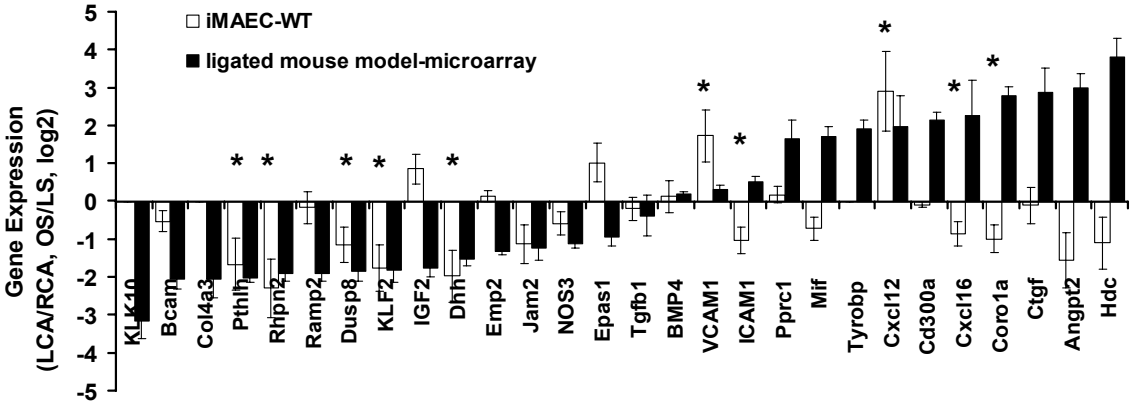

Figure 5.5 Validation of shear-sensitive mRNAs in iMAEC-WT by qPCR. *Total RNAs were collected from iMAEC-WT exposed to OS or LS for 24hr. qPCR analysis was then performed taqman qPCR system with pre-designed primers. mRNA copy numbers were normalized against 18S and are shown as mean± SEM (n=4). p*< 0.05 (OS vs, LS).*

Validation of mechanosensitive genes at the protein level in mouse and human arterial endothelium

To further examine the validity of the mechanosensitive genes discovered *in vivo*, we examined protein expression levels of two newly identified mechanosensitive genes (*Jam2* and *Lmo4*) and two previously known ones (*Angpt2* and *BMP4*). Immunohistochemical staining confirmed that all four protein expression levels changed consistent to the mRNA results (Figure 5.6).

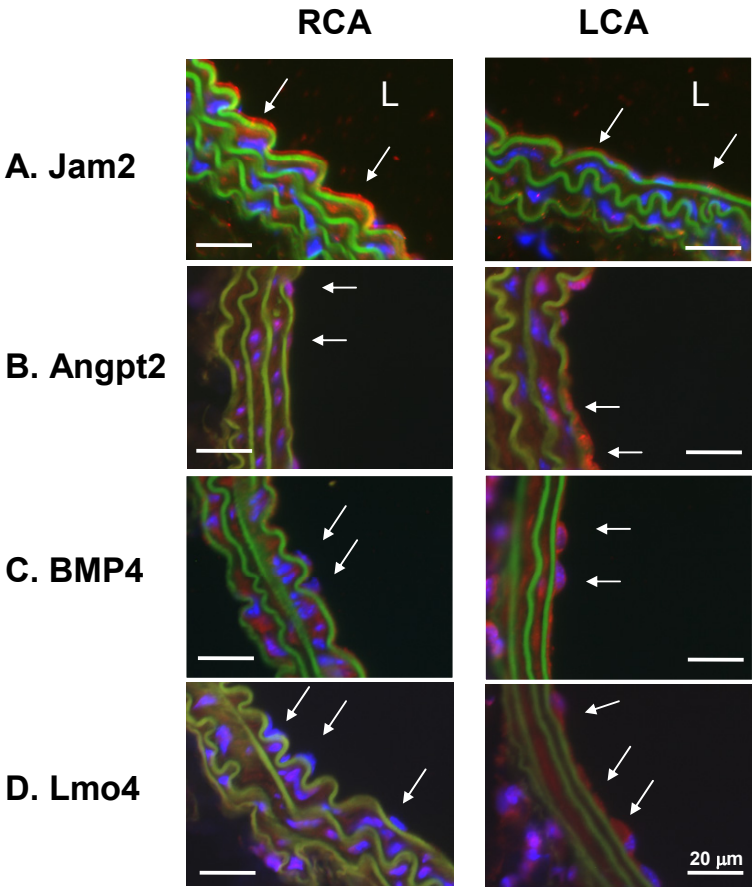

Figure 5.6 Disturbed flow in LCA decreases protein expression of Jam2, while upregulating Angpt2, BMP4, and Lmo4. *C57BL/6 mice underwent partial ligation and LCA and RCA were collected 2 days post-ligation. Paraffin sections were stained with specific antibodies for Jam2 (**A**), Angpt2 (**B**), BMP4 (**C**) and Lmo4 (**D**). Nuclei were counterstained with Hoechst (blue). Arrows indicates the protein expression in endothelial cells and L indicates lumen. Images are representative of n=4 mice*

Disturbed flow in LCA increased expression of Angpt2, BMP4 and Lmo4 proteins in endothelium, while decreasing Jam2 (Figure 5.6). In addition, Lmo4 expression was easily detected in the flow-disturbed lesser curvature (LC) region of aortic arch, but not in stable flow regions in the greater curvature (GC) and thoracic aorta (TA) in C57BL/6 mice (Figure 5.7). Moreover, Lmo4 was specifically expressed in human coronary artery endothelium in an asymmetric pattern (Figure 5.7). These results not only confirm that disturbed flow induced in our mouse carotid model changes protein expression of some of the expected mechanosensitive genes, but also provide further evidence supporting the validity of the newly discovered mechanosensitive genes.

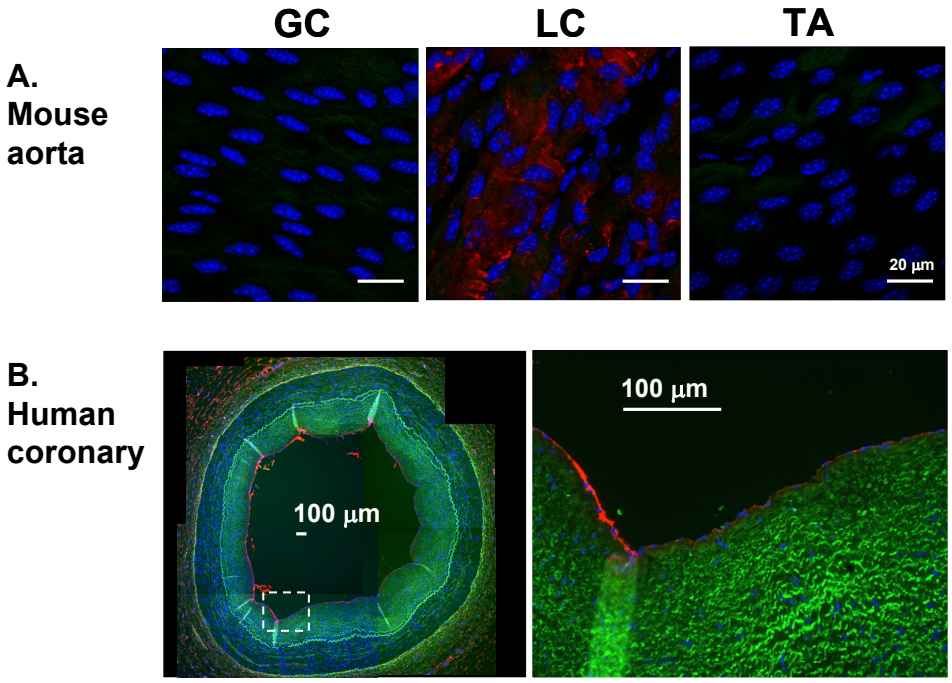

Figure 5.7 Lmo4 is differentially expressed in mouse aortic arch and human coronary artery. *(**A**), En face staining of greater curvature (GC), lesser curvature (LC) of the arch, and the thoracic aorta (TA) was performed with Lmo4 antibody (Red). Blue signal indicates nuclei stained with DAPI; green signal indicates elastic laminae detected by autofluorescence. Shown are representative images of 7 different mice. Paraffin sections of human coronary artery were stained for Lmo4 protein expression (**B**). Overall staining patterns were shown at low magnification (x5) and zoomed views (20X) of the indicated areas (broken box).*

Discussion

Although the association between localization of atherosclerotic lesions and local hemodynamics has been recognized for over several decades, compelling evidence directly demonstrating the cause-and-effect relationship between disturbed flow and atherosclerosis has been scarce, largely due to a lack of adequate animal models to test the hypothesis directly. We recently have provided evidence directly demonstrating that disturbed flow acutely caused by partial ligation of carotid artery rapidly induces endothelial dysfunction in one week and atherosclerosis in two weeks [28]. We further developed a novel method of endothelial RNA extraction from mouse carotid intima [28]. The availability of sufficient quantity of endothelial RNA from mouse carotid intima enabled us to carry out genome-wide high-throughput screening studies to identify mechanosensitive genes in the mouse model. Using this novel method and mouse model, we identified 62 (27 up and 35 down) genes at 12 hr and 523 (228 up and 295 down) genes at 48 hr after the partial ligation that changed significantly in the flow-disturbed LCA endothelium compared to the contra-lateral RCA (Figure 5.1). The microarray results were further validated for 46 selected genes by qPCR (Figure 5.2). To our great surprise, all 40 up- or down-regulated genes tested were validated by qPCR. Four of those genes (two previously known mechanosensitive genes: *BMP4* and *Angpt2*; two novel mechanosensitive genes: *Lmo4* and *Jam2*) were further validated by immunostaining of mouse carotid artery (Figure 5.6). In particular, expression of Lmo4 was validated by immunostaining of mouse aortic arch and human coronary artery (Figure 5.7). Gene ontology analyses using the mechanosensitive genes suggest that disturbed flow rapidly controls expression of endothelial genes involved in cell morphology and proliferation pathways, followed by additional genes regulating inflammatory and immune responses by 48 hrs post-ligation (Table 5.1). These

secondary responses involving inflammation and immune responses may lead to subsequent endothelial dysfunction by 1 week and atherosclerosis by 2 weeks. This is the first *in vivo* genome-wide DNA microarray study revealing the gene expression profiles in response to acute exposure to flow-disturbance using mouse carotid endothelium. While confirming some of the previously known mechanosensitive genes, this study reports numerous novel mechanosensitive genes that have never been reported previously to our knowledge.

Our study uncovers one interesting group of mechanosensitive genes as immediate and persistent responders that were up- or down-regulated by disturbed flow in LCA endothelium both at 12 and 48 hr time points (Table 5.4).

Table 5.4. Common mechanosensitive genes between 12hr and 48hr

Up-regulated (LCA/RCA)	Down-regulated (LCA/RCA)
Ctgf	2310046K01Rik
Ctps	BC020535
Fosl2	Dab2ip
Got2	Dhh
Lmo4	E030024M20Rik
	Eln
	F2rl1
	Icam2
	Id1
	Inmt
	Klf2
	Klf4
	Klk10
	Kras
	Lims2
	Lsr
	P4ha2
	Pdlim2
	Ptprj
	Rab11fip5
	Rhpn2
	Slc9a3r2
	Tek
	Timp3

These genes include some of the well-known mechanosensitive genes such as *Klf2* and *Klf4* [11, 20, 26] while the majority of them have never been reported previously as mechanosensitive genes such as transcription regulators *Lmo4, Fosl2,* and *Id1*. These early and persistent responders could represent the primary mechanosensitive genes that respond immediately to disturbed flow in endothelium, potentially playing a key role in vascular biology and atherosclerosis.

Lmo4 (LIM-only protein 4) is a potential oncogene and associated with growth, migration and invasion of breast cancer cells [32-34]. In our study, we found that Lmo4 expression is upregulated in disturbed flow regions including mouse LCA endothelium and aortic arch. Interestingly, Lmo4 expression in human coronary artery was found specifically in endothelial cells in an asymmetric manner, consistent with the idea of its flow-dependent expression. Interestingly, oscillatory shear stress stimulates endothelial cell proliferation [36-39] suggesting a potential role for Lmo4 overexpressed in flow-disturbed regions in the pro-atherogenic response.

Previously, several DNA microarray studies have been reported generating the lists of potential mechanosensitive genes using cultured endothelial cells exposed to various shear stress conditions, laminar, pulsatile laminar, oscillatory shear and turbulent flow. In most studies, gene expression profiles in endothelial cells exposed to laminar shear were compared to that of static culture conditions [9-17], while a few compared laminar shear to that of oscillatory or turbulent shear[14, 38, 40], better simulating pathophysiological conditions. These microarray studies have identified many mechanosensitive genes such as *Klf2, Klf4*, *BMP-4*, cathepsins, and *Angpt2* and subsequent studies have revealed functional significance of these mechanosensitive genes in regulation of inflammation, thrombosis, vascular remodeling, angiogenesis and arteriogenesis [11, 19-22, 26-27], demonstrating the critical use of these microarray studies in studying vascular

biology and diseases. Since cultured endothelial cells are prone to phenotypic change during extended culture (no flow condition) and *in vitro* shear conditions cannot exactly replicate *in vivo* conditions, we wanted to examine whether the mechanosensitive genes found in our mouse endothelium *in vivo* were similar or different to those found *in vitro*. Our initial comparison was carried out between the 42 confirmed mechanosensitive genes *in vivo* and our HUVEC array result using the same microarray platform. These comparisons showed that ~55% mechanosensitive genes examined here were conserved while the remaining ~45% were either dysregulated or lost. Similarly, we found that ~50% of the *in vivo* genes were also conserved, while ~50% were not when our *in vivo* data were compared to another independent study recently reported by Conway et. al.[14]. These results demonstrate that approximately half of the mechanosensitive genes found *in vivo* can be confirmed *in vitro*, while the other half may not be found *in vitro* due to phenotypic changes in cultured cells. These findings clearly demonstrate the critical need of *in vivo* models in studying flow-dependent vascular responses and diseases.

Recently, Davies and colleagues have conducted *in vivo* DNA microarray studies using endothelial RNAs obtained directly from the flow-disturbed inner aortic arch and undisturbed flow region of normal pig aorta [35, 41-42]. When we compared our list of 42 confirmed mechanosensitive genes found *in vivo* to that of pig endothelial array result (Table S7), we found only 2 (*Klf4* and *eNOS*) were found in their list. This discrepancy could be due to following reasons: First, this may represent the difference in the acute mouse model vs. chronic pig aorta model. Since pig aortic arch is exposed to chronic changes including flow-disturbance for many months from birth, the observed gene profile changes may be complex and may not be solely attributed to flow-disturbance. On the other hand, we isolated endothelial RNA samples within 12 to 48 hrs following

partial ligation, enabling us to study direct effect of flow-disturbance on endothelial gene expression *in vivo*. Second, while the inner curvature of pig aortic arch is a well-known naturally occurring flow-disturbed region, it may be difficult to identify a distinct region exposed to disturbed flow and to obtain RNA samples from the small area only. In contrast, our mouse carotid artery (LCA) is exposed to flow-disturbance occurring nearly homogeneously along the length of the common carotid artery as we recently demonstrated [28]. Third, unlike our mouse array study using the mouse genome-wide probes, the pig array was carried out against human probes due to the lack of porcine specific arrays. This could have resulted in underestimation of mechanosensitive genes in the pig array study. One advantage of our study using the mouse model is that the identified mechanosensitive genes could easily be further examined for their pathophysiological importance in transgenic or knockout mice.

One caveat of in vivo studies such as ours is the potential contamination of RNAs originating from leukocytes accumulated in the carotid intima or medial smooth muscle cells. However, as we have recently demonstrated, our intimal RNA isolation method is free of markers of smooth muscle cells (α-SMA) and leukocytes (CD11b) as determined by qPCR [28]. In addition, we did not find discernible CD11b positive staining in the intima of LCA and RCA within two days of partial ligation [28], although we found them in the adventitia [28]. This was the reason that we limited our experimental time points to 12 and 48 hrs to prevent potential contamination of infiltrating cells in the LCA intima. Furthermore, we examined whether additional markers of infiltrating leukocytes in our microarray results. CD3, CD4, CD28, CD11b, CD43, CD16 and CD56 are either not detectable or not significantly different between LCA and RCA, suggesting there is no obvious contamination of T cells, B cells or macrophages in our RNA samples. While we cannot completely rule out the possibility of infiltrating cells affect our gene lists, we

are especially confident for those mechanosensitive genes such as well-known *Klf2*, *Klf4*, *eNOS* and the novel *Jam2*, *Klk10* and *Dhh* that are highly expressed in the contralateral RCA, but that are decreased in flow-disturbed LCA.

In summary, we have carried out *in vivo* genome-wide microarray studies using mouse carotid endothelium exposed to disturbed flow. From this study, we identified more than 500 mechanosensitive genes that change in response to disturbed flow within 2 days. Based on our analysis of confirmed 42 mechanosensitive genes identified in mouse carotid endothelium, we estimate ~50% of the *in vivo* mechanosensitive genes are novel while the rest confirms the previous results reported in cultured endothelial cells. These findings suggest that while the *in vitro* flow studies are valid and play important roles in studying detailed mechanistic studies, it highlights the critical and unique need of *in vivo* models to study vascular biology and diseases since many of the mechanosensitive genes are lost or dysregulated during culture. These novel mechanosensitive genes identified in this study need to be further studied to determine their functional importance in cells and animal models in the future. They may provide novel therapeutic and diagnostic targets of vascular diseases such as atherosclerosis.

References

1. Ross R. Atherosclerosis--an inflammatory disease. *N Engl J Med*. 1999;340:115-126

2. Libby P. Inflammation in atherosclerosis. *Nature*. 2002;420:868-874

3. Ku DN, Giddens DP, Zarins CK, Glagov S. Pulsatile flow and atherosclerosis in the human carotid bifurcation. Positive correlation between plaque location and low oscillating shear stress. *Arteriosclerosis*. 1985;5:293-302

4. VanderLaan PA, Reardon CA, Getz GS. Site specificity of atherosclerosis: Site-selective responses to atherosclerotic modulators. *Arterioscler Thromb Vasc Biol*. 2004;24:12-22

5. Berk BC. Atheroprotective signaling mechanisms activated by steady laminar flow in endothelial cells. *Circulation*. 2008;117:1082-1089

6. Davies PF, Mundel T, Barbee KA. A mechanism for heterogeneous endothelial responses to flow in vivo and in vitro. *J Biomech*. 1995;28:1553-1560

7. Jo H, Song H, Mowbray A. Role of nadph oxidases in disturbed flow- and bmp4-induced inflammation and atherosclerosis. *Antioxid Redox Signal*. 2006;8:1609-1619

8. Chien S. Effects of disturbed flow on endothelial cells. *Ann Biomed Eng*. 2008;36:554-562

9. Garcia-Cardena G, Comander JI, Blackman BR, Anderson KR, Gimbrone MA. Mechanosensitive endothelial gene expression profiles: Scripts for the role of hemodynamics in atherogenesis? *Ann N Y Acad Sci*. 2001;947:1-6

10. Zhao Y, Chen BP, Miao H, Yuan S, Li YS, Hu Y, Rocke DM, Chien S. Improved significance test for DNA microarray data: Temporal effects of shear stress on endothelial genes. *Physiol Genomics*. 2002;12:1-11

11. Dekker RJ, van Soest S, Fontijn RD, Salamanca S, de Groot PG, VanBavel E, Pannekoek H, Horrevoets AJ. Prolonged fluid shear stress induces a distinct set of endothelial cell genes, most specifically lung kruppel-like factor (klf2). *Blood*. 2002;100:1689-1698

12. Chen BP, Li YS, Zhao Y, Chen KD, Li S, Lao J, Yuan S, Shyy JY, Chien S. DNA microarray analysis of gene expression in endothelial cells in response to 24-h shear stress. *Physiol Genomics*. 2001;7:55-63

13. McCormick SM, Eskin SG, McIntire LV, Teng CL, Lu CM, Russell CG, Chittur KK. DNA microarray reveals changes in gene expression of shear stressed human umbilical vein endothelial cells. *Proc Natl Acad Sci U S A*. 2001;98:8955-8960

14. Conway DE, Williams MR, Eskin SG, McIntire LV. Endothelial cell responses to atheroprone flow are driven by two separate flow components: Low time-average shear stress and fluid flow reversal. *American journal of physiology*. 2010;298:H367-374

15. Himburg HA, Dowd SE, Friedman MH. Frequency-dependent response of the vascular endothelium to pulsatile shear stress. *American journal of physiology*. 2007;293:H645-653

16. Chu TJ, Peters DG. Serial analysis of the vascular endothelial transcriptome under static and shear stress conditions. *Physiol Genomics*. 2008;34:185-192

17. Dai G, Kaazempur-Mofrad MR, Natarajan S, Zhang Y, Vaughn S, Blackman BR, Kamm RD, Garcia-Cardena G, Gimbrone MA, Jr. Distinct endothelial phenotypes evoked by arterial waveforms derived from atherosclerosis-susceptible and -resistant regions of human vasculature. *Proc Natl Acad Sci U S A*. 2004;101:14871-14876

18. Chang K, Weiss D, Suo J, Vega JD, Giddens D, Taylor WR, Jo H. Bone morphogenic protein antagonists are coexpressed with bone morphogenic protein 4 in endothelial cells exposed to unstable flow in vitro in mouse aortas and in human coronary arteries: Role of bone morphogenic protein antagonists in inflammation and atherosclerosis. *Circulation*. 2007;116:1258-1266

19. Sorescu GP, Sykes M, Weiss D, Platt MO, Saha A, Hwang J, Boyd N, Boo YC, Vega JD, Taylor WR, Jo H. Bone morphogenic protein 4 produced in endothelial cells by oscillatory shear stress stimulates an inflammatory response. *J Biol Chem*. 2003;278:31128-31135

20. SenBanerjee S, Lin Z, Atkins GB, Greif DM, Rao RM, Kumar A, Feinberg MW, Chen Z, Simon DI, Luscinskas FW, Michel TM, Gimbrone MA, Jr., Garcia-Cardena G, Jain MK. Klf2 is a novel transcriptional regulator of endothelial proinflammatory activation. *J Exp Med*. 2004;199:1305-1315

21. Tressel SL, Kim H, Ni CW, Chang K, Velasquez-Castano JC, Taylor WR, Yoon YS, Jo H. Angiopoietin-2 stimulates blood flow recovery after femoral artery occlusion by inducing inflammation and arteriogenesis. *Arterioscler Thromb Vasc Biol*. 2008;28:1989-1995

22. Tressel SL, Huang RP, Tomsen N, Jo H. Laminar shear inhibits tubule formation and migration of endothelial cells by an angiopoietin-2 dependent mechanism. *Arterioscler Thromb Vasc Biol*. 2007;27:2150-2156

23. Platt MO, Ankeny RF, Shi GP, Weiss D, Vega JD, Taylor WR, Jo H. Expression of cathepsin k is regulated by shear stress in cultured endothelial cells and is increased in endothelium in human atherosclerosis. *American journal of physiology*. 2007;292:H1479-1486

24. Platt MO, Ankeny RF, Jo H. Laminar shear stress inhibits cathepsin l activity in endothelial cells. *Arterioscler Thromb Vasc Biol*. 2006;26:1784-1790

25. Won D, Zhu SN, Chen M, Teichert AM, Fish JE, Matouk CC, Bonert M, Ojha M, Marsden PA, Cybulsky MI. Relative reduction of endothelial nitric-oxide synthase expression and transcription in atherosclerosis-prone regions of the mouse aorta and in an in vitro model of disturbed flow. *Am J Pathol*. 2007;171:1691-1704

26. Villarreal G, Jr., Zhang Y, Larman HB, Gracia-Sancho J, Koo A, Garcia-Cardena G. Defining the regulation of klf4 expression and its downstream transcriptional targets in vascular endothelial cells. *Biochem Biophys Res Commun*. 2009

27. Sorescu GP, Song H, Tressel SL, Hwang J, Dikalov S, Smith DA, Boyd NL, Platt MO, Lassegue B, Griendling KK, Jo H. Bone morphogenic protein 4 produced in endothelial cells by oscillatory shear stress induces monocyte adhesion by stimulating reactive oxygen species production from a nox1-based nadph oxidase. *Circ Res*. 2004;95:773-779

28. Nam D, Ni CW, Rezvan A, Suo J, Budzyn K, Llanos A, Harrison D, Giddens D, Jo H. Partial carotid ligation is a model of acutely induced disturbed flow, leading to rapid endothelial dysfunction and atherosclerosis. *Am J Physiol Heart Circ Physiol*. 2009;297:H1535-1543

29. Bolstad BM, Irizarry RA, Astrand M, Speed TP. A comparison of normalization methods for high density oligonucleotide array data based on variance and bias. *Bioinformatics*. 2003;19:185-193

30. Tusher VG, Tibshirani R, Chu G. Significance analysis of microarrays applied to the ionizing radiation response. *Proc Natl Acad Sci U S A*. 2001;98:5116-5121

31. Schmittgen TD, Livak KJ. Analyzing real-time pcr data by the comparative c(t) method. *Nat Protoc*. 2008;3:1101-1108

32. Sum EY, Shackleton M, Hahm K, Thomas RM, O'Reilly LA, Wagner KU, Lindeman GJ, Visvader JE. Loss of the lim domain protein lmo4 in the mammary gland during pregnancy impedes lobuloalveolar development. *Oncogene*. 2005;24:4820-4828

33. Sum EY, Segara D, Duscio B, Bath ML, Field AS, Sutherland RL, Lindeman GJ, Visvader JE. Overexpression of lmo4 induces mammary hyperplasia, promotes cell invasion, and is a predictor of poor outcome in breast cancer. *Proc Natl Acad Sci U S A*. 2005;102:7659-7664

34. Visvader JE, Venter D, Hahm K, Santamaria M, Sum EY, O'Reilly L, White D, Williams R, Armes J, Lindeman GJ. The lim domain gene lmo4 inhibits differentiation of mammary epithelial cells in vitro and is overexpressed in breast cancer. *Proc Natl Acad Sci U S A*. 2001;98:14452-14457

35. Passerini AG, Polacek DC, Shi C, Francesco NM, Manduchi E, Grant GR, Pritchard WF, Powell S, Chang GY, Stoeckert CJ, Jr., Davies PF. Coexisting proinflammatory and antioxidative endothelial transcription profiles in a disturbed flow region of the adult porcine aorta. *Proc Natl Acad Sci U S A*. 2004;101:2482-2487

36. Davies PF, Dewey CF, Jr., Bussolari SR, Gordon EJ, Gimbrone MA, Jr. Influence of hemodynamic forces on vascular endothelial function. In vitro studies of shear stress and pinocytosis in bovine aortic cells. *J Clin Invest*. 1984;73:1121-1129

37. Guo D, Chien S, Shyy JY. Regulation of endothelial cell cycle by laminar versus oscillatory flow: Distinct modes of interactions of amp-activated protein kinase and akt pathways. *Circ Res*. 2007;100:564-571

38. Garcia-Cardena G, Comander J, Anderson KR, Blackman BR, Gimbrone MA, Jr. Biomechanical activation of vascular endothelium as a determinant of its functional phenotype. *Proc Natl Acad Sci U S A*. 2001;98:4478-4485

39. Lin K, Hsu PP, Chen BP, Yuan S, Usami S, Shyy JY, Li YS, Chien S. Molecular mechanism of endothelial growth arrest by laminar shear stress. *Proc Natl Acad Sci U S A*. 2000;97:9385-9389

40. Brooks AR, Lelkes PI, Rubanyi GM. Gene expression profiling of human aortic endothelial cells exposed to disturbed flow and steady laminar flow. *Physiol Genomics*. 2002;9:27-41

41. Civelek M, Manduchi E, Riley RJ, Stoeckert CJ, Jr., Davies PF. Chronic endoplasmic reticulum stress activates unfolded protein response in arterial endothelium in regions of susceptibility to atherosclerosis. *Circ Res*. 2009;105:453-461

42. Passerini AG, Shi C, Francesco NM, Chuan P, Manduchi E, Grant GR, Stoeckert CJ, Jr., Karanian JW, Wray-Cahen D, Pritchard WF, Davies PF. Regional determinants of arterial endothelial phenotype dominate the impact of gender or short-term exposure to a high-fat diet. *Biochem Biophys Res Commun*. 2005;332:142-148

CHAPTER 6

DISCOVERY OF MECHANOSENSITIVE MICRORNAS USING IN VIVO MODEL OF MOSUE CAROTID ARTERY ENDOTHELIUM EPXOSED TO DISTURBED FLOW

Summary

As we have shown in Chapter 5, using the partial carotid mouse model, we identified numerous mechanosensitive genes helping us to understand the mechanism by which disturbed flow induces atherosclerosis. However, this type of systematic regulation of gene expression requires different levels of control at the transcriptional, post-transcriptional, and translational levels. MicroRNAs (miRNAs) are a newly discovered group of endogenous small RNAs that regulate gene expression at the post-transcriptional level. They have been shown to regulate cell proliferation, differentiation, apoptosis[1-3], and also play diverse roles in fundamental biological processes in endothelial cells. In this study, we carried out a miRNA microarray analysis to explore the expression profiles of miRNAs in partially ligated mouse carotid endothelium. The microarray results were validated by qPCR and further bioinformatics analyses were performed to discover the correlation between the potential target genes regulated by flow-sensitive miRNAs and those shear-sensitive mRNAs identified in Chapter 5.

Introduction

MicroRNAs (miRNAs) are small non-coding RNAs (~22 nucleotides), which regulate gene expression at the post-transcriptional level[4-5]. They interact with the 3' untranslated region (3' UTR) of specific target mRNAs in a sequence-specific manner[6]. Each miRNA is thought to target multiple mRNAs, resulting in mRNA degradation or translational inhibition[4]. The expression of miRNAs is tightly controlled and highly tissue, developmental stage, and disease specific. In endothelial cells (EC), it has become clear that miRNAs play diverse roles in fundamental biological processes, such as cell migration[7], angiogenesis[8-9], and inflammation[10]. In addition, miR-19a and mir-23b have been shown to play a role in EC proliferation modulated by laminar shear stress in cultured HUVEC[11-12]. However, the role of miRNAs in disturbed flow induced inflammation and atherosclerosis still need to be determined.

Atherosclerosis is an inflammatory disease [13-14] preferentially occurring in arterial regions exposed to disturbed flow, which is characterized by low and oscillatory shear stress, while straight arterial regions exposed to stable flow are protected from atherosclerosis[15-16]. Despite the association between the two, *in vivo* evidence directly linking disturbed flow conditions to atherosclerosis has been scarce. In Chapter 4, we have shown that disturbed flow caused by partial ligation of mouse carotid artery rapidly induces endothelial dysfunction by 1 week, and robust plaques formation by two weeks in hyperlipidemic mice, directly demonstrating the causal relationship between disturbed flow and atherosclerosis [17]. In addition, using carotid arteries from the same mouse model, we have developed a novel method of obtaining endothelial RNA samples that are nearly free of contamination from smooth muscle cells and leukocytes RNAs [17].

In this study, we carried out miRNA microarray analysis on endothelial RNAs obtained from the flow-disturbed left common carotid arterial (LCA) and contralateral right carotid arterial (RCA) after 12 or 48 hours of partial ligation in mouse. The results were validated by qPCR in which 7 of 14 selected miRNAs were confirmed including miR-712, miR-223, miR-195, and miR-30c. We also analyzed the potential target genes of these shear-sensitive miRNAs and made correlations with mechanosensitive mRNAs we described in Chapter 5.

Methods

Partial carotid ligation and flow pattern validation by high resolution ultrasound

All animal studies were performed with male C57Bl/6 mice according to the approved IACUC protocol by Emory University. Mice (Jackson Laboratories) were partially ligated between 6 to 8 weeks of age as recently described [17]. Briefly, three of four caudal branches of left common carotid artery (LCA) - left external carotid, internal carotid, and occipital artery - were ligated with 6-0 silk suture while the superior thyroid artery was left intact in anesthetized mice. Six hours post-surgery, each animal was examined by VEVO 770 High-resolution *in vivo* micro-imaging ultrasound system to determine whether ligation induced low and oscillatory shear stress in the LCA [17].

Intimal RNA isolation from carotid arteries

Total RNA from intima were separately obtained from LCA and RCA at 12, and 48 hr post-ligation as described previously [17]. Briefly, LCA and RCA were quickly flushed with 150 μl of QIAzol lysis reagent (QIAGEN) using 29G insulin syringe into a microfuge tube. The eluate was then used for total intimal RNA isolation using miRNeasy mini kit (QIAGEN).

Microarray Procedures

Total intimal RNAs were obtained from LCA and RCA at 12hr and 48hr post-ligation. Intimal RNAs from three LCAs or RCAs were pooled to obtain ~30 ng total RNA. All RNA samples used for the microarray study passed a quality control test using Agilent BioAnalyze NanoChip. Each sample was linearly amplified by WT-Ovation RNA amplification system (NuGEN) and used for the microarray study using Illumina Mouse v2 MicroRNA expression beadchip array with 656 mouse miRNAs (Illumina) at the Emory Biomarker Service Center. After hybridization, BeadChips are scanned on the Illumina BeadArray Reader.

Microarray Data Analysis and Bioinformatics

The microarray data was statistically analyzed by Significance Analysis of Microarrays software (SAM) [18]. The differentially expressed genes between LCA and RCA were identified for those which showed more than 1.5 fold-changes at <10% false discovery rate. The potential target genes of miRNAs were analyzed by TargetScan.

Quantitative real time PCR (qPCR) validation

Total RNA was polyadenylated and reverse transcribed for use in a two-step qRT-PCR using the NCode miRNA First-Strand cDNA Synthesis and qRT-PCR kits (Invitrogen). The resulting cDNA was subjected to qRT-PCR using the NCode universal reverse primer in conjunction with a sequence-specific forward primer for selected miRNAs. A master mix was prepared for each PCR, which included SYBR GreenER™ qRT-PCR SuperMix, forward primer, Universal qRT-PCR Primer, ROX reference dye and template cDNA. Snorna202 was used as the internal control. The reactions were monitored using a preheated real-time instrument (ABI StepOne Plus). The PCR conditions were

2 min at 50 °C and 10 min at 95 °C, followed by 40 cycles of 95 °C for 4 s and 57 °C for 30 s. Fold changes between LCA and RCA were determined using the ΔΔCt method [19].

Results

Discovery of mechanosensitive miRNAs regulated by disturbed flow in mouse carotid endothelium in vivo.

Table 6.1. miRNAs expression in mouse carotids differentially regulated by ligation.

Gene ID	Gene Name	Fold Change	q-value(%)	Gene ID	Gene Name	Fold Change	q-value(%)
Upregulated by LCA 12hr post lidation				**Downgulated by LCA 12hr post lidation**			
ILMN_3167162	mmu-miR-291b-5p	17.26	0.00	ILMN_3169121	mmu-miR-742*	0.17	0.00
ILMN_3169017	mmu-miR-511	2.29	0.00				
ILMN_3169029	mmu-miR-1186	1.52	0.00				
Upregulated by LCA 48hr post lidation				**Downgulated by LCA 12hr post lidation**			
ILMN_3167999	mmu-miR-712	71.52	0.00	ILMN_3168388	mmu-miR-7a	0.33	0.00
ILMN_3167081	mmu-miR-330*	33.71	0.00	ILMN_3168172	mmu-miR-29b	0.42	0.00
ILMN_3167002	mmu-miR-200c	27.26	0.00	ILMN_3169003	mmu-miR-574-5p	0.61	0.00
ILMN_3169007	mmu-miR-92b	10.29	0.00	ILMN_3168985	mmu-miR-327	0.37	5.03
ILMN_3166979	mmu-miR-223	7.47	0.00	ILMN_3167551	mmu-let-7d	0.54	5.03
ILMN_3169129	solexa-1127-427	5.26	0.00	ILMN_3167191	mmu-miR-195	0.32	7.37
ILMN_3168964	mmu-miR-615-5p	2.64	0.00	ILMN_3167374	mmu-miR-26b	0.50	7.37
ILMN_3167491	mmu-miR-128a:9.1	2.16	0.00	ILMN_3167729	mmu-miR-30c	0.57	7.37
ILMN_3168517	mmu-miR-93	2.12	0.00	ILMN_3168503	mmu-miR-692	0.61	7.37
ILMN_3169147	solexa-284-1594	1.91	0.00	ILMN_3169001	mmu-miR-509-5p	0.62	7.37
ILMN_3167373	mmu-miR-423-3p	1.90	0.00	ILMN_3167681	mmu-miR-221	0.46	8.43
ILMN_3168413	mmu-miR-324-3p	1.78	0.00	ILMN_3168494	mmu-miR-181d	0.61	8.43
ILMN_3167894	mmu-miR-146b	23.34	3.69	ILMN_3166942	mmu-miR-691	0.64	8.43
ILMN_3167032	mmu-miR-699	20.43	3.69	ILMN_3169125	mmu-miR-877*	0.29	10.29
ILMN_3169151	solexa-308-1456	2.16	3.69	ILMN_3168346	mmu-miR-152	0.53	10.29
ILMN_3169111	mmu-miR-138*	1.91	3.69	ILMN_3167224	mmu-miR-30d	0.58	10.29
ILMN_3167774	mmu-miR-210	1.66	3.69	ILMN_3169002	mmu-miR-509-3p	0.60	10.29
ILMN_3169046	mmu-miR-669e	64.09	6.70	ILMN_3169095	mmu-miR-20a*	0.67	10.29
ILMN_3168958	mmu-miR-770-5p	18.56	6.70				
ILMN_3169138	solexa-200-2167	14.35	6.70				
ILMN_3168922	mmu-miR-128	10.88	6.70				
ILMN_3168301	mmu-miR-339-5p	3.20	6.70				
ILMN_3167248	mmu-miR-703	1.59	6.70				
ILMN_3168165	mmu-miR-342-3p	2.67	7.97				
ILMN_3168045	mmu-miR-17*	61.94	9.83				
ILMN_3167226	mmu-miR-296-5p	43.12	9.83				
ILMN_3169104	mmu-miR-93*	2.33	9.83				

We carried out a miRNA microarray study using Illumina BeadChip array containing 656 mouse miRNAs and endothelial RNAs obtained from the flow-disturbed LCA and contralateral RCA at 12 and 48 hours following the partial ligation of LCA of C57BL/6 mice. We found, using a false discovery rate (FDR) of 10%, 45 (27 up- and 18 down-regulated) out of 656 miRNAs were significantly altered by more than 50% in the flow-disturbed LCA endothelium compared to the RCA 48 hours after ligation (Table 6.1). At

12 hours, only 4 miRNAs (3 up- and 1 down-) were differentially regulated in LCA endothelium compared to the RCA (Table 6.1). The significantly altered miRNAs in individual samples were analyzed by hierarchical clustering to examine the intra- and inter-group variations. As shown in the heat maps (Figure 6.1), the samples had slight variations within each group.

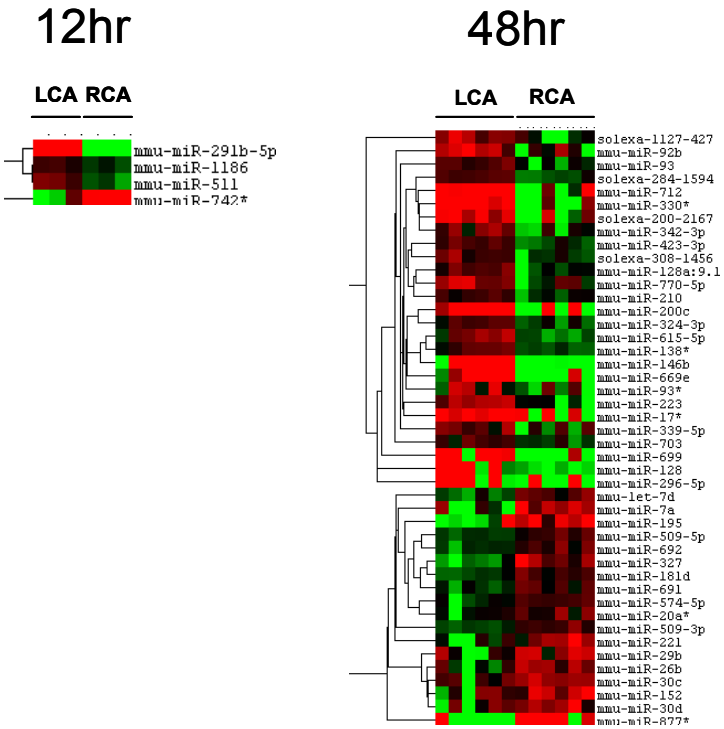

Figure 6.1 The expression of miRNAs in response to disturbed flow in mouse carotid artery endothelium in vivo. *Total RNAs were obtained from intima of mouse left carotid (flow-disturbed LCA) and right carotid (contralateral control, RCA) 12 and 48 hrs post-ligation. Hierarchical clustering analyses of mechanosensitive miRNAs found in LCA endothelium compared to that of RCA are shown as heat maps. Each column represents a single sample pooled from 3 different LCAs or RCAs, and each row represents a single miRNA probe.*

Validation of mechanosensitive miRNAs by qPCR

We selected 14 miRNAs (7 up-, 7 down-regulated genes) plus 9 additional miRNAs of interests that were not significantly changed 48 hours post-ligation and tested by qPCR assay. These RNAs used for qPCR validation were independent from those used in the microarray study. Our qPCR results validated the microarray results for the 48 hr time point for the 3 up- and 3-down regulated genes (Figure 6.2A and B). We also selected 9 additional miRNAs of interests which did not change significantly according to the microarray result, but 5 of 9 miRNAs showed significantly difference between LCA and RCA by qPCR (Figure 6.2C). These results suggest that our microarray result using 10% FDR underestimated the number of mechanosensitive miRNAs that changed significantly.

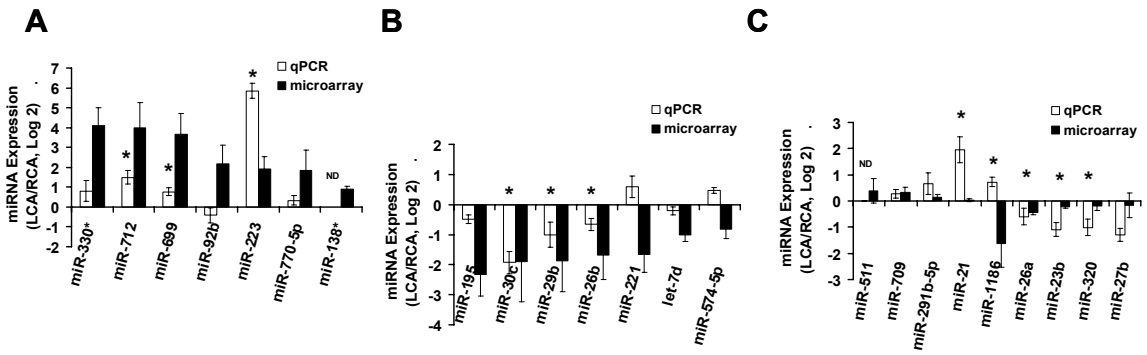

Figure 6.2 Validation of mechanosensitive miRNAs by qPCR. *Total RNAs from intima of LCA or RCA at 48 hours after ligation were collected. Differentially expressed miRNAs were selected for qPCR analyses Each RNA sample was pooled from 3 different mouse carotid, representing total of 9 (n=3) mice. Microarray results and qPCR validation results for 48 hours time points are shown as fold-increase* ***(A)*** *or fold-decrease* ***(B)*** *of miRNAs expressed in LCA over RCA in log2 scale are shown as mean± SEM (n=5~7), *< 0.05 (LCA vs.RCA). In* ***(C)****, 9 miRNAs of interests that did not reach statistical significance (>10% FDR) were examined by qPCR. Shown are mean± SEM (n=5~7), *< 0.05 (LCA vs.RCA).*

For the 12 hour time point, none of the 3 significantly upregulated miRNAs (miR-511, miR-1186, and miR-291-5p) were confirmed by qPCR analysis (Figure 6.3). Overall, we were able to validate 50% of miRNAs at 48 hours while none of the three miRNAs were validated at 12 hours. These results demonstrate the high variability of 12 hour microarray; however, the 48 hour time point microarray results provided a reliable list of mechanosensitive miRNA.

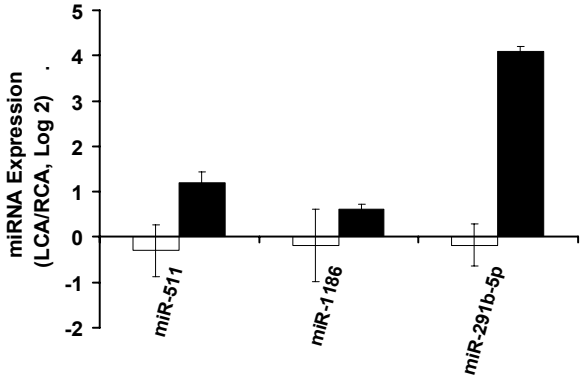

Figure 6.3 Validation of mechanosensitive miRNAs by qPCR. *Total RNAs from intima of LCA or RCA at 12 hour after ligation were collected. Differentially expressed miRNAs were selected for qPCR analyses. Each RNA sample was pooled from 3 different mouse carotid, representing total of 9 (n=3) mice. Microarray results and qPCR validation results for 12 hour time points are shown as fold-difference of miRNAs expressed in LCA over RCA in log2 scale as mean± SEM (n=3)*

Validation of mechanosensitive miRNAs in iMAEC-WT

To further confirm the expression of miRNAs in response to different flow patterns, we used iMAEC-WT cell line, described in Chapter 3, to validate the mechanosensitive miRNAs. iMAEC-WT were exposed to LS or OS for 1 day and the expression level of miRNAs was determined by qPCR. Nineteen miRNAs were selected for qPCR analysis based on the microarray results and highly expressed miRNAs in ECs that have been

reported in literature. In iMAEC-WT exposed to LS or OS, seven of the nineteen selected miRNAs showed significant shear dependence (Figure 6.4). Of those, the response of miR-712, miR-29b, miR-7a, and miR-320 to OS was consistent with the mouse carotid endothelium exposed to acute disturbed flow. In contrast, miR-423-3p showed the opposite response to OS and the remaining 12 miRNAs were not affected by shear stress. These results suggest several mechanosensitive miRNAs exhibit similar responses in iMAEC to OS. The results from iMAEC culture provide a convincing evidence to support our *in vivo* findings using the partial carotid ligation model. These results also suggest the need of an *in vivo* model for studying endothelial biology due to phenotypic drift of cultured endothelial cells.

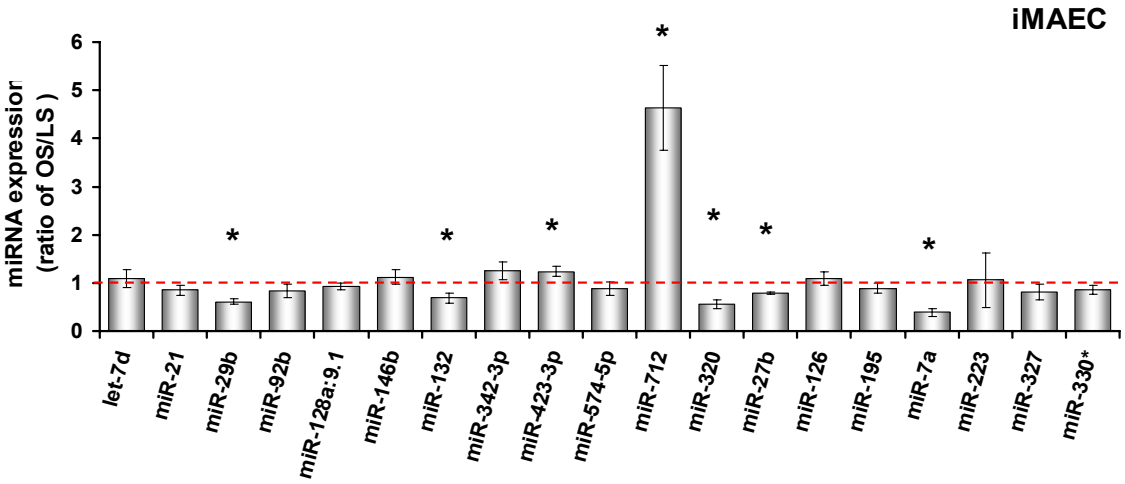

Figure 6.4 Validation of mechanosensitive miRNAs in iMAEC-WT. *Total RNAs from iMAEC-WT exposed to LS or OS for 1 day were collected. Differentially expressed miRNAs were selected for qPCR analyses. qPCR validation results in iMAEC are normalized with snoRNA202 and shown as fold-difference of miRNAs in OS over LS as mean± SEM (n=3)*

The correlation between mechanosensitive miRNAs and mRNAs

To determine the function of mechanosensitive miRNAs identified *in vivo*, and provide the potential regulation network of miRNAs, we utilized bioinformatics approaches to find a correlations between the miRNAs targets and shear-sensitive mRNAs. A extensive *in silico* analysis using TargetScan[20], a program to search for potential targets of mechanosensitive miRNAs, generated thousands of candidates. We compared the resultant list with our mRNA expression profiles from Chapter 5 to provide potential links between mechanosensitive miRNAs to their corresponding mRNAs. The Venn diagrams (Figure 6.5) showed two categories of regulatory correlation. Group A: the predicted targets of upregulated miRNAs and doweregulated mRNAs in LCA (Figure 6.5A), and the group B: the the predicted targets of downregulated miRNAs and upregulated mRNA (Figure 6.5B).

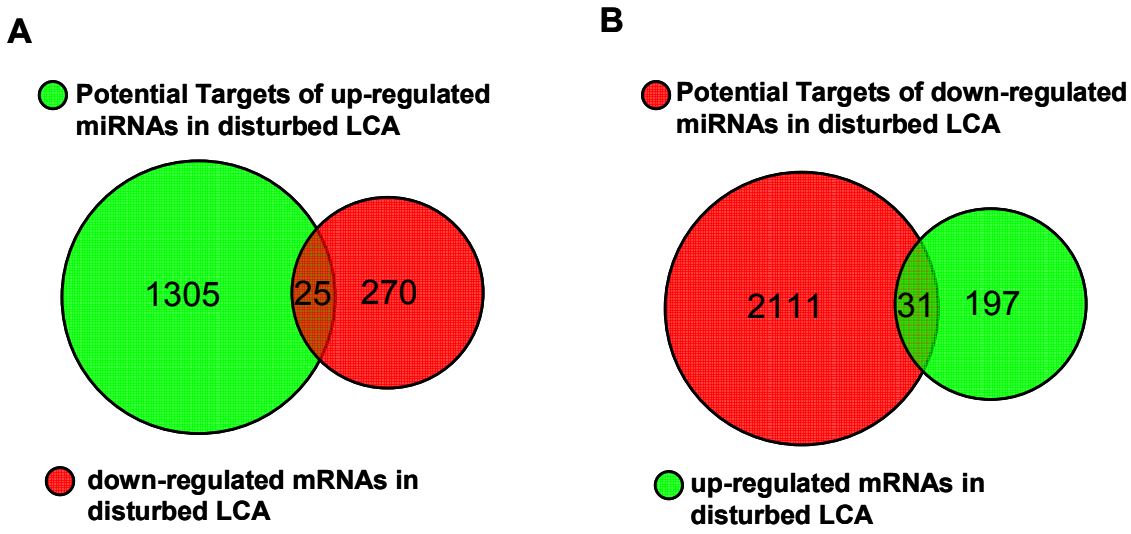

Figure 6.5 Venn diagrams show the correlations between potential targets of mechanosensitive miRNAS and mechanosensitive genes.

There are 25 and 31 genes falling in group A and B, respectively, and the detailed list is shown in Table 6.2. These two groups of genes showed a reverse direction of regulation between miRNAs and mRNAs by disturbed flow. This is consistent with the finding of the inhibitory effect of miRNAs on gene expression. Furthermore, approximately 10 to 15% (25/295, and 31/228) of mechanosensitive mRNAs were found to be potential targets of shear-sensitive miRNAs, suggesting the importance of the mechanosensitive miRNAs and mRNAs identified in this dissertation. In addition, it is believed that miRNA regulates gene expression in a post-transcriptional manner[4-5] which hampers the discovery of its target genes by using the results from mRNA microarray. This suggests our analysis underestimates the number of genes involved in the regulatory network of mechanosensitive miRNAs.

Table 6.2 Predicted mechanosensitive targets and miRNAs

Up-regulated in LCA	Dwon-regulated in LCA	Down-regulated in LCA	Up-regulated in LCA
Targets	**miRNAs**	**Targets**	**miRNAs**
GAS7	miR-29b, miR-let-7d, miR-30c, miR-691, miR-181,miR-30d	PRDM16	miR-712, miR-200c, miR-92b, miR-128
THBS1	miR-let-7d, miR-327, miR-691	HS3ST1	miR-712, miR-200c
TNFRSF1B	miR-let-7d, miR-152	RHPN2	miR-324-3p, miR-92b
SEMA6B	miR-30c, miR-30d	FBLN2	miR-128
PDGFB	miR-29b, miR-let-7d	TBC1D9B	miR-128
PRKCD	miR-26b, miR-181d	ADCY6	miR-128
FRZB	miR-30c, miR-30d	AGRN	miR-128
GOT2	miR-30c, miR-30d	NUMB	miR-146b
GADD45A	miR-152	SORT1	miR-146b
SAMHD1	miR-181d	KCTD10	miR-200c
TXNDC5	miR-181d	SEMA3F	miR-200c
EVI2A	miR-181d	ARL6IP2	miR-223
CXCL12	miR-221	KCTD12	miR-324-3p
BLOC1S2	miR-26b	IGF2	miR-324-3p
ERO1LB	miR-26b	PDLIM2	miR-339-5p
HOMER1	miR-26b	RRAS	miR-699
PDE4B	miR-26b	PKP4	miR-699
CTGF	miR-26b	PCOLCE2	miR-92b
TMEM132A	miR-29b	WWP2	miR-92b
IFI30	miR-29b	NKX2-3	miR-92b
PTPRC	miR-327	KLF2	miR-92b
PREP	miR-327	NAGK	miR-93
RASSF4	miR-692	DUSP8	miR-93
TGFBI	miR-692	MTERFD2	miR-93
GPATCH3	miR-let-7d	RAB11FIP5	miR-93
GOLT1B	miR-let-7d		
MYO1F	miR-let-7d		
SMAP2	miR-let-7d		
TTLL4	miR-let-7d		
BZW2	miR-let-7d		
EDN1	miR-let-7d		

Discussion

Evidence is now emerging showing the importance of miRNAs in cardiovascular disease. However, the particular miRNAs involved in atherosclerosis have not been identified. Here, we provide a list of miRNAs, which expression was altered in response to an acute stimulation of disturbed flow, a key pathophysiological factor in atherosclerosis. These miRNAs may be the regulators of inflammation in the early stages of atherosclerosis. The bioinformatics approaches used in this study, to predict the target genes of mechanosensitive miRNAs, identified two groups of targets which correlate with the profiles of shear-sensitive mRNAs. Because most miRNAs regulate gene expression post-transcriptionally[4-5], the gene number inside the miRNAs regulatory network is underestimated. However, the genes (miRNAs and mRNAs) provided here may play critical roles in cellular inflammation and atherosclerosis.

In this study, we performed miRNA microarray analysis using endothelial RNA collected from the mouse carotid artery exposed to disturbed flow. Our result showed higher variability between samples and groups which resulted in a low validation rate (50%). This may be due to the variability between mice or a limitation in the experimental design. Given the small size of a mouse carotid, we could not obtain a sufficient quantity of total endothelium RNA to carry out our study. The RNA samples, therefore, were amplified before the direct hybridization on microarray chip. On average, the expression levels of miRNAs are lower than that of mRNAs [21-22], which increases the difficulty in detection minimally expressed miRNAs. These limitations may contribute to the increased variability in our study and reduced the reliability of our microarray results.

Identification of miRNA regulated genes is a major obstacle in the bioinformatics field. Current prediction methods of miRNAs targets are based on the seeding region of

miRNAs that bind to the target site(s) on a given mRNA by sequence complementarities. These methods also consider additional pairing by other nucleotides, which has been hypothesized to be important in miRNA binding[23]. The tolerance for extensive mismatches outside the seed region is intended to increase the number of potential targets under miRNA control. However, this also generates a large number of the false-positive targets. In addition, one miRNA can target hundreds of genes and a single gene can be regulated by multiple miRNAs. This makes it difficult to clarify the regulatory network among miRNAs and mRNAs through systematic experiments. In this study, we have narrowed down the number of shear sensitive miRNAs and mRNAs and also provide two lists of genes which show a promising correlation between miRNA and mRNAs. These new targets warrant future investigation to determine their functional importance in atherosclerosis.

Reference

1. Chen CZ, Li L, Lodish HF, Bartel DP. Microrna modulate hematopoietic lineage differentiation. *Science*. 2004;303:83-86

2. Xu P, Guo M, Hay BA. Microrna and the regulation of cell death. *Trends Genet*. 2004;20:617-624

3. Mendell JT. Miriad roles for the mir-17-92 cluster in development and disease. *Cell*. 2008;133:217-222

4. van Rooij E, Olson EN. Microrna: Powerful new regulators of heart disease and provocative therapeutic targets. *J Clin Invest*. 2007;117:2369-2376

5. Small EM, Frost RJ, Olson EN. Microrna add a new dimension to cardiovascular disease. *Circulation*. 2010;121:1022-1032

6. Zhao Y, Srivastava D. A developmental view of microrna function. *Trends Biochem Sci*. 2007;32:189-197

7. Poliseno L, Tuccoli A, Mariani L, Evangelista M, Citti L, Woods K, Mercatanti A, Hammond S, Rainaldi G. Microrna modulate the angiogenic properties of huvecs. *Blood*. 2006;108:3068-3071

8. Suarez Y, Fernandez-Hernando C, Pober JS, Sessa WC. Dicer dependent microrna regulate gene expression and functions in human endothelial cells. *Circ Res*. 2007;100:1164-1173

9. Kuehbacher A, Urbich C, Zeiher AM, Dimmeler S. Role of dicer and drosha for endothelial microrna expression and angiogenesis. *Circ Res*. 2007;101:59-68

10. Harris TA, Yamakuchi M, Ferlito M, Mendell JT, Lowenstein CJ. Microrna-126 regulates endothelial expression of vascular cell adhesion molecule 1. *Proc Natl Acad Sci U S A*. 2008;105:1516-1521

11. Wang KC, Garmire LX, Young A, Nguyen P, Trinh A, Subramaniam S, Wang N, Shyy JY, Li YS, Chien S. Role of microrna-23b in flow-regulation of rb phosphorylation and endothelial cell growth. *Proc Natl Acad Sci U S A*. 2010;107:3234-3239

12. Qin X, Wang X, Wang Y, Tang Z, Cui Q, Xi J, Li YS, Chien S, Wang N. Microrna-19a mediates the suppressive effect of laminar flow on cyclin d1 expression in human umbilical vein endothelial cells. *Proc Natl Acad Sci U S A*. 2010;107:3240-3244

13. Ross R. Atherosclerosis--an inflammatory disease. *N Engl J Med*. 1999;340:115-126

14. Libby P. Inflammation in atherosclerosis. *Nature*. 2002;420:868-874

15. Ku DN, Giddens DP, Zarins CK, Glagov S. Pulsatile flow and atherosclerosis in the human carotid bifurcation. Positive correlation between plaque location and low oscillating shear stress. *Arteriosclerosis*. 1985;5:293-302

16. VanderLaan PA, Reardon CA, Getz GS. Site specificity of atherosclerosis: Site-selective responses to atherosclerotic modulators. *Arterioscler Thromb Vasc Biol*. 2004;24:12-22

17. Nam D, Ni CW, Rezvan A, Suo J, Budzyn K, Llanos A, Harrison D, Giddens D, Jo H. Partial carotid ligation is a model of acutely induced disturbed flow, leading to rapid endothelial dysfunction and atherosclerosis. *American journal of physiology*. 2009;297:H1535-1543

18. Tusher VG, Tibshirani R, Chu G. Significance analysis of microarrays applied to the ionizing radiation response. *Proc Natl Acad Sci U S A*. 2001;98:5116-5121

19. Schmittgen TD, Livak KJ. Analyzing real-time pcr data by the comparative c(t) method. *Nat Protoc*. 2008;3:1101-1108

20. Lewis BP, Shih IH, Jones-Rhoades MW, Bartel DP, Burge CB. Prediction of mammalian microrna targets. *Cell*. 2003;115:787-798

21. Yu Z, Jian Z, Shen SH, Purisima E, Wang E. Global analysis of microrna target gene expression reveals that mirna targets are lower expressed in mature mouse and drosophila tissues than in the embryos. *Nucleic Acids Res*. 2007;35:152-164

22. Zhang BH, Pan XP, Cox SB, Cobb GP, Anderson TA. Evidence that mirnas are different from other rnas. *Cell Mol Life Sci*. 2006;63:246-254

23. Grimson A, Farh KK, Johnston WK, Garrett-Engele P, Lim LP, Bartel DP. Microrna targeting specificity in mammals: Determinants beyond seed pairing. *Mol Cell*. 2007;27:91-105

CHAPTER 7

MICRORNA-663 UPREGULATED BY OSCILLATORY SHEAR STRESS PLAYS A KEY ROLE IN INFLAMMATORY RESPONSE IN HUMAN UMBILICAL VEIN ENDOTHELIAL CELLS

Summary

The mechanisms by which oscillatory shear (OS) induces, while high laminar shear stress (LS) prevents atherosclerosis are still unclear. Here, we examined the hypothesis that OS induces inflammatory response, a critical atherogenic event, in endothelial cells by a miRNA-dependent mechanism. By miRNA microarray analysis using total RNA from human umbilical vein endothelial cells (HUVECs) that were exposed to OS or LS for 24hr, we identified 21 miRNAs that were differentially expressed. Of the 21 miRNAs, 13 were further examined by qPCR, which validated the result for 10 miRNAs (77%). Of those, the most OS-sensitive miRNA, miR-663 (increased by 3-fold) were studied further for its functional significance. Treatment of HUVECs with the miR-663 antagonist (miR-663-LNA) significantly blocked OS-induced monocyte adhesion, but not OS-induced apoptosis, compared to a scrambled LNA control (control-LNA). DNA microarray study performed under the same conditions revealed 32 up-regulated and 3 down-regulated genes, 6 of which are known to be involved in inflammatory response. We identified 10 OS-sensitive miRNAs including miR-663, which plays a key role in OS-induced inflammatory responses by mediating the expression of inflammatory gene network in HUVECs. These OS-sensitive miRNAs may mediate atherosclerosis induced by disturbed flow.

Introduction

Atherosclerosis is an inflammatory disease that occurs preferentially at particular areas of disturbed flow characterized by low and oscillatory wall shear stress (OS) in branched or curved arteries [1-2]. In contrast, straight arterial regions are exposed to high and stable shear stress (LS) and are well protected from atherosclerosis[2]. In Chapter 4, I have shown that disturbed flow caused by partial ligation of mouse carotid artery induce robust atherosclerosis rapidly within two weeks upon high-fat diet[3], directly demonstrating the causal relationship between disturbed flow and atherosclerosis[3]. However, the underlying mechanisms by which disturbed flow induces atherosclerosis still remain unclear.

Gene expression profiles are dramatically altered when endothelial cells (ECs) are exposed to LS or OS. For instance, LS is known to increase expression of atheroprotective genes including kruppel-like factor 2 (*KLF2*), kruppel-like factor 4 (*KLF4)*, and endothelial nitric oxide synthase (*eNOS)*, while OS stimulates inflammation by overexpression of bone morphogenic protein-4 (*BMP4*) and adhesion molecules, such as vascular cell adhesion molecule-1 (VCAM-1), intercellular adhesion molecule-1 (ICAM-1), and E-selectin[4-8]. Numerous studies have shown differences between LS- and OS-dependent gene and protein regulation; however, the detailed mechanisms underlying shear dependent gene expression has not been fully elucidated.

MicroRNAs (miRNAs) are a large class of conserved, noncoding, small RNAs that are typically 18 to 22 nucleotides in length. They repress gene expression post-transcriptionally by interacting with the 3' untranslated region (3' UTR) of specific target mRNAs in a sequence-specific manner[9]. Nearly 800 miRNAs are encoded in the human genome, and each is thought to target multiple mRNAs, resulting in mRNA degradation

or translational inhibition[10]. Studies have demonstrated that miRNAs control cell proliferation, differentiation, and apoptosis[11-13]. In ECs, it has become clear that miRNAs play diverse roles in fundamental biological processes, such as cell migration, angiogenesis, and inflammation. In human ECs, knockdown of Dicer or Drosha, two key enzymes for miRNA biogenesis, *in vitro* causes a decrease in angiogenesis[14-15]. More specifically, let-7f and miR-27b have been shown to exert pro-angiogenic effects[15], while overexpression of miR-221/222 in HUVEC inhibits tube formation, migration, and wound healing in response to stem cell factor, suggesting it has an anti-angiogenic effect[16]. The role of miRNAs in vascular inflammation, in particular in leukocyte activation and infiltration into the vascular wall, has recently been reported. Harris et al. identified miR-126 as an inhibitor of VCAM-1 expression, a mediator of leukocyte adherence to endothelial cells[17]. Finally, Ji et al. found that downregulation of miR-21 decreased neointima formation in the rat carotid artery after angioplasty which indicates that miR-21 is a mediator of neointima lesion formation[18].

Though several insights have been made regarding miRNAs governing cellular responses in ECs, the effect of shear stress on miRNAs expression remains unclear. Recently, Chien S. and colleagues showed that miR-19a and mir-23b were upregulated by laminar shear compared to static control demonstrating that miRNAs play roles in EC proliferation modulated by shear stress [19-20]. Given the differential gene regulation between LS and OS, we hypothesized that shear-sensitive miRNAs play critical roles in regulating gene expression and subsequently mediate OS-induced inflammation. To test the hypothesis, we screened the miRNA expression profiles of human umbilical vein endothelial cells (HUVEC) exposed to LS or OS. Through validation studies, we identified 10 OS-sensitive miRNAs. Next, we determined the functional importance of the most OS-induced miRNA, miR-663, and found its specific role in endothelial

inflammatory response, but not in apoptosis, through the alteration of ICAM-1 but not VCAM-1 expression. We then carried out an additional genome-wide array study to discover the potential target genes of miR-663. This DNA microarray study identified 35 potential miR-663 targets, which include a network of inflammatory genes and transcription factors such as *KLF4*. Collectively, these results suggest that OS induces inflammatory responses in ECs by altering miRNA expression such as upregulation of miR-663, which in turn mediate expression of network of genes.

Methods

Cell Culture and Shear Studies

HUVEC were purchased from BD biosciences, cultured in M199 media (Cellgro) with 20% fetal bovine serum (FBS, Hyclone), and used between passage 5 and 6. Confluent cells were exposed to unidirectional LS (15 dyn/cm^2) or OS (± 5 dyn/cm^2 at 1 Hz frequency) for 24 hr using a cone-and-plate shear device as described by us previously[8, 21].

Microarray Analysis of miRNA Expression and qPCR validation

Total RNA was isolated with the miRNeasy Mini Kit (QIAGEN) using HUVEC exposed to LS or OS for 1 day. Microarray assay was performed using a service provider (LC Sciences) as described previously[22]. Briefly, total RNA samples were size fractionated and small RNAs (< 300 nt) were 3'-extended with a poly(A) tail. An oligonucleotide tag was then ligated to the poly(A) tail for fluorescent dye staining; two different tags (for Cy3 and Cy5 dyes) were used in dual-sample experiments. Hybridization was performed overnight on a μParaflo microfluidic chip (Chip ID miRHuman 12.0 version, LC

Sciences). After the fluorescence images were collected, the ratio (Cy3/Cy5, log2 transformed, balanced) and *p*-values were calculated using Student t-test. Significant signals were those with less than 0.05 *p*-values. We then validated the array data by qPCR. Briefly, the isolated total RNA was polyadenylated and reverse transcribed for use in a two-step qPCR using the NCode miRNA First-Strand cDNA Synthesis and qRT-PCR kits (Invitrogen). The resulting cDNA was subjected to qPCR using the NCode universal reverse primer in conjunction with a sequence-specific forward primer for selected miRNAs. A master mix was prepared for each PCR, which included SYBR GreenER™ qPCR SuperMix, forward primer, Universal qPCR Primer, ROX reference dye and template cDNA. RNU6B was used as the internal control. The reactions were monitored using a preheated real-time instrument (ABI StepOne Plus). The PCR conditions were 2 min at 50 °C and 10 min at 95 °C, followed by 40 cycles of 95 °C for 4 s and 57 °C for 30 s.

HUVEC transfection with miR-663-LNA antagonist or pre-miR-663 precursor

HUVECs were transfected with miRCURY LNA (Locked Nucleic Acids) (miR-663 LNA and scrambled miR as a control, Exiqon) or miRNA precursor (pre-miR-663 and pre-miR-control, Ambion) in a dose-dependent manner (from 25nM to 100nM or 10nM to 30 mM, respectively) using Oligofectamine (Invitrogen) as described previously[7]. One day following transfection, cells were exposed to shear stress. The antagonistic efficacy of miRNA-LNA was assayed by qPCR.

Monocyte adhesion assay

One day post-transfection, HUVECs were exposed to OS or LS for 1 day and monocyte adhesion was determined using THP-1 cells as we previously described[7-8].

Caspase 3 activity

One day post-transfection, HUVECs were exposed to OS or LS for 1 day and Caspase-3 activity in the cell lysate was then determined by using the Caspase-3 Fluorescent Assay Kit (BD Biosciences) according to the manufacturer's instructions.

Preparation of protein samples and Western blot analysis

Following experimental treatments, cell lysates were prepared and analyzed by Western blot analysis as described previously by us[8]. Equal aliquots of protein samples (20 μg each) were resolved on an SDS-PAGE gel, transferred to a polyvinylidene difluoride membrane and incubated with antibodies specific to ICAM-1, VCAM-1 and Actin (Santa Cruz).

mRNA microarray analysis and qPCR validation

Total RNA samples were extracted using miReasy mini kit (QIAQEN) from HUVECs transfected with miR-663-LNA or control miR-LNA after 24 hr shear exposure (LS or OS). All RNA samples passed quality control using Agilent BioAnalyze NanoChip before the gene chip study was carried out in the Emory Biomarker Service Center at the Emory University. A HumanHT-12 v3 Expression BeadChip array (Illumina) was used in this study and the data was statistically analyzed by SAM (Significance Analysis of Microarrays[23]). The differentially expressed genes were identified as significant if expression level in OS-exposed ECs was different by more than 50% of LS and at the false discovery rate of 10% (*q*-value). Total RNA of each sample was reverse transcribed into cDNA using SuperScript III and random primers (Invitrogen) as we described. Briefly, qPCR was performed on selected genes using Brilliant II SYBR Green QPCR Master Mix (Stratagene) with custom designed primers on a Real-Time PCR System (ABI StepOne Plus). All qPCR results were normalized based on 18S RNA

expression in each sample. Fold changes between samples were determined using the ΔΔCt method[24]

Resutls

Identification of miRNAs differentially regulated by OS and LS

To determine whether miRNA expression is changed in ECs exposed to OS compared to LS, we performed shear stress experiments in cultured HUVECs. We collected total RNA from HUVECs exposed to OS or LS for 1 day, and carried out microarray analysis using μParaflo microfluidic chip containing 856 human miRNA probes. This analysis revealed that 244 miRNAs of the 856 examined were detectable in HUVECs. Of the 244 detected miRNAs, 21 miRNAs (9 higher and 12 lower) were differentially expressed by more than 50% ($p<0.05$) in OS-exposed cells compared to LS (Table 7.1).

Table 7.1 Shear sensitive miRNA

miRNA	Fold change (OS/LS) log2 scale	p-value
hsa-miR-663	2.02	0.005
hsa-miR-1275	0.95	0.015
*hsa-miR-424**	0.42	0.026
hsa-miR-1469	1.66	0.029
hsa-miR-638	1.79	0.031
hsa-miR-421	0.95	0.032
hsa-miR-939	1.64	0.043
hsa-miR-149*	2.51	0.046
hsa-miR-1231	1.89	0.049
hsa-miR-151-3p	-0.54	0.005
hsa-miR-320a	-1.03	0.006
hsa-miR-320c	-1.08	0.006
hsa-miR-320d	-1.18	0.006
has-miR-139-5p	-1.87	0.008
hsa-miR-320b	-1.20	0.019
hsa-miR-192	-1.41	0.023
hsa-miR-125a-3p	-0.84	0.023
hsa-miR-191	-0.19	0.027
hsa-miR-194	-1.12	0.033
hsa-miR-195	-0.54	0.032
hsa-miR-27b	-0.89	0.048

Verification of shear-sensitive miRNAs by qPCR

To validate the microarray data, qPCR was used as an independent measure of miRNA expression. Of the 21 miRNAs identified by the array result, we selected top 13 based on their potential abundance and fold-stimulation as determined by the microarray data (Table 7.1). In addition, we also examined miR-126 expression since it is a well-known endothelial specific miRNA[17] although it was not shear-sensitive in our array result. Ten miRNAs of the 13 examined were confirmed by qPCR results as OS-sensitive (Figure 7.1). These include miR-663, miR-1275, and miR-638 that were up-regulated, while miR-320a,b,c, miR-151-3p, miR-195, miR-27b, and miR-139-5p that were down-regulated by OS compared to LS in HUVECs. As expected, miR-126 was highly expressed in ECs but its level was not altered by OS compared to LS.

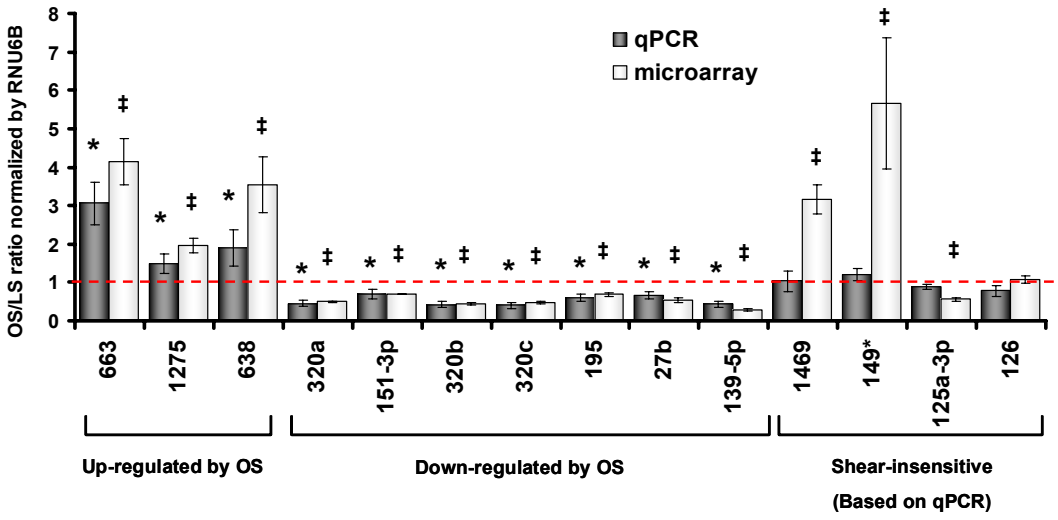

Figure 7.1 Validation of shear-sensitive miRNAs by qPCR. *HUVECs were exposed to LS or OS for 24 hr, and total RNA was collected for miRNAs expression analysis either by microarray or qPCR. miRNAs expression were normalized by RNU6B and were shown as mean± SEM (n=4 for qPCR and n=3 for microarray), * p<0.05 (OS vs LS by qPCR), and ‡<0.05 (OS vs LS by microarray)*

Modulation of miR-663 expression in HUVECs

Since miR-663 expression was the most OS-sensitive miRNA, we decided to study its functional significance in ECs. Two approaches were used to modulate miR-663 expression: 1) inhibition of miR-663, we transfected HUVECs with miR-663-LNA or control-LNA, 2) overpression of miR-663, HUVECs were transfected with pre-miR-663 or pre-miR-control. Transfection of miR-663-LNA decreased while pre-miR-663 increased endogenous miR-663 level in a concentration-dependent manner (Figure 7.2A, 7.3A). Furthermore, miR-663-LNA (100nM) significantly inhibited OS-induced miR-663 expression (Figure 7.2B), demonstrating that this is an efficient approach to inhibit miR-663 in HUVECs. In addition, pre-miR-663 (10 nM) dramatically increased miR-663 expression both in LS and OS condition (Figure 7.3B).

miR-663 plays an important role in OS-induced monocyte adhesion but not in apoptosis of endothelial cells.

To test whether miR-663 plays a key role in endothelial function, we examined whether miR-663-LNA prevents two well-characterized OS-induced events in endothelial cells: inflammation[7-8] and apoptosis[25] as measured by monocyte adhesion and caspase-3 activity assays, respectively. As shown previously, exposure of HUVECs to OS increased monocyte adhesion to ECs by more than 4-fold compared to that of LS in cells treated with control-LNA (Figure 7.2C). However, miR-663-LNA treatment significantly inhibited OS-induced monocyte adhesion by ~70% of the control-LNA group. Next, we examined the effect of miR-663-LNA on OS-induced caspase-3 activity. As expected, OS exposure significantly increased caspase-3 activity compared to LS in HUVEC treated with control LNA. Unlike monocyte adhesion study, however, miR-663-LNA did not affect OS-induced caspase-3 activity.

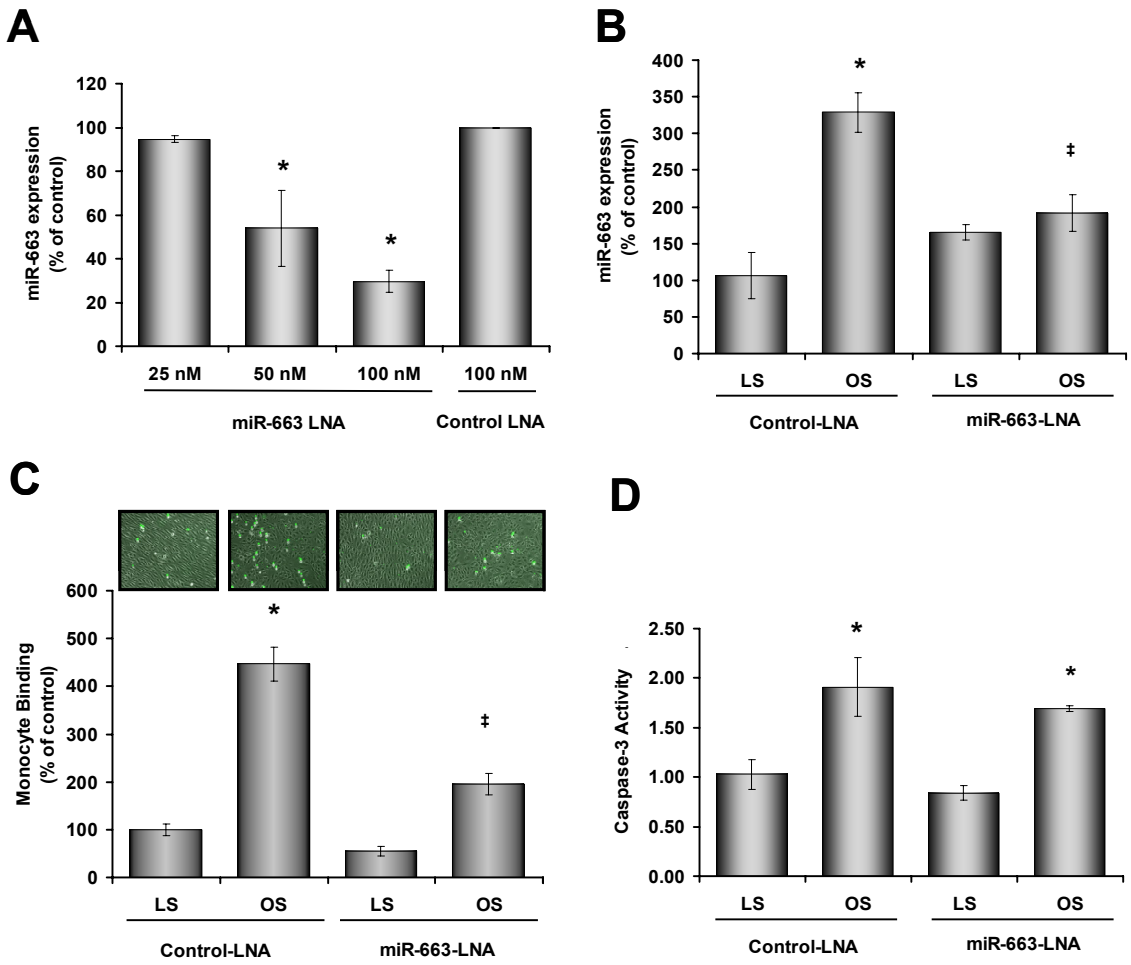

Figure 7.2 Inhibition of miR-663 by miR-663-LNA mediates OS-induced monocyte adhesion to ECs without affecting endothelial apoptosis. *A, Endogenous miR-663 expression is inhibited by miR-LNA transfection. HUVECs were transfected with miR-663-LNA at 25nM, 50nM, and 100nM. As a control, Control-LNA (100nM) was also transfected. miR-663 expression was assayed by qRT-PCR and normalized by RNU6B. Data shown as mean± SEM (n=3), * p<0.05 vs. control group. B, miR-663-LNA inhibits OS-induced miR-663 expression. HUVECs were transfected with miR-663-LNA or Control-LNA (100 nM) one day before shear exposure (LS or OS for 24 hr). miR-663 expression was assayed by qRT-PCR and normalized by RNU6B. Data shown as mean± SEM. * p<0.05 vs Control-LNA in LS-exposed cells and ‡<0.05 vs Control-LNA in OS-exposed cells. C, miR-663 mediates OS-induced monocyte adhesion. One day before shear experiments (LS or OS, 24hr), ECs were transfected with control miR-LNA or miR-663-LNA (100nM). After shear, monocyte adhesion assay was performed. Representative images are shown and quantified results are shown as mean± SEM (n=3), * p<0.05 vs Control in LS-exposed cells and ‡<0.05 vs Control OS-exposed cells. D. miR-663 does not mediate OS-induced caspase-3 activation. Transfected HUVECs with control LNA or miR-663-LNA were exposed to OS or LS for 1 day, and caspase-3 activity was determined using the cell lysate. Data shown as mean± SEM. * p<0.05 vs control-LNA in LS-exposed cells.*

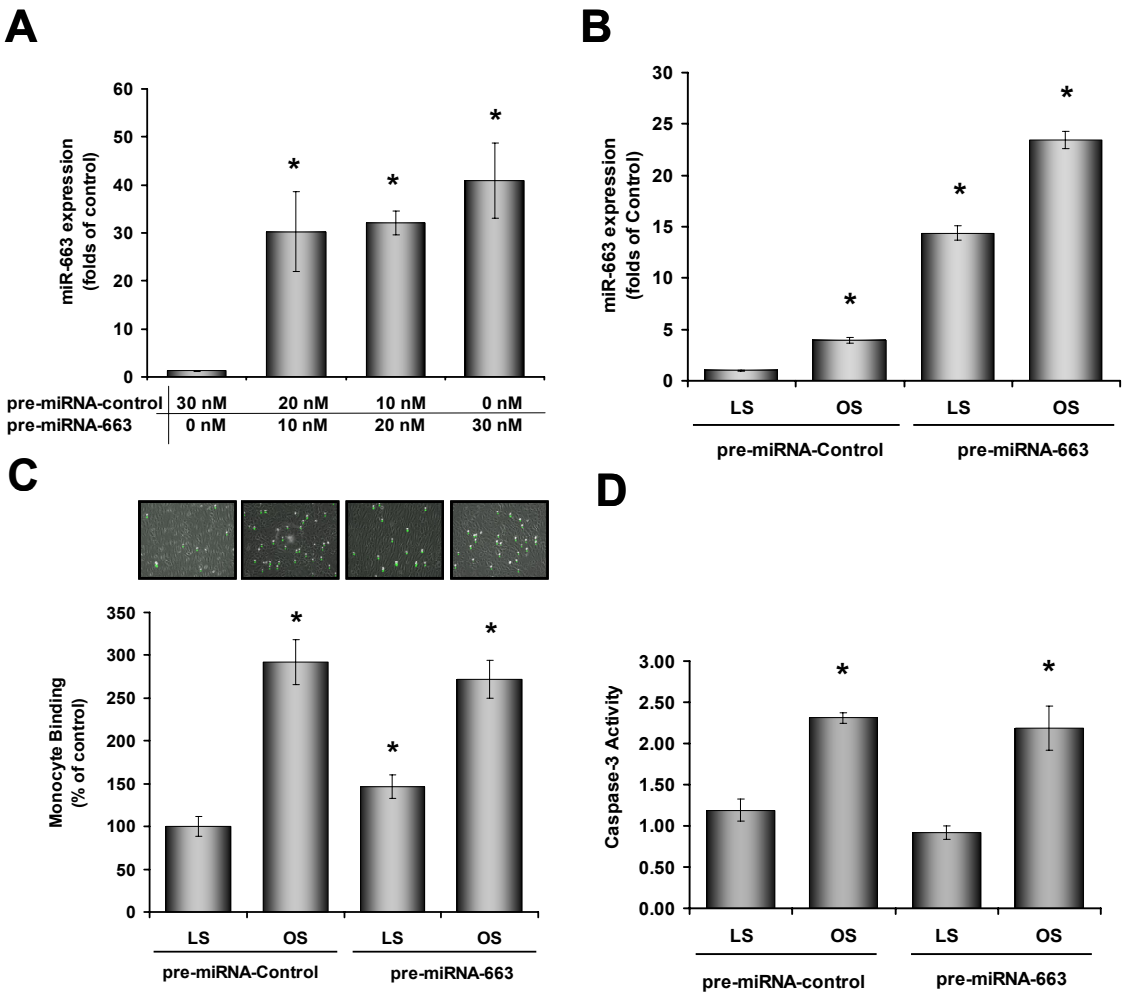

Figure 7.3 Overexpression of miR-663 partially induced monocyte adhesion to ECs without affecting endothelial apoptosis *A, Endogenous miR-663 expression is increased by pre-miRNA transfection. HUVECs were transfected with pre-miR-663 at 10nM, 20nM, and 30nM. miR-663 expression was assayed by qRT-PCR and normalized by RNU6B. Data shown as mean± SEM (n=3), * p<0.05 vs. control group. B, pre-miR-663 increases miR-663 expression under shear condition. HUVECs were transfected with pre-miR-663 or pre-miR-control (10 nM) one day before shear exposure (LS or OS for 24 hr). miR-663 expression was assayed by qRT-PCR and normalized by RNU6B. Data shown as mean± SEM. * p<0.05 vs pre-miR-control in LS-exposed cells. C, pre-miR-663 partially induced monocyte adhesion under LS conditon. One day before shear experiments (LS or OS, 24hr), ECs were transfected with pre-miR-663 or pre-miR-control (10nM). After shear, monocyte adhesion assay was performed Representative images are shown and quantified results are shown as mean± SEM (n=3), * p<0.05 vs pre-miR-control in LS-exposed cells. D. miR-663 does not mediate OS-induced caspase-3 activation. Transfected HUVECs with pre-miR-663 or pre-miR-control (10nM) were exposed to OS or LS for 1 day, and caspase-3 activity was determined using the cell lysate. Data shown as mean± SEM. * p<0.05 vs pre-miR-control in LS-exposed cells.*

In addition, we also performed a DNA fragmentation assay, another assay for cell apoptosis, to examine whether miR-663 is not involved in apoptosis. Again, as expected, DNA fragmentation significantly elevated in OS treated cells compared to LS, but miR-663-LNA didn't affect OS-induced DNA fragmentation (Figure 7.4). These results suggest that miR-663 has a specific role in OS-induced inflammatory pathway, but not in apoptosis pathway. Moreover, overexpression of miR-663 in EC exposed to LS partially increased monocyte adhesion (Figure 7.3C) but didn't affect LS-inhibited caspase activity (Figure 7.3D). These further support that the expression of miR-663 mediates monocyte adhesion modulating by shear stress.

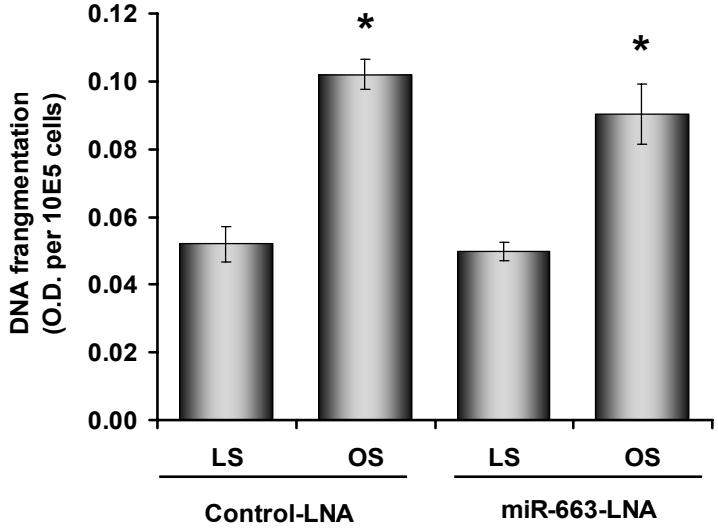

Figure 7.4 miR-663 does not mediate OS-induced DNA fragmentation. *BrdU labeled HUVECs were transfected with control LNA or miR-663-LNA (100 nM) and exposed to OS or LS for 1 day, DNA fragmentation by ELISA assay was determined using the fraction of cell cytosol. Data shown as mean± SEM. * p<0.05 vs Control-LNA in LS-exposed cells.*

miR-663 specifically altered ICAM-1 but not VCAM-1 expression in ECs

To investigate how miR-663 regulated monocyte adhesion, we examined whether miR-663 regulates the expression of adhesion molecules, such as ICAM-1 and VCAM-1, in

ECs transfected with miR-663. As shown in Figure 7.5, miR-663-LNA significantly decreased ICAM-1 protein expression while VCAM-1 was not affected, suggesting a potential mechanism that the effect of miR-663 on OS-induced monocyte adhesion could be mediated by ICAM-1. However, the total protein expression of ICAM-1 didn't show significant difference between LS and OS (Figure 7.5) and failed to correlate to OS-induced monocyte adhesion.

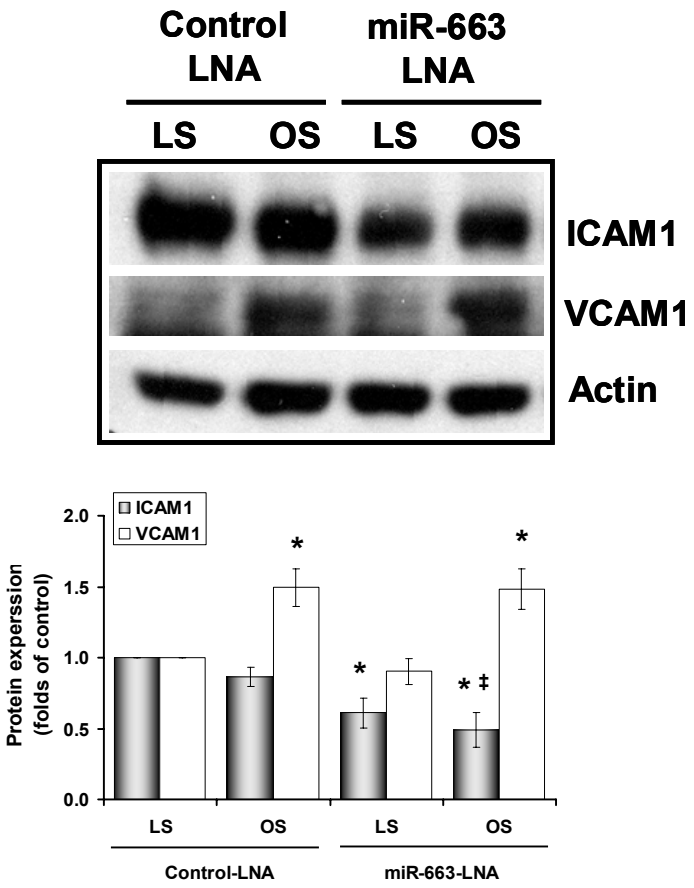

Figure 7.5 miR-663-LNA inhibits ICAM-1 but not VCAM-1 expression *HUVECs were transfected with miR-663-LNA or Control-LNA (100 nM) one day before shear exposure (LS or OS for 24 hr). Total protein were collected and protein expression of ICAM-1 and VCAM-1 were examined by Western blot. Quantatification of the blot were shown as mean± SEM. * p<0.05 vs Control-LNA in LS-exposed cells and ‡<0.05 vs Control-LNA in OS-exposed cells.*

miR-663 doesn't involved TNF-α-induced monocyte adhesion as well as ICAM-1 expression.

To test whether miR-663 is specifically in OS-induced cellular inflammation, we performed a control experiment to examine the role of miR-663 in cytokine-induced EC inflammation. TNF-α dramatically induced monocyte adhesion by 8 folds (Figure 7.6) and increased ICAM-1 and VCAM-1 expression robustly. However, miR-663-LNA didn't affect TNF-α induced monocyte adhesion and adhesion molecules expression (Figure 7.6), demonstrating the specific role of miR-663 in OS- but not cytokine-induced EC inflammation.

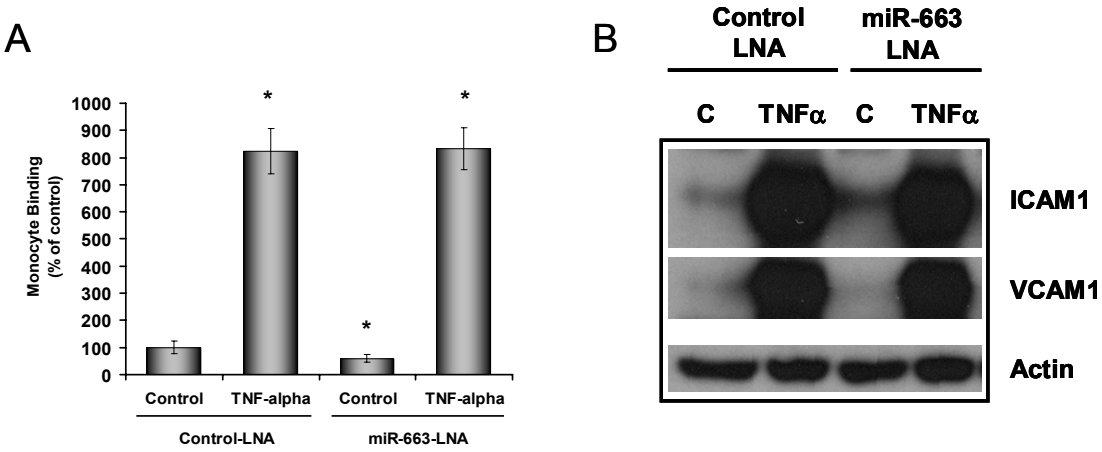

Figure 7.6 A, miR-663 does not mediate TNF-α-induced monocyte adhesion. *One day before TNF-α treatment, HUVECs were transfected with control miR-LNA or miR-663-LNA (100nM). TNF-α (40ng/ml) treated cells were incubated for overnight (16hr), and then monocyte adhesion assay was performed. Representative images are shown and quantified results are shown as mean± SEM (n=3), * p<0.05 vs Control in LS-exposed cells.* ***B****, HUVECs were transfected with miR-663-LNA or Control-LNA (100 nM) one day before TNF-α treatment (40ng/ml, 16hr). Total protein were collected and protein expression of ICAM-1 and VCAM-1 were examined by Western blot.*

miRNA-663 altered mRNA expression in ECs exposed to OS

The function of miR-663 has not been reported previously. Given the role of miR-663 in OS-induced inflammation, the potential target of miR-663 appears to be adhesion molecules. However, since miR-663-LNA significantly inhibited ICAM-1 but not VCAM-1 expression as shown in Figure 7.5, the sequence of miR-663 is not complementary to ICAM-1 3'-UTR, suggesting that ICAM-1 can not be the direct target of miR-663. In addition, extensive *in silico* analysis using web-based programs including TargetScan[26] and MiRanda[27] to search for potential targets of miR-663 produced no obviously identifiable pro-inflammatory genes. These results suggested that miR-663 may regulate a network of genes, rather than a single or a small number of target genes to regulate inflammatory response.

To test this hypothesis, we performed an additional genome-wide microarray to identify mRNAs regulated by miR-663 in HUVECs exposed to OS. ECs were transfected with control miR-LNA or miR-663-LNA and then subjected to either LS or OS for 24 hr. Microarrays were then performed using Illumina BeadChip and the data was first analyzed to determine gene expression profiles between cells exposed to OS and LS in control or miR-663-LNA-treated cells. As shown in the heatmap (Figure 7.7A), OS up-regulated 1,056 gene probes, while down-regulating 903 compared to LS in control-LNA treated ECs. Among those, many well-studied shear-sensitive genes identified in our array data, including *KLF2, KLF4, eNOS, BMP4, ANGPT2* and *VCAM-1*, were shown to be regulated in a manner that is consistent with the previous findings [4, 6], providing confidence on our current array data. We also found that 854 and 698 gene probes were up- and down-regulated, respectively, by OS compared to LS in miR-663-LNA treated ECs (detailed gene list has been deposited to GEO:GSE20739).

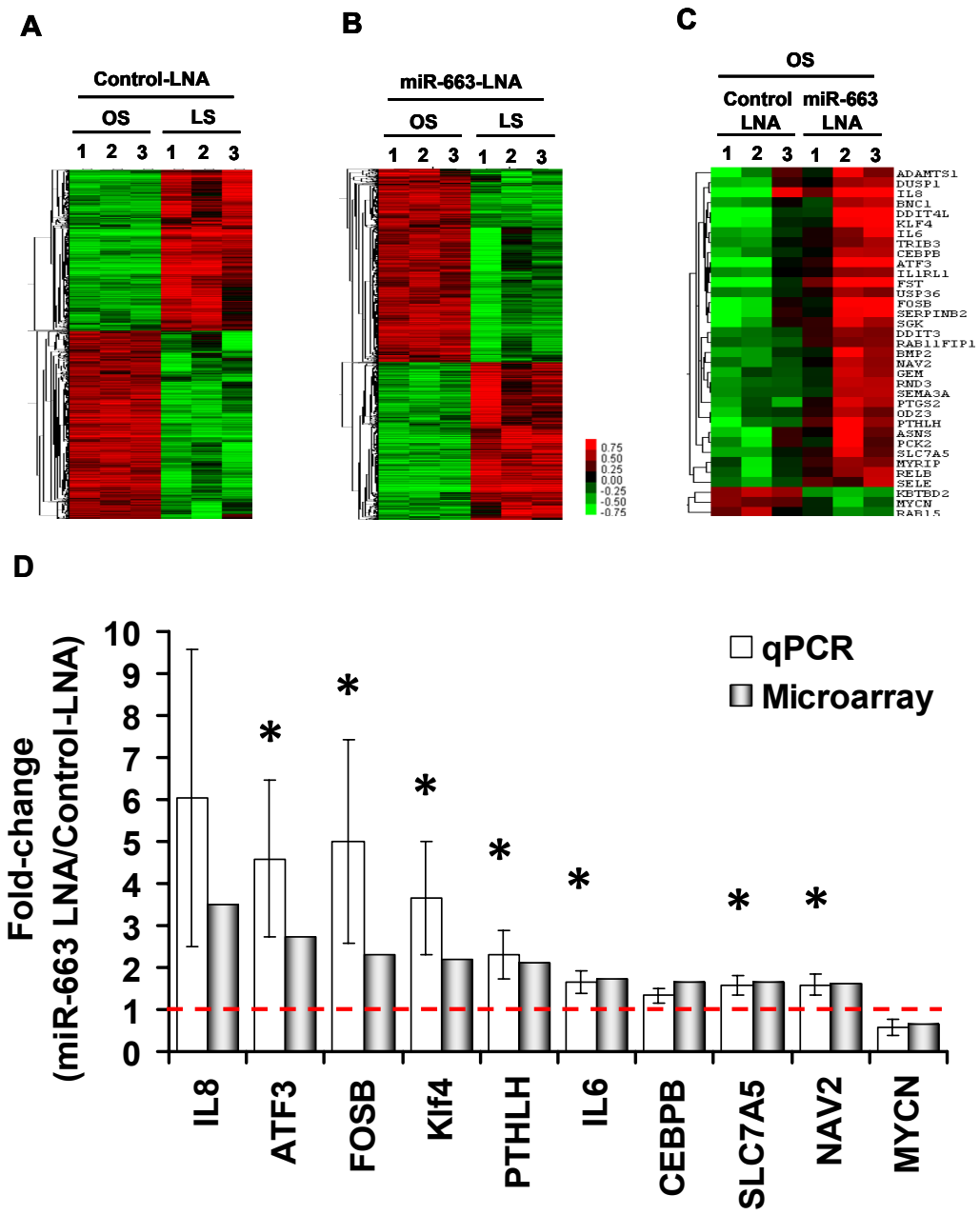

Figure 7.7 Gene expression profiles and qPCR validation between LS and OS either treated with control miR-LNA or miR-663-LNA. *HUVECs were transfected with miR-663-LNA or control miR-LNA (100 nM) one day before shear experiments (LS or OS for 24 hr). Total RNA samples were collected and microarray analysis was performed. Genes which showed differential expression are presented as heatmaps. Expression of shown genes is significantly different in between the two compared groups in A, B and C by more than 50% at a false discovery rate of 1% (A and B) and 10% (C). D, Selected genes were further validated by qPCR. mRNAs expression were normalized by 18S and were shown as mean± SEM (n=3 for qPCR * p<0.05 (miR-663 LNA-OS vs Control LNA-OS),*

More importantly, we determined which gene expression was altered in a miR-663-dependent manner by comparing miR-663-LNA treated ECs to control-LNA group under OS condition. The results showed that 32 genes were up-regulated, while 3 were down-regulated in cells treated with OS and the miR-663 inhibitor (Figure 7.7C and Table 7.2). In contrast, only one gene exhibited a significant difference between control-LNA and miR-663-LNA in LS-treated ECs (Table 7.2). Next, we validated the microarray results by qPCR. We selected 10 genes for qPCR validation using total RNA samples from ECs treated with miR-663-LNA or Control-LNA under OS condition. Our qPCR results validated 7 of 10 genes including *KLF4, FOSB, SLC7A5* and *NAV2* (Figure 7.7).

Table 7.2 mRNAs regulated by miR-663

Gene ID	Gene Name	Fold Change (miR-663-LNA/Control-LNA)	q-value(%)	Direct target predicted by TargetScan
Gene differentially expressed (control-LNA-OS vs miR-663-LNA OS)				
ILMN_1668125	MYRIP	1.55	0.00	No
ILMN_1676984	DDIT3	1.53	0.00	No
ILMN_1692219	RAB11FIP1	1.52	0.00	No
ILMN_1700081	FST	5.48	6.14	No
ILMN_1666733	IL8	3.51	6.14	No
ILMN_2374865	ATF3	2.72	6.14	No
ILMN_1696537	DDIT4L	2.61	6.14	No
ILMN_1751607	FOSB	2.31	6.14	Yes
ILMN_2137789	KLF4	2.20	6.14	No
ILMN_2314169	PTHLH	2.13	6.14	No
ILMN_2150851	SERPINB2	1.97	6.14	No
ILMN_1677511	PTGS2	1.79	6.14	No
ILMN_1702487	SGK	1.78	6.14	No
ILMN_1699651	IL6	1.73	6.14	No
ILMN_1722718	BMP2	1.70	6.14	No
ILMN_1693014	CEBPB	1.65	6.14	Yes
ILMN_1811258	RELB	1.65	6.14	No
ILMN_1720373	SLC7A5	1.64	6.14	Yes
ILMN_1759513	RND3	1.63	6.14	No
ILMN_1739393	SELE	1.61	6.14	No
ILMN_2399300	NAV2	1.61	6.14	Yes
ILMN_1677092	GEM	1.58	6.14	No
ILMN_1765641	SEMA3A	1.57	6.14	No
ILMN_2336094	ODZ3	1.55	6.14	No
ILMN_1781285	DUSP1	1.53	6.14	No
ILMN_1697227	USP36	1.52	6.14	No
ILMN_1787815	TRIB3	1.52	6.14	No
ILMN_2242900	IL1RL1	1.50	6.14	No
ILMN_1796417	ASNS	1.73	7.52	No
ILMN_1751465	BNC1	1.51	7.52	No
ILMN_1673566	ADAMTS1	1.54	9.52	No
ILMN_1671791	PCK2	1.52	9.52	No
ILMN_1784540	KBTBD2	0.52	0.00	No
ILMN_1731699	RAB15	0.67	10.58	No
ILMN_2219767	MYCN	0.64	10.58	No
Gene differentially expressed (control-LNA-LS vs miR-663-LNA LS)				
ILMN_1784540	KBTBD2	0.52	0	No

Furthermore, we determined which of the 35 genes (32 up-regulated and 3 down-regulated) in OS-treated cells were potential targets of miR-663 by *in silico* analysis using TargetScan (Table 7.2) and MiRanda (data not shown). This analysis revealed 4 of 35 genes are potential direct targets of miR-663: *SLC7A5, NAV2,* and two transcription factors *FOSB* and *CEBPB*. To test our hypothesis whether these 35 genes regulated by miR-663 play a key role in OS-mediated inflammatory response, we carried out DAVID (**D**atabase for **A**nnotation, **V**isualization and **I**ntegrated **D**iscovery) analysis. The functional annotation result showed that inflammatory responses were indeed affected by miR-663 (Table 7.3).

Table 7.3 Functional Annotation for genes regulated by miR-663 under OS condition.

Term	Count	%	*p*-Value
negative regulation of cellular process	13	37.14%	2.31E-06
organ development	13	37.14%	8.50E-06
regulation of cell proliferation	9	25.71%	9.24E-06
negative regulation of cell proliferation	7	20.00%	1.27E-05
inflammatory response	**6**	**17.14%**	4.75E-04
tissue development	6	17.14%	8.15E-04
epidermis development	4	11.43%	0.004192
ectoderm development	4	11.43%	0.005121
negative regulation of cellular metabolic process	5	14.29%	0.010025
regulation of transcription, DNA-dependent	***12***	***34.29%***	0.011825

Moreover, additional cellular processes such as regulation of transcription and cell proliferation were also regulated by miR-663 (Table 7.3). Total of seven transcription factors (*FOSB, CEBPB, DDIT3, ATF3, KLF4, BNC1* and *MYCN)* were identified as direct or indirect targets of miR-663 in OS-treated cells. These results suggest that miR-663 is

a shear-sensitive miRNA, regulating expression of many genes including the transcription factors, which in turn induce inflammatory response in ECs.

Discussion

In this study, we identified 10 OS-sensitive miRNAs in cultured ECs by performing a genome-wide miRNA microarray and subsequent validation by qRT-PCR study (Figure 7.1). We next determined the functional importance of the most OS-sensitive miRNA, miR-663 as a pro-inflammatory gene. Using the miR-663 specific inhibitor (mi663-LNA), we found that miR-663 specifically mediated OS-induced monocyte adhesion to endothelial cells while it did not have any effect on OS-induced apoptosis (Figure 7.2). This observation was further supported by overexpression of miR-663 which partially induced monocyte adhesion in LS condition. We then performed an additional genome-wide DNA microarray study to identify potential gene targets regulated by miR-663 in HUVECs since ICAM-1 downregualted by miR-663-LNA is not the direct target of miR-663. From the study, we found 35 potential genes regulated (Table 7.2); however, in silico analysis such as Targetscan and MiRanda screening of these 35 genes showed that only 4 genes are predicted to be the potential target of miR-663. Among those miR-663 regulated genes, several are transcription factors, including *KLF4, FOSB*, and *ATF3,* and could subsequently regulate a number of genes that are related to inflammatory responses.

Through microarray analysis, we identified 4 genes (*FOSB, CEBPB, SLC7A5,* and *NAV2*) that were up-regulated in miR-663-LNA treated ECs and were also predicted as potential targets of miR-663 by TargetScan (Table 7.2). These four genes fall in poorly conserved targets category, suggesting the species specificity in this study.

Interestingly, of 1639 potential targets of miR-663 by TargetScan, there are only 34 conserved sites while 2064 poorly conserved sites remain. This could be due to the species-specific expression of miR-663 discovered only in primates (Human, Chimpanzee, and Monkey). *FOSB* and *CEBPB* are transcription factors known to play roles in cell proliferation and inflammatory responses, respectively [28-29]. SLC7A5 acts as a L-type amino acid exchanger[30] and NAV2 (neuron navigator 2) is involved in neuronal development[31]. Since their function in ECs is unclear, further studies need to be conducted. In addition, the rest of the miR-663-regulated genes that were not predicted as direct targets of miR-663 include several more transcription factors. Of note, *KLF4* may play an important role in mediating the effects of miR-663. *KLF2* and *KLF4* are key regulators of endothelial function and are induced by atheroprotective shear stress[32]. Overexpression of KLF4 in human ECs significantly reduced TNF-α induction of E-selectin and VCAM-1, suggesting KLF4 has an anti-inflammatory effect through inhibiting adhesion molecules[33]. Recently, Villarreal et. al. also showed that a significant degree of mechanistic and functional conservation between KLF4 and KLF2[34]. Collectively, these transcription factors have been shown to coordinate transcriptional programs important for vasodilation, anti-inflammation, and anti-thrombotic effect in vascular endothelial cells. Our data shows inhibiting miR-663 with miR-663-LNA restores KLF4 expression in ECs under OS. This warrants further investigation of the role of miR-663 and KLF4 in OS-induced inflammation.

Recently, miR-126 has been shown to regulate VCAM-1 expression while mediating TNF-α-stimulated leukocyte adherence to ECs[17]. In addition, miR-31 and miR-17-3p were shown to regulate E-selectin and ICAM-1, respectively, in TNF-induced ECs[35]. Inhibition of miR-31 or miR-17-3p decreased neutrophil adhesion to ECs. In our study, we have shown miR-663 is involved in OS-induced monocyte binding, and miR-663-LNA

decreases ICAM-1 but not VCAM-1 expression (Figure 7.5). However, the total protein expression of ICAM-1 didn't show significant difference between LS and OS which failed to correlate the monocyte adhesion results. This controversial result has been reported previously[36] and the effect of ICAM-1 on monocyte adhesion seems to be determined by the "effective" ICAM-1located in correct location rather than the total protein level. Collectively, these studies suggested the diverse regulation of miRNAs in a single biological process.

A critical unexplored aspect of miRNA function is the subtlety and complexity of gene regulatory networks. In a setting where one miRNA can regulate hundreds of genes and one gene can be regulated by a number of miRNAs, lack of knowledge in the mechanisms that govern miRNA-mRNA as well as miRNA-miRNA interactions is a major issue. Current prediction methods of miRNAs targets are based on the seeding region of miRNAs that bind to the target site(s) on a given mRNA by sequence complementarities. These methods also consider additional pairing by other nucleotides, which has been hypothesized to be important in miRNA binding[37]. The tolerance for extensive mismatches outside the seed region is indeed to increase the number of potential targets under miRNA control. Unfortunately, this complexity of interactions hinders the discovery of actual miRNA targets. In addition, factors contributing to the control of inducible or repressible miRNA expression and miRNA-coordinated expression with other regulatory molecules are not well-known and need to be investigated. For instance, depleting miRNA 221 and 222 in HUVEC affects the miRNA profile showing 9 up-regulated and 23 down-regulated miRNAs[16]. This observation demonstrates the complex network involving co-expression of miRNAs and transcription factors that can be altered by a single miRNA variations[16]. In our study, we examined 8 shear-sensitive miRNA expressions while knocking down miR-663 under

OS condition. The results showed the minor alteration of those 8 miRNAs, suggesting the complex network between miR-663 and other shear-sensitive miRNAs. Because of this complexity, any individual biological process mediated by miRNA may require a number of different factors that contribute to the final outcome. This type of synergy makes it difficult to identify a single gene as a direct mediator responsible for the effect of miRNA on any given biological function.

In summary, this is the first report identifying oscillatory shear-sensitive miRNAs in HUVECs and demonstrating miR-663 involvement in OS-induced cellular inflammation. We also demonstrate a gene network regulated by miR-663 under OS condition. Given the complexity of miRNA regulatory networks, miRNAs may be better a therapeutic target than mRNAs or proteins. We have recently demonstrated that disturbed flow conditions such as OS are causally linked to atherosclerosis development. The shear-sensitive miRNAs, discovered in this study, could be potential therapeutic targets for the treatment of atherosclerosis.

References

1. Ku DN, Giddens DP, Zarins CK, Glagov S. Pulsatile flow and atherosclerosis in the human carotid bifurcation. Positive correlation between plaque location and low oscillating shear stress. *Arteriosclerosis*. 1985;5:293-302

2. VanderLaan PA, Reardon CA, Getz GS. Site specificity of atherosclerosis: Site-selective responses to atherosclerotic modulators. *Arterioscler Thromb Vasc Biol*. 2004;24:12-22

3. Nam D, Ni CW, Rezvan A, Suo J, Budzyn K, Llanos A, Harrison D, Giddens D, Jo H. Partial carotid ligation is a model of acutely induced disturbed flow, leading to rapid endothelial dysfunction and atherosclerosis. *Am J Physiol Heart Circ Physiol*. 2009;297:H1535-1543

4. Dai G, Kaazempur-Mofrad MR, Natarajan S, Zhang Y, Vaughn S, Blackman BR, Kamm RD, Garcia-Cardena G, Gimbrone MA, Jr. Distinct endothelial phenotypes evoked by arterial waveforms derived from atherosclerosis-susceptible and -resistant regions of human vasculature. *Proc Natl Acad Sci U S A*. 2004;101:14871-14876

5. Dekker RJ, van Soest S, Fontijn RD, Salamanca S, de Groot PG, VanBavel E, Pannekoek H, Horrevoets AJ. Prolonged fluid shear stress induces a distinct set of endothelial cell genes, most specifically lung kruppel-like factor (klf2). *Blood*. 2002;100:1689-1698

6. McCormick SM, Eskin SG, McIntire LV, Teng CL, Lu CM, Russell CG, Chittur KK. DNA microarray reveals changes in gene expression of shear stressed human umbilical vein endothelial cells. *Proc Natl Acad Sci U S A*. 2001;98:8955-8960

7. Sorescu GP, Song H, Tressel SL, Hwang J, Dikalov S, Smith DA, Boyd NL, Platt MO, Lassegue B, Griendling KK, Jo H. Bone morphogenic protein 4 produced in endothelial cells by oscillatory shear stress induces monocyte adhesion by stimulating reactive oxygen species production from a nox1-based nadph oxidase. *Circ Res*. 2004;95:773-779

8. Sorescu GP, Sykes M, Weiss D, Platt MO, Saha A, Hwang J, Boyd N, Boo YC, Vega JD, Taylor WR, Jo H. Bone morphogenic protein 4 produced in endothelial cells by oscillatory shear stress stimulates an inflammatory response. *J Biol Chem*. 2003;278:31128-31135

9. Zhao Y, Srivastava D. A developmental view of microrna function. *Trends Biochem Sci*. 2007;32:189-197

10. van Rooij E, Olson EN. Micrornas: Powerful new regulators of heart disease and provocative therapeutic targets. *J Clin Invest*. 2007;117:2369-2376

11. Chen CZ, Li L, Lodish HF, Bartel DP. Micrornas modulate hematopoietic lineage differentiation. *Science*. 2004;303:83-86

12. Xu P, Guo M, Hay BA. Micrornas and the regulation of cell death. *Trends Genet*. 2004;20:617-624

13. Mendell JT. Miriad roles for the mir-17-92 cluster in development and disease. *Cell*. 2008;133:217-222

14. Suarez Y, Fernandez-Hernando C, Pober JS, Sessa WC. Dicer dependent micrornas regulate gene expression and functions in human endothelial cells. *Circ Res*. 2007;100:1164-1173

15. Kuehbacher A, Urbich C, Zeiher AM, Dimmeler S. Role of dicer and drosha for endothelial microrna expression and angiogenesis. *Circ Res*. 2007;101:59-68

16. Poliseno L, Tuccoli A, Mariani L, Evangelista M, Citti L, Woods K, Mercatanti A, Hammond S, Rainaldi G. Micrornas modulate the angiogenic properties of huvecs. *Blood*. 2006;108:3068-3071

17. Harris TA, Yamakuchi M, Ferlito M, Mendell JT, Lowenstein CJ. Microrna-126 regulates endothelial expression of vascular cell adhesion molecule 1. *Proc Natl Acad Sci U S A*. 2008;105:1516-1521

18. Ji R, Cheng Y, Yue J, Yang J, Liu X, Chen H, Dean DB, Zhang C. Microrna expression signature and antisense-mediated depletion reveal an essential role of microrna in vascular neointimal lesion formation. *Circ Res*. 2007;100:1579-1588

19. Wang KC, Garmire LX, Young A, Nguyen P, Trinh A, Subramaniam S, Wang N, Shyy JY, Li YS, Chien S. Role of microrna-23b in flow-regulation of rb phosphorylation and endothelial cell growth. *Proc Natl Acad Sci U S A*. 2010;107:3234-3239

20. Qin X, Wang X, Wang Y, Tang Z, Cui Q, Xi J, Li YS, Chien S, Wang N. Microrna-19a mediates the suppressive effect of laminar flow on cyclin d1 expression in human umbilical vein endothelial cells. *Proc Natl Acad Sci U S A*. 2010;107:3240-3244

21. Boo YC, Jo H. Flow-dependent regulation of endothelial nitric oxide synthase: Role of protein kinases. *Am J Physiol Cell Physiol*. 2003;285:C499-508

22. Lin Y, Liu X, Cheng Y, Yang J, Huo Y, Zhang C. Involvement of micrornas in hydrogen peroxide-mediated gene regulation and cellular injury response in vascular smooth muscle cells. *J Biol Chem*. 2009;284:7903-7913

23. Tusher VG, Tibshirani R, Chu G. Significance analysis of microarrays applied to the ionizing radiation response. *Proc Natl Acad Sci U S A*. 2001;98:5116-5121

24. Schmittgen TD, Livak KJ. Analyzing real-time pcr data by the comparative c(t) method. *Nat Protoc*. 2008;3:1101-1108

25. Mueller CF, Widder JD, McNally JS, McCann L, Jones DP, Harrison DG. The role of the multidrug resistance protein-1 in modulation of endothelial cell oxidative stress. *Circ Res*. 2005;97:637-644

26. Lewis BP, Shih IH, Jones-Rhoades MW, Bartel DP, Burge CB. Prediction of mammalian microrna targets. *Cell*. 2003;115:787-798

27. Betel D, Wilson M, Gabow A, Marks DS, Sander C. The microrna.Org resource: Targets and expression. *Nucleic Acids Res*. 2008;36:D149-153

28. Milde-Langosch K. The fos family of transcription factors and their role in tumourigenesis. *Eur J Cancer*. 2005;41:2449-2461

29. Li H, Gade P, Xiao W, Kalvakolanu DV. The interferon signaling network and transcription factor c/ebp-beta. *Cell Mol Immunol*. 2007;4:407-418

30. del Amo EM, Urtti A, Yliperttula M. Pharmacokinetic role of l-type amino acid transporters lat1 and lat2. *Eur J Pharm Sci*. 2008;35:161-174

31. Clagett-Dame M, McNeill EM, Muley PD. Role of all-trans retinoic acid in neurite outgrowth and axonal elongation. *J Neurobiol*. 2006;66:739-756

32. Suzuki T, Aizawa K, Matsumura T, Nagai R. Vascular implications of the kruppel-like family of transcription factors. *Arterioscler Thromb Vasc Biol*. 2005;25:1135-1141

33. Methe H, Balcells M, Alegret Mdel C, Santacana M, Molins B, Hamik A, Jain MK, Edelman ER. Vascular bed origin dictates flow pattern regulation of endothelial adhesion molecule expression. *Am J Physiol Heart Circ Physiol*. 2007;292:H2167-2175

34. Villarreal G, Jr., Zhang Y, Larman HB, Gracia-Sancho J, Koo A, Garcia-Cardena G. Defining the regulation of klf4 expression and its downstream transcriptional targets in vascular endothelial cells. *Biochem Biophys Res Commun*. 2009;391:984-989

35. Suarez Y, Wang C, Manes TD, Pober JS. Cutting edge: Tnf-induced micrornas regulate tnf-induced expression of e-selectin and intercellular adhesion molecule-1 on human endothelial cells: Feedback control of inflammation. *J Immunol*. 2010;184:21-25

36. Conway DE, Williams MR, Eskin SG, McIntire LV. Endothelial cell responses to atheroprone flow are driven by two separate flow components: Low time-average shear stress and fluid flow reversal. *Am J Physiol Heart Circ Physiol*. 2010;298:H367-374

37. Grimson A, Farh KK, Johnston WK, Garrett-Engele P, Lim LP, Bartel DP. Microrna targeting specificity in mammals: Determinants beyond seed pairing. *Mol Cell*. 2007;27:91-105

CHAPTER 8

DISCUSSION

Limitations

There are several limitations in the work presented here and are described in detail below.

iMAEC lines

Cultured mouse endothelial cells, given the wide availability of transgenic mice, can be a useful tool to study endothelial cell biology. In this study, a simple method for generating iMAEC lines that maintain an endothelial phenotype was demonstrated. This method overcomes the proliferative limitation of mouse endothelial cells, allowing the expansion of a few cells from the mouse aorta. However, this method also has limitations. The primary MAEC were infected with retrovirus encoding polyoma middle T antigen, a tumor antigen originally isolated from mouse polyoma virus[1]. Middle T antigen is tightly bound to the membrane[2-3] and serves as a docking port for many signaling molecules that are necessary for cellular transformation in tissue culture[4-5]. Signaling molecules include Src-family protein tyrosine kinases (PTKs), protein phosphatase 2A (PP2A), PLC-γ, and PI3K[6]. More specifically, middle T antigen activates the PI3K/Akt signaling pathway[7] which blocks apoptosis and prevents cell cycle withdrawal. Because middle T antigen constitutively activates proliferative signaling pathways, using iMAEC lines to study cell functions related to cell growth, proliferation, and apoptosis is not appropriate. In addition, the alteration of signaling pathways in iMAEC lines causes significant differences from primary MAEC. Finally, interpretation of iMAEC responses to stimuli should be examined carefully.

Partial carotid ligation model

The mouse model of partial carotid ligation presented in this study showed a distinct flow pattern characterized by low and oscillatory flow in LCA after surgery. This model rapidly induced endothelial cell dysfunction within one week and atherosclerosis in two weeks. Because this model provides accelerated disease progression, several precautions and limitations should be addressed. First, the disturbed flow pattern generated in LCA is simpler than the naturally occurring flow disturbance at curves or bifurcations of the arterial tree. The different EC responses between the partial ligation model and naturally occurring flow disturbed flow may not only be due to acute flow disturbance, but may be resultant from different disturbed flow patterns. Second, partial carotid ligation induces robust atherosclerotic plaques in ApoE null mice fed a high-fat diet within two weeks suggesting a different pathology from naturally occurring atherosclerosis. Progression of atherosclerosis is chronic and takes months and years to develop in mice and humans, respectively. The accelerated atherosclerosis caused by partial carotid ligation saves time and effort, however the detailed mechanisms and features may be lost due to different patho-physiology. Finally, the method for endothelial RNA isolation from the carotid has its limitation. Low and oscillatory shear stress caused by partial ligation induces cellular inflammation which leads to leukocyte and neutrophil infiltration. Our results suggest that the endothelium is free of immune cell infiltration at two days post-ligation. However, significant macrophage/leukocyte adhesion to endothelium was observed in longer time points. To avoid the endothelial RNA contamination from immune cells, the time frame for intimal RNA preparation is limited to two days post-ligation.

The difference between in vivo and in vitro

This study was performed both in mouse carotid artery and in cultured HUVEC. The mechanosensitive miRNAs and mRNAs identified *in vivo* showed distinctive difference from those *in vitro*. Several reasons could explain the divergence: 1) *in vivo* study performed in mice is not compatible to those in human cells because of the species diversity. We identified several mouse-specific miRNAs such as miR-712 which is not feasible to be validated in human cells. The situation is similar to miR-663, a human specific miRNA, which can not be used in the mouse model to test the functional relevance. 2) The developed iMAEC line, created to prevent intraspecies inconsistency, shows that many genes appear to have been significantly dysregulated during culture. This brought a fundamental question of *in vitro* cell culture system. The environment from which these endothelial cells come is very different from culturing condition. This may have an effect on the endothelial cell phenotype and it affects the results in our study. Furthermore, i*n vivo condition,* the endothelial cells are in close proximity to other cell types in a 3-dimentional interactive environment compared to the culture condition of pure endothelial cells in 2-dimentional cultured dish. 3) The flow pattern and shear intensity are dramatically different in mouse and in cultured cells. The shear patterns used in cultured cells are simplified waveform with average physiological shear magnitude of 15 dynes/cm^2 (LS);however, the shear stress waveform over a cardiac cycle in mouse carotid is pulsatile and can easily reach over 100 dynes/cm^2 during peak systole. Therefore, the gap between experimental conditions from *in vitro* and *in vivo* is the major limitation of this study.

Functional validation in vivo

Because of the difference between *in vitro* and *in vivo*, it is more valuable to validate the functional importance of our novel miRNAs and mRNAs using mouse model than to do the study using cultured cells regarding the physiological relevance; however, the

transgenic mice of interest are not widely commercially available and require a huge effort to generate these mouse lines. In addition, the techniques for transient gene manipulation *in vivo* are still under developments. Therefore, to investigate the functional importance from the list of miRNAs and mRNAs by screening study performed in mice is just not feasible at this point.

Predictions of miRNA target genes

In a setting where one miRNA can regulate hundreds of genes and one gene can be regulated by a number of miRNAs, lack of knowledge in the mechanisms that govern miRNA-mRNA as well as miRNA-miRNA interactions is a major issue. Current prediction methods of miRNAs targets are based on the seeding region of miRNAs that bind to the target site(s) on a given mRNA by sequence complementarities. These methods also consider additional pairing by other nucleotides, which has been hypothesized to be important in miRNA binding[8]. The tolerance for extensive mismatches outside the seed region increases the number of potential targets under miRNA control. Unfortunately, this complexity of interactions hinders the discovery of actual miRNA targets. In fact, the popular program such as TargetScan which is used for this purpose will show hundreds or thousands "potential" target genes of any given single miRNA. The miRNA-mRNA interaction should be validated by experiments such as the 3'UTR reporter assay[9-10] and then by inspecting protein expression while altering the level of miRNA[9]. There is no systematic way to perform this type of study but the learning process of trial-and-error.

In addition, because of the complexity of biological system, any individual biological process mediated by miRNA may require a number of different factors that contribute to

the final outcome. This type of synergy makes it difficult to identify a single gene as a direct mediator responsible for the effect of miRNA on any given biological function.

Future Directions

We provided the lists of novel mechanosensitive miRNAs and mRNAs in this study; however, the detailed mechanisms and functional importance have not been determined yet. Better understanding of gene regulation and disease progression require the mechanisms dissected from the current study. The findings described in this dissertation have laid the groundwork for additional future studies of mechanosensitive miRNAs and mRNAs in endothelial cells. Advancement of this work may focus on both *in vitro* and *in vivo* experimental approaches.

In vivo functional validation

A straightforward approach to validate the functional importance of mechanosensitive genes is to use the same mouse model by knocking down the gene of interest, known as the "loss-of-function" study. This approach could be achieved by acquiring the transgenic mouse with the deletion of specific gene in genomic locus. It could also be performed by infusion of pharmacologic inhibitors to the mouse for inhibiting the function or silencing the expression of the genes. Several studies have reported that the successful delivery of targeting siRNA for gene silencing is practical[11-13]; however, the delivery of RNAi to endothelial cells in specific regions is a major challenge. In our mouse model, we create a disturbed flow pattern locally in LCA by partially carotid ligation. The ideal condition to examine gene function would be to knockdown the gene of interest specifically in the endothelium of carotid arteries. Local RNAi delivery techniques are currently being developed in our lab and the procedure is shown in Figure 8.1 as a proof of concept.

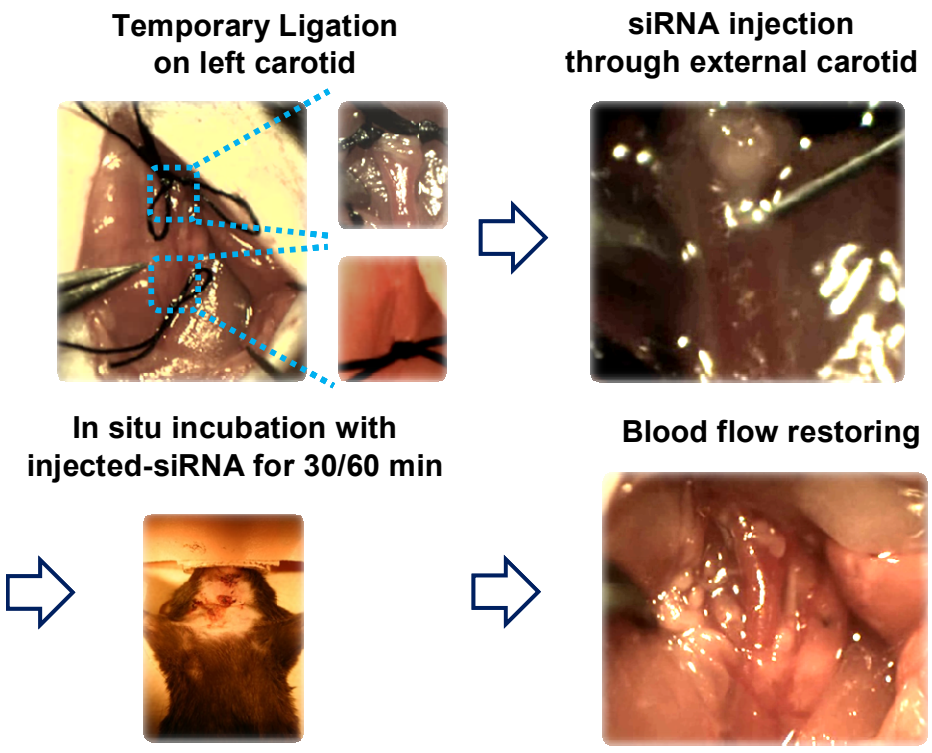

Figure 8.1 Experimental procedure of RNAi delivery to carotid artery.

RNAi molecules were mixed with transfection reagents and directly injected to carotid artery. Temporary ligation of the carotid was used to stop the blood flow and loss of materials. The delivery of RNAi specifically to endothelium through the use of this technique has been demonstrated by imaging the fluorescence labeling siRNA molecules as shown in figure 8.2. This method for locally delivery of siRNA appears to be convincing while more control experiments need to be done to validate the efficacy of this new technique.

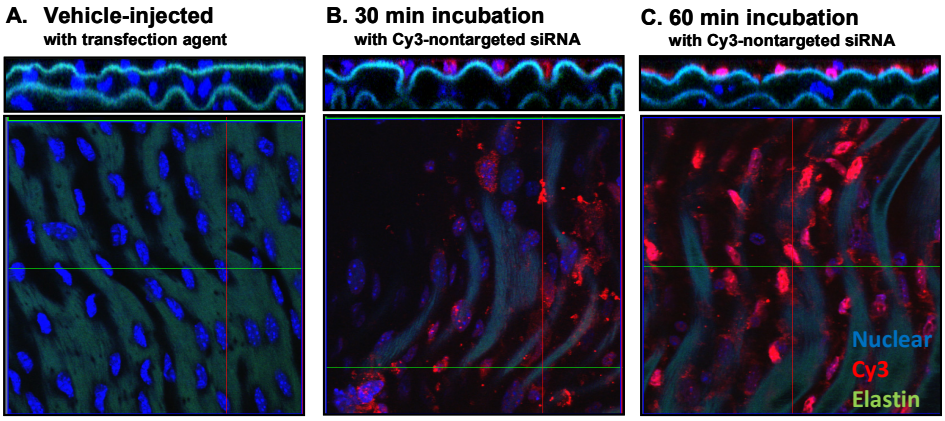

Figure 8.2 Delivery of siRNA to carotid endothelium. *Representative examples of carotid tissues obtained from Cy3-labeled nontargeted-siRNA-transfected (B, C) or untransfected (A) mouse carotid artery. The En-Face carotid tissue observed using confocal microscopy [blue fluorescence of nuclear (DAPI), red fluorescence of Cy3-labeled siRNAs, green fluorescence of elastic tissue]. Note the presence of Cy3-labelded siRNA in the endothelial cells in B and C.*

Several types of inhibiting molecules can be applied by this technique including lentiviral-based shRNA for silencing mRNA or miRNA[14-17]. In addition, LNA oligonucleotides could also been locally or systematically administrated to mouse to suppress the function of miRNA as described previously[18-19]. Overall, dissecting the list of novel mechanosensitive miRNAs and mRNAs regarding the function significance using *in vivo* knockdown technique would further expand the contribution of this dissertation.

Studying molecular mechanisms using cell culture

To support and explain the significance of the *in vivo* functional study, it requires detailed investigation of underlying molecular mechanisms. Given the complicated environment *in vivo*, the mechanistic study is difficult to design and perform in animal. In Chapter 3, the method we described to generate the iMAEC lines could be used to study the underlying molecular mechanisms of specific miRNA or mRNA. The iMAEC lines provide

a useful tool to study the mechanisms in the absence of specific miRNA and mRNA granted that the corresponding transgenic mouse is available.

Identified target genes and regulating network of miRNA

As we discussed in Chapter 7, the current method to find the target genes of miRNA only based on sequence complimentary. It generates a long list of predicted target genes of single miRNA with a large portion of false-positive candidates. Since we believe that the regulation of miRNA seems to be a tuning process involving a set of genes which cooperatively work as a network, the individual target gene(s) of specific miRNA still need to be identified. For a selected miRNA, the potential target genes based on sequence prediction could be confirmed by 3'UTR reporter assay and by checking protein expression levels after modulating miRNA levels.

Summary

Cardiovascular disease is the leading cause of death among developed countries and is rapidly becoming the major cause of death in the developing world[20]. Atherosclerosis is a major contributor to cardiovascular disease and accounts for an estimated one-third of deaths worldwide[21]. In an effort to develop effective treatments for this pervasive pathology, research is now focused on the mechanisms of atherogenesis. In order to address the hemodynamic components of disease pathogenesis, researchers have focused on mechanotransduction of flow-dependent shear stress in the vascular endothelium as a source of novel pathological mechanisms[22-23]. Understanding how unidirectional, laminar blood flow protects vessels from atherogenesis, while disturbed, oscillatory blood flow promotes it, stands to provide enormous insight into disease pathogenesis and may provide powerful, specific new therapies for cardiovascular disease intervention.

The overall *objective* of this dissertation was to determine which microRNAs (miRNAs) and mRNAs are regulated by different flow conditions in vascular endothelial cells *in vitro* and in mouse carotid artery endothelium *in vivo*, and to identify which miRNAs mediate flow-dependent vascular inflammation. These results allow us to identify novel targets either for therapeutic intervention or for early clinical detection of atherosclerosis. The *overall hypothesis* of this project was that *oscillatory shear (OS) and laminar shear (LS) stress differentially alter the expression of mechanosensitive miRNAs each capable of regulating complex networks of gene expression, which in turn leads to inflammation in endothelial cells.* This hypothesis was tested using both *in vitro* and *in vivo* approaches, high throughput microarray analyses, and functional validation of specific targets by PCR as outlined in these three specific aims:

- **Specific Aim 1: Develop a novel mouse model of experimentally inducible disturbed flow and a method for isolating endothelial cell RNA with intensive validation of minimal contamination, to examine the expression profiles of miRNA and mRNA *in vivo*.**

- **Specific Aim 2: Identify flow-sensitive miRNAs and mRNAs in partially ligated murine carotid endothelium and cultured HUVEC.**

- **Specific Aim 3: Investigate the role of mechanosensitive miRNA-663 in HUVEC undergoing OS-induced cellular inflammation.**

To achieve these specific aims, our first developed a mouse model which modifies the flow pattern in the left common carotid artery. We ligate three of the four caudal branches of the LCA - left external, left internal, and occipital arteries. We then

characterized the low and oscillatory shear stress induced by the partial carotid ligation procedure. This procedure induces accelerated endothelial dysfunction in one week and advanced atherosclerotic plaques by 2 weeks in ApoE knockout mice fed a high fat diet[24]. Using this model, I developed a simple method to isolate endothelial RNA from the partially ligated left common carotid as well as the contralateral right common carotid[24]. This method was then fine-tuned to provide total RNA samples in sufficient quantity with little to no appreciable contamination from cells populating the underlying medial and adventitial layers of the artery. In addition, the time points (12hr and 48hr post-ligation) we selected for RNA samples collection are free of infiltrating immune cells common in areas of disturbed flow. In addition, I also developed a method to generate iMAEC line for use *in vitro* for validation purpose. The methods used to develop iMAEC lines described in this dissertation can be applied to generate additional MAEC lines, using various knockout mouse lines, to provide a critical tool to investigate the vascular biology and pathobiology.

To investigate the mRNA expression profiles *in vivo*, we carried out genome-wide microarray assays using endothelial RNA isolated from the flow-disturbed left and contralateral right common carotid arteries (LCA and RCA) in wildtype C57BL/6 mice. We found that 62 and 523 genes significantly changed in flow-disturbed LCA endothelium compared to the RCA by 12hr and 48hr post-ligation respectively. The array results for 44 out of 46 genes were validated by qPCR, including well-known shear-responsive genes, *Klf2*, *eNOS*, and *BMP4*, as well as numerous novel mechanosensitive genes such as *Klk10*, *Dhh*, *Jam2* and *Lmo4.* Lmo4 protein was specifically expressed in the flow disturbed mouse aortic arch endothelium and in human coronary endothelium in an asymmetric pattern. Comparison of *in vivo*, *ex vivo*, and *in vitro* endothelial gene expression patterns suggests that many mechanosensitive genes found *in vivo* appear

to have been significantly dysregulated during culture. Gene ontology analyses revealed that disturbed flow induced cell proliferation and morphology by 12hr, followed by inflammatory and immune responses by 48hr.

To provide further insight into the possible mechanisms of observed mechanosensitive gene changes we performed microarrays looking at miRNA expression profiles using RNA samples isolated as described above. We found that 27 and 18 miRNAs were significantly either up- or down-regulated, respectively, in flow-disturbed LCA endothelium compared to the RCA 48 hours post-ligation. However, only 4 miRNAs showed significant differences between LCA and RCA as of 12 hours post-ligation. The array results were also validated by qPCR confirming several mechanosensitive miRNAs such as miR-23b, miR-29b, miR-30c, and miR-712, which have not been reported previously. Further analyses between mechanosensitive miRNAs and mRNAs reveal approximately 10 to 15% (25/295, and 31/228) of mechanosensitive mRNAs found to be potential targets of shear-sensitive miRNAs based on the sequence complementary prediction by TargetScan. This also suggests the significance of these mechanosensitive miRNAs and mRNAs identified in this dissertation and these targets could play an important role involving in the mechanisms underling the effect of shear stress on cardiovascular disease.

To further study the functional importance of mechanosensitive miRNAs, we examined the miRNAs expression profiles in cultured HUVEC exposed to OS or LS for 24hr. Given the difference between *in vitro* and *in vivo* system, the new data set was obtained and detailed functional validation was performed. After validation by PCR, we identified 10 OS-sensitive (3 up- and 7 down-regulated by OS) miRNAs. Of those, the most significant OS-induced miRNA, miR-663, was selected for determining its functional

importance. miR-663 plays a specific role in endothelial inflammatory response, but not in apoptosis, in an ICAM-1 dependent manner. In order to identify potential target genes of miR663, we carried out an additional genome-wide DNA microarray, which uncovered 35 potential miR-663 targets, including a network of inflammatory genes and transcription factors such as *KLF4, ATF3, and FOSB*. Since these transcriptional factors have been known to serve as master regulators in several biological functions including inflammation, these results suggest that miR-663 is a shear-sensitive miRNA, regulating expression of many genes including the transcription factors, which in turn may induce inflammatory response in ECs.

Collectively, OS significantly altered the gene expression profiles including miRNA and mRNA compared to LS. These mechanosensitive genes regulated by miRNAs seem to be involved in OS-induced EC inflammation in the earliest stage of atherosclerosis development. In particular, miR-663, an OS-induced miRNA, is shown to mediate cellular inflammation by regulating a network of genes further supporting the notion that flow-sensitive miRNAs and mRNA play important roles in disturbed flow-induced cardiovascular diseases.

Conclusions

The findings from the partial carotid ligation model show that acute exposure to disturbed flow results in accelerated endothelial dysfunction and atherosclerosis *in vivo*. High-throughput microarrays reveal distinct expression profiles of both miRNAs and mRNAs in mouse endothelium exposed to disturbed flow suggesting the regulatory mechanisms by which miRNAs regulate mRNAs resulting in EC inflammation, the earliest stage of atherosclerosis. While the similarity between the *in vitro* and *in vivo*

results demonstrate the validity and complementary nature of both systems, the dysregulated or lost genes in cultured endothelial cells highlights the critical importance of *in vivo* models in studying flow-dependent vascular biology and atherosclerosis. This *in vivo* study provides new insight into the mechanisms of flow induced atherosclerosis. In particular, I first reported that an upregulation of miR-663 due to OS in HUVEC causes monocyte adhesion, but not endothelial apoptosis, in an ICAM-1 dependent manner. miR-663 regulates a group of genes including transcriptional factors and inflammatory genes which may also mediate OS-induced EC inflammation. Collectively, revealing the profiles of miRNAs and mRNAs regulated by hemodynamic flow provides a better understanding in vascular diseases and provide potential target for developing effective preventative therapeutic approaches in cardiovascular diseases.

References

1. Schaffhausen BS, Roberts TM. Lessons from polyoma middle t antigen on signaling and transformation: A DNA tumor virus contribution to the war on cancer. *Virology*. 2009;384:304-316

2. Ito Y. Polyoma virus-specific 55k protein isolated from plasma membrane of productively infected cells is virus-coded and important for cell transformation. *Virology*. 1979;98:261-266

3. Dilworth SM, Hansson HA, Darnfors C, Bjursell G, Streuli CH, Griffin BE. Subcellular localisation of the middle and large t-antigens of polyoma virus. *EMBO J*. 1986;5:491-499

4. Treisman R, Novak U, Favaloro J, Kamen R. Transformation of rat cells by an altered polyoma virus genome expressing only the middle-t protein. *Nature*. 1981;292:595-600

5. Carmichael GG, Schaffhausen BS, Dorsky DI, Oliver DB, Benjamin TL. Carboxy terminus of polyoma middle-sized tumor antigen is required for attachment to membranes, associated protein kinase activities, and cell transformation. *Proc Natl Acad Sci U S A*. 1982;79:3579-3583

6. Cheng J, DeCaprio JA, Fluck MM, Schaffhausen BS. Cellular transformation by simian virus 40 and murine polyoma virus t antigens. *Semin Cancer Biol*. 2009;19:218-228

7. Dahl J, Jurczak A, Cheng LA, Baker DC, Benjamin TL. Evidence of a role for phosphatidylinositol 3-kinase activation in the blocking of apoptosis by polyomavirus middle t antigen. *J Virol*. 1998;72:3221-3226

8. Grimson A, Farh KK, Johnston WK, Garrett-Engele P, Lim LP, Bartel DP. Microrna targeting specificity in mammals: Determinants beyond seed pairing. *Mol Cell*. 2007;27:91-105

9. Orom UA, Lund AH. Experimental identification of microrna targets. *Gene*. 2010;451:1-5

10. Didiano D, Hobert O. Molecular architecture of a mirna-regulated 3' utr. *RNA*. 2008;14:1297-1317

11. Love KT, Mahon KP, Levins CG, Whitehead KA, Querbes W, Dorkin JR, Qin J, Cantley W, Qin LL, Racie T, Frank-Kamenetsky M, Yip KN, Alvarez R, Sah DW, de Fougerolles A, Fitzgerald K, Koteliansky V, Akinc A, Langer R, Anderson DG. Lipid-like materials for low-dose, in vivo gene silencing. *Proc Natl Acad Sci U S A*. 2010;107:1864-1869

12. Takeshita F, Minakuchi Y, Nagahara S, Honma K, Sasaki H, Hirai K, Teratani T, Namatame N, Yamamoto Y, Hanai K, Kato T, Sano A, Ochiya T. Efficient delivery of small interfering rna to bone-metastatic tumors by using atelocollagen in vivo. *Proc Natl Acad Sci U S A*. 2005;102:12177-12182

13. Morin A, Gallou-Kabani C, Mathieu JR, Cabon F. Systemic delivery and quantification of unformulated interfering rnas in vivo. *Curr Top Med Chem*. 2009;9:1117-1129

14. Li Y, Liang XY, Wei LN, Xiong YL, Yang X, Shi HG, Yang ZH. Study of rna interference inhibiting rat ovarian androgen biosynthesis by depressing 17alpha-hydroxylase/17, 20-lyase activity in vivo. *Reprod Biol Endocrinol*. 2009;7:73

15. Lee DS, Rumi MA, Konno T, Soares MJ. In vivo genetic manipulation of the rat trophoblast cell lineage using lentiviral vector delivery. *Genesis*. 2009;47:433-439

16. Singer O, Verma IM. Applications of lentiviral vectors for shrna delivery and transgenesis. *Curr Gene Ther*. 2008;8:483-488

17. Stern P, Astrof S, Erkeland SJ, Schustak J, Sharp PA, Hynes RO. A system for cre-regulated rna interference in vivo. *Proc Natl Acad Sci U S A*. 2008;105:13895-13900

18. Worm J, Stenvang J, Petri A, Frederiksen KS, Obad S, Elmen J, Hedtjarn M, Straarup EM, Hansen JB, Kauppinen S. Silencing of microrna-155 in mice during acute inflammatory response leads to derepression of c/ebp beta and down-regulation of g-csf. *Nucleic Acids Res*. 2009;37:5784-5792

19. Elmen J, Lindow M, Schutz S, Lawrence M, Petri A, Obad S, Lindholm M, Hedtjarn M, Hansen HF, Berger U, Gullans S, Kearney P, Sarnow P, Straarup EM, Kauppinen S. Lna-mediated microrna silencing in non-human primates. *Nature*. 2008;452:896-899

20. Nabel EG. Cardiovascular disease. *N Engl J Med*. 2003;349:60-72

21. Ross R. The pathogenesis of atherosclerosis: A perspective for the 1990s. *Nature*. 1993;362:801-809

22. Caro CG. Discovery of the role of wall shear in atherosclerosis. *Arterioscler Thromb Vasc Biol*. 2009;29:158-161

23. Davies PF. Hemodynamic shear stress and the endothelium in cardiovascular pathophysiology. *Nat Clin Pract Cardiovasc Med*. 2009;6:16-26

24. Nam D, Ni CW, Rezvan A, Suo J, Budzyn K, Llanos A, Harrison D, Giddens D, Jo H. Partial carotid ligation is a model of acutely induced disturbed flow, leading to rapid endothelial dysfunction and atherosclerosis. *Am J Physiol Heart Circ Physiol*. 2009;297:H1535-1543

APPENDIX A

mRNA expression profiles in response to disturb flow *in vivo*

Table A1. mRNA expression profiles in mouse ligated carotid endothelium (LCA) and controlateral right carotid endothelium (RCA) at 12 hr post-ligation

Gene_ID	Gene	LCA1	LCA2	LCA3	RCA1	RCA2	RCA3	LCA/RCA		q-value%
		signal	signal	signal	signal	signal	signal	ratio	SEM	
ILMN_1235698	Bmp4	817.172	753.4	861.735	525.787	490.672	560.74	1.54	0.01	0.00
ILMN_2593496	Got2	228.157	261.709	287.046	122.4	159.325	184.514	1.69	0.09	0.00
ILMN_2909150	Ctgf	1789.72	1892.92	2115.17	308.975	514.682	378.377	5.02	0.67	0.00
ILMN_2932964	Ctps	384.078	391.404	348.456	173.17	207.548	172.161	2.04	0.10	0.00
ILMN_1239386	Galntl2	347.417	330.933	257.781	155.923	125.391	88.3212	2.60	0.20	0.00
ILMN_2451036	LOC100047093	1679.33	1519.85	1469.16	1051.6	759.426	647.492	1.96	0.20	0.00
ILMN_1244612	Galntl2	1221.87	1278.77	1161.78	657.66	809.722	552.401	1.85	0.15	0.00
ILMN_2694569	LOC631037	474.404	495.195	339.706	339.191	325.196	176.209	1.62	0.16	9.02
ILMN_1228475	Ulk1	450.358	528.455	411.063	277.396	374.191	209.711	1.67	0.16	9.02
ILMN_1236958	Gabarapl1	1892.92	1951.06	1614.44	1209.61	1229.78	1100.19	1.54	0.04	9.02
ILMN_2642403	Lmo4	298.879	281.02	303.95	181.468	150.419	152.839	1.83	0.10	9.02
ILMN_1231490	2410006H16Rik	144.038	123.159	107.22	73.0421	55.7899	45.2832	2.18	0.11	9.37
ILMN_2596560	Phactr1	710.084	709.029	688.767	326.108	282.42	392.486	2.15	0.22	9.37
ILMN_1213034	2010312A17Rik	173.498	230.831	148.483	110.302	174.393	87.3967	1.53	0.11	9.37
ILMN_2741621	Birc2	120.616	100.17	108.414	71.0796	52.6087	61.0963	1.79	0.06	9.37
ILMN_2790373	Snn	224.13	181.408	273.396	140.47	102.953	175.678	1.64	0.06	9.56
ILMN_1258158	Aldh6a1	225.876	231.851	168.556	143.021	129.896	86.1761	1.77	0.11	9.56
ILMN_2888552	Slc1a4	250.203	230.504	195.269	132.684	116.778	106.532	1.90	0.04	9.56
ILMN_2977558	Dapk2	167.93	180.36	215.294	45.5269	36.7138	43.489	4.52	0.41	9.56
ILMN_2909336	Gpm6a	593.102	381.618	391.008	292.334	177.744	150.528	2.26	0.17	9.56
ILMN_1238215	Ctgf	732.024	776.478	1051.6	120.253	143.62	147.488	6.21	0.50	9.56
ILMN_2471996	AI317223	108.143	120.993	118.385	47.364	45.7351	44.5681	2.53	0.12	9.56
ILMN_1234487	Angpt2	132.058	117.781	107.494	76.0581	53.367	52.736	1.99	0.14	9.56
ILMN_1216764	Ier3	1302.13	1165	979.313	783.446	833.397	485.736	1.69	0.18	9.56
ILMN_1252481	Fosl2	574.427	804.603	664.416	333.518	431.408	369.402	1.80	0.04	9.56
ILMN_1215136	Scn3b	132.921	89.9995	114.408	87.8651	40.9282	70.6479	1.78	0.21	9.56
ILMN_1223313	Fn3k	159.775	128.891	117.762	113.407	74.5454	64.4237	1.66	0.13	9.56
ILMN_2711966	Mrpl1	116.087	130.869	159.467	60.179	69.4427	89.0209	1.87	0.04	9.56
ILMN_1230596	E030033D05Rik	693.063	576.728	582.878	403.333	322.458	404.28	1.65	0.11	10.00
ILMN_1232928	Timp3	551.733	494.594	560.043	887.528	857.985	901.938	0.61	0.01	0.00
ILMN_2604029	Klf2	115.137	72.2157	81.7463	332.636	262.923	286.216	0.30	0.02	0.00
ILMN_2686883	Gnaq	211.461	223.549	217.127	328.862	336.292	323.963	0.66	0.01	0.00
ILMN_2697304	Eln	591.147	1039.74	1188.16	1347.98	1656.34	1809.24	0.57	0.07	0.00
ILMN_1235077	Capn2	119.518	141.371	167.639	239.745	255.197	275.515	0.55	0.03	0.00
ILMN_2595664	Dhh	451.157	431.692	574.427	954.708	928.442	976.693	0.51	0.04	0.00
ILMN_2672190	Id1	222.28	186.727	161.345	347.956	311.966	303.761	0.59	0.03	0.00
ILMN_2880906	Pdlim2	213.178	176.138	142.426	359.282	355.997	319.709	0.51	0.04	2.54
ILMN_2750053	Ptprj	542.797	505.843	544.872	974.098	1042.64	956.522	0.54	0.03	2.54
ILMN_2424721	Pdgfa	240.649	195.966	227.271	406.149	371.926	437.338	0.55	0.02	4.78
ILMN_2634083	Cdkn1a	155.98	186.659	260.502	298.461	351.312	447.08	0.55	0.02	7.17
ILMN_2618408	Icam2	383.167	332.636	393.431	671.942	634.329	780.865	0.53	0.02	7.17
ILMN_2745876	BC020535	380.535	331.058	331.058	566.348	575.882	585.862	0.60	0.03	7.17
ILMN_1220170	Tek	472.59	480.064	498.934	693.063	798.297	773.345	0.64	0.02	7.17
ILMN_2498731	E030024M20Rik	176.277	217.963	169.109	399.759	379.243	386.73	0.48	0.05	7.17
ILMN_2950503	Dab2ip	156.906	174.016	152.106	249.206	256.373	226.339	0.66	0.02	7.17
ILMN_2999439	Klf4	171.955	165.37	119.236	345.631	349.432	250.068	0.48	0.01	7.17
ILMN_2675760	2310046K01Rik	196.939	182.573	118.636	341.139	380.047	322.807	0.48	0.06	7.17
ILMN_2976129	Tinagl	398.491	427.274	629.718	740.839	757.994	858.775	0.61	0.06	7.17
ILMN_2773211	Kras	54.4353	68.3277	62.5253	102.517	120.555	117.508	0.54	0.01	7.17
ILMN_2608133	Rhpn2	281.73	437.953	347.3	728.041	736.412	677.373	0.50	0.06	7.17
ILMN_1216781	Rab11fip5	227.547	241.386	221.022	430.174	422.569	358.315	0.57	0.03	7.17
ILMN_2587084	C230009C22Rik	80.5051	101.966	105.303	137.694	172.615	168.081	0.60	0.01	7.17
ILMN_2866267	F2rl1	164.217	151.751	175.17	271.486	277.509	328.971	0.56	0.02	7.17
ILMN_2789562	P4ha2	324.92	314.45	235.263	445.015	447.244	406.84	0.67	0.05	7.17
ILMN_1247916	Lims2	139.682	106.904	73.1437	252.02	187.496	171.197	0.52	0.05	7.17
ILMN_1231445	Inmt	41.3145	36.7486	52.4461	106.073	122.761	135.324	0.36	0.03	7.17
ILMN_2683586	Capn2	197.623	233.652	272.105	354.01	364.537	376.849	0.64	0.05	7.45
ILMN_2710274	Slc9a3r2	652.56	539.922	456.409	1092.35	1089.95	1185.03	0.49	0.06	7.45
ILMN_1229745	Sertad4	220.611	385.796	269.127	423.909	534.873	406.474	0.63	0.06	7.45
ILMN_3140516	Rapgef1	128.303	168.44	136.418	209.651	285.033	249.165	0.58	0.02	7.45
ILMN_2641228	Hspa12b	269.897	282.867	229.154	584.68	503.675	595.72	0.47	0.05	7.45
ILMN_2738345	Lims2	172.243	149.716	140.761	236.444	237.036	234.543	0.65	0.04	9.70
ILMN_2699637	Lsr	96.655	116.2	184.641	238.637	214.482	283.553	0.53	0.07	9.70
ILMN_1243407	Klk10	367.059	413.861	459.284	1033.42	1624.18	1376.8	0.31	0.03	9.70
ILMN_2689207	Col6a3	42.4081	40.3794	52.2117	85.3355	86.7083	105.74	0.49	0.01	9.70
ILMN_2774056	Cmklr1	54.6829	52.8889	45.0754	87.0237	87.8331	80.0749	0.60	0.02	9.70
ILMN_1212703	Kras	201.053	156.063	193.432	349.833	316.052	429.296	0.51	0.04	9.70

Table A2. mRNA expression profiles in mouse ligated carotid endothelium (LCA) and controlateral right carotid endothelium (RCA) at 48 hr post-ligation

Gene_ID	Gene	LCA1	LCA2	LCA3	RCA1	RCA2	RCA3	LCA/RCA		q-value%
		signal	signal	signal	signal	signal	signal	ratio	SEM	
ILMN_2743013	Ncf4	123.319	153.945	130.835	30.4068	62.8657	37.0913	3.34	0.47	0.00
ILMN_2939681	Lyzs	187.153	212.471	201.707	48.2658	81.8811	65.3634	3.19	0.37	0.00
ILMN_2878071	Lyz	429.584	479.76	438.107	126.971	197.15	116.669	3.19	0.39	0.00
ILMN_2867147	Tyrobp	596.259	655.812	588.908	118.44	229.035	163.324	3.83	0.64	0.00
ILMN_2935386	6330548G22Rik	212.163	282.065	276.212	92.8085	176.527	162.691	1.86	0.21	3.14
ILMN_1245129	Ifitm1	71.9507	87.6932	87.4224	26.9705	46.1087	43.6963	2.19	0.24	3.14
ILMN_2767918	Ifi30	63.2231	78.1292	88.1417	35.5067	49.5621	59.3177	1.61	0.09	3.14
ILMN_3120652	Smap2	624.053	648.638	606.324	388.744	414.294	402.025	1.56	0.03	3.14
ILMN_2511249	scl0002785.1_49	121.224	120.312	141.507	68.7494	71.6649	93.8944	1.65	0.08	3.14
ILMN_1223257	Ccl4	72.8491	70.5143	75.7351	30.5678	29.4904	30.6628	2.41	0.03	3.14
ILMN_2718801	Fosl2	69.6099	80.6075	73.0887	40.0656	49.4381	41.3171	1.71	0.04	3.40
ILMN_3009860	Sell	87.2527	91.0993	92.5678	30.1647	35.8777	30.1431	2.83	0.16	3.40
ILMN_2712986	Chi3l3	207.973	251.51	222.01	31.4937	42.6378	33.2733	6.39	0.25	3.40
ILMN_3127739	Sf3b4	216.219	162.509	202.788	125.774	86.2596	121.33	1.76	0.06	7.51
ILMN_2737713	Edn1	822.014	651.046	605.525	349.556	261.932	134.351	3.11	0.70	7.51
ILMN_1252076	Lyz2	211.03	262.556	252.771	30.1063	44.3544	34.4201	6.76	0.43	7.51
ILMN_2470131	6720475J19Rik	66.5284	72.9085	74.02	32.1014	33.5133	35.5536	2.11	0.03	7.51
ILMN_2888834	Apob48r	157.947	141.914	178.439	30.6259	29.1935	39.4368	4.85	0.18	7.51
ILMN_2920849	Pira4	78.3787	85.1096	78.5584	35.4018	34.4845	31.7957	2.38	0.09	7.51
ILMN_1240256	Slc9a3r1	287.558	265.65	261.411	148.796	127.151	147.717	1.93	0.09	7.51
ILMN_1251066	BC067047	100.997	84.065	83.4896	58.3733	38.659	45.1855	1.92	0.13	7.51
ILMN_3117876	Chi3l3	226.687	287.435	252.441	42.0187	53.0328	37.5862	5.84	0.44	7.51
ILMN_2714796	Coro1a	324.182	389.274	409.327	41.4145	77.2405	49.7029	7.03	1.00	7.51
ILMN_1249242	Dnajc2	324.869	289.343	304.17	214.517	187.064	176.265	1.60	0.07	7.51
ILMN_1221354	9330156H06Rik	53.8499	51.2482	49.4678	34.5135	33.36	30.5358	1.57	0.02	8.59
ILMN_1225192	Nfkbid	100.098	103.557	88.8847	30.247	33.5903	31.3071	3.08	0.14	8.59
ILMN_2699531	Rgs10	218.763	212.256	200.079	152.404	144.844	119.11	1.53	0.08	8.59
ILMN_1217928	C230067O06Rik	151.306	202.394	168.605	81.602	115.268	93.6139	1.80	0.03	8.59
ILMN_1217849	Laptm5	864.305	1021.15	1041.96	158.069	302.342	147.426	5.30	1.07	8.59
ILMN_3013874	EG434858	94.9012	96.9803	118.144	55.2752	50.6449	69.941	1.77	0.07	8.59
ILMN_2731760	Myo1f	94.678	99.1485	109.74	33.263	40.0031	36.5386	2.78	0.16	8.59
ILMN_3089584	Cd74	467.7	422.95	350.281	123.912	165.07	47.2612	4.58	1.46	8.59
ILMN_1221817	Cd74	357.567	326.853	274.567	109.381	139.16	40.3052	4.14	1.36	8.59
ILMN_2652511	Hist1h2bj	261.488	457.748	306.074	155.764	324.703	168.345	1.64	0.12	8.59
ILMN_2571683	9830169E20Rik	278.327	367.707	303.171	122.441	173.871	152.507	2.13	0.08	8.59
ILMN_1259561	Prep	80.1438	95.7846	87.9637	44.4471	51.3282	47.8638	1.84	0.02	8.59
ILMN_2659151	Thbs1	499.943	608.123	543.083	178.973	189.039	121.282	3.50	0.51	8.59
ILMN_1248139	Gp49a	141.482	190.374	162.124	31.4862	43.9857	33.6517	4.55	0.14	8.59
ILMN_1254513	4930553M18Rik	283.914	396.799	323.464	124.799	188.748	155.469	2.15	0.06	8.59
ILMN_2637165	2310001H17Rik	168.303	159.675	137.582	106.278	78.8015	62.7342	1.93	0.18	8.59
ILMN_2965903	Hdc	914.47	811.755	1004.96	43.2749	115.778	54.5811	15.52	4.33	8.59
ILMN_1245109	3830430K15Rik	70.8322	80.3457	64.5523	29.8251	47.0862	29.5065	2.09	0.20	8.59
ILMN_2699923	Asprv1	64.1191	67.7721	64.8877	32.6039	41.3551	33.0468	1.86	0.11	8.59
ILMN_3160218	Amica1	315.159	265.168	248.355	31.1891	42.8909	31.6534	8.04	1.14	8.59
ILMN_2712668	Pfkfb4	145.68	181.907	188.39	33.3639	56.7406	37.4467	4.20	0.53	8.59
ILMN_2777491	Fhod1	193.803	259.093	304.499	78.9357	158.901	168.632	1.96	0.25	8.59
ILMN_2565252	B130015M16Rik	164.343	211.942	177.849	99.37	125.727	95.0685	1.74	0.07	8.59
ILMN_1244977	H2-DMb1	114.585	84.6889	85.6722	74.4329	42.7625	52.7834	1.71	0.14	8.59
ILMN_2646630	Lrrc33	129.658	118.721	142.842	39.0084	35.3955	31.1459	3.75	0.42	8.59
ILMN_2996904	Obfc2a	65.4459	62.6891	76.221	36.5757	36.6565	43.5082	1.75	0.02	8.59
ILMN_2603689	Fmnl1	72.0529	84.8952	81.4144	31.1145	33.0254	27.6943	2.61	0.18	8.67
ILMN_2686244	Rassf4	95.5648	119.131	107.044	32.9869	33.8311	32.7233	3.23	0.18	8.67
ILMN_2609323	Lst1	116.537	118.7	98.3757	52.9958	34.3275	30.5178	2.96	0.39	8.67
ILMN_1226525	H2-Ab1	511.746	477.066	513.215	181.965	144.138	64.5439	4.69	1.64	9.45
ILMN_3102376	Fcgr2b	54.4655	58.6859	57.6539	30.2046	38.2377	31.9347	1.71	0.09	9.45
ILMN_1258723	Bop1	90.0959	76.221	82.9635	48.7119	40.8353	51.7244	1.77	0.08	9.45
ILMN_2766780	Lyzs	53.1439	56.7818	58.3109	31.9626	39.1244	36.9594	1.56	0.06	9.45
ILMN_2644587	Bzw2	79.8605	96.644	130.336	48.2566	55.0492	95.6831	1.59	0.12	9.45
ILMN_2669404	Lmnb2	464.079	819.59	639.564	229.616	514.085	295.852	1.93	0.17	9.45
ILMN_2416628	Pscd4	298.021	248.589	359.701	105.753	79.7443	117.302	3.00	0.09	9.45
ILMN_2712151	1810033B17Rik	63.4892	54.3306	58.1757	37.5892	34.0434	35.1195	1.65	0.03	9.45
ILMN_1247377	Mpeg1	94.1206	86.877	107.877	35.9544	39.3979	41.2287	2.48	0.14	9.45
ILMN_2692960	Ero1lb	91.8589	89.118	99.0977	46.7554	54.0509	51.1508	1.85	0.10	9.45
ILMN_1241302	Csf3r	66.924	67.8597	60.6093	29.2848	34.0753	32.6814	2.04	0.13	9.45
ILMN_2606144	Cd300lf	203.567	303.984	266.307	28.857	46.6458	32.5913	7.25	0.49	9.45
ILMN_2685023	Hmha1	81.0002	87.1227	92.5342	30.4157	38.2413	26.7233	2.80	0.35	9.45
ILMN_1229530	Csk	337.99	252.528	271.937	253.677	161.416	153.79	1.56	0.13	9.45
ILMN_2820260	Wdr77	99.2368	98.7058	137.238	48.9736	45.0733	68.385	2.07	0.06	9.45

Table A2. -Continued

Gene_ID	Gene	LCA1	LCA2	LCA3	RCA1	RCA2	RCA3	LCA/RCA		q-value%
		signal	signal	signal	signal	signal	signal	ratio	SEM	
ILMN_2607880	Tkt	231.327	253.954	270.961	132.288	134.951	189.084	1.69	0.13	9.45
ILMN_2956092	Rassf4	97.4455	129.891	111.895	32.3396	35.7787	32.92	3.35	0.18	9.45
ILMN_2909150	Ctgf	2112.78	2237.06	2417.67	607.917	342.627	143.338	8.96	4.05	9.45
ILMN_2687586	Cxcl16	489.811	523.719	544.239	192.637	302.815	213.647	2.27	0.27	9.45
ILMN_2924831	Gas7	105.126	136.965	94.9113	37.2214	87.2888	42.8033	2.20	0.36	9.45
ILMN_1238215	Ctgf	788.6	844.157	975.014	177.849	107.824	57.0806	9.78	3.78	9.45
ILMN_2685393	Ccr5	85.57	95.7537	111.699	27.3557	29.427	28.7345	3.42	0.23	9.45
ILMN_2607675	LOC641240	386.96	384.085	387.646	167.878	123.286	61.3794	3.91	1.22	9.45
ILMN_2619861	Nipsnap1	104.972	183.746	134.089	64.3865	126.451	86.1648	1.55	0.05	9.45
ILMN_2673776	E2f2	126.665	157.947	160.624	60.1764	99.7358	77.5122	1.92	0.17	9.45
ILMN_2910934	Cd52	206.319	271.354	326.853	34.496	57.7126	69.3713	5.13	0.42	9.45
ILMN_2694857	Gpatch3	79.3019	54.5587	78.5897	53.227	29.8892	58.6097	1.55	0.14	9.45
ILMN_1256883	Rad51	70.8423	101.832	70.4245	28.8867	50.97	34.1362	2.17	0.14	9.45
ILMN_2559943	A230055O06Rik	148.961	146.605	155.192	101.43	93.0909	87.6985	1.60	0.09	9.45
ILMN_2629971	Fzr1	52.8148	61.3323	64.5439	35.3009	38.5166	44.1843	1.52	0.04	9.45
ILMN_1213364	LOC638892	228.097	290.785	316.083	138.476	155.98	202.311	1.69	0.09	9.45
ILMN_1223317	Lgals3	70.0863	64.7204	75.4575	32.4776	33.2499	31.0613	2.18	0.14	9.45
ILMN_2748875	Fcer1g	100.123	163.572	119.655	31.5826	61.3874	33.5504	3.13	0.26	9.45
ILMN_1235392	LOC668183	115.284	121.459	135.66	47.1985	54.1764	41.9853	2.64	0.30	9.45
ILMN_1239569	Lsg1	103.294	116.788	132.113	49.7742	74.3494	94.3037	1.68	0.20	9.45
ILMN_1230157	Rnd3	221.61	170.703	242.565	89.7682	83.3089	121.401	2.17	0.15	9.45
ILMN_2787257	Coro1a	272.453	320.607	392.791	43.5109	65.6973	51.2859	6.27	0.80	9.45
ILMN_2781030	Napsa	134.677	111.621	133.666	34.3081	45.1231	45.4002	3.11	0.43	9.45
ILMN_1230440	1700041B20Rik	96.4732	128.642	139.576	45.1958	59.9518	63.2417	2.16	0.02	9.45
ILMN_1252804	Map4k1	71.8466	60.3193	66.8166	49.0154	29.6923	42.226	1.69	0.17	9.45
ILMN_1236387	BC024537	469.549	434.196	339.932	305.973	212.732	190.717	1.79	0.15	9.45
ILMN_2887986	Cd300a	237.52	423.177	337.449	47.2138	128.411	65.4145	4.49	0.60	9.45
ILMN_1227434	Itgb7	83.795	78.8353	79.6518	50.4758	34.0096	31.6193	2.17	0.26	9.45
ILMN_2749063	Dock10	121.947	113.393	83.2968	60.1824	36.46	31.4292	2.60	0.31	9.45
ILMN_2460168	Wdr1	164.099	240.009	239.87	94.2181	182.106	153.171	1.54	0.12	9.45
ILMN_1244123	Slc38a2	617.278	625.837	600.028	411.409	327.222	277.441	1.86	0.19	9.45
ILMN_1219712	Ctps	186.691	153.171	195.687	105.577	78.5897	85.897	2.00	0.15	9.45
ILMN_1222471	Gmfg	111.062	108.082	127.702	52.6678	53.123	48.4808	2.26	0.19	9.45
ILMN_2816180	Lbh	293.83	322.267	337.268	135.811	183.486	126.057	2.20	0.27	9.45
ILMN_2769285	Sema6b	273.399	417.44	342.393	122.095	182.171	116.952	2.49	0.22	9.45
ILMN_2642403	Lmo4	292.83	226.864	246.03	161.313	138.716	149.292	1.70	0.06	9.45
ILMN_2657409	Rps18	121.768	81.1019	131.02	66.7005	43.6392	77.7686	1.79	0.05	9.45
ILMN_3113420	Ptpn6	116.265	94.4267	115.182	39.6456	40.0271	32.1489	2.96	0.35	9.45
ILMN_2665666	Pstpip1	64.4405	80.309	74.7295	29.2007	30.2943	37.1943	2.29	0.19	9.45
ILMN_2747456	Ivns1abp	590.533	756.968	781.699	182.197	184.423	122.369	4.58	0.94	9.45
ILMN_2690603	Spp1	65.9903	53.5652	58.918	28.6354	27.6908	27.5881	2.12	0.11	9.45
ILMN_1218123	Aif1	148.664	155.192	172.53	43.6865	71.7701	41.9966	3.22	0.57	9.45
ILMN_2633062	9130422G05Rik	70.3247	73.2567	65.3731	49.2978	43.418	38.5776	1.60	0.09	9.45
ILMN_2787785	Akna	65.5509	84.5019	85.8354	35.0572	55.3759	45.1822	1.77	0.12	9.45
ILMN_1224876	Znhit1	136.738	147.426	134.253	69.9344	101.869	65.8559	1.81	0.18	9.45
ILMN_2685392	Ccr5	84.029	83.7625	103.879	34.0272	29.3048	30.2587	2.92	0.28	9.45
ILMN_1255766	Sh3bp2	278.066	241.807	383.771	151.535	113.675	198.318	1.97	0.09	9.45
ILMN_2524817	Dnahc17	73.2993	94.2797	102.733	41.2589	52.5195	54.4876	1.82	0.03	9.45
ILMN_1228657	Fcgr2b	57.0806	57.6871	58.8866	30.3894	37.3815	30.0423	1.79	0.13	9.45
ILMN_2628629	Cdh1	68.05	69.4677	66.7291	41.0275	41.4125	46.8406	1.59	0.08	9.45
ILMN_2671984	Ptprc	97.5611	89.882	107.976	44.1995	36.937	31.766	2.68	0.37	9.45
ILMN_2619961	4933429F08Rik	61.1867	61.4304	54.6537	34.5111	41.7481	34.1263	1.62	0.09	9.45
ILMN_2663930	Slfn1	160.255	155.284	214.321	32.0282	34.0124	30.4836	5.53	0.76	9.45
ILMN_2675223	Cd33	92.3515	112.121	130.542	29.4763	40.0378	33.5334	3.28	0.32	9.45
ILMN_1230287	4732429D16Rik	117.416	159.803	120.705	39.1662	42.5963	39.0152	3.28	0.24	9.45
ILMN_2639925	Narg1	85.7018	88.9274	95.44	61.2866	58.5311	58.9547	1.51	0.06	9.45
ILMN_2705628	Clec4d	130.394	101.072	151.713	32.5298	33.4012	42.0911	3.55	0.29	9.45
ILMN_1226517	Ttll4	115.468	115.212	144.219	62.1325	74.5314	79.9557	1.74	0.10	9.45
ILMN_2757428	Bloc1s2	127.436	146.689	153.895	74.0141	108.02	92.7563	1.58	0.11	9.45
ILMN_3158135	Sema6b	137.319	196.419	162.365	77.6723	100.185	73.5688	1.98	0.13	9.45
ILMN_1228320	Cfp	88.6197	156.385	120.428	35.1701	69.8271	43.9795	2.50	0.14	9.45
ILMN_2737302	Cxcl12	272.912	328.145	351.831	103.238	99.8966	67.5787	3.71	0.77	9.45
ILMN_1247626	As3mt	52.1732	45.421	47.4531	33.0136	30.0851	33.0534	1.51	0.04	9.45
ILMN_1252335	Agpat6	1062.84	973.937	1072.38	612.669	610.072	806.167	1.55	0.12	9.45
ILMN_3008858	Ctsc	84.114	98.5505	129.243	28.2129	35.5427	42.4797	2.93	0.08	9.45
ILMN_2655024	Il17ra	224.335	282.901	245.501	91.3833	59.972	47.6047	4.11	0.84	9.45
ILMN_1236290	Ets1	80.5701	117.178	108.323	37.5733	48.1691	46.8349	2.30	0.08	9.45
ILMN_2891646	Hist1h2bm	220.447	420.2	283.212	137.976	291.864	148.961	1.65	0.14	9.45
ILMN_2689785	Cd68	78.7163	86.6409	84.1276	44.8606	42.4945	30.8189	2.17	0.29	9.45

Table A2. -Continued

Gene_ID	Gene	LCA1	LCA2	LCA3	RCA1	RCA2	RCA3	LCA/RCA		q-value%
		signal	signal	signal	signal	signal	signal	ratio	SEM	
ILMN_2631161	Fcgr4	171.804	267.6	234.549	32.5079	33.593	25.6287	7.47	1.14	9.45
ILMN_2544890	Pde4b	111.57	95.7741	107.701	67.3081	56.1154	47.1862	1.88	0.20	9.45
ILMN_2767057	3110082I17Rik	202.788	205.627	226.076	95.0387	128.583	157.37	1.72	0.21	9.45
ILMN_1224353	Rcc2	251.425	226.076	164.073	169.787	113.35	92.9437	1.75	0.15	9.45
ILMN_1239102	H2-Eb1	226.402	180.13	196.204	94.0991	85.3377	37.1224	3.27	1.01	9.45
ILMN_3073899	Pira11	75.7727	69.0438	64.2367	39.2087	37.5585	40.449	1.79	0.10	9.45
ILMN_2747060	Coro1a	84.3514	110.019	114.992	33.7275	41.0687	31.6302	2.94	0.35	9.45
ILMN_2913716	H2-Ab1	386.625	341.736	380.835	184.893	124.201	60.6329	3.71	1.30	9.45
ILMN_2653132	Clec7a	60.2752	70.4402	71.6424	34.7265	31.5234	33.6207	2.03	0.15	9.45
ILMN_2842338	Tbc1d10c	75.4891	97.3202	94.4267	41.8572	48.4452	40.463	2.05	0.15	9.45
ILMN_2887983	Cd300a	245.024	447.291	350.996	49.8912	107.791	59.5509	4.98	0.50	9.45
ILMN_1240566	Cep170	128.61	107.81	115.212	53.65	56.509	65.9948	2.02	0.20	9.45
ILMN_1221736	Samhd1	188.324	222.395	201.868	110.729	106.165	69.5941	2.23	0.35	9.45
ILMN_2634248	Syncrip	213.302	188.295	187.853	155.698	100.997	91.2002	1.76	0.21	9.45
ILMN_2957167	4931417G12Rik	52.8908	77.2405	73.7782	30.2857	51.7699	40.0315	1.69	0.10	9.45
ILMN_2963974	Gemin4	79.7541	95.2519	87.846	54.2831	55.062	51.4061	1.64	0.08	9.45
ILMN_2742152	Gadd45a	135.198	174.665	208.666	34.586	33.3604	35.3309	5.02	0.59	9.45
ILMN_1219333	9830134K01Rik	64.5167	58.1718	78.6184	33.8243	37.9753	53.7238	1.63	0.14	9.45
ILMN_3157568	Bcl2l11	131.316	122.924	136.543	88.1417	59.0194	64.8877	1.89	0.20	9.45
ILMN_2601155	Frzb	144.679	148.101	125.241	60.5082	70.7536	74.7254	2.05	0.21	9.45
ILMN_2529254	LOC223653	64.022	66.7712	72.0714	44.0204	37.9957	41.6299	1.65	0.10	9.45
ILMN_1249486	Mgl1	337.781	337.449	485.498	30.8081	127.473	114.992	5.94	2.55	9.45
ILMN_2894211	8430408G22Rik	73.0131	64.3754	55.1521	33.3645	31.603	30.255	2.02	0.11	9.45
ILMN_2896805	Psmd12	148.101	171.203	206.836	77.8464	126.685	133.269	1.60	0.16	9.45
ILMN_2906473	Gbl	266.679	253.353	242.375	151.35	179.604	165.538	1.55	0.11	9.45
ILMN_2821148	Serhl	165.843	202.624	140.398	68.4558	80.9844	69.9344	2.31	0.15	9.45
ILMN_2685194	Lass6	63.7303	76.289	85.0273	30.4902	30.7031	29.9149	2.47	0.22	9.45
ILMN_3139875	Acot1	87.6059	100.282	128.563	50.5489	56.6237	68.9806	1.79	0.04	9.45
ILMN_1254577	AI607873	98.2401	82.2416	110.359	31.6262	36.8739	32.9902	2.89	0.34	9.45
ILMN_2526163	LOC380753	58.693	65.5098	61.1632	40.2658	37.0268	37.1696	1.62	0.09	9.45
ILMN_2593496	Got2	250.005	371.042	377.416	158.659	239.539	216.55	1.62	0.06	9.45
ILMN_2618714	Pdgfb	200.589	324.339	300.63	70.2625	100.932	76.9535	3.32	0.31	9.45
ILMN_1255419	Zfpn1a1	57.952	64.6896	67.9671	32.1947	33.5807	27.0043	2.08	0.22	9.45
ILMN_1259488	Mgea6	187.932	197.963	206.784	94.9623	137.195	99.8402	1.83	0.20	9.45
ILMN_2836137	E2f2	124.543	144.472	159.718	60.1469	89.7572	68.5264	2.00	0.21	9.45
ILMN_2734729	H2-Aa	120.771	96.1291	106.339	50.4609	54.0207	36.4385	2.36	0.33	9.45
ILMN_2742592	Hist1h2be	278.749	573.009	385.54	163.776	384.401	179.161	1.78	0.19	9.45
ILMN_1254035	Myo10	52.187	68.5964	67.1637	29.357	32.4906	30.9367	2.02	0.12	9.45
ILMN_1256359	Smox	47.721	59.4659	60.5905	30.2443	32.779	33.8997	1.73	0.07	9.45
ILMN_1226606	Tmem132a	252.95	378.103	472.027	165.737	220.591	333.247	1.55	0.09	9.45
ILMN_1247832	Cd74	120.225	110.307	90.2238	32.0138	55.4824	31.8229	2.86	0.51	9.45
ILMN_2704919	Ube2t	48.4476	55.7575	45.7454	31.1464	31.3181	28.5945	1.65	0.07	9.45
ILMN_2494707	LOC381232	43.9483	48.7864	47.4492	29.6229	35.3182	28.389	1.51	0.08	9.45
ILMN_2727663	Tgfbi	72.3304	106.531	103.039	30.5145	37.1042	30.3291	2.88	0.30	9.45
ILMN_2435584	scl0001978.1_6	323.084	457.449	504.059	193.521	224.73	275.432	1.85	0.11	9.45
ILMN_1214071	Ifitm1	202.756	267.787	337.874	38.3514	80.5801	54.5967	4.93	0.85	9.45
ILMN_2552295	Vcam1	99.9333	87.1573	106.544	57.7501	62.3063	71.5858	1.54	0.10	9.45
ILMN_2814974	Klra2	79.6905	108.516	122.823	28.4786	34.4396	30.6148	3.32	0.36	9.45
ILMN_2922899	Plcb2	52.2083	58.4757	67.5014	31.1035	32.6911	51.2296	1.59	0.14	9.45
ILMN_1247540	Vcan	58.4595	59.6001	48.5533	33.6529	35.992	32.7154	1.63	0.07	9.45
ILMN_2810405	Myo1g	112.665	99.2771	135.567	31.0478	42.2243	32.4181	3.39	0.54	9.45
ILMN_2655336	Vcan	87.1722	118.57	99.0153	48.9433	52.8628	33.8756	2.32	0.33	9.45
ILMN_1231012	Lcp2	50.4248	55.6685	62.1287	31.9881	31.7046	32.196	1.75	0.10	9.45
ILMN_2915232	Cotl1	247.673	182.837	170.062	55.2838	37.2057	65.6713	3.99	0.71	9.45
ILMN_1222059	Thbs1	1191.26	1623.56	1613.82	427.005	537.658	171.413	5.07	2.17	9.45
ILMN_2936380	Sgpl1	76.1673	67.9833	77.8775	41.7466	47.3443	50.033	1.61	0.11	9.45
ILMN_2585233	Selpl	64.5884	56.231	48.213	40.1101	34.137	32.8397	1.58	0.05	9.45
ILMN_1242661	Itgb2	73.5594	89.9637	81.0295	44.1862	39.8288	44.1643	1.92	0.18	9.45
ILMN_3072427	Il1rn	74.4756	61.3546	56.0791	41.3113	36.8553	35.6531	1.68	0.07	9.45
ILMN_2577664	Fcgr2b	78.645	78.9582	57.4285	32.4023	36.5747	30.8478	2.15	0.16	9.45
ILMN_2715234	Rnmtl1	82.8654	96.7753	106.862	41.0073	46.4818	78.4749	1.82	0.23	9.45
ILMN_3043669	Sla	73.9528	70.2469	59.4795	46.4209	32.0101	36.2508	1.81	0.19	9.45
ILMN_2957862	Noc4l	209.341	237.52	306.964	113.482	158.699	166.487	1.73	0.12	9.45
ILMN_1222803	Hspa9	229.715	320.263	370.133	137.138	212.354	207.089	1.66	0.08	9.45
ILMN_2547840	2200005K02Rik	192.637	186.067	173.103	76.4028	76.0771	110.319	2.18	0.31	9.45
ILMN_1227907	Gmfg	147.447	136.477	186.773	61.2671	61.0607	55.4081	2.67	0.35	9.45
ILMN_1242457	Fpr2	153.684	97.4913	151.142	36.5815	31.2652	28.003	4.24	0.66	9.45
ILMN_2752224	Mrps28	88.4381	103.684	105.415	45.7269	78.8944	63.7256	1.63	0.18	9.45

Table A2. -Continued

Gene_ID	Gene	LCA1	LCA2	LCA3	RCA1	RCA2	RCA3	LCA/RCA		q-value%
		signal	signal	signal	signal	signal	signal	ratio	SEM	
ILMN_2657478	Cd53	63.5755	90.9569	83.7725	32.9734	35.9727	32.8526	2.34	0.20	9.45
ILMN_1249498	Plek	57.0174	79.9951	73.4948	33.2295	37.6965	35.3666	1.97	0.13	9.45
ILMN_1251669	Evi2a	82.2689	132.097	115.193	33.7059	39.7659	38.5166	2.92	0.26	9.45
ILMN_1220418	Hcst	136.677	92.8745	122.8	34.3575	39.3619	34.6893	3.29	0.48	9.45
ILMN_2746501	Csf3r	69.2868	58.1453	64.0938	29.6236	35.7204	32.6136	1.98	0.21	9.45
ILMN_2859847	Pygl	51.0557	68.4258	73.4562	32.046	35.2159	45.1164	1.72	0.11	9.45
ILMN_2666487	Ruvbl1	147.172	174.969	206.183	93.454	129.946	126.422	1.52	0.09	9.45
ILMN_2745425	Rcc1	161.416	220.994	195.97	73.0225	54.1906	80.9498	2.90	0.59	9.45
ILMN_1248604	D030029G14Rik	70.6935	73.0021	65.1351	50.3384	48.6371	30.7995	1.67	0.22	9.45
ILMN_2485839	Tnfrsf1b	107.917	132.878	95.6707	61.9638	68.3193	60.2337	1.76	0.10	9.45
ILMN_3155245	Arhgap25	140.997	187.482	152.592	51.9362	121.34	105.778	1.90	0.41	9.45
ILMN_2495068	scl000854.1_75	89.4428	92.8338	77.9331	43.8873	45.8507	51.9321	1.85	0.18	9.45
ILMN_2720634	Prmt5	113.534	152.14	170.153	65.5098	88.5023	80.2057	1.86	0.13	9.45
ILMN_2653619	Ctage5	246.576	238.368	234.446	120.932	175.409	125.929	1.75	0.20	9.45
ILMN_2637714	Rasa3	261.901	368.445	303.324	166.879	189.742	114.384	2.05	0.32	9.45
ILMN_2595732	LOC100046232	298.299	340.374	365.872	147.385	97.7021	57.3349	3.96	1.28	9.45
ILMN_1215085	Fkbp10	149.929	234.822	253.158	88.4708	148.241	133.604	1.72	0.09	9.45
ILMN_1220893	Zfp281	116.143	125.99	133.604	84.3139	80.2212	73.3344	1.59	0.13	9.45
ILMN_2803674	S100a9	644.295	504.87	463.707	181.349	273.803	135.985	2.94	0.55	9.45
ILMN_1252673	Cugbp2	121.93	89.3088	116.804	95.8404	52.6885	68.2533	1.56	0.14	9.45
ILMN_2864309	OTTMUSG00000(	78.8015	59.7396	57.4533	47.3468	42.2183	31.526	1.63	0.12	9.45
ILMN_2702508	Ebna1bp2	291.764	429.095	456.204	202.915	270.278	273.803	1.56	0.07	9.45
ILMN_1213708	4732462B05Rik	175.328	163.203	138.554	95.4991	110.484	95.1137	1.59	0.12	9.45
ILMN_2539454	LOC100042952	220.177	238.713	206.103	130.672	135.961	155.122	1.59	0.13	9.45
ILMN_3074985	H2afz	479.432	814.589	587.133	322.458	501.453	372.378	1.56	0.04	9.45
ILMN_2620069	Rpo1-4	123.776	103.052	112.023	89.5179	38.5027	67.0893	1.91	0.39	9.45
ILMN_2669441	Eftud2	243.605	396.587	404.776	156.045	237.52	222.43	1.68	0.07	9.45
ILMN_2918499	Abcb1b	75.4227	66.5557	69.6153	56.9205	32.488	42.3462	1.67	0.21	9.45
ILMN_1220996	Ptpn6	169.716	153.499	232.057	57.1494	45.5891	39.1416	4.09	0.93	9.92
ILMN_1245750	Prkcd	71.4567	111.699	104.522	37.7644	49.2345	62.7581	1.94	0.18	9.92
ILMN_2686044	Eif5a	2057.08	2738.78	2694.64	1466.51	1470.72	1701.41	1.62	0.13	9.92
ILMN_1254630	Ptpre	56.8771	73.2747	66.0706	38.1517	38.9873	40.061	1.67	0.11	9.92
ILMN_2833243	C330023M02Rik	67.7556	59.0485	53.0734	38.0122	33.6462	36.813	1.66	0.11	9.92
ILMN_1226785	Homer1	70.2128	54.5932	82.3784	39.7392	31.219	39.3394	1.87	0.11	9.92
ILMN_2712066	Pgd	574.081	478.684	597.984	395.758	321.509	301.621	1.64	0.17	9.92
ILMN_1250947	Txndc5	374.85	615.608	490.31	231.068	325.412	188.832	2.04	0.29	9.92
ILMN_2837779	Trpv2	55.1453	49.2566	45.0145	30.2019	31.773	30.266	1.62	0.10	9.92
ILMN_2685668	Nek6	65.568	64.9197	61.8051	34.4664	35.2325	44.87	1.71	0.17	9.92
ILMN_2820893	Selplg	140.46	92.6037	122.352	35.6979	42.4189	30.2311	3.39	0.60	9.92
ILMN_1237948	Tes	60.1162	75.3485	85.4126	31.5681	39.833	32.3082	2.15	0.25	9.92
ILMN_2593143	Dock10	48.1056	50.8025	59.1494	33.7463	31.4091	33.7003	1.60	0.10	9.92
ILMN_3154691	Sirpb1	79.5718	57.0543	73.5632	29.8909	31.5653	36.2726	2.17	0.26	9.92
ILMN_2633275	Golt1b	59.4795	59.6169	62.258	32.6962	39.2804	47.3007	1.55	0.15	9.92
ILMN_1257019	BC037034	446.474	352.563	517.081	293.505	222.2	266.214	1.68	0.13	9.92
ILMN_2507890	Ddx27	129.975	113.289	154.104	64.471	76.3964	77.5963	1.83	0.17	9.92
ILMN_2672190	Id1	62.2339	107.621	200.265	183.975	227.904	325.688	0.48	0.08	0.00
ILMN_2588249	S3-12	78.0149	38.9636	34.8013	149.177	114.816	108.516	0.39	0.06	0.00
ILMN_3113303	Atp2b2	116.025	76.6974	77.1416	289.127	267.296	256.483	0.33	0.04	0.00
ILMN_2619136	Pthlh	48.2381	53.4097	41.8714	190.072	194.052	195.665	0.25	0.02	0.00
ILMN_2687547	Sdpr	853.481	561.222	546.579	1374.31	1156.68	1137.1	0.53	0.05	2.91
ILMN_2765224	Bcam	246.143	178.001	127.729	772.164	787.544	699.336	0.24	0.04	2.91
ILMN_1237224	Kctd12	143.312	94.4929	79.4847	254.883	218.563	190.497	0.47	0.05	2.91
ILMN_3037580	Rbms2	148.529	77.8341	70.8423	251.425	167.529	168.541	0.49	0.05	3.26
ILMN_1228233	Gstm1	100.51	82.4163	69.1176	163.203	153.355	134.751	0.56	0.03	3.26
ILMN_1240938	AW212394	291.864	256.664	238.824	544.239	550.372	531.947	0.48	0.03	3.26
ILMN_2595664	Dhh	296.17	457.271	327.064	924.811	1021.15	1000.24	0.37	0.04	3.26
ILMN_2728539	Exdl2	51.7371	53.091	64.6525	81.1776	84.9802	94.8571	0.65	0.02	3.26
ILMN_2630182	Syp	43.117	38.0969	36.6536	86.5402	77.1416	80.5596	0.48	0.01	3.26
ILMN_1222685	1200016G03Rik	112.383	66.7949	66.1079	210.203	149.539	160.951	0.46	0.04	6.00
ILMN_1245307	Fbln2	72.3688	102.79	95.5123	127.322	151.656	151.713	0.63	0.03	6.00
ILMN_2628567	Phlda3	35.6836	38.3845	38.6554	57.5053	60.4906	61.8387	0.63	0.00	6.00
ILMN_1236168	C030034J23Rik	230.646	77.2548	72.6993	443.702	255.527	254.035	0.37	0.08	6.00
ILMN_2710159	MGC41689	204.383	168.578	108.339	514.959	422.262	380.345	0.36	0.04	6.00
ILMN_1253178	Aldh3a1	111.994	88.4553	97.9298	256.664	226.402	264.792	0.40	0.02	6.00
ILMN_2576994	C230096K16Rik	157.077	142.681	108.976	226.946	202.788	180.299	0.67	0.03	6.00
ILMN_2697304	Eln	1000.24	1705.22	1208.86	1988.5	2515.64	2212.67	0.58	0.05	6.00
ILMN_2904686	Cyb5r3	229.213	260.79	249.825	405.187	403.518	421.073	0.60	0.02	6.87

Table A2. -Continued

Gene_ID	Gene	LCA1	LCA2	LCA3	RCA1	RCA2	RCA3	LCA/RCA		q-value%
		signal	signal	signal	signal	signal	signal	ratio	SEM	
ILMN_1212935	Fzd4	76.9535	72.4573	71.6006	114.847	106.663	111.264	0.66	0.01	6.87
ILMN_1258578	Ahnak	382.316	306.669	385.115	595.809	508.434	634.982	0.62	0.01	6.87
ILMN_2658804	Rras	127.353	132.034	92.5633	196.565	215.554	175.816	0.60	0.04	6.87
ILMN_2441501	Clstn1	45.3194	52.187	51.0351	77.2405	83.4216	79.0062	0.62	0.02	6.87
ILMN_2769567	F2rl1	235.524	159.184	167.442	376.455	282.065	279.041	0.60	0.02	6.87
ILMN_1238603	Pcolce2	82.5011	66.228	59.1973	149.202	134.56	140.146	0.49	0.04	6.87
ILMN_3066763	Arl4a	90.8471	148.592	98.3375	285.216	298.602	269.817	0.39	0.05	6.87
ILMN_2557319	D530030K12Rik	173.467	202.984	205.466	299.497	301.047	316.914	0.63	0.03	6.87
ILMN_2598103	Emp2	417.299	445.245	436.385	1126.37	997.387	1145.03	0.40	0.02	6.87
ILMN_2605539	Sgcd	65.639	50.9856	44.1843	112.578	93.1222	96.3487	0.53	0.04	6.87
ILMN_2772855	Plek2	37.2072	51.4746	51.8662	88.2238	93.4264	95.4991	0.51	0.04	6.87
ILMN_2736783	Kctd12	512.111	295.475	269.308	884.251	732.913	601.71	0.48	0.05	6.87
ILMN_2712873	Cyb5r3	146.274	176.566	153.984	233.764	280.452	267.013	0.61	0.02	6.87
ILMN_2625920	Aoc3	131.367	35.614	35.7044	263.466	148.796	138.005	0.33	0.08	6.87
ILMN_3061923	Rbms2	176.925	138.5	95.6101	261.411	241.544	177.17	0.60	0.04	6.87
ILMN_2691641	Gja5	1008.44	1000.24	868.589	1637.38	1613.82	1662.57	0.59	0.03	6.87
ILMN_1240266	Ankrd25	188.414	244.001	208.29	413.715	435.703	377.164	0.52	0.03	6.87
ILMN_2765101	Nkx6-2	186.73	243.29	238.939	284.65	354.738	368.284	0.66	0.01	6.87
ILMN_2639809	Nucb1	141.533	126.85	125.096	219.022	194.959	214.159	0.63	0.02	6.87
ILMN_2710419	Plec1	529.3	401.323	461.117	830.81	639.564	782.283	0.62	0.01	6.87
ILMN_2798086	Fchsd2	222.609	201.439	228.433	345.459	366.42	376.647	0.60	0.03	6.87
ILMN_1220170	Tek	422.95	326.735	317.866	699.822	620.507	685.316	0.53	0.04	6.87
ILMN_1230039	Hyal2	127.702	148.38	187.358	294.463	367.707	407.887	0.43	0.02	6.87
ILMN_2745370	Sult1a1	252.628	126.991	73.8402	405.668	327.311	277.179	0.43	0.10	6.87
ILMN_1257053	Trrp1	37.8964	49.098	61.3483	107.439	124.856	118.44	0.42	0.05	6.87
ILMN_2839886	Mxd4	81.9997	70.0674	59.3453	143.589	137.012	110.093	0.54	0.02	6.87
ILMN_2908132	Gja5	1742.7	1605.47	1567.3	2583.93	2583.93	2738.78	0.62	0.03	6.87
ILMN_1220023	Snhg10	50.3966	54.7987	77.4215	112.852	138.5	151.214	0.45	0.03	6.87
ILMN_3109360	Plec1	98.3757	100.702	128.226	166.972	160.833	179.957	0.64	0.04	6.87
ILMN_2502860	Ern1	222.809	172.126	184.279	321.206	288.074	318.448	0.62	0.04	6.87
ILMN_3139103	Adam15	83.5285	67.1136	94.1663	228.742	214.244	284.473	0.34	0.02	6.87
ILMN_1215859	Serpina1b	33.3142	35.683	34.7094	59.6241	58.8416	56.4895	0.59	0.02	6.87
ILMN_1213456	Dhrs7	99.8878	118.25	94.9623	198.193	209.535	216.993	0.50	0.04	6.87
ILMN_2725493	2700078K21Rik	40.2563	47.9145	43.114	99.6693	102.504	115.053	0.42	0.03	6.87
ILMN_2713835	Nos3	128.411	151.047	109.104	249.905	311.942	274.064	0.47	0.03	6.87
ILMN_1214275	Ddef2	130.455	87.759	63.6744	166.922	135.33	110.019	0.67	0.06	7.51
ILMN_2596117	Kctd10	275.84	316.914	308.662	457.748	479.924	534.928	0.61	0.02	7.51
ILMN_2953751	Sec14l1	111.699	133.722	117.914	204.504	201.06	202.615	0.60	0.04	7.51
ILMN_2715195	Stxbp3a	87.9518	88.8714	91.8696	148.916	134.164	142.943	0.63	0.02	7.51
ILMN_2801891	Cygb	63.3289	27.8296	36.1873	107.03	85.1764	82.1725	0.45	0.08	7.51
ILMN_1236917	Tmem59	122.279	128.864	122.134	208.611	233.426	197.73	0.59	0.02	7.51
ILMN_1224018	Foxk1	45.8532	62.8697	45.1941	100.662	114.552	114.358	0.47	0.04	7.51
ILMN_3022252	Arhgef15	358.839	287.917	182.699	550.372	423.744	368.566	0.61	0.06	7.51
ILMN_2646052	C4a	62.815	42.36	38.3445	89.4502	63.9564	60.3816	0.67	0.02	7.51
ILMN_1217742	Atp2b4	205.67	93.0616	122.622	356.859	310.617	326.853	0.42	0.08	7.51
ILMN_1221146	Cytl1	882.036	477.684	479.432	1479.31	1325.04	1332.33	0.44	0.08	7.51
ILMN_1230578	LOC100045421	30.9348	33.1017	43.1599	71.006	64.9596	74.3976	0.51	0.04	7.51
ILMN_2710274	Slc9a3r2	423.177	347.456	309.668	1050.18	1016.65	1198.69	0.33	0.04	8.11
ILMN_2630039	E130014J05Rik	64.2269	119.518	77.3166	128.519	166.304	140.248	0.59	0.07	8.11
ILMN_2738345	Lims2	123.066	109.173	96.2198	313.307	238.461	264.652	0.40	0.03	8.11
ILMN_1253182	Hs3st1	144.693	109.309	125.627	196.419	182.637	192.889	0.66	0.04	8.11
ILMN_1245446	5730405I09Rik	103.851	70.1408	77.6978	143.21	125.096	126.027	0.63	0.05	8.11
ILMN_2970167	Wwp2	99.4163	83.5547	89.5852	168.455	132.499	146.379	0.61	0.01	8.11
ILMN_2942674	Lims2	114.145	103.081	86.1846	317.148	250.321	302.675	0.35	0.04	8.11
ILMN_1243080	Taf9b	78.8229	129.813	96.5937	141.805	200.649	146.191	0.62	0.03	8.11
ILMN_1243407	Klk10	72.4259	166.042	96.5406	1021.15	810.832	1025.49	0.12	0.04	8.11
ILMN_2416218	5530400B01Rik	43.8792	53.688	70.2938	116.319	132.471	172.365	0.40	0.01	8.11
ILMN_2511768	Ttc17	94.7962	84.1399	94.3132	147.573	156.757	149.929	0.60	0.03	8.11
ILMN_2940642	St6galnac2	181.706	108.618	98.5505	341.863	306.268	338.523	0.39	0.07	8.11
ILMN_2659879	Adcy6	94.5228	77.2323	64.5074	174.869	137.052	123.01	0.54	0.01	8.11
ILMN_2744414	Nme3	55.2283	61.5117	98.0606	97.0437	112.407	157.92	0.58	0.02	8.11
ILMN_2778181	Plekha6	34.0601	39.3109	39.4733	82.2512	77.6384	94.4418	0.45	0.03	8.11
ILMN_1213850	Col4a3	290.506	100.468	80.1506	614.723	472.324	567.125	0.28	0.10	8.11
ILMN_2638114	Ptn	32.7443	27.7131	31.5817	53.9461	44.1532	50.6546	0.62	0.01	8.11
ILMN_1225825	LOC100039175	149.292	113.675	75.9107	236.689	211.11	203.404	0.51	0.08	8.11
ILMN_1248397	Smarcd3	48.44	46.5846	60.204	92.1682	79.7314	107.24	0.56	0.02	8.11
ILMN_1239381	Klf3	161.902	147.573	159.426	504.059	372.064	480.324	0.35	0.02	8.11
ILMN_2633386	LOC100044190	183.189	208.452	165.737	381.449	369.561	296.068	0.53	0.03	8.11

Table A2. -Continued

Gene_ID	Gene	LCA1	LCA2	LCA3	RCA1	RCA2	RCA3	LCA/RCA		q-value%
		signal	signal	signal	signal	signal	signal	ratio	SEM	
ILMN_2669062	Pi16	544.239	258.436	259.511	1241.79	1032.64	1305.32	0.30	0.07	8.11
ILMN_2479359	Tmod3	100.151	96.7873	87.0908	178.613	149.639	157.483	0.59	0.03	8.11
ILMN_2433213	Klf7	197.15	148.324	162.419	301.34	292.51	263.754	0.59	0.04	8.11
ILMN_1259554	Marveld1	295.742	218.699	200.156	578.387	409.629	486.774	0.49	0.04	8.11
ILMN_3094506	Arhgef15	249.151	184.614	195.81	379.653	368.445	396.069	0.55	0.05	8.11
ILMN_2755833	Lrrc3b	42.248	35.4296	34.0641	70.0455	66.1659	56.2598	0.58	0.02	8.11
ILMN_2723024	BC004044	34.7697	43.6311	49.7896	57.1241	66.6586	67.272	0.67	0.04	8.11
ILMN_1234318	Ubxd1	282.467	213.541	225.574	403.757	401.323	379.425	0.61	0.05	8.11
ILMN_2699637	Lsr	127.923	87.5939	111.784	337.268	221.61	294.463	0.38	0.01	8.11
ILMN_2999439	Klf4	107.856	84.3514	84.215	299.601	295.852	372.58	0.29	0.04	8.11
ILMN_1231439	Aatk	157.92	175.917	186.73	293.83	336.911	395.84	0.51	0.02	8.11
ILMN_2675760	2310046K01Rik	172.059	111.635	195.131	563.411	360.928	502.928	0.33	0.03	8.11
ILMN_2661422	Ramp2	504.87	475.438	389.274	1054.3	917.819	1088.19	0.45	0.05	8.11
ILMN_1248994	4933407C03Rik	127.219	101.735	75.8184	223.594	193.564	210.536	0.48	0.06	8.11
ILMN_1260405	D330008E13Rik	98.0606	73.3663	45.7439	136.276	100.97	85.327	0.66	0.06	8.11
ILMN_2675232	Klk8	96.2111	93.4264	80.4456	196.733	199.298	229.119	0.44	0.04	8.11
ILMN_2608133	Rhpn2	259.918	187.358	208.938	747.241	740.239	966.087	0.27	0.04	8.11
ILMN_1248740	Sema3f	587.133	651.489	606.935	1186.2	1161.24	1409.35	0.50	0.04	8.11
ILMN_2609025	Elmo1	134.465	110.413	101.262	208.907	163.203	153.499	0.66	0.01	8.11
ILMN_1230129	Adamts1	122.238	124.704	151.871	201.488	178.513	233.764	0.65	0.03	8.11
ILMN_1231802	Tbc1d9b	33.741	37.4625	38.1107	54.4372	52.911	57.5937	0.66	0.03	8.11
ILMN_2790842	Jam2	124.676	102.814	90.6203	272.976	221.491	279.166	0.42	0.05	8.11
ILMN_1242787	4930557M22Rik	41.1506	42.8033	41.6011	68.2616	62.2175	64.0826	0.65	0.02	8.11
ILMN_1228031	Dusp8	87.1472	164.237	131.982	446.474	539.755	367.087	0.29	0.05	8.11
ILMN_1224589	Tmem77	79.4451	72.5412	54.4581	119.991	100.057	92.3784	0.66	0.04	8.11
ILMN_2485594	B130005I07Rik	34.2484	40.5641	40.2952	58.0717	58.3733	59.1772	0.66	0.03	8.11
ILMN_1237264	Trspap1	53.9897	45.0626	66.6205	98.3551	82.5496	96.286	0.60	0.05	8.11
ILMN_2678355	Amigo2	200.895	159.649	181.816	378.103	379.425	465.668	0.45	0.04	8.11
ILMN_1218934	Rdm1	103.409	86.2467	55.7304	179.384	135.081	125.527	0.55	0.06	8.11
ILMN_2777082	P4ha2	216.879	359.701	623.623	776.328	864.305	964.159	0.45	0.11	8.11
ILMN_2430542	Nos3	121.33	136.738	98.4581	221.353	283.725	260.402	0.47	0.05	8.11
ILMN_3003864	Cgnl1	334.932	239.642	156.385	591.126	537.82	564.432	0.43	0.08	8.11
ILMN_2653215	Nagk	157.705	141.767	138.349	240.257	259.054	216.306	0.61	0.03	8.11
ILMN_2788593	Nos3	113.98	123.912	103.799	233.023	284.88	206.059	0.48	0.02	8.11
ILMN_2640248	Lama5	200.724	203.499	200.036	371.901	326.735	309.207	0.60	0.03	8.11
ILMN_2635631	Sema3f	417.684	390.156	391.19	787.544	729.074	923.072	0.50	0.04	8.11
ILMN_2876325	Fbxo34	49.326	60.209	66.0396	88.1484	104.785	125.057	0.55	0.01	8.11
ILMN_3111298	Mcfd2	169.684	219.692	244.888	265.869	350.281	403.059	0.62	0.01	8.11
ILMN_1241903	Klf4	43.9331	32.111	37.4217	91.3567	96.1915	113.289	0.38	0.05	8.11
ILMN_3132949	Fbln2	70.0583	73.3238	82.0111	119.96	110.92	115.302	0.65	0.04	8.11
ILMN_2920759	Clip1	185.174	121.682	112.001	278.804	181.042	182.837	0.65	0.02	8.11
ILMN_1218949	Mterfd2	301.69	105.697	77.5773	482.642	314.461	367.212	0.39	0.12	8.11
ILMN_2706730	Ptprr	60.4528	46.3893	39.1565	116.04	127.268	128.836	0.40	0.06	8.11
ILMN_1230880	Myst4	71.5004	53.07	53.6116	109.8	83.1432	99.9707	0.61	0.04	8.11
ILMN_2461707	Rbms2	130.959	100.308	98.508	170.765	157.257	161.466	0.67	0.05	8.11
ILMN_2427021	Megf6	48.688	63.0216	48.2948	109.131	101.175	100.334	0.52	0.05	8.11
ILMN_1241892	Sod3	134.538	92.696	68.8795	177.599	158.954	135.213	0.62	0.07	8.11
ILMN_3033533	Add1	274.507	256.824	219.692	383.771	398.773	399.875	0.64	0.05	8.11
ILMN_1254927	Ly6c1	364.13	200.724	143.763	660.535	688.27	620.507	0.36	0.10	8.11
ILMN_1248947	Mal	137.485	72.275	127.908	256.938	195.398	204.444	0.51	0.07	8.11
ILMN_1221264	Klf4	44.6148	39.8925	33.0754	133.999	95.2519	115.346	0.35	0.04	8.11
ILMN_2590034	Ltbp4	782.283	543.771	452.054	1055.94	966.087	914.47	0.60	0.07	8.11
ILMN_2596346	Dcn	90.4845	51.7102	45.442	124.329	91.8195	71.5224	0.64	0.05	8.11
ILMN_2706853	Scamp1	762.104	595.205	641.17	1039.71	1045.49	961.692	0.66	0.05	8.11
ILMN_2599955	Btbd3	305.366	227.618	142.411	494.447	533.091	453.325	0.45	0.09	8.11
ILMN_2578183	E330020K23Rik	30.5007	36.3718	42.1806	60.0792	56.6584	65.6786	0.60	0.04	8.11
ILMN_2715558	Arhgap17	163.203	148.815	145.273	255.256	206.389	235.048	0.66	0.03	8.11
ILMN_1235230	Pdlim3	282.316	197.642	198.515	366.616	338.784	320.983	0.66	0.06	8.11
ILMN_2759079	Ppap2a	118.721	159.764	187.064	237.352	236.32	268.555	0.62	0.06	8.11
ILMN_1228245	Prickle1	51.8263	58.89	39.0885	75.7577	93.4373	64.3906	0.64	0.02	8.11
ILMN_3137804	Pbx1	91.7399	62.7876	56.8554	132.442	112.466	88.0602	0.63	0.04	8.11
ILMN_2618408	Icam2	465.668	496.633	413.078	912.268	862.8	1029.2	0.50	0.05	8.11
ILMN_1249888	Adcy6	56.1244	54.8139	75.563	147.893	147.525	132.797	0.44	0.06	8.11
ILMN_1215879	Pkhd1l1	52.5954	48.9358	42.2605	76.8252	81.1776	80.1112	0.60	0.05	8.11
ILMN_1218241	Slc9a3r2	38.2593	41.671	40.0713	62.9502	78.0995	78.1575	0.55	0.03	8.11
ILMN_3049559	C4b	133.533	61.2284	57.7642	205.866	137.617	104.479	0.55	0.06	8.11
ILMN_1255416	Ly6a	1104.46	830.81	652.951	1597.38	1529.47	1518.64	0.55	0.08	8.11
ILMN_1257193	Ppm1a	75.7351	83.5746	96.6313	129.487	117.852	150.578	0.65	0.04	8.11

Table A2. -Continued

Gene_ID	Gene	LCA1	LCA2	LCA3	RCA1	RCA2	RCA3	LCA/RCA		q-value%
		signal	signal	signal	signal	signal	signal	ratio	SEM	
ILMN_1241605	LOC383884	54.6585	35.6853	30.1919	72.1759	60.7634	49.4577	0.65	0.05	8.11
ILMN_2700166	Ccnd2	360.795	240.15	297.852	494	455.732	446.189	0.64	0.06	8.11
ILMN_1225657	2410095B20Rik	55.062	45.0902	42.8424	86.3618	65.8265	73.194	0.64	0.03	8.11
ILMN_2896843	Cd248	48.8687	32.4954	63.9994	83.2478	88.5625	110.744	0.51	0.07	8.11
ILMN_2513922	Prdm16	41.6079	39.0039	49.0403	72.0203	63.8746	69.0167	0.63	0.04	8.11
ILMN_2614380	Map3k1	303.793	241.665	168.945	421.91	364.13	354.311	0.62	0.07	8.11
ILMN_1248895	Cachd1	45.9188	30.615	37.0233	73.8569	57.0335	55.5248	0.61	0.04	8.11
ILMN_1260571	Spna2	191.048	142.571	131.147	262.266	248.325	198.585	0.65	0.04	8.11
ILMN_2640570	Pak4	163.982	189.45	223.33	358.386	531.947	489.502	0.42	0.03	8.11
ILMN_1243249	2810410A03Rik	357.198	212.915	220.079	590.533	392.919	533.911	0.52	0.06	8.11
ILMN_2733887	Mknk2	233.221	162.634	149.901	445.245	339.737	451.189	0.44	0.06	8.11
ILMN_1239673	LOC672215	38.9745	56.0613	42.9084	70.3618	107.621	83.5746	0.53	0.01	8.11
ILMN_2963704	Sfxn3	923.072	763.426	796.198	1214.35	1179.22	1320.67	0.67	0.05	8.11
ILMN_2513570	AW123240	70.483	82.906	100.857	106.085	131.761	160.851	0.64	0.01	8.11
ILMN_2670375	Itm2b	521.35	428.866	444.289	693.644	733.971	731.408	0.65	0.05	8.11
ILMN_1219447	Zmym3	96.3626	95.5384	112.893	150.021	187.095	200.265	0.57	0.04	8.11
ILMN_2761918	Mmrn2	832.829	513.691	565.535	1176.27	1137.1	1117.52	0.56	0.08	8.11
ILMN_2789562	P4ha2	118.522	161.927	292.11	399.875	381.449	449.139	0.46	0.10	8.11
ILMN_2493521	Tnrc6c	104.466	79.4961	75.2412	172.817	127.106	117.736	0.62	0.01	8.11
ILMN_2728538	Exdl2	44.8324	54.019	62.6551	81.9711	82.4037	86.0639	0.64	0.05	8.11
ILMN_2658407	Elmo1	71.0764	87.6985	118.356	137.513	140.496	157.305	0.63	0.07	8.11
ILMN_1223049	Tns1	200.969	141.404	106.994	294.114	299.497	269.623	0.52	0.09	8.11
ILMN_2855515	Pnpla6	117.852	129.658	98.6394	192.188	178.238	183.746	0.63	0.06	8.11
ILMN_2913222	Efcab4a	140.581	122.414	150.052	233.506	271.492	317.274	0.51	0.05	8.11
ILMN_2577853	Rw1-pending	51.684	62.4702	45.4828	87.8284	84.5065	76.4736	0.64	0.05	8.11
ILMN_1224866	Ptgs1	51.6725	47.1747	45.0369	93.0616	83.8402	104.383	0.52	0.04	8.36
ILMN_2933431	Pps	41.1925	37.794	45.5791	60.2271	65.7182	76.1147	0.62	0.03	8.36
ILMN_2750053	Ptprj	373.419	266.465	251.024	794.088	808.417	1007.42	0.35	0.06	8.36
ILMN_2641228	Hspa12b	271.621	215.554	218.699	489.109	443.208	577.363	0.47	0.05	8.36
ILMN_2947526	Ecm1	166.998	102.742	128.992	238.573	209.463	258.307	0.56	0.07	8.36
ILMN_2757019	She	201.575	205.773	198.377	278.935	307.14	335.692	0.66	0.04	8.36
ILMN_2509327	Wipf3	40.1571	38.7539	34.6308	62.1871	60.3744	66.7522	0.60	0.04	8.36
ILMN_2633897	Pde6d	51.1288	51.3888	55.3458	83.1158	86.9641	76.8633	0.64	0.04	8.36
ILMN_2615035	Mgst3	182.197	234.446	175.219	285.806	419.386	356.011	0.56	0.04	8.36
ILMN_3126277	Palmd	498.667	563.001	504.87	813.914	869.588	1010.49	0.59	0.04	8.36
ILMN_2743320	Myst4	67.7135	56.8771	54.8654	111.326	82.5011	93.5353	0.63	0.03	8.36
ILMN_2592823	Cdc42ep5	94.1107	66.2064	50.5887	155.469	105.431	90.3429	0.60	0.02	8.36
ILMN_1241293	Cldn5	842.223	502.602	537.82	1549.02	1292.13	1759.24	0.41	0.07	8.36
ILMN_2727687	Numb	52.3817	86.2716	98.0765	105.144	123.575	130.094	0.65	0.08	8.36
ILMN_3111877	Rbms2	442.828	318.448	305.33	577.363	548.363	554.129	0.63	0.07	8.36
ILMN_2727309	LOC100044204	125.856	57.9598	43.5082	256.167	131.843	135.526	0.42	0.05	8.36
ILMN_3159275	Ahnak	349.427	201.707	230.212	467.7	326.305	427.005	0.63	0.06	8.36
ILMN_2877069	Tspo	157.145	164.622	154.671	250.749	309.742	241.544	0.60	0.03	8.36
ILMN_2678477	Gja5	74.3285	72.6458	56.9453	134.907	150.052	164.073	0.46	0.06	8.36
ILMN_3052632	Epas1	1613.82	1001.67	864.305	2304.22	2020.1	2174.36	0.53	0.09	8.36
ILMN_2592881	Jam2	71.4685	66.0291	56.2363	117.134	114.911	130.702	0.54	0.06	8.36
ILMN_3132223	C630004H02Rik	195.894	129.579	158.008	291.764	257.511	228.301	0.62	0.06	8.36
ILMN_2466164	Wfdc1	31.943	35.1659	34.2332	75.9107	75.1312	59.7646	0.49	0.04	8.36
ILMN_3115796	Cd40	32.134	105.198	63.9726	116.069	157.662	116.921	0.50	0.12	8.36
ILMN_2720083	Bace2	138.364	104.127	136.076	242.001	299.277	303.036	0.46	0.06	8.36
ILMN_2705128	Muted	364.511	371.22	449.541	552.21	656.598	612.669	0.65	0.05	8.36
ILMN_1220234	Serpina1e	39.344	35.033	39.7792	83.5948	115.575	108.964	0.38	0.05	8.36
ILMN_2599008	Kirrel3	52.7322	38.3915	38.4879	91.0124	64.9092	84.7187	0.54	0.04	8.36
ILMN_2588295	Rarres2	31.8438	55.6936	36.7392	81.0295	115.357	70.0633	0.47	0.04	8.36
ILMN_2881681	Tnrc6c	189.907	114.468	129.592	391.19	279.551	235.579	0.48	0.04	8.36
ILMN_2865335	Krt80	316.475	196.959	141.215	470.301	382.959	417.299	0.51	0.10	8.36
ILMN_2432550	Trib2	126.182	63.1931	70.2625	326.405	176.977	202.624	0.36	0.01	8.36
ILMN_2756665	Cbr2	53.5133	115.954	74.4169	150.439	183.243	199.513	0.45	0.09	8.36
ILMN_2736379	Nfia	421.636	355.867	235.579	588.515	468.921	449.797	0.67	0.07	8.36
ILMN_2572849	C920007D24Rik	44.6002	57.6022	52.6758	76.0338	110.563	107.761	0.53	0.03	8.36
ILMN_1225988	Zdhhc3	28.6758	42.7422	73.3151	83.7998	103.178	107.044	0.48	0.10	8.36
ILMN_2862179	Ccl11	32.7051	30.762	32.7544	55.4121	47.2542	47.8454	0.64	0.03	8.36
ILMN_1257077	Jag1	81.2723	72.5674	72.5891	113.421	112.962	128.205	0.64	0.04	8.46
ILMN_2799596	AI662250	60.6924	87.4522	58.3217	112.918	123.184	123.184	0.57	0.07	8.46
ILMN_3139693	Rab11fip5	238.322	181.183	257.913	326.305	334.612	358.203	0.66	0.06	8.46
ILMN_2991660	Mif4gd	63.2658	53.2608	51.634	94.7868	89.6643	72.7436	0.66	0.03	8.46
ILMN_3079421	Pde6d	72.8345	89.553	76.3914	144.693	128.743	134.877	0.59	0.06	8.46
ILMN_2765032	Kcnn4	42.161	43.3855	43.2686	68.959	83.8463	90.9059	0.53	0.04	8.46

Table A2. -Continued

Gene_ID	Gene	LCA1	LCA2	LCA3	RCA1	RCA2	RCA3	LCA/RCA		q-value%
		signal	signal	signal	signal	signal	signal	ratio	SEM	
ILMN_2622089	5430432N15Rik	292.288	377.416	350.853	673.927	584.801	741.828	0.52	0.07	8.46
ILMN_2868457	Lrrc1	30.4015	44.1971	43.52	69.7624	77.6978	66.0829	0.55	0.06	8.46
ILMN_2549903	6230401I02Rik	424.33	447.474	551.141	788.6	752.523	737.73	0.63	0.06	8.46
ILMN_2963700	Sfxn3	514.465	415.733	420.048	681.141	740.801	699.822	0.64	0.06	8.46
ILMN_1220360	Unc13b	306.803	147.945	199.844	441.338	386.378	458.732	0.50	0.10	8.46
ILMN_1258788	Snx27	87.4803	97.8215	97.2554	130.203	177.528	162.064	0.61	0.04	8.46
ILMN_2913166	Serping1	221.237	90.8912	101.459	317.398	256.531	205.41	0.52	0.10	8.46
ILMN_3129160	Epas1	268.311	207.224	148.553	403.919	367.087	392.919	0.54	0.08	8.46
ILMN_2803249	Inmt	29.4014	27.4922	29.0673	67.8443	61.8051	50.9721	0.48	0.04	8.46
ILMN_2618148	C330008K14Rik	40.7916	54.0309	52.6678	94.1524	83.3205	97.8215	0.54	0.06	8.46
ILMN_2495363	Wasf2	121.426	96.8233	81.3992	194.621	137.447	155.714	0.62	0.05	8.46
ILMN_2722864	Ncam1	59.7314	39.6274	37.8231	99.9707	98.385	114.019	0.44	0.08	8.46
ILMN_2872058	Ctsh	544.057	486.774	372.676	796.198	832.829	865.29	0.57	0.07	8.65
ILMN_2877029	Cytl1	872.013	510.394	509.037	1368.43	1338.51	1524.36	0.45	0.09	8.65
ILMN_2745876	BC020535	329.37	207.778	148.101	496.633	474.132	487.371	0.47	0.10	8.65
ILMN_1225570	Serpina1d	29.0837	30.3817	34.1942	72.9833	57.8335	61.5255	0.49	0.05	8.65
ILMN_2627179	Ell3	32.2903	72.5006	82.3609	63.2503	104.714	100.838	0.67	0.09	8.65
ILMN_3163577	Scn3b	70.2625	36.8987	42.4418	117.436	120.904	134.089	0.41	0.10	8.65
ILMN_2908133	Gja5	658.524	494	473.41	820.708	825.317	761.05	0.67	0.06	8.65
ILMN_3150811	Tsc22d3	283.414	203.971	167.529	391.439	419.129	370.712	0.55	0.09	8.65
ILMN_1242286	Ermp1	71.0934	116.357	85.7468	112.943	155.042	152.14	0.65	0.05	8.65
ILMN_1238936	D130063P19Rik	46.7383	40.8882	47.1953	69.0167	67.9597	85.8136	0.61	0.04	8.65
ILMN_3112526	Ldb2	66.8084	69.3189	81.2723	117.148	146.556	180.184	0.50	0.04	8.65
ILMN_1233340	Pkp4	681.517	589.246	550.781	932.625	873.975	1013.33	0.65	0.06	8.65
ILMN_2454786	Tpcn1	151.871	93.1508	91.3389	218.634	219.409	176.434	0.55	0.08	8.65
ILMN_3163020	Klc1	133.391	100.303	105.02	171.278	172.876	158.988	0.67	0.06	8.65
ILMN_1232123	Traf3ip2	51.1805	47.9913	49.6801	77.2158	77.9778	94.7022	0.60	0.04	8.65
ILMN_1231520	Trpv4	88.4863	66.2779	61.6668	141.914	121.081	152.958	0.52	0.06	8.65
ILMN_2449620	5830427D02Rik	37.9178	41.6011	31.6109	56.5784	72.4921	52.5811	0.62	0.03	8.65
ILMN_2740628	Ndrg3	37.3127	38.5466	43.304	75.1993	64.4612	65.2556	0.59	0.05	8.65
ILMN_2931918	4432416J03Rik	38.8503	36.6663	38.3514	63.8012	60.5082	77.5385	0.57	0.04	8.65
ILMN_2834370	Cutc	123.078	113.35	106.029	185.206	162.097	197.642	0.63	0.05	8.65
ILMN_2610442	Wscd1	146.262	151.656	70.179	271.621	227.266	140.91	0.57	0.05	8.65
ILMN_2663211	Stbd1	137.695	84.2408	73.0131	178.031	147.945	153.32	0.61	0.09	8.65
ILMN_2688236	Atp2a3	4083.11	3028.05	2825.87	5196.2	4906.71	5196.2	0.65	0.07	8.65
ILMN_1212703	Kras	153.355	215.024	240.758	304.499	292.288	343.464	0.65	0.07	8.65
ILMN_2870522	Plekha6	62.1625	100.997	51.8263	368.961	249.825	343.276	0.24	0.08	8.65
ILMN_2790839	Jam2	276.563	154.216	145.886	434.397	404.776	475.933	0.44	0.10	8.65
ILMN_2621038	Hoxa7	42.0135	66.9511	66.9422	63.7045	107.24	105.47	0.64	0.01	8.65
ILMN_2745367	Myo1c	76.7253	95.945	141.976	145.352	130.394	201.207	0.66	0.06	8.65
ILMN_1253304	Stmn2	49.4318	56.2363	47.9572	134.21	206.725	225.925	0.28	0.05	9.10
ILMN_2473692	1110059G02Rik	57.9107	56.6484	51.2859	79.1824	88.9048	91.6038	0.64	0.05	9.10
ILMN_2923607	Phlda3	117.163	144.375	121.826	234.21	210.536	259.773	0.55	0.07	9.10
ILMN_1238331	Rom1	155.714	129.458	122.095	253.353	290.506	327.602	0.48	0.07	9.10
ILMN_1250469	Bcl9l	640.55	599.17	494.447	1066.43	1231.62	1387.11	0.48	0.07	9.10
ILMN_2507400	9330180L10Rik	84.7187	85.897	86.9195	142.571	119.75	155.22	0.62	0.05	9.10
ILMN_3161897	Dync1li2	123.393	126.126	136.104	195.082	184.662	247.673	0.62	0.04	9.10
ILMN_2686087	Cutc	53.3624	58.8209	75.3768	108.356	90.7635	139.828	0.56	0.05	9.10
ILMN_1229828	Adamts10	50.3671	46.1116	35.9946	70.8726	85.0851	72.5674	0.58	0.07	9.10
ILMN_2700408	Mgll	40.2028	42.4966	37.1282	76.9833	79.917	100.429	0.47	0.05	9.10
ILMN_2624451	4933407C03Rik	244.182	167.616	135.02	359.109	386.96	381.449	0.49	0.10	9.10
ILMN_2474515	9430020K01Rik	103.424	90.278	72.5598	131.218	135.37	128.458	0.67	0.06	9.10
ILMN_1259753	Sp4	50.6371	55.206	37.5402	73.3093	84.6086	79.7982	0.60	0.07	9.10
ILMN_2727481	Palmd	336.989	385.54	327.944	603.342	548.933	682.097	0.58	0.06	9.10
ILMN_2597769	Igf2	75.7692	79.9773	74.05	342.482	211.942	246.143	0.30	0.05	9.10
ILMN_2697760	Nkx2-3	77.9397	81.6723	110.832	125.057	169.488	164.891	0.59	0.06	9.10
ILMN_2622354	Arfl4	40.3359	35.7265	42.8769	80.0266	56.3296	73.1443	0.57	0.04	9.10
ILMN_2838317	Pqlc3	34.9174	44.4537	43.4826	75.8462	65.2609	77.7796	0.57	0.06	9.10
ILMN_2604029	Klf2	58.2625	38.0564	43.8004	144.138	205.143	146.915	0.30	0.06	9.10
ILMN_1246346	B230107H12Rik	82.2304	66.1079	54.0231	105.721	112.744	96.9221	0.64	0.07	9.10
ILMN_1222365	2610200O14Rik	65.5176	55.4662	47.6255	102.801	100.303	70.0863	0.62	0.04	9.10
ILMN_1251524	Them4	42.7651	56.1845	62.6502	69.3859	92.0097	81.4395	0.67	0.05	9.10
ILMN_2993109	Ddit4	922.125	499.199	581.594	1117.52	912.268	1003.24	0.65	0.09	9.10
ILMN_2646166	Ndrl	247.3	151.787	269.623	318.341	303.324	379.264	0.66	0.08	9.10
ILMN_2729153	Nos3	119.927	139.333	86.6722	205.941	262.556	267.257	0.48	0.08	9.45
ILMN_1237671	Setmar	31.0571	72.4921	60.8733	88.7598	100.6	105.764	0.55	0.11	9.45
ILMN_2634689	Itgb4	134.351	77.9847	72.1687	212.051	200.796	239.87	0.44	0.10	9.45
ILMN_1217061	Casp9	170.256	158.484	187.693	225.646	274.673	302.527	0.65	0.05	9.45

Table A2. -Continued

Gene_ID	Gene	LCA1	LCA2	LCA3	RCA1	RCA2	RCA3	LCA/RCA		q-value%
		signal	signal	signal	signal	signal	signal	ratio	SEM	
ILMN_2833781	Pwwp2b	91.1142	80.24	83.0716	139.828	158.284	187.064	0.53	0.06	9.45
ILMN_2857957	Mgll	39.4813	41.585	37.6306	65.7594	86.7752	92.0097	0.50	0.06	9.45
ILMN_1232928	Timp3	410.301	495.592	463.428	882.937	705.192	882.036	0.56	0.07	9.45
ILMN_2622500	Zbtb7c	40.4978	43.1366	62.7662	269.948	166.341	339.932	0.20	0.03	9.45
ILMN_1249637	Peg13	73.4438	39.8558	40.1235	93.3435	75.1746	62.6477	0.65	0.07	9.45
ILMN_2765047	Chrd	39.5724	37.3638	36.3189	76.4122	110.281	113.999	0.39	0.06	9.45
ILMN_1217606	1500005K14Rik	37.6023	54.0652	75.9536	132.689	140.354	120.098	0.43	0.10	9.45
ILMN_2683095	Ap1g2	161.527	207.089	168.476	273.399	311.432	220.177	0.67	0.05	9.45
ILMN_2498731	E030024M20Rik	112.001	87.8961	90.4651	322.372	206.583	358.107	0.34	0.05	9.45
ILMN_1232295	Sort1	171.734	208.772	116.669	240.758	260.586	222.395	0.68	0.08	9.45
ILMN_2614889	B3gnt8	95.0234	102.037	101.684	436.16	252.441	362.178	0.30	0.05	9.45
ILMN_2602185	9/9/2009	117.453	124.175	176.172	229.783	233.697	379.854	0.50	0.02	9.45
ILMN_2661299	Pmp22	44.1811	36.6886	40.3481	62.54	64.7739	56.354	0.66	0.05	9.45
ILMN_2504268	Gcap26	32.6939	35.1222	38.4518	123.988	197.394	123.881	0.25	0.04	9.45
ILMN_2620233	Fmo5	63.5324	32.9711	33.755	80.7574	66.9208	66.7679	0.59	0.10	9.45
ILMN_2876579	Ubxd1	161.466	125.073	111.58	230.049	204.198	246.498	0.59	0.07	9.45
ILMN_3144575	Itgb4	205.627	157.832	108.067	306.426	383.213	329.111	0.47	0.10	9.45
ILMN_2755424	Bcorl1	51.0598	64.9965	109.709	89.9531	105.528	180.982	0.60	0.01	9.45
ILMN_2880906	Pdlim2	74.2399	78.1829	87.5498	274.469	201.897	367.928	0.30	0.05	9.45
ILMN_2798993	Nr1d2	228.653	136.121	142.541	272.053	228.301	236.689	0.68	0.08	9.45
ILMN_2702547	4930519N16Rik	35.6221	33.5482	31.201	65.5301	98.8013	82.9635	0.42	0.06	9.45
ILMN_2759563	2410008K03Rik	52.6433	77.8949	68.6875	103.753	114.783	145.475	0.55	0.06	9.45
ILMN_2583163	D430023I21Rik	67.3631	49.3736	59.3074	92.4817	97.8458	90.0475	0.63	0.07	9.45
ILMN_2674367	Agrn	267.522	165.156	208.09	390.656	375.927	493.489	0.52	0.08	9.45
ILMN_3138157	Arl6ip2	57.947	33.4486	34.9759	104.205	55.4453	69.9793	0.55	0.03	9.92
ILMN_2615557	Dab2ip	469.35	537.658	403.059	780.909	692.179	769.706	0.63	0.07	9.92
ILMN_1238479	Mgst3	85.2191	97.2455	67.7363	110.046	140.652	121.577	0.67	0.06	9.92
ILMN_1228942	Cd59a	135.902	168.823	180.93	367.928	274.064	423.744	0.47	0.07	9.92
ILMN_2846812	Sp100	138.5	96.3988	94.1524	261.965	157.43	167.484	0.57	0.02	9.92
ILMN_2664224	Ephx1	205.941	115.592	116.265	277.548	245.235	283.099	0.54	0.10	9.92
ILMN_2419858	E230020D15Rik	81.8134	51.9907	44.456	101.794	94.213	83.0312	0.63	0.09	9.92
ILMN_2416876	Gm967	81.6857	60.0294	56.7679	125.607	147.447	157.606	0.47	0.09	9.92
ILMN_2913089	Brd9	91.6038	110.439	129.057	170.062	161.466	166.378	0.67	0.07	9.92
ILMN_2741464	Fgd5	61.8191	97.8936	70.3934	111.062	165.498	175.739	0.52	0.06	9.92
ILMN_2702997	Thap7	39.0791	44.4453	54.4245	123.286	95.008	96.1765	0.45	0.07	9.92
ILMN_1242571	Pkn3	561.836	461.474	374.85	762.104	884.251	861.78	0.56	0.09	9.92
ILMN_1227126	Ppp2r3a	38.6953	42.6033	34.5624	57.6406	57.293	62.445	0.66	0.06	9.92
ILMN_2790188	4921533L14Rik	116.247	90.4346	93.7405	222.43	204.383	302.815	0.42	0.06	9.92
ILMN_2742627	Six2	82.4274	57.474	118.55	139.091	130.835	150.836	0.61	0.10	9.92
ILMN_1256136	Nme7	52.9252	38.1628	45.2995	75.9807	70.4637	93.1356	0.57	0.06	9.92
ILMN_1222004	Rbbp9	43.8743	37.2039	39.9486	82.1031	56.425	81.2136	0.56	0.05	9.92
ILMN_2418725	Zdhhc3	35.5653	40.9597	72.5309	72.6642	88.8714	94.4003	0.57	0.10	9.92
ILMN_2706268	Scara3	67.0842	85.0897	102.554	189.608	154.716	163.475	0.51	0.08	9.92
ILMN_1225835	Mfap5	133.695	111.675	86.8026	295.475	265.168	389.609	0.37	0.07	9.92

APPENDIX B

miRNA expression profiles in response to disturb flow *in vivo*

Table B1. miRNA expression profiles in mouse ligated carotid endothelium (LCA) and controlateral right carotid endothelium (RCA) at 12 hr post-ligation

		LCA1	LCA2	LCA3	RCA1	RCA2	RCA3	LCA/RCA		
Illumina_ID	NAME	signal	signal	signal	signal	signal	signal	ratio	SEM	p-value
ILMN_3167971	mmu-let-7a	22202.67	21782.33	21667.17	22315.71	22315.71	22161.04	0.98	0.01	0.105
ILMN_3167970	mmu-let-7b	23433.92	23433.92	23433.92	23680.80	23433.92	23433.92	1.00	0.00	0.423
ILMN_3169089	mmu-let-7b*	800.62	372.29	415.58	476.38	505.71	999.71	0.94	0.38	0.667
ILMN_3168513	mmu-let-7c	21667.58	22202.67	22428.75	22315.71	22315.71	22315.71	0.99	0.01	0.439
ILMN_3169088	mmu-let-7c-2*,mmu-let-7a*	3713.96	5585.17	4940.75	5195.25	5378.71	6990.17	0.82	0.11	0.244
ILMN_3167551	mmu-let-7d	20752.09	20992.67	21373.50	21286.75	21286.75	21556.58	0.98	0.00	0.083
ILMN_3167347	mmu-let-7d*	12550.09	13339.00	14293.80	16613.34	15355.88	16048.71	0.84	0.04	0.070
ILMN_3168463	mmu-let-7e	17060.42	18162.42	17927.75	19224.38	19306.34	18942.21	0.92	0.02	0.058
ILMN_3167189	mmu-let-7f	19910.46	19624.21	18540.67	19762.92	20035.00	20031.88	0.97	0.02	0.348
ILMN_3168365	mmu-let-7g	17593.50	18860.25	18923.05	18693.67	19516.46	19306.34	0.96	0.01	0.076
ILMN_3169053	mmu-let-7g*	3251.71	2225.83	2184.38	2635.33	2290.04	2481.46	1.03	0.11	0.786
ILMN_3168316	mmu-let-7i	12142.67	14644.79	17273.88	12185.25	14490.50	14938.83	1.05	0.05	0.396
ILMN_3168724	mmu-let-7i*	823.08	576.83	1026.17	686.92	814.83	1213.67	0.92	0.15	0.497
ILMN_3167634	mmu-miR-100	6498.04	7087.13	7157.13	6531.29	7087.13	6787.25	1.02	0.02	0.477
ILMN_3168157	mmu-miR-101a:9.1	5081.96	5902.71	5212.71	6002.96	6618.08	5262.96	0.91	0.04	0.166
ILMN_3168940	mmu-miR-101b	1655.79	2433.42	410.50	1117.42	390.04	4382.00	2.60	1.86	0.822
ILMN_3167027	mmu-miR-103	9078.00	11072.67	13431.75	10784.96	11307.67	10569.67	1.03	0.13	0.841
ILMN_3168930	mmu-miR-106a	2873.00	2162.75	1145.58	1364.83	1417.33	1711.92	1.43	0.42	0.451
ILMN_3167574	mmu-miR-106b	1557.54	2764.00	1146.58	2431.25	1687.38	674.46	1.33	0.34	0.734
ILMN_3167552	mmu-miR-10a	9409.67	10749.50	11307.67	10530.29	10609.83	12550.09	0.94	0.04	0.235
ILMN_3169105	mmu-miR-10a*	985.25	699.29	695.96	639.96	993.71	774.13	1.05	0.25	0.966
ILMN_3167276	mmu-miR-10b	4904.46	6208.42	5111.25	5759.54	5671.54	9675.00	0.82	0.16	0.397
ILMN_3169068	mmu-miR-10b*	1519.13	1397.96	1263.29	1415.08	1486.83	1796.92	0.91	0.11	0.457
ILMN_3169029	mmu-miR-1186	15549.92	16122.04	13591.17	9716.46	11211.92	8856.92	1.52	0.05	0.004
ILMN_3169030	mmu-miR-1187	8143.17	7063.71	6879.71	8129.33	11386.92	5957.83	0.93	0.16	0.558
ILMN_3169043	mmu-miR-1192	2190.63	790.13	931.21	783.25	903.08	5986.96	1.28	0.79	0.586
ILMN_3169049	mmu-miR-1195	17897.21	17489.71	17519.63	17877.96	17742.04	16794.88	1.01	0.02	0.630
ILMN_3169050	mmu-miR-1196	6663.29	5410.33	6803.17	2331.50	6311.83	3935.00	1.81	0.58	0.310
ILMN_3168794	mmu-miR-1197	1332.08	1026.63	958.29	1081.00	1245.08	1705.67	0.87	0.20	0.496
ILMN_3169052	mmu-miR-1199	381.54	374.58	343.88	436.38	523.92	727.79	0.69	0.12	0.183
ILMN_3167670	mmu-miR-125a-5p	19859.34	20501.34	20203.75	20372.50	20297.04	20752.09	0.99	0.01	0.364
ILMN_3168389	mmu-miR-125b-5p	18717.67	18942.21	19224.38	19762.92	19683.67	19762.92	0.96	0.01	0.034
ILMN_3167695	mmu-miR-126-3p	20028.09	21782.33	21401.50	21512.50	21893.33	21937.00	0.97	0.02	0.222
ILMN_3168399	mmu-miR-126-5p	23927.67	23927.67	23927.67	23680.80	23927.67	23927.67	1.00	0.00	0.423
ILMN_3167031	mmu-miR-127	2276.04	3057.17	4612.92	3619.13	4444.63	2669.17	1.01	0.36	0.834
ILMN_3168922	mmu-miR-128	1381.25	2267.38	932.58	1005.54	1098.88	1411.75	1.37	0.40	0.533
ILMN_3168183	mmu-miR-129-5p	7239.00	474.63	426.08	1447.83	1481.38	779.13	1.96	1.52	0.566
ILMN_3168497	mmu-miR-130a	7613.17	9623.17	9987.38	8046.96	9514.75	7303.79	1.11	0.13	0.500
ILMN_3168212	mmu-miR-132	2618.17	1185.17	3966.54	2684.13	847.88	745.17	2.57	1.38	0.378
ILMN_3168314	mmu-miR-133a	5287.13	4804.79	3454.17	1627.04	2172.54	2834.29	2.23	0.59	0.123
ILMN_3167661	mmu-miR-133a*	710.08	755.92	501.58	626.54	728.42	782.04	0.94	0.15	0.667
ILMN_3167874	mmu-miR-135b	1192.38	1030.42	915.13	1223.42	1224.04	1608.04	0.80	0.12	0.264
ILMN_3167501	mmu-miR-138	1069.33	1110.17	1613.25	886.54	1195.21	1093.87	1.20	0.16	0.360
ILMN_3167136	mmu-miR-140	6153.13	8524.88	8017.63	7366.79	8084.50	6450.58	1.04	0.12	0.774
ILMN_3168302	mmu-miR-140*	10530.29	13087.38	12724.30	14799.08	12408.71	12885.42	0.92	0.10	0.499
ILMN_3168509	mmu-miR-142-5p	368.33	377.33	350.29	423.08	512.88	624.75	0.72	0.09	0.137
ILMN_3166958	mmu-miR-143	8524.88	13643.17	14834.71	11860.67	14513.50	10530.29	1.02	0.20	0.990
ILMN_3168030	mmu-miR-144:9.1	3167.75	2654.67	2486.92	2881.79	2527.96	2752.88	1.02	0.06	0.794
ILMN_3167456	mmu-miR-145	11725.58	15839.21	14799.08	16495.71	16705.21	17273.88	0.84	0.07	0.140
ILMN_3168483	mmu-miR-146a	1975.25	3765.46	774.92	1999.25	3631.25	1026.17	0.93	0.09	0.715
ILMN_3169120	mmu-miR-146b*	405.79	681.13	768.04	421.96	505.71	641.79	1.17	0.11	0.239
ILMN_3168105	mmu-miR-148a	3847.54	4486.00	4520.58	4916.63	4270.04	2250.46	1.28	0.37	0.675
ILMN_3168426	mmu-miR-148b	4495.54	6662.38	5499.79	6067.67	3473.42	5548.96	1.22	0.36	0.745
ILMN_3167902	mmu-miR-149	3006.96	4403.79	2539.17	2558.04	1465.63	755.79	2.51	0.68	0.139
ILMN_3167703	mmu-miR-150	6626.88	7842.67	10569.67	9324.67	7267.58	12553.00	0.88	0.11	0.302
ILMN_3168367	mmu-miR-151-3p	5839.50	8170.08	9324.67	9219.58	9219.58	10910.88	0.79	0.08	0.104
ILMN_3168819	mmu-miR-151-5p	13722.80	16970.75	19224.38	16314.25	17335.13	18149.54	0.96	0.06	0.616
ILMN_3168346	mmu-miR-152	8043.75	10972.09	12185.25	9273.08	11386.92	9219.58	1.05	0.14	0.764
ILMN_3167522	mmu-miR-154	2544.88	2933.79	2897.54	1049.71	437.79	568.21	4.74	1.25	0.021
ILMN_3166946	mmu-miR-155	4551.38	2656.46	4908.25	7169.00	7698.29	7818.71	0.54	0.10	0.044
ILMN_3167434	mmu-miR-15a	817.08	3195.75	2874.58	1155.38	2523.13	1163.54	1.48	0.52	0.368
ILMN_3167060	mmu-miR-15b	12090.50	13630.05	14359.21	16970.75	13630.05	16406.00	0.86	0.08	0.244
ILMN_3167989	mmu-miR-16	13087.38	14644.79	15291.05	13935.55	13842.80	13630.05	1.04	0.05	0.541
ILMN_3167785	mmu-miR-17	6103.83	3205.46	6239.08	3736.04	4634.79	8436.67	1.02	0.31	0.794
ILMN_3167127	mmu-miR-181a	7397.04	8397.25	9026.42	8426.71	7544.00	7087.13	1.09	0.11	0.568
ILMN_3169069	mmu-miR-181a-2*	1074.83	1050.88	935.54	922.38	1170.46	1437.13	0.90	0.15	0.497
ILMN_3168257	mmu-miR-181b	4039.83	5620.04	6417.33	4980.50	3714.42	4210.00	1.28	0.24	0.402
ILMN_3168494	mmu-miR-181d	761.88	723.33	536.42	681.25	924.71	732.25	0.88	0.12	0.375
ILMN_3167698	mmu-miR-184	420.75	414.25	377.54	454.75	576.33	712.42	0.72	0.11	0.179
ILMN_3167152	mmu-miR-185	3336.38	3569.17	3745.88	3456.04	5645.46	5075.00	0.78	0.10	0.175
ILMN_3168167	mmu-miR-187	486.88	2498.29	2497.54	3243.83	674.33	1785.33	1.75	1.04	0.962
ILMN_3167745	mmu-miR-188-5p	556.29	435.00	772.08	561.54	579.00	620.46	1.00	0.14	0.993
ILMN_3168282	mmu-miR-18a	6138.21	5009.29	4112.79	4472.00	4213.42	3711.08	1.22	0.08	0.125
ILMN_3169094	mmu-miR-18a*	1535.67	353.13	285.79	420.46	438.67	510.63	1.67	0.99	0.593
ILMN_3167167	mmu-miR-190	1030.25	1916.54	846.75	432.13	467.63	545.21	2.68	0.75	0.151
ILMN_3167253	mmu-miR-191	14513.50	16630.75	18426.17	17310.13	15355.88	19508.05	0.96	0.07	0.539
ILMN_3169072	mmu-miR-191*	1686.67	1013.21	1148.71	1088.54	1162.04	1774.17	1.02	0.27	0.884
ILMN_3167506	mmu-miR-192	1750.17	3385.46	2410.75	765.92	902.75	5470.58	2.16	0.96	0.942
ILMN_3168366	mmu-miR-193	5844.42	5403.00	3685.50	2599.67	6098.58	8113.83	1.20	0.54	0.804
ILMN_3169073	mmu-miR-193*	2384.63	4065.71	3635.92	1806.83	2655.33	1841.04	1.61	0.19	0.072
ILMN_3168982	mmu-miR-193b	877.75	738.96	1441.92	2055.71	2408.92	1874.67	0.50	0.14	0.093
ILMN_3167122	mmu-miR-194	6182.42	5481.79	5555.54	5368.38	6009.46	4277.46	1.12	0.11	0.437
ILMN_3167191	mmu-miR-195	6852.08	7487.21	8299.67	7842.67	7397.04	7210.42	1.01	0.08	0.926
ILMN_3168308	mmu-miR-196b	4058.54	6094.58	5234.21	5237.75	5196.17	5902.71	0.94	0.12	0.663
ILMN_3168924	mmu-miR-199a-3p,mmu-miR-199b	14513.50	9273.08	6933.96	9712.79	8318.79	7895.42	1.16	0.18	0.445
ILMN_3167976	mmu-miR-199a-5p	2653.83	5986.96	4322.00	4809.33	7302.00	5464.71	0.72	0.08	0.039
ILMN_3167626	mmu-miR-199b*	2733.00	5932.42	3756.58	3569.17	1044.54	5620.04	2.37	1.65	0.762
ILMN_3169106	mmu-miR-19a*	379.54	697.46	307.92	440.08	446.13	583.08	0.98	0.31	0.871
ILMN_3167260	mmu-miR-19b	5237.75	5367.54	2840.54	2560.54	1628.96	1789.04	2.31	0.51	0.086
ILMN_3168294	mmu-miR-200b	3862.79	3466.29	3406.92	4653.17	3827.54	3935.00	0.87	0.02	0.046
ILMN_3169074	mmu-miR-200b*	976.67	829.38	713.21	859.00	1022.63	1274.50	0.84	0.17	0.392
ILMN_3169108	mmu-miR-200c*	1376.71	741.29	692.75	827.17	869.21	1369.58	1.01	0.34	0.833
ILMN_3168487	mmu-miR-203	4656.54	3591.08	1653.50	4402.58	497.58	6757.96	2.84	2.20	0.830
ILMN_3169015	mmu-miR-208b	688.54	596.88	559.54	643.92	807.17	962.83	0.80	0.14	0.281
ILMN_3167510	mmu-miR-20a	3661.83	7576.46	5368.38	5985.17	3316.42	3278.13	1.51	0.49	0.560
ILMN_3169095	mmu-miR-20a*	15078.58	9026.42	6028.38	10455.75	9873.38	7899.17	1.04	0.21	0.783
ILMN_3167333	mmu-miR-20b	895.46	859.17	622.33	847.67	977.00	1272.92	0.81	0.17	0.372
ILMN_3167371	mmu-miR-21	18162.42	19728.46	19267.92	21150.75	20853.67	20992.67	0.91	0.03	0.071
ILMN_3167774	mmu-miR-210	4146.71	4507.83	5531.54	5813.42	3567.58	6498.04	0.94	0.17	0.544
ILMN_3168266	mmu-miR-211	856.46	550.46	478.83	672.71	2329.83	947.54	0.67	0.31	0.355
ILMN_3167761	mmu-miR-212	16421.25	7544.25	6618.08	10317.63	8368.38	7544.00	1.12	0.23	0.596

Table B1. -Continued

Illumina_ID	NAME	LCA1 signal	LCA2 signal	LCA3 signal	RCA1 signal	RCA2 signal	RCA3 signal	LCA/RCA ratio	SEM	p-value
ILMN_3167046	mmu-miR-214	5171.13	5914.96	7197.58	5902.71	7950.75	5183.38	1.00	0.20	0.853
ILMN_3167234	mmu-miR-215	1395.33	1279.46	1091.67	1208.83	1400.08	1582.58	0.92	0.13	0.545
ILMN_3167177	mmu-miR-216b	716.79	596.54	469.21	621.83	793.00	1011.00	0.79	0.20	0.364
ILMN_3168380	mmu-miR-218	1616.88	619.21	2655.33	2027.83	5158.17	5342.50	0.47	0.20	0.167
ILMN_3169109	mmu-miR-218-2*	1009.21	437.79	375.96	491.00	586.42	739.38	1.10	0.48	0.995
ILMN_3167523	mmu-miR-219	830.13	709.04	795.71	778.17	922.71	1161.25	0.84	0.12	0.286
ILMN_3167773	mmu-miR-22	10516.96	12408.71	12096.79	12468.00	12550.09	11364.00	0.97	0.06	0.624
ILMN_3169097	mmu-miR-22*	1624.92	3614.46	3375.83	2135.83	1148.25	3192.25	1.66	0.75	0.511
ILMN_3167681	mmu-miR-221	8397.25	3744.25	6153.13	4277.63	5359.13	2274.04	1.79	0.59	0.374
ILMN_3167963	mmu-miR-222	3991.13	6270.00	7169.00	7397.04	6375.63	5531.54	0.94	0.22	0.714
ILMN_3166979	mmu-miR-223	9409.67	10301.67	7738.83	4277.67	5907.00	7193.33	1.67	0.33	0.142
ILMN_3168515	mmu-miR-224	2501.92	3814.08	1380.13	6412.04	3481.21	4594.54	0.60	0.25	0.227
ILMN_3168226	mmu-miR-23a	14490.50	15832.75	16959.00	19108.79	18428.05	18149.54	0.85	0.05	0.106
ILMN_3167997	mmu-miR-23b	20444.34	19859.34	20268.67	21036.00	20630.17	20297.04	0.98	0.01	0.174
ILMN_3168211	mmu-miR-24	19224.38	19437.21	19612.88	20035.00	19632.05	19552.80	0.98	0.01	0.347
ILMN_3169098	mmu-miR-24-2*	2821.08	1560.50	3605.67	5197.08	1263.13	4027.58	0.89	0.20	0.406
ILMN_3168476	mmu-miR-25	11307.67	11072.67	12754.96	11048.25	13220.33	13643.17	0.93	0.05	0.315
ILMN_3168005	mmu-miR-26a	18942.21	20031.88	20031.88	20221.58	20297.04	20630.17	0.96	0.01	0.139
ILMN_3167374	mmu-miR-26b	16705.21	17060.42	16620.50	17260.67	16585.38	17927.75	0.97	0.03	0.465
ILMN_3168323	mmu-miR-27a	20031.88	21147.75	21036.00	21782.33	21556.58	21667.58	0.96	0.02	0.154
ILMN_3169102	mmu-miR-27a*	825.88	741.67	533.46	823.25	867.67	1109.08	0.78	0.16	0.315
ILMN_3168409	mmu-miR-27b	12885.42	15078.58	15466.67	15749.50	15466.67	15922.46	0.92	0.05	0.268
ILMN_3167223	mmu-miR-28	4512.25	3482.17	6039.29	5724.00	10376.21	10102.34	0.57	0.13	0.132
ILMN_3169107	mmu-miR-28*	1343.38	1007.04	1306.83	1297.67	759.88	1234.58	1.14	0.09	0.194
ILMN_3168514	mmu-miR-291a-3p	615.88	620.38	545.88	663.54	818.92	865.17	0.77	0.09	0.139
ILMN_3167737	mmu-miR-293	3314.42	2684.88	2392.96	3083.13	2539.17	2682.50	1.01	0.06	0.873
ILMN_3169076	mmu-miR-293*	666.38	589.75	525.92	650.29	769.33	1057.54	0.76	0.15	0.285
ILMN_3167176	mmu-miR-295	469.79	495.17	637.08	670.42	768.83	1107.92	0.64	0.04	0.060
ILMN_3169078	mmu-miR-295*	2188.58	1733.54	1389.88	1576.63	1512.50	3558.17	0.97	0.30	0.659
ILMN_3168154	mmu-miR-297a	5583.21	4911.04	4569.75	4845.71	4589.63	4077.96	1.11	0.02	0.050
ILMN_3168963	mmu-miR-297c*,mmu-miR-297a*,mmu-miR-297b-3p	389.04	719.71	2846.50	1451.13	4041.79	3652.75	0.41	0.19	0.163
ILMN_3168928	mmu-miR-299	907.50	795.33	619.54	814.08	922.04	1027.25	0.86	0.15	0.417
ILMN_3167035	mmu-miR-29a	12237.42	14227.92	13684.08	15355.88	14300.75	15219.84	0.90	0.06	0.215
ILMN_3169100	mmu-miR-29a*	1452.92	1203.67	1646.50	1280.67	1348.92	1717.00	1.00	0.07	0.894
ILMN_3168172	mmu-miR-29b	8863.54	10671.04	9566.58	10569.67	12816.42	12408.71	0.81	0.02	0.021
ILMN_3167643	mmu-miR-29c	11130.09	12724.30	10376.21	11516.63	12237.42	11522.00	0.97	0.04	0.537
ILMN_3169080	mmu-miR-302a*	509.92	474.13	420.00	500.17	650.63	848.92	0.75	0.15	0.259
ILMN_3167279	mmu-miR-302b	405.50	404.42	334.17	456.25	551.79	655.58	0.71	0.11	0.160
ILMN_3167455	mmu-miR-30a	7499.04	9903.00	9623.17	8672.92	8397.25	12007.58	0.95	0.12	0.612
ILMN_3167158	mmu-miR-30a*	6764.50	7672.17	8070.50	8424.63	7944.17	9514.75	0.87	0.05	0.121
ILMN_3167448	mmu-miR-30b	7128.54	10071.75	8593.58	7589.21	10186.71	6425.67	1.09	0.13	0.586
ILMN_3167729	mmu-miR-30c	15549.92	16869.34	15594.17	16709.13	16597.08	17172.46	0.95	0.03	0.280
ILMN_3169085	mmu-miR-30c-2*	3190.25	2180.88	2140.83	2618.17	2269.79	2562.38	1.00	0.11	0.950
ILMN_3167224	mmu-miR-30d	10671.04	12885.42	11860.67	13457.67	12378.79	13630.05	0.90	0.07	0.300
ILMN_3168138	mmu-miR-30e	430.54	2043.00	2363.79	1647.25	1426.46	2394.46	0.89	0.34	0.733
ILMN_3167711	mmu-miR-30e*	5959.33	7840.33	7728.54	6860.08	8503.96	5086.96	1.10	0.21	0.783
ILMN_3167403	mmu-miR-320	13550.42	15549.92	17594.09	16018.79	16421.25	18310.17	0.92	0.04	0.137
ILMN_3167956	mmu-miR-323-3p	794.88	845.08	774.33	736.88	1028.46	1197.54	0.85	0.13	0.319
ILMN_3168413	mmu-miR-324-3p	3418.75	5410.33	2169.13	4336.17	6055.29	4730.92	0.71	0.13	0.149
ILMN_3167905	mmu-miR-326	4738.33	6241.50	8017.63	7939.92	5620.04	7185.54	0.94	0.17	0.700
ILMN_3168985	mmu-miR-327	2087.13	1735.46	1752.54	1891.71	1864.88	2070.79	0.96	0.08	0.632
ILMN_3168198	mmu-miR-328	10071.75	11725.58	12406.09	14146.46	11995.75	15555.46	0.83	0.08	0.161
ILMN_3168522	mmu-miR-329	460.42	440.00	2024.58	2124.75	2204.79	2212.17	0.44	0.24	0.142
ILMN_3167996	mmu-miR-335-5p	359.63	415.75	420.67	495.17	534.25	3951.13	0.54	0.22	0.382
ILMN_3168934	mmu-miR-337-5p	4956.08	4400.17	3812.13	4336.17	3769.50	3774.08	1.11	0.05	0.159
ILMN_3167344	mmu-miR-338-3p	1377.92	904.21	972.87	2845.54	1101.92	1264.71	0.69	0.10	0.251
ILMN_3168936	mmu-miR-339-3p	1148.71	940.83	816.67	952.71	1059.04	1358.13	0.90	0.17	0.545
ILMN_3168301	mmu-miR-339-5p	3541.04	2899.58	3208.92	3342.75	1159.38	1404.71	1.95	0.45	0.141
ILMN_3166998	mmu-miR-340-3p	488.38	546.67	701.00	1733.54	676.08	795.50	0.66	0.19	0.324
ILMN_3168866	mmu-miR-340-5p	412.58	750.38	495.00	444.13	457.38	725.17	1.08	0.29	0.952
ILMN_3167123	mmu-miR-341:9.1	2359.71	2326.92	2451.04	2443.96	2386.08	2666.04	0.95	0.02	0.132
ILMN_3168165	mmu-miR-342-3p	4143.88	4955.54	7397.04	4554.83	4904.46	4907.83	1.14	0.18	0.513
ILMN_3167891	mmu-miR-344	406.29	3605.67	1515.04	3333.88	4204.21	6039.29	0.41	0.23	0.143
ILMN_3168939	mmu-miR-345-3p	3031.63	1393.33	1162.42	1380.13	2237.17	1722.63	1.16	0.52	0.926
ILMN_3168128	mmu-miR-345-5p	635.88	1390.96	1820.04	1492.00	631.75	790.13	1.64	0.61	0.650
ILMN_3167734	mmu-miR-346	20031.88	7738.83	7128.50	11651.71	7658.38	6311.17	1.29	0.22	0.364
ILMN_3168429	mmu-miR-34a	413.00	1792.17	2465.71	2223.42	563.71	2888.33	1.41	0.91	0.740
ILMN_3168326	mmu-miR-350	849.79	2454.21	4417.75	3947.92	1504.25	500.29	3.56	2.67	0.799
ILMN_3168297	mmu-miR-365	7233.79	7814.25	8574.75	9675.00	7798.63	9737.17	0.88	0.07	0.234
ILMN_3168444	mmu-miR-369-3p	555.50	1056.42	426.38	563.13	660.29	790.13	1.04	0.31	0.973
ILMN_3168318	mmu-miR-374	9675.00	9458.17	9987.38	11211.92	10784.96	13087.38	0.83	0.04	0.071
ILMN_3167229	mmu-miR-375	1205.67	1049.71	833.33	998.63	1150.58	1308.25	0.92	0.16	0.597
ILMN_3168505	mmu-miR-376a	651.25	1356.67	445.75	635.42	746.17	841.96	1.12	0.38	0.817
ILMN_3167566	mmu-miR-376b	1098.88	950.04	755.92	910.21	1100.50	1168.71	0.91	0.16	0.548
ILMN_3167006	mmu-miR-378	1737.42	2283.75	3006.96	903.08	2321.83	4980.50	1.17	0.39	0.683
ILMN_3168180	mmu-miR-378*	1097.08	682.58	1311.33	764.75	1628.92	1225.63	0.97	0.30	0.697
ILMN_3167443	mmu-miR-379	3912.96	3067.92	4782.00	3036.63	3109.21	1640.54	1.73	0.60	0.296
ILMN_3167239	mmu-miR-382	2964.67	734.38	5926.54	1193.71	988.54	7544.25	1.34	0.57	0.976
ILMN_3169113	mmu-miR-382*	657.00	905.67	846.75	539.00	661.29	917.54	1.17	0.13	0.400
ILMN_3168946	mmu-miR-409-5p	676.13	559.54	423.08	3863.46	653.00	653.00	0.56	0.20	0.366
ILMN_3167988	mmu-miR-411	511.21	1827.79	425.29	2201.50	3205.46	1074.25	0.40	0.10	0.057
ILMN_3168062	mmu-miR-411*:9.1	9571.33	2465.58	2452.38	3584.17	3688.67	3005.04	1.38	0.64	0.604
ILMN_3167373	mmu-miR-423-3p	3850.17	4361.21	4058.58	4713.58	3801.42	3385.46	1.05	0.12	0.827
ILMN_3168947	mmu-miR-425	2731.67	4989.50	1839.50	4003.67	3406.96	2360.04	0.98	0.25	0.942
ILMN_3167614	mmu-miR-451	1537.04	915.13	1768.13	1446.75	996.38	1214.79	1.15	0.16	0.427
ILMN_3168131	mmu-miR-453	4605.00	838.50	497.75	920.42	692.75	3747.17	2.12	1.48	0.932
ILMN_3167131	mmu-miR-455	880.33	1036.38	1265.46	2669.17	686.75	824.25	1.12	0.40	0.693
ILMN_3167714	mmu-miR-455*	1770.46	1560.50	1505.38	1859.63	1735.75	2008.42	0.87	0.06	0.180
ILMN_3168948	mmu-miR-463	1185.67	1106.75	1018.08	1130.87	1282.67	1609.83	0.85	0.12	0.336
ILMN_3167236	mmu-miR-465a-3p,mmu-miR-465b-3p,mmu-miR-465c-3p,mmu-miR-465a-3p,mmu-miR-465b-3p,mmu-miR-465c-3p,mmu-miR-465a-3p,mmu-miR-465b-3p,mmu-miR-465c-3p	1009.12	833.04	776.75	902.25	1050.71	1328.29	0.83	0.16	0.365
ILMN_3168989	mmu-miR-465c-5p	2000.92	1558.92	1566.46	1860.33	1797.04	2238.04	0.88	0.11	0.389
ILMN_3167875	mmu-miR-466a-3p,mmu-miR-466b-3p,mmu-miR-466c-3p,mmu-miR-466e-3p,mmu-miR-466a-3p,mmu-miR-466b-3p,mmu-miR-466c-3p,mmu-miR-466e-3p,mmu-miR-466b-3-3p,mmu-miR-466a-3p,mmu-miR-466b-3p,mmu-miR-466c-3p,mmu-miR-466e-3p,mmu-miR-466a-3p,mmu-miR-466b-3p,mmu-miR-466c-	1671.54	2335.04	2465.38	3714.42	1005.87	4041.79	1.13	0.60	0.544
ILMN_3168949	mmu-miR-466a-5p	4515.21	3839.79	3424.92	4204.21	3820.92	3652.29	1.01	0.04	0.847
ILMN_3169037	mmu-miR-466f	4638.13	3137.46	2934.33	3437.33	2795.75	3635.92	1.09	0.16	0.661

Table B1. -Continued

Illumina_ID	NAME	LCA1 signal	LCA2 signal	LCA3 signal	RCA1 signal	RCA2 signal	RCA3 signal	LCA/RCA ratio	SEM	p-value
ILMN_3168994	mmu-miR-466f-3p	19773.67	21036.00	20046.63	17008.34	18428.05	15061.84	1.21	0.06	0.046
ILMN_3168993	mmu-miR-466f-5p	3607.46	588.42	529.17	2281.38	757.92	872.42	0.99	0.30	0.660
ILMN_3168995	mmu-miR-466g	8615.25	8068.79	4353.08	7939.92	6634.75	6888.83	0.98	0.18	0.918
ILMN_3169027	mmu-miR-466i	18403.92	20752.09	19052.54	14146.46	16495.67	12264.00	1.37	0.09	0.026
ILMN_3169023	mmu-miR-466l	659.71	597.04	512.54	670.13	776.58	1031.83	0.75	0.14	0.255
ILMN_3168950	mmu-miR-467a	4760.21	3773.67	3127.88	3798.67	3084.75	3316.67	1.14	0.10	0.295
ILMN_3169039	mmu-miR-467f	13339.00	11995.75	10910.88	8045.29	9490.50	8752.25	1.39	0.13	0.079
ILMN_3169048	mmu-miR-467h	2613.58	1986.50	1929.25	2309.21	2135.38	2246.83	0.97	0.08	0.798
ILMN_3168457	mmu-miR-484	6448.42	6523.42	7945.04	7063.71	6685.13	8623.25	0.94	0.02	0.096
ILMN_3167240	mmu-miR-486	3670.83	4158.63	3541.04	2980.63	915.46	6138.21	2.12	1.23	0.817
ILMN_3167805	mmu-miR-487b	733.29	650.63	549.21	701.00	833.83	1005.08	0.79	0.14	0.288
ILMN_3168506	mmu-miR-489	6101.46	6060.25	5626.25	5644.04	5270.29	4831.13	1.13	0.03	0.026
ILMN_3168999	mmu-miR-493	3883.25	611.13	540.63	1219.96	813.46	3067.92	1.37	0.92	0.990
ILMN_3168446	mmu-miR-494	4595.67	4564.79	4233.29	5646.21	4829.42	4803.79	0.88	0.04	0.111
ILMN_3167437	mmu-miR-497	2369.67	2334.00	3830.25	3541.04	2026.46	642.58	2.59	1.69	0.607
ILMN_3169000	mmu-miR-504	22161.04	3251.71	3991.13	12793.30	4591.04	2322.75	1.39	0.34	0.417
ILMN_3169017	mmu-miR-511	5985.63	5676.83	4482.13	2517.96	2840.54	1786.92	2.29	0.15	0.006
ILMN_3168686	mmu-miR-532-3p	5222.71	5011.83	5698.58	5783.96	4594.83	6073.17	0.98	0.06	0.622
ILMN_3167658	mmu-miR-540-3p	1146.58	1064.29	1003.17	1006.92	1267.83	1499.04	0.88	0.14	0.417
ILMN_3167074	mmu-miR-542-3p	4287.42	3947.83	3635.96	4098.25	3718.92	3631.25	1.04	0.02	0.178
ILMN_3167043	mmu-miR-546	753.33	670.42	674.04	692.75	932.96	1054.12	0.82	0.14	0.279
ILMN_3168117	mmu-miR-547	799.71	763.04	474.38	581.79	665.17	643.17	1.09	0.19	0.710
ILMN_3169004	mmu-miR-574-3p	4864.08	7330.58	6787.25	6662.38	7275.21	4345.08	1.10	0.24	0.867
ILMN_3169003	mmu-miR-574-5p	10644.21	10530.29	10890.25	12926.25	12954.42	14359.21	0.80	0.02	0.018
ILMN_3169020	mmu-miR-582-5p	2503.00	1979.63	2027.83	2291.54	2031.38	2162.46	1.00	0.05	0.943
ILMN_3169005	mmu-miR-590-5p	545.42	469.21	327.25	551.88	566.88	596.25	0.79	0.13	0.247
ILMN_3167257	mmu-miR-592	7254.04	7185.54	6958.50	8574.75	8114.00	8715.50	0.84	0.03	0.031
ILMN_3167379	mmu-miR-615-3p	6650.54	5950.79	5444.38	5444.38	5839.50	4835.58	1.12	0.06	0.180
ILMN_3168964	mmu-miR-615-5p	361.75	420.63	332.50	480.46	469.33	538.79	0.76	0.08	0.112
ILMN_3167305	mmu-miR-652	7197.58	7087.13	9056.71	7885.33	6417.33	8239.46	1.04	0.06	0.634
ILMN_3168475	mmu-miR-654-3p	8672.92	2441.04	4160.67	3739.54	2629.29	2068.88	1.75	0.42	0.264
ILMN_3169006	mmu-miR-654-5p	644.58	544.13	433.42	607.21	730.75	819.29	0.78	0.15	0.282
ILMN_3168959	mmu-miR-666-3p	677.13	1178.71	331.38	433.71	489.33	530.83	1.53	0.52	0.441
ILMN_3167968	mmu-miR-667	1973.58	1795.00	395.88	2165.88	521.63	3515.88	1.49	1.00	0.651
ILMN_3166951	mmu-miR-669c	1498.17	4065.71	1937.54	4782.00	3031.63	780.29	1.38	0.63	0.826
ILMN_3169026	mmu-miR-669d	1662.58	512.33	622.21	2907.83	2440.25	884.75	0.49	0.15	0.141
ILMN_3168279	mmu-miR-676	5726.75	5088.00	5086.96	5129.63	5141.79	5499.13	1.01	0.06	0.896
ILMN_3167814	mmu-miR-678	779.25	737.79	940.83	730.88	981.58	1007.25	0.92	0.09	0.412
ILMN_3167520	mmu-miR-679	5228.38	4369.00	4377.54	4757.17	4578.75	4277.63	1.03	0.04	0.603
ILMN_3168259	mmu-miR-682	6199.79	6417.33	4563.75	1549.71	4416.25	1374.17	2.92	0.76	0.050
ILMN_3166975	mmu-miR-683	12550.09	12289.58	11024.80	7267.58	9680.58	5028.21	1.73	0.27	0.046
ILMN_3167156	mmu-miR-690	17526.21	19632.05	16042.00	12816.42	18001.00	11652.84	1.28	0.09	0.067
ILMN_3166942	mmu-miR-691	1275.25	1047.46	959.33	993.08	1245.08	1575.58	0.91	0.20	0.565
ILMN_3168503	mmu-miR-692	709.38	511.38	483.67	594.83	698.67	877.75	0.83	0.19	0.403
ILMN_3167541	mmu-miR-694	3619.13	2360.04	2253.08	2304.33	2933.79	2198.13	1.13	0.23	0.680
ILMN_3166950	mmu-miR-697	359.42	398.75	320.92	384.63	509.92	529.75	0.77	0.09	0.162
ILMN_3167754	mmu-miR-700	592.29	953.38	1178.71	1110.63	1695.50	3865.58	0.47	0.08	0.196
ILMN_3167918	mmu-miR-701	742.38	625.54	634.67	1164.54	846.54	1162.42	0.64	0.06	0.049
ILMN_3167248	mmu-miR-703	13309.42	12993.84	10890.25	6593.67	10256.34	2899.58	2.35	0.74	0.067
ILMN_3168285	mmu-miR-706	22050.04	22428.75	21556.58	20853.67	21401.50	20035.00	1.06	0.01	0.013
ILMN_3167086	mmu-miR-707	7393.58	3160.46	2006.38	2487.04	2041.17	2891.42	1.74	0.66	0.419
ILMN_3168249	mmu-miR-708	20880.92	17489.71	15832.75	19306.34	17385.92	18310.17	0.98	0.06	0.843
ILMN_3168185	mmu-miR-708*	436.71	412.17	357.67	451.63	561.54	644.17	0.75	0.12	0.195
ILMN_3167605	mmu-miR-709	7939.92	9219.58	10530.29	9458.17	8456.17	8426.71	1.06	0.12	0.712
ILMN_3167133	mmu-miR-712*	475.71	437.38	395.21	502.50	598.58	813.88	0.72	0.13	0.221
ILMN_3167549	mmu-miR-719	16032.33	4829.42	2888.33	6685.13	3965.54	4504.46	1.42	0.52	0.479
ILMN_3167188	mmu-miR-720	8355.92	9518.08	8073.08	8046.96	8974.83	7816.54	1.04	0.01	0.052
ILMN_3167283	mmu-miR-742	512.92	559.13	544.25	718.25	838.50	1288.46	0.60	0.09	0.136
ILMN_3166970	mmu-miR-743a	512.21	439.58	399.96	551.67	648.50	1012.42	0.67	0.15	0.233
ILMN_3167180	mmu-miR-744	2333.21	4804.21	5759.54	5401.71	4005.08	2455.21	1.33	0.56	0.870
ILMN_3167621	mmu-miR-758	2437.71	1093.79	1064.54	1208.63	1242.46	1822.08	1.16	0.44	0.872
ILMN_3168003	mmu-miR-761	2497.54	3091.08	2527.79	2135.42	2772.96	5786.21	0.91	0.24	0.548
ILMN_3167967	mmu-miR-762	1446.96	2176.50	1248.04	1192.38	1307.04	1736.79	1.20	0.27	0.644
ILMN_3168100	mmu-miR-763	478.42	476.58	1785.33	550.13	603.54	762.67	1.33	0.50	0.539
ILMN_3168958	mmu-miR-770-5p	3437.33	2517.96	6028.38	5331.38	1896.54	4585.63	1.10	0.23	0.960
ILMN_3168388	mmu-miR-7a	3246.50	1230.08	5498.75	4399.25	1627.04	1111.58	2.15	1.40	0.640
ILMN_3169112	mmu-miR-7a*	21556.58	4591.04	3752.42	18149.54	5470.58	11386.92	0.79	0.25	0.649
ILMN_3168519	mmu-miR-7b	410.71	428.83	350.42	468.13	562.29	693.67	0.72	0.11	0.173
ILMN_3166949	mmu-miR-805	17424.79	17890.58	16812.92	13935.55	17785.17	11698.59	1.23	0.12	0.188
ILMN_3168967	mmu-miR-871	875.92	832.04	961.00	964.46	1104.50	1487.58	0.77	0.08	0.145
ILMN_3169012	mmu-miR-872	802.50	841.96	523.46	542.29	633.13	588.00	1.23	0.18	0.313
ILMN_3169013	mmu-miR-873	2217.58	1856.42	1678.29	1962.58	1838.92	2169.00	0.97	0.10	0.772
ILMN_3169014	mmu-miR-875-3p	997.42	1231.29	841.17	368.63	6311.71	4967.00	1.02	0.84	0.247
ILMN_3167525	mmu-miR-878-3p	523.96	544.25	485.46	556.83	758.92	964.79	0.72	0.13	0.203
ILMN_3169011	mmu-miR-878-5p	378.33	372.83	318.42	395.42	505.96	586.50	0.75	0.12	0.194
ILMN_3169123	mmu-miR-881*	608.92	519.63	533.46	607.00	759.71	967.62	0.75	0.13	0.218
ILMN_3168975	mmu-miR-883b-3p	436.17	409.08	322.04	447.08	516.29	524.58	0.79	0.10	0.193
ILMN_3168974	mmu-miR-883b-5p	891.42	685.83	644.25	685.46	915.13	1133.29	0.87	0.22	0.488
ILMN_3166986	mmu-miR-92a	11130.09	12468.00	13055.59	13087.38	13643.17	15132.88	0.88	0.02	0.026
ILMN_3169007	mmu-miR-92b	568.21	1272.92	2520.71	1678.79	602.58	780.79	1.89	0.84	0.654
ILMN_3168517	mmu-miR-93	3298.00	3786.21	5610.58	2960.92	3130.79	3484.75	1.31	0.15	0.200
ILMN_3169104	mmu-miR-93*	2218.92	1742.42	3284.63	821.88	892.21	1004.83	2.64	0.38	0.068
ILMN_3168174	mmu-miR-96	2956.13	2387.38	2265.33	2793.04	2402.46	2720.04	0.96	0.07	0.634
ILMN_3167422	mmu-miR-98	4673.38	5104.42	6270.00	6153.13	6924.92	3930.38	1.03	0.28	0.833
ILMN_3167809	mmu-miR-99a	3041.96	5247.96	4829.42	3175.67	2623.29	2876.79	1.55	0.31	0.216
ILMN_3168262	mmu-miR-99b	5680.17	8199.42	7544.00	7046.67	5875.79	8199.42	1.04	0.18	0.937
ILMN_3169129	solexa-1127-427	5367.54	3744.83	8170.75	6730.33	5605.75	8137.96	0.82	0.10	0.201
ILMN_3169133	solexa-1328-360	2313.75	1752.17	5676.83	7613.17	3116.63	2474.88	1.05	0.62	0.685
ILMN_3169134	solexa-1416-339_2	450.25	419.04	309.42	457.83	469.33	542.13	0.82	0.13	0.296
ILMN_3169137	solexa-1837-257	9903.00	1498.17	1411.75	1820.04	654.92	1465.63	2.90	1.33	0.370
ILMN_3169138	solexa-200-2167	1874.67	2549.42	3271.42	996.96	1044.54	2582.88	1.86	0.34	0.053
ILMN_3168343	solexa-2054-231	1689.88	1343.33	1230.08	1461.08	1476.21	1896.54	0.91	0.15	0.541
ILMN_3169142	solexa-239-1823	7759.88	8752.25	8686.04	9987.38	9466.25	6965.38	0.98	0.14	0.757
ILMN_3169146	solexa-27-9416	16495.71	18408.50	20501.34	17560.71	19026.83	17471.05	1.03	0.07	0.762
ILMN_3169149	solexa-3024-155	606.13	608.79	580.25	672.63	835.96	1041.42	0.73	0.10	0.159
ILMN_3169150	solexa-3062-153	5645.46	6506.71	7738.83	7290.83	6412.04	9712.79	0.86	0.08	0.209
ILMN_3169151	solexa-308-1456	6231.13	7976.88	9409.67	6231.13	8025.50	10071.75	0.98	0.02	0.382
ILMN_3169152	solexa-3253-144	7950.75	7275.21	6417.33	3827.54	3951.13	4526.21	1.78	0.19	0.041
ILMN_3169153	solexa-403-1161	4967.00	6707.58	7514.00	5237.75	6860.08	8017.63	0.95	0.01	0.096
ILMN_3167558	solexa-4153-111	1215.29	977.67	978.87	905.46	1150.58	1313.79	0.98	0.18	0.766
ILMN_3169158	solexa-5560-82	10569.67	11130.09	13044.92	12289.58	10591.50	11019.96	1.03	0.09	0.820
ILMN_3169159	solexa-5593-81	2001.96	902.42	809.67	857.13	1521.75	5641.96	1.02	0.67	0.503

Table B1. -Continued

Illumina_ID	NAME	LCA1 signal	LCA2 signal	LCA3 signal	RCA1 signal	RCA2 signal	RCA3 signal	LCA/RCA ratio	SEM	p-value
ILMN_3169160	solexa-564-789	635.42	485.33	620.21	615.25	646.67	935.29	0.82	0.11	0.257
ILMN_3169161	solexa-622-718	4158.63	4729.42	5056.29	2894.67	6138.21	812.13	2.81	1.72	0.491
ILMN_3169162	solexa-897-515	858.38	1481.38	1335.92	2856.25	2239.50	1059.13	0.74	0.28	0.336
ILMN_3168529	mmu-miR-106a:9.1	358.54	406.29	391.54	471.46	600.92	722.04	0.66	0.06	0.079
ILMN_3168955	mmu-miR-1224	335.71	373.88	300.29	388.13	2031.38	425.96	0.58	0.21	0.363
ILMN_3167491	mmu-miR-128a:9.1	1453.65	2245.81	798.21	1018.06	688.98	363.96	2.29	0.53	0.163
ILMN_3169092	mmu-miR-15a*	1395.33	354.71	292.71	2132.46	1289.33	566.25	0.48	0.11	0.080
ILMN_3169071	mmu-miR-186*	574.29	551.67	413.38	544.63	704.29	599.54	0.84	0.11	0.264
ILMN_3169055	mmu-miR-27b*	385.96	340.63	1538.00	452.38	2772.96	1072.08	0.80	0.38	0.526
ILMN_3169077	mmu-miR-294*	341.96	1307.04	273.42	394.54	404.08	3316.67	1.39	0.95	0.601
ILMN_3169101	mmu-miR-29c*	505.71	1592.33	1942.42	2464.38	3731.21	508.13	1.48	1.17	0.525
ILMN_3167828	mmu-miR-31*	614.38	508.38	382.46	559.21	621.96	644.46	0.84	0.15	0.364
ILMN_3168288	mmu-miR-34b-5p	343.92	1174.21	292.63	415.83	447.29	555.17	1.33	0.66	0.708
ILMN_3168943	mmu-miR-362-3p	418.79	436.71	704.38	1382.08	558.25	474.63	0.86	0.34	0.505
ILMN_3168438	mmu-miR-376b*	1509.79	3406.96	3714.42	5646.21	4929.63	442.04	3.12	2.64	0.749
ILMN_3167115	mmu-miR-669b	583.25	341.58	340.00	412.00	684.83	468.13	0.88	0.28	0.572
ILMN_3169035	mmu-miR-669h-3p	1062.38	392.42	575.75	592.08	464.29	503.58	1.26	0.28	0.435
ILMN_3167514	mmu-miR-671-5p	331.38	351.58	326.08	393.63	461.04	593.58	0.72	0.09	0.142
ILMN_3168277	mmu-miR-681	324.71	559.13	316.17	448.08	5086.96	561.21	0.47	0.18	0.377
ILMN_3167808	mmu-miR-101a	4318.83	3935.00	4041.79	1548.58	1528.21	112.88	13.72	11.04	0.022
ILMN_3169040	mmu-miR-1190	5605.75	5272.50	4843.54	3600.13	4881.71	273.33	6.79	5.47	0.197
ILMN_3168025	mmu-miR-134	1851.17	310.29	1692.54	749.58	415.33	2393.96	1.31	0.58	0.870
ILMN_3166992	mmu-miR-139-5p	2170.25	5954.17	2477.67	3069.42	327.67	6071.04	6.43	5.87	0.903
ILMN_3169086	mmu-miR-148a*	537.13	580.25	737.33	422.04	734.58	352.92	1.38	0.38	0.536
ILMN_3169054	mmu-miR-15b*	1074.25	1560.25	3127.88	4143.88	2692.13	286.50	3.92	3.50	0.819
ILMN_3168478	mmu-miR-199a-3p:9.1	7658.38	6657.50	4256.88	6241.50	5367.54	329.46	5.13	3.90	0.123
ILMN_3167787	mmu-miR-19a	1392.75	3951.13	274.71	1089.33	2892.50	488.46	1.07	0.25	0.409
ILMN_3167196	mmu-miR-204	2598.92	2659.42	1078.96	1725.67	3269.50	131.92	3.50	2.35	0.510
ILMN_3167837	mmu-miR-31	476.96	1187.21	663.71	1497.17	2368.79	70.75	3.40	2.99	0.444
ILMN_3168391	mmu-miR-361	1028.88	3042.92	3481.21	1760.29	103.17	4569.75	10.28	9.61	0.799
ILMN_3168146	mmu-miR-434-3p	159.29	1188.71	1328.29	3977.00	2327.67	2986.88	0.33	0.15	0.115
ILMN_3169009	mmu-miR-466d-3p	390.04	114.33	2052.83	2345.54	2535.71	2793.50	0.32	0.21	0.076
ILMN_3167553	mmu-miR-491	325.00	357.08	321.00	353.79	450.42	589.96	0.75	0.11	0.211
ILMN_3168956	mmu-miR-551b	910.13	520.88	1237.50	365.92	365.83	553.75	2.05	0.32	0.100
ILMN_3169032	mmu-miR-669f	493.67	2204.79	1521.96	1091.67	3134.25	113.04	4.87	4.30	0.962
ILMN_3167160	mmu-miR-684	7944.17	8299.67	6612.00	3797.58	7022.29	77.71	29.45	27.82	0.120
ILMN_3168126	mmu-miR-685	1151.08	5195.25	4277.63	4185.46	994.79	119.42	13.77	11.12	0.537
ILMN_3167032	mmu-miR-699	1224.04	2964.67	2140.17	994.96	3342.75	324.21	2.91	1.85	0.485
ILMN_3168037	mmu-miR-702	2705.71	1997.08	1557.33	3228.63	4591.04	239.88	2.59	1.96	0.649
ILMN_3167999	mmu-miR-712	1206.92	2008.42	3316.67	6350.46	142.67	3385.46	5.08	4.50	0.647
ILMN_3169121	mmu-miR-742*	58.71	589.75	2022.17	3866.42	4529.50	5359.04	0.17	0.11	0.002
ILMN_3169125	mmu-miR-877*	4173.58	2333.21	475.63	157.38	1610.29	3112.67	9.37	8.58	0.750
ILMN_3169155	solexa-447-1003	731.33	1492.00	948.71	596.33	71.92	2544.33	7.45	6.65	0.989
ILMN_3169056	mmu-miR-29b*	120.71	2720.04	2273.71	337.08	4854.67	4338.46	0.48	0.06	0.144
ILMN_3168929	mmu-miR-34b-3p	262.50	281.67	1015.58	381.33	413.13	568.38	1.05	0.37	0.764
ILMN_3168374	mmu-miR-693-3p	323.96	1404.71	837.04	294.83	2176.50	506.71	1.13	0.29	0.717
ILMN_3169103	mmu-miR-92a*	426.96	430.79	329.58	364.96	558.67	390.83	0.93	0.12	0.526
ILMN_3168320	mmu-miR-1	629.92	70.71	65.54	753.71	2334.00	4495.54	0.29	0.27	0.209
ILMN_3167231	mmu-miR-101b:9.1	876.88	96.67	655.08	611.88	4847.96	91.46	2.87	2.18	0.527
ILMN_3169051	mmu-miR-1198	501.58	153.75	1689.96	5186.50	64.58	2431.88	1.06	0.68	0.350
ILMN_3169061	mmu-miR-125b*	367.08	319.54	314.29	375.13	443.04	605.96	0.74	0.13	0.229
ILMN_3167008	mmu-miR-129-3p	4128.71	4291.58	2429.75	1487.46	85.63	98.96	25.82	13.68	0.034
ILMN_3168045	mmu-miR-17*	105.79	947.33	2608.96	397.63	1215.96	99.96	9.05	8.53	0.557
ILMN_3168280	mmu-miR-181c	1460.00	153.42	774.04	851.54	2497.54	169.08	2.12	1.32	0.738
ILMN_3167628	mmu-miR-196a	368.79	112.79	2876.79	2682.50	138.17	6590.46	0.46	0.20	0.201
ILMN_3169099	mmu-miR-26b*	397.75	924.71	930.71	95.79	451.92	62.87	7.00	3.95	0.082
ILMN_3168927	mmu-miR-296-3p	1121.00	2142.58	2945.58	240.17	3026.13	229.25	6.07	3.57	0.476
ILMN_3166969	mmu-miR-324-5p	835.63	1509.79	182.75	790.88	1482.33	194.17	1.01	0.03	0.347
ILMN_3167611	mmu-miR-331-3p	603.54	906.46	1658.96	87.17	1977.33	92.33	8.45	5.11	0.703
ILMN_3168410	mmu-miR-425*	542.79	823.29	191.00	1560.25	264.50	2585.75	1.18	0.97	0.381
ILMN_3168991	mmu-miR-466c-5p	1895.63	284.79	858.38	353.92	368.33	430.79	2.71	1.37	0.320
ILMN_3168996	mmu-miR-466h	2806.79	851.04	249.08	2043.00	1428.17	384.96	0.87	0.25	0.970
ILMN_3167922	mmu-miR-541	1150.58	1818.92	902.75	840.92	112.63	133.67	8.09	4.32	0.152
ILMN_3167846	mmu-miR-665	244.63	638.79	455.17	752.54	215.29	1853.17	1.18	0.89	0.447
ILMN_3168520	mmu-miR-668	295.13	4164.88	5160.88	1942.42	3541.33	77.13	22.75	22.09	0.564
ILMN_3167536	mmu-miR-669a	1079.38	1023.88	688.54	159.04	100.33	893.13	5.92	2.76	0.283
ILMN_3169131	solexa-1278-371	915.33	499.92	806.42	1781.92	98.00	251.96	2.94	1.33	0.953
ILMN_3169147	solexa-284-1594	198.13	1990.33	5317.46	1320.92	1827.79	221.00	8.43	7.82	0.543
ILMN_3168578	solexa-5306-86	330.46	432.46	642.46	77.75	75.79	481.96	3.76	1.29	0.045
ILMN_3167755	mmu-miR-182	424.63	260.00	252.46	299.17	919.50	570.83	0.71	0.36	0.338
ILMN_3167244	mmu-miR-410	313.75	323.25	272.88	1031.21	422.33	519.79	0.53	0.13	0.198
ILMN_3168422	mmu-miR-693-5p	290.71	343.67	322.50	345.54	454.25	532.50	0.73	0.07	0.110
ILMN_3169127	solexa-103-3961	290.67	332.17	1234.58	834.33	1355.75	98.92	4.36	4.06	0.846
ILMN_3169140	solexa-201-2163	989.17	363.75	530.33	436.17	147.58	214.42	2.40	0.07	0.069
ILMN_3169145	solexa-2564-185	335.71	513.75	399.79	135.63	165.92	497.83	2.12	0.68	0.371
ILMN_3169156	solexa-4983-92	941.29	344.17	2614.13	347.13	398.83	344.54	3.72	2.01	0.309
ILMN_3169045	mmu-miR-1194	2111.83	1377.13	292.63	184.96	181.08	154.13	6.97	2.77	0.171
ILMN_3168012	mmu-miR-142-3p	964.67	333.58	440.21	241.75	1734.04	267.50	1.94	1.11	0.816
ILMN_3167894	mmu-miR-146b	855.00	1248.04	177.13	780.79	213.92	204.50	2.60	1.62	0.398
ILMN_3168019	mmu-miR-206	1404.71	2655.33	94.75	5488.83	101.42	116.88	9.08	8.55	0.814
ILMN_3168406	mmu-miR-291b-3p	798.17	257.38	428.67	81.13	756.92	88.33	5.01	2.74	0.657
ILMN_3167162	mmu-miR-291b-5p	2615.58	2294.50	2501.92	133.54	136.25	162.88	17.26	1.24	0.002
ILMN_3168984	mmu-miR-297c	79.67	3435.04	78.25	86.17	462.08	3233.04	2.79	2.33	0.975
ILMN_3167913	mmu-miR-299*	144.88	522.17	1512.04	173.75	235.29	1013.96	1.51	0.40	0.242
ILMN_3168116	mmu-miR-301a	489.29	305.04	987.42	248.29	428.08	268.58	2.12	0.86	0.371
ILMN_3169084	mmu-miR-30c-1*	99.08	98.50	373.79	98.71	2055.71	658.21	0.54	0.28	0.346
ILMN_3168935	mmu-miR-338-5p	652.54	984.04	161.58	900.88	194.42	203.38	2.19	1.43	0.652
ILMN_3168938	mmu-miR-342-5p	76.42	2631.63	685.46	452.92	84.58	90.21	12.96	9.33	0.396
ILMN_3167138	mmu-miR-376c	84.25	1343.38	1022.88	1155.58	95.54	275.58	5.95	4.19	0.705
ILMN_3168987	mmu-miR-421	1717.83	178.21	1020.92	517.79	212.83	227.83	2.88	1.07	0.214
ILMN_3168006	mmu-miR-434-5p	1383.08	202.67	648.88	197.54	7738.83	188.71	3.49	2.01	0.555
ILMN_3169022	mmu-miR-467e	241.38	1512.04	1293.83	239.75	1860.33	291.92	2.08	1.18	0.643
ILMN_3168236	mmu-miR-483*	257.21	207.83	1296.04	1249.63	234.29	2892.50	0.51	0.20	0.197
ILMN_3167221	mmu-miR-485	486.00	855.25	71.13	1105.00	77.96	80.42	4.10	3.44	0.913
ILMN_3167583	mmu-miR-490	261.17	352.21	307.58	390.17	422.08	588.42	0.68	0.09	0.126
ILMN_3167912	mmu-miR-501-3p	99.83	112.00	399.79	508.71	234.42	1066.17	0.35	0.08	0.126
ILMN_3168957	mmu-miR-671-3p	847.63	217.04	125.50	1398.75	3889.04	178.54	0.45	0.20	0.335
ILMN_3168059	mmu-miR-674	431.67	293.25	2402.46	655.58	89.54	88.46	10.36	8.43	0.433
ILMN_3168270	mmu-miR-674*	82.96	68.54	330.96	2426.33	4164.88	69.58	1.60	1.58	0.245
ILMN_3169119	mmu-miR-744*	5413.58	134.42	245.58	934.50	157.25	653.17	2.34	1.73	0.480
ILMN_3167710	mmu-miR-759	196.63	1023.17	2382.83	250.58	285.88	3380.38	1.69	0.95	0.854
ILMN_3168479	mmu-miR-760:9.1	786.08	616.96	75.54	87.38	80.08	2243.08	5.58	2.80	0.770

Table B1. -Continued

Illumina_ID	NAME	LCA1 signal	LCA2 signal	LCA3 signal	RCA1 signal	RCA2 signal	RCA3 signal	LCA/RCA ratio	SEM	p-value
ILMN_3169124	mmu-miR-872*	1170.21	2083.71	2271.33	249.63	311.92	312.79	6.21	0.78	0.040
ILMN_3168976	mmu-miR-874	433.04	202.71	663.58	1048.04	245.50	311.71	1.12	0.52	0.751
ILMN_3167447	mmu-miR-9	426.00	4092.00	993.71	61.29	63.08	61.33	29.34	17.96	0.259
ILMN_3169058	mmu-miR-99b*	166.50	81.88	586.96	743.08	82.21	608.13	0.73	0.25	0.402
ILMN_3168979	mmu-miR-105	275.25	309.33	265.96	345.17	402.50	488.00	0.70	0.08	0.113
ILMN_3167116	mmu-miR-302a	265.21	288.33	271.08	363.29	387.96	589.17	0.64	0.09	0.143
ILMN_3168071	mmu-miR-450b-3p	272.38	307.50	262.92	327.92	386.63	483.42	0.72	0.09	0.148
ILMN_3168056	mmu-miR-673-5p	2440.25	93.29	89.08	2045.67	391.96	102.50	0.77	0.28	0.904
ILMN_3167983	mmu-miR-704	736.67	1343.13	199.54	225.13	250.08	395.54	3.05	1.41	0.335
ILMN_3168106	mmu-miR-764-5p	161.71	164.67	1593.63	185.46	389.88	6239.08	0.52	0.18	0.392
ILMN_3169016	mmu-miR-877	2352.79	270.04	585.17	264.63	329.71	455.71	3.66	2.62	0.405
ILMN_3167353	mmu-miR-107	105.83	138.42	523.92	620.29	132.00	139.58	1.66	1.08	0.889
ILMN_3169044	mmu-miR-1193	198.63	78.00	1126.00	735.71	74.33	74.71	5.46	4.81	0.747
ILMN_3168361	mmu-miR-181a-1*	97.75	62.21	571.54	869.96	65.96	64.67	3.30	2.78	0.832
ILMN_3169070	mmu-miR-183*	265.75	320.38	271.75	325.79	400.17	442.08	0.74	0.06	0.093
ILMN_3168073	mmu-miR-186	182.29	194.88	452.96	208.71	236.33	2024.58	0.64	0.21	0.398
ILMN_3168981	mmu-miR-18b	592.13	159.38	864.96	175.13	183.83	219.92	2.73	0.94	0.220
ILMN_3167472	mmu-miR-32	371.88	218.25	361.75	246.25	255.88	301.17	1.19	0.19	0.406
ILMN_3167081	mmu-miR-330*	213.54	228.88	1038.75	833.83	281.63	318.50	1.44	0.92	0.971
ILMN_3167584	mmu-miR-351	161.92	174.92	807.79	494.50	202.29	202.38	1.73	1.14	0.795
ILMN_3168477	mmu-miR-381	101.08	1110.63	1658.96	265.46	119.08	130.50	7.47	3.68	0.257
ILMN_3167820	mmu-miR-409-3p	504.88	60.00	638.17	62.17	60.46	73.04	5.95	2.49	0.190
ILMN_3168962	mmu-miR-423-5p	101.42	752.13	663.58	108.21	122.00	139.54	3.95	1.56	0.192
ILMN_3167383	mmu-miR-431	508.38	152.08	786.88	152.54	159.17	170.08	2.97	1.07	0.217
ILMN_3167973	mmu-miR-433	100.21	651.67	364.17	115.46	123.25	134.75	2.95	1.28	0.256
ILMN_3168193	mmu-miR-433*	349.92	295.79	263.50	330.08	356.71	532.63	0.79	0.16	0.353
ILMN_3168187	mmu-miR-450a-5p	85.63	658.67	375.38	192.21	97.29	107.88	3.57	1.83	0.339
ILMN_3167599	mmu-miR-467b	245.88	301.38	272.00	311.08	385.92	392.71	0.75	0.03	0.031
ILMN_3167334	mmu-miR-485*	940.79	193.46	179.00	365.88	241.08	255.21	1.36	0.61	0.552
ILMN_3167052	mmu-miR-495	80.08	98.17	366.96	1149.42	100.67	100.92	1.56	1.07	0.578
ILMN_3167017	mmu-miR-500	290.63	458.25	417.88	117.88	107.42	122.54	3.38	0.52	0.035
ILMN_3169118	mmu-miR-503*	1870.67	70.50	659.79	188.63	69.17	78.54	6.45	2.75	0.265
ILMN_3168199	mmu-miR-532-5p	2933.79	93.88	1582.58	98.25	95.50	99.83	15.57	8.34	0.221
ILMN_3167979	mmu-miR-539	131.83	638.17	635.75	142.13	144.88	159.83	3.10	1.09	0.192
ILMN_3167513	mmu-miR-551b:9.1	170.38	832.04	286.50	187.63	196.54	196.33	2.20	1.03	0.363
ILMN_3169046	mmu-miR-669e	3541.33	668.71	210.33	142.75	155.42	198.08	10.06	7.43	0.341
ILMN_3169033	mmu-miR-669i	2345.17	50.83	49.00	266.25	443.92	49.04	3.31	2.76	0.540
ILMN_3168011	mmu-miR-672	175.75	163.46	4591.04	3220.42	184.38	196.67	8.10	7.63	0.856
ILMN_3167845	mmu-miR-677	90.17	94.96	1019.25	100.17	108.08	2444.38	0.73	0.16	0.413
ILMN_3168148	mmu-miR-713	988.58	118.83	601.63	123.00	133.50	146.54	4.34	2.07	0.229
ILMN_3167900	mmu-miR-715	629.75	205.21	220.42	189.83	224.08	571.25	1.54	0.90	0.928
ILMN_3168502	mmu-miR-718	283.50	387.33	258.63	328.13	381.38	476.71	0.81	0.14	0.334
ILMN_3167961	mmu-miR-764-3p	50.08	219.96	51.33	283.71	843.96	1904.92	0.15	0.07	0.205
ILMN_3168969	mmu-miR-880	507.38	47.17	294.00	47.75	70.88	50.75	5.69	2.88	0.247
ILMN_3169130	solexa-1201-400	287.04	217.50	740.50	257.21	258.67	393.50	1.28	0.31	0.447
ILMN_3169139	solexa-2011-236	2148.33	67.08	63.71	2527.96	64.00	62.21	0.97	0.06	0.430
ILMN_3169157	solexa-5067-90	527.96	782.58	77.88	87.54	81.29	82.25	5.53	2.52	0.207
ILMN_3169096	mmu-miR-21*	291.63	305.75	248.83	328.63	361.92	402.96	0.78	0.08	0.151
ILMN_3168932	mmu-miR-325	271.79	275.46	257.75	317.54	389.08	526.92	0.68	0.11	0.163
ILMN_3169002	mmu-miR-509-3p	180.54	468.13	213.04	247.79	297.83	435.54	0.93	0.33	0.761
ILMN_3169082	mmu-miR-106b*	47.75	1007.25	148.96	46.67	47.75	50.54	8.35	6.39	0.366
ILMN_3169042	mmu-miR-1191	570.04	83.96	80.63	86.79	87.08	92.88	2.80	1.88	0.441
ILMN_3167099	mmu-miR-130b	171.50	1315.46	182.17	191.88	221.00	278.29	2.50	1.73	0.486
ILMN_3169083	mmu-miR-130b*	118.63	128.50	124.04	129.67	144.17	947.38	0.65	0.26	0.404
ILMN_3168348	mmu-miR-133b	256.88	276.75	250.42	290.46	367.04	434.21	0.74	0.09	0.144
ILMN_3167823	mmu-miR-135a	413.88	194.75	211.88	237.04	221.33	505.13	1.02	0.39	0.760
ILMN_3167624	mmu-miR-136	102.50	407.42	112.63	114.79	104.58	122.88	1.90	1.00	0.466
ILMN_3169063	mmu-miR-136*	99.54	1064.54	100.17	112.50	121.29	124.58	3.49	2.64	0.446
ILMN_3168064	mmu-miR-141	213.63	215.54	192.21	242.88	264.63	445.83	0.71	0.14	0.263
ILMN_3169067	mmu-miR-154*	698.92	212.54	168.54	196.38	243.46	194.88	1.77	0.90	0.490
ILMN_3169093	mmu-miR-16*	281.83	239.29	239.21	256.42	1641.67	308.04	0.67	0.28	0.406
ILMN_3167529	mmu-miR-183	215.25	236.42	185.00	1212.88	215.33	267.92	0.66	0.27	0.389
ILMN_3167217	mmu-miR-201	152.58	158.21	143.67	1387.29	169.58	169.67	0.63	0.26	0.405
ILMN_3169075	mmu-miR-203*	369.79	141.75	167.21	164.17	158.33	394.92	1.19	0.55	0.927
ILMN_3167091	mmu-miR-205	136.67	146.54	143.25	155.96	1284.63	228.00	0.54	0.22	0.372
ILMN_3167495	mmu-miR-207	258.21	282.79	236.50	306.25	381.33	454.42	0.70	0.10	0.137
ILMN_3169117	mmu-miR-20b*	279.25	189.13	305.75	132.79	143.33	198.50	1.65	0.23	0.076
ILMN_3167457	mmu-miR-24-1*	60.63	725.33	202.75	61.00	56.08	60.92	5.75	3.65	0.316
ILMN_3168926	mmu-miR-290-3p	139.79	152.21	134.21	149.17	3798.67	181.21	0.57	0.27	0.414
ILMN_3167645	mmu-miR-297b-5p	619.54	199.00	198.63	196.58	240.88	241.67	1.60	0.78	0.543
ILMN_3167235	mmu-miR-302c*	133.96	133.92	124.25	140.58	4760.21	167.58	0.57	0.28	0.416
ILMN_3166938	mmu-miR-322	118.04	1700.29	142.75	137.08	142.42	188.92	4.52	3.71	0.447
ILMN_3167910	mmu-miR-325*	83.79	646.67	77.33	77.92	81.75	88.33	3.29	2.31	0.428
ILMN_3169110	mmu-miR-33*	105.46	802.50	103.38	117.13	120.67	139.58	2.76	1.94	0.464
ILMN_3168933	mmu-miR-330	133.29	128.83	306.38	135.00	151.88	171.38	1.21	0.29	0.535
ILMN_3168944	mmu-miR-335-3p	78.75	91.13	90.21	1727.25	155.33	123.17	0.45	0.21	0.389
ILMN_3168937	mmu-miR-341	345.33	119.63	108.38	136.38	131.88	148.71	1.39	0.57	0.576
ILMN_3169081	mmu-miR-34c*	130.25	159.75	720.17	162.42	289.08	170.92	1.86	1.18	0.604
ILMN_3167597	mmu-miR-374*	72.83	77.25	854.42	76.63	73.08	80.58	4.20	3.20	0.422
ILMN_3167098	mmu-miR-380-3p	1205.04	84.42	80.58	84.75	87.58	99.29	5.33	4.44	0.434
ILMN_3167050	mmu-miR-452	120.54	131.71	125.42	1260.63	150.00	175.63	0.56	0.24	0.389
ILMN_3166954	mmu-miR-465a-5p	304.79	234.54	210.08	278.67	286.75	395.46	0.81	0.16	0.372
ILMN_3168990	mmu-miR-466b-5p	109.13	384.63	104.58	104.38	119.00	109.38	1.74	0.74	0.423
ILMN_3169008	mmu-miR-466d-5p	3772.96	232.96	202.92	279.46	246.96	317.00	5.03	4.24	0.444
ILMN_3169041	mmu-miR-466j	265.75	295.38	259.54	329.79	341.21	416.25	0.77	0.07	0.122
ILMN_3167338	mmu-miR-467a*,mmu-miR-467d*,mmu-miR-467a*,mmu-miR-467d*	76.75	76.67	1431.83	81.58	77.33	78.25	6.74	5.78	0.425
ILMN_3168997	mmu-miR-467c	100.54	1476.75	83.42	63.46	61.29	78.96	8.91	7.59	0.406
ILMN_3167917	mmu-miR-471:9.1	135.50	102.29	109.12	113.00	103.29	1144.46	0.76	0.34	0.435
ILMN_3167781	mmu-miR-488*	205.75	279.96	239.54	333.29	325.88	389.75	0.70	0.08	0.076
ILMN_3167642	mmu-miR-499	65.79	69.25	67.13	71.71	1852.67	80.08	0.60	0.28	0.417
ILMN_3168526	mmu-miR-501-5p	53.63	53.83	55.67	55.25	533.75	56.83	0.68	0.29	0.419
ILMN_3167125	mmu-miR-505	99.29	89.17	83.50	88.71	5954.17	94.58	0.67	0.34	0.423
ILMN_3167887	mmu-miR-543	53.42	748.67	51.50	52.75	50.83	53.88	5.57	4.58	0.424
ILMN_3169019	mmu-miR-598	157.67	194.67	522.71	198.79	265.33	274.92	1.14	0.38	0.699
ILMN_3169025	mmu-miR-669g	53.83	57.13	56.04	55.42	3752.42	58.83	0.65	0.32	0.422
ILMN_3168082	mmu-miR-676*	65.08	68.25	985.00	67.92	72.21	71.17	5.25	4.30	0.427
ILMN_3168248	mmu-miR-696	1630.38	155.42	180.71	170.75	188.17	194.00	3.77	2.89	0.441
ILMN_3167423	mmu-miR-705	270.75	147.54	74.83	75.88	813.67	83.33	1.55	1.03	0.601
ILMN_3168961	mmu-miR-760	117.79	131.63	157.42	252.96	216.96	1727.17	0.39	0.15	0.345
ILMN_3168397	mmu-miR-801:9.1	80.96	91.29	1157.88	88.67	113.21	130.54	3.53	2.67	0.439
ILMN_3168968	mmu-miR-879	196.54	242.88	227.38	381.33	299.71	260.08	0.73	0.11	0.192

Table B1. -Continued

Illumina_ID	NAME	LCA1 signal	LCA2 signal	LCA3 signal	RCA1 signal	RCA2 signal	RCA3 signal	LCA/RCA ratio	SEM	p-value
ILMN_3169128	solexa-110-3896	178.33	188.25	164.17	208.54	198.58	479.04	0.72	0.19	0.352
ILMN_3167930	solexa-231-1844	835.54	110.04	104.04	119.79	120.13	128.58	2.90	2.04	0.451
ILMN_3169143	solexa-2402-197	150.38	150.50	136.46	812.33	173.00	178.42	0.61	0.21	0.368
ILMN_3167725	solexa-4179-110	190.63	110.96	833.83	99.38	97.25	102.96	3.72	2.20	0.345
ILMN_3169154	solexa-4327-106	65.25	69.54	67.04	66.17	2149.54	76.42	0.63	0.30	0.420
ILMN_3169036	mmu-miR-1188	114.17	127.04	117.50	150.00	157.71	304.54	0.65	0.13	0.241
ILMN_3168921	mmu-miR-125a-3p	53.88	53.88	54.75	56.17	382.04	56.17	0.69	0.28	0.416
ILMN_3169028	mmu-miR-1-2-as	149.63	162.33	154.17	189.46	191.67	311.96	0.71	0.11	0.208
ILMN_3168356	mmu-miR-290-5p	268.58	284.46	228.92	328.38	328.17	367.42	0.77	0.07	0.110
ILMN_3168420	mmu-miR-429	271.92	308.04	226.83	337.04	359.42	304.25	0.80	0.03	0.013
ILMN_3168664	mmu-miR-431*	134.46	70.71	70.88	314.29	69.21	72.79	0.81	0.19	0.421
ILMN_3168954	mmu-miR-450a-3p	220.04	254.38	240.00	273.38	325.88	461.75	0.70	0.09	0.163
ILMN_3168992	mmu-miR-466e-5p	256.92	271.21	251.67	313.83	343.63	430.04	0.73	0.07	0.115
ILMN_3167855	mmu-miR-467b*	309.42	79.88	76.04	78.00	82.08	92.42	1.92	1.02	0.470
ILMN_3169115	mmu-miR-470*	250.21	258.63	243.21	292.54	338.29	371.50	0.76	0.06	0.079
ILMN_3169021	mmu-miR-582-3p	287.83	286.25	234.25	335.58	338.92	399.29	0.76	0.09	0.147
ILMN_3168278	mmu-miR-710	158.96	198.33	197.58	190.21	254.17	394.04	0.71	0.10	0.208
ILMN_3168403	mmu-miR-721	225.42	235.83	221.25	256.42	303.63	349.75	0.76	0.07	0.117
ILMN_3168978	mmu-miR-876-3p	72.71	77.08	80.63	81.58	87.58	411.21	0.66	0.23	0.389

Table B2. miRNA expression profiles in mouse ligated carotid endothelium (LCA) and controlateral right carotid endothelium (RCA) at 48 hr post-ligation

Illumia_ID	NAME	LCA1	LCA2	LCA3	LCA4	LCA5	LCA6	RCA1	RCA2	RCA3	RCA4	RCA4	RCA6	LCA/RCA		
		signal	signal	signal	signal	signal	signal	signal	signal	signal	signal	signal	signal	ratio	SEM	p-value
ILMN_3167971	mmu-let-7a	12936.67	9184.083	13760.83	10428.17	11896.83	12936.67	12811.67	15395	17161.5	1800.25	16716.83	17505.17	1.61	0.84	0.481
ILMN_3167970	mmu-let-7b	23384.17	16401	25891.08	25463.42	23384.17	23985.08	28579.5	28579.5	28579.5	25463.42	27525.75	28579.5	0.83	0.06	0.034
ILMN_3169089	mmu-let-7b*	1009.083	461.25	594	453.5	453.5	443.0833	648.1667	533.5	332.0833	773	312.75	426.25	1.21	0.19	0.546
ILMN_3167551	mmu-let-7d	9184.083	7508.083	5693.167	12656	6873.917	8873.167	18895.42	17161.5	15807.75	11469	16401	21350.83	0.54	0.11	0.008
ILMN_3167347	mmu-let-7d*	16401	17505.17	19786	17505.17	19786	19786	17505.17	21350.83	18895.42	18895.42	15807.75	15100.5	1.05	0.08	0.708
ILMN_3168365	mmu-let-7g	6534	7416.333	723	10534.83	9633	10534.83	10684.58	12251	13133.08	13760.83	12095.75	9871.417	0.65	0.14	0.056
ILMN_3169053	mmu-let-7g*	4131.917	1351.583	2006.667	1308.5	1018.333	1244.667	1912.583	1655.25	763.8333	1703.417	836.25	1351.583	1.42	0.32	0.316
ILMN_3168316	mmu-let-7i	6873.917	8536.417	1137.167	11048.17	8653.917	7277.917	9871.417	10089.58	10428.17	6175.917	13760.83	12811.67	0.77	0.23	0.155
ILMN_3167634	mmu-miR-100	14561.83	17845.75	14561.83	14252.67	15100.5	15100.5	13665.33	8461.333	12656	13962.67	13133.08	10223.75	1.33	0.17	0.068
ILMN_3168157	mmu-miR-101a:9.1	198.9167	567.8333	218.6667	209.75	169	188.8333	214.6667	883.3333	272	4992.583	3532.167	6534	0.42	0.17	0.078
ILMN_3167231	mmu-miR-101b:9.1	2912.75	7111.083	7611	3419.333	277.5833	198.9167	198.9167	9871.417	6873.917	9184.083	4712.75	628.6667	2.87	2.36	0.264
ILMN_3167027	mmu-miR-103	28579.5	28579.5	28579.5	28579.5	28579.5	28579.5	22194.33	22194.33	27087.58	27525.75	27087.58	27525.75	1.13	0.05	0.040
ILMN_3168930	mmu-miR-106a	1070.583	979.5	1679.417	1137.167	1214.667	1182.333	1703.417	1538.583	783.8333	1912.583	683.8333	979.5	1.16	0.27	0.851
ILMN_3168529	mmu-miR-106a:9.1	293.6667	180.9167	344.75	272	203.5833	187.1667	265.1667	355.8333	205.1667	414.6667	222.9167	312.75	0.91	0.18	0.365
ILMN_3169105	mmu-miR-10a*	414.6667	355.8333	1943.917	1368.417	1294.083	1117.667	2048.417	1506.5	648.1667	2227.667	410.75	603.1667	1.51	0.55	0.761
ILMN_3169068	mmu-miR-10b*	603.1667	344.75	628.6667	477.1667	369.25	414.6667	827.8333	586.0833	355.8333	661.5	576.5	863.9167	0.82	0.19	0.137
ILMN_3169029	mmu-miR-1186	4647.833	268.5833	695.1667	4817.25	477.1667	1574.333	6093.417	12497.5	3850	671.25	3776.083	3776.083	1.45	1.15	0.219
ILMN_3169030	mmu-miR-1187	1117.667	172.8333	5646.75	3389.167	3389.167	1034.583	1655.25	307.8333	2559.167	1173.75	1278.083	4075.75	1.54	0.48	0.538
ILMN_3169043	mmu-miR-1192	447.5833	559	1308.5	5198.25	815.3333	836.25	1538.583	918.5	334.9167	1329.583	361.75	671.25	2.04	0.65	0.385
ILMN_3169049	mmu-miR-1195	13665.33	13760.83	17845.75	18348.58	17161.5	16716.83	17161.5	15807.75	16716.83	15395	14252.67	16209.25	1.03	0.07	0.773
ILMN_3168794	mmu-miR-1197	1048.917	715.25	1351.583	827.8333	783.8333	1009.083	1450.5	1294.083	676.3333	1574.333	550.0833	908.8333	1.06	0.24	0.614
ILMN_3168389	mmu-miR-125b-5p	8221.333	9346.417	2120.25	6369.833	2867	6873.917	12656	8005.833	10534.83	4313.5	10223.75	13133.08	0.72	0.21	0.090
ILMN_3167695	mmu-miR-126-3p	6434.583	4712.75	7820.25	576.5	471.5	483.6667	893.75	676.3333	342	754.6667	329.0833	421.6667	6.73	3.44	0.088
ILMN_3168399	mmu-miR-126-5p	13962.67	8394.833	15100.5	8816.583	13133.08	6746.5	26650.33	16209.25	21350.83	2912.75	28579.5	24957.08	0.92	0.43	0.049
ILMN_3168922	mmu-miR-128	4347.25	4243.5	3389.167	268.5833	4075.75	405.3333	355.8333	277.5833	209.75	339.1667	209.75	2905.8333	10.88	3.23	0.025
ILMN_3167491	mmu-miR-128a:9.1	4322.792	6732.167	5200.25	5535.458	5341.708	6958.167	1032.417	2814.458	3950.917	2901.375	3897.583	3872.792	2.16	0.44	0.002
ILMN_3168183	mmu-miR-129-5p	695.1667	918.5	731.5833	648.1667	554.5	461.25	515.6667	773	586.0833	1117.667	559	1189.333	0.96	0.16	0.471
ILMN_3168497	mmu-miR-130a	1480.333	1679.417	2699.75	1891.5	1800.25	1703.417	5752.583	2281.917	1117.667	3026	2730.417	7416.333	0.82	0.33	0.151
ILMN_3168212	mmu-miR-132	332.0833	218.6667	613.3333	334.9167	342	339.1667	554.5	671.25	1390.25	544.25	3443.417	443.0833	0.47	0.10	0.144
ILMN_3168314	mmu-miR-133a	2317.417	1408.083	5427.667	3361.167	1943.917	783.8333	7190.917	3443.417	2006.667	1034.583	1635.083	2048.417	1.38	0.53	0.787
ILMN_3167661	mmu-miR-133a*	661.5	471.5	676.3333	510.9167	436.5833	503.4167	849.1667	594	366.1667	806.8333	387.8333	405.3333	1.07	0.18	0.793
ILMN_3168348	mmu-miR-133b	342	245	405.3333	254.4167	245	265.1667	339.1667	387.8333	224.5833	344.75	170.9167	216.8333	1.14	0.18	0.809
ILMN_3167874	mmu-miR-135b	979.5	586.0833	1173.75	763.8333	676.3333	731.5833	1048.917	1034.583	576.5	1538.583	510.9167	937.1667	1.02	0.24	0.557
ILMN_3167501	mmu-miR-138	613.3333	307.8333	524.1667	443.0833	366.1667	379.75	576.5	443.0833	254.4167	603.1667	220.4167	332.0833	1.23	0.22	0.632
ILMN_3167136	mmu-miR-140	146.6667	3804.083	351.4167	329.0833	283.8333	383.1667	806.8333	979.5	2520.75	298.8333	4647.833	5752.583	0.91	0.62	0.245
ILMN_3166958	mmu-miR-143	11743.58	15395	11283.75	16716.83	9871.417	14851.75	19786	13665.33	15395	16209.25	17845.75	15395	0.83	0.10	0.140
ILMN_3168030	mmu-miR-144:9.1	2559.167	2754.917	2947.25	2162.667	2365.333	1891.5	2983.667	2404.333	1450.5	3119.333	1538.583	1968.583	1.20	0.20	0.598
ILMN_3167456	mmu-miR-145	18348.58	17161.5	17505.17	19786	17845.75	16401	20911.25	17845.75	21755.67	21350.83	20911.25	20911.25	0.87	0.03	0.006
ILMN_3168483	mmu-miR-146a	628.6667	2983.667	265.1667	259.8333	3119.333	453.5	224.5833	318.6667	2867	467.4167	1294.083	4877.833	2.55	1.44	0.737
ILMN_3169120	mmu-miR-146b*	344.75	648.1667	393.6667	290.5833	274.9167	304.25	414.6667	461.25	1538.583	443.0833	238.3333	293.6667	0.89	0.16	0.381
ILMN_3167902	mmu-miR-149	3361.167	6237.917	783.8333	1480.333	3776.083	4243.5	6369.833	510.9167	1968.583	715.25	1746.167	1009.083	3.60	1.81	0.369
ILMN_3168367	mmu-miR-151-3p	11632.25	8005.833	11156.33	8310.833	7820.25	7111.083	5798.167	9286.417	9739.083	8653.917	12936.67	5646.75	1.14	0.20	0.832
ILMN_3168819	mmu-miR-151-5p	27087.58	26179.5	26650.33	27087.58	27525.75	27525.75	27087.58	27525.75	26650.33	28579.5	26179.5	26179.5	1.00	0.02	0.964
ILMN_3167060	mmu-miR-15b	13760.83	10822.92	18348.58	15807.75	12251	17161.5	13133.08	18348.58	16209.25	8736.833	15100.5	17845.75	1.06	0.17	0.923
ILMN_3167989	mmu-miR-16	10534.83	14851.75	13133.08	14851.75	12095.75	15807.75	13364.42	14561.83	13665.33	14561.83	16209.25	11743.58	0.98	0.09	0.702
ILMN_3167785	mmu-miR-17	8736.833	11048.17	7508.083	11632.25	9346.417	9184.083	8736.833	7064.083	12497.5	8095.417	8310.833	1912.583	1.75	0.63	0.339
ILMN_3167127	mmu-miR-181a	13364.42	15807.75	12656	14561.83	12936.67	12095.75	9346.417	10684.58	10089.58	13364.42	12251	11283.75	1.23	0.08	0.024
ILMN_3169069	mmu-miR-181a-2*	773	1854.583	3970.25	849.1667	3026	763.8333	1278.083	964.4167	503.4167	1390.25	603.1667	783.8333	2.84	1.22	0.219
ILMN_3168257	mmu-miR-181b	8536.417	7820.25	754.6667	497.0833	6237.917	2559.167	2067.5	815.3333	3443.417	5259.667	8005.833	8394.833	2.52	1.55	0.913
ILMN_3167755	mmu-miR-182	268.5833	145.8333	280.1667	224.5833	214.6667	220.4167	298.8333	220.4167	159.4167	342	187.1667	283.8333	0.98	0.17	0.540
ILMN_3169070	mmu-miR-183*	426.25	230.1667	436.5833	369.25	304.25	277.5833	369.25	339.1667	320.5	576.5	355.8333	510.9167	0.87	0.13	0.267
ILMN_3167152	mmu-miR-185	1506.5	1776	2227.667	1329.583	1173.75	2208.917	1891.5	1776	937.1667	2208.917	1070.583	1137.167	1.30	0.29	0.584
ILMN_3169071	mmu-miR-186*	165.5833	156.75	410.75	320.5	293.6667	293.6667	489.4167	286.8333	146.6667	361.75	156.75	188.8333	1.33	0.38	0.984
ILMN_3168167	mmu-miR-187	3026	3254.25	4817.25	232.5833	191.4167	4209.083	318.6667	6534	149.1667	11156.33	863.9167	304.25	9.39	5.15	0.813
ILMN_3167745	mmu-miR-188-5p	248	334.9167	893.75	676.3333	1574.333	603.1667	1070.583	613.3333	283.8333	586.0833	178.0833	298.8333	2.66	1.31	0.517
ILMN_3168282	mmu-miR-18a	5150.25	11469	7713.917	10089.58	9739.083	7416.333	4556.833	7561.333	6369.833	4243.5	4556.833	8095.417	1.55	0.24	0.055
ILMN_3169094	mmu-miR-18a*	559	8221.333	908.8333	6695.167	5427.667	5198.25	5427.667	5198.25	393.6667	5150.25	1703.417	471.5	3.25	1.61	0.351
ILMN_3167253	mmu-miR-191	26650.33	27525.75	26179.5	27525.75	27087.58	27087.58	25463.42	27087.58	27525.75	27087.58	26650.33	27087.58	1.01	0.01	0.601
ILMN_3169072	mmu-miR-191*	510.9167	263.1667	620.6667	467.4167	431.5833	576.5	1189.333	783.8333	421.6667	3389.167	483.6667	763.8333	0.67	0.20	0.195
ILMN_3167506	mmu-miR-192	5985.583	620.6667	1009.083	5798.167	908.8333	2606.083	7508.083	874.25	3254.25	1182.333	2317.417	567.8333	1.95	0.89	0.857
ILMN_3168366	mmu-miR-193	1746.167	6434.583	4313.5	9871.417	9286.417	9346.417	11896.83	7508.083	7508.083	13665.33	4313.5	7111.083	0.96	0.28	0.432
ILMN_3169073	mmu-miR-193*	3655.333	3318.75	2208.917	7508.083	6746.5	3970.25	2606.083	7351.417	4992.583	7611	3730.333	5587.833	0.97	0.22	0.512
ILMN_3168982	mmu-miR-193b	8461.333	6695.167	5798.167	6093.417	2824.917	4777.167	715.25	1018.333	9633	2317.417	6623.167	5693.167	3.82	1.86	0.510
ILMN_3167122	mmu-miR-194	6913.75	5985.583	8816.583	4075.75	6623.167	6695.167	4486.667	4031.417	5302.583	6237.917	4877.833	4031.417	1.39	0.16	0.092
ILMN_3167191	mmu-miR-195	393.6667	1308.5	477.1667	1278.083	2404.333	10089.58	6746.5	9346.417	3776.083	8310.833	6695.167	9286.417	0.32	0.16	0.016
ILMN_3167628	mmu-miR-196a	7904.5	1244.667	9985.333	8536.417	6988.917	6913.75	9633	8873.167	4486.667	5752.583	5493.5	5493.5	1.20	0.28	0.875
ILMN_3167916	mmu-miR-196a*	410.75	286.8333	461.25	379.75	410.75	312.75	458.75	550.0833	447.5833	908.8333	447.5833	379.75	0.77	0.10	0.125
ILMN_3168308	mmu-miR-196b	4556.833	1828.917	11048.17	5532	4379.5	5371.667	11469	11048.17	4288.5	9346.417	1912.583	6175.917	1.15	0.42	0.466
ILMN_3167104	mmu-miR-197	576.5	387.8333	806.8333	559	510.9167	550.0833	453.5	503.4167	405.3333	863.9167	293.6667	477.1667	1.26	0.22	0.546
ILMN_3168924	mmu-miR-199a-3p,	14252.67	11156.33	12936.67	9739.083	9184.083	7508.083	16209.25	13364.42	14851.75	12095.75	18895.42	9004.417	0.79	0.06	0.052
ILMN_3168478	mmu-miR-199a-3p:	5798.167	8873.167	3594	5111.333	8221.333	9286.417	12095.75	8736.833	9438.917	7190.917	12656	6623.167	0.77	0.15	0.128
ILMN_3167976	mmu-miR-199a-5p	6369.833	6093.417	9286.417	8221.333	12497.5	11048.17	1968.583	9739.083	8310.833	12656	7904.5	11896.83	1.36	0.40	0.917
ILMN_3167787	mmu-miR-19a	180.9167	209.75	232.5833	178.0833	170.9167	180.9167	293.6667	6988.917	187.1667	293.6667	221.3333	4817.25	0.55	0.19	0.173
ILMN_3167260	mmu-miR-19b	3419.333	3492.75	3289.5	2208.917	4434.333	2520.75	3492.75	2912.75	2659.417	3318.75	979.5	1538.583	1.71	0.58	0.284
ILMN_3168294	mmu-miR-200b	1308.5	1173.75	1746.167	1214.667	1351.583	1308.5	2754.917	1943.917	1214.667	2659.417	1368.417	1746.167	0.79	0.15	0.122
ILMN_3169074	mmu-miR-200b*	671.25	458.75	979.5	715.25	628.6667	676.3333	1154.917	1048.917	524.1667	1137.167	431.5833	773	0.97	0.23	0.399
ILMN_3169108	mmu-miR-200c*	620.6667	272	387.8333	280.1667	236.5833	214.6667	290.5833	304.25	214.6667	312.75	366.1667	436.5833	1.15	0.27	0.868
ILMN_3169015	mmu-miR-208b	849.1667	554.5	874.25	567.8333	503.4167	544.25	883.3333	836.25	453.5	731.5833	320.5	515.6667	1.16	0.20	0.814
ILMN_3167510	mmu-miR-20a	1635.083	3419.333	2067.5	1263.167	1746.167	4947.75	2404.333	8653.917	4379.5	2281.917	3204.833	1480.333	1.00	0.47	0.336
ILMN_3169095	mmu-miR-20a*	9985.333	1746.167	9633	10684.58	10822.92	11632.25	15395	11156.33	11283.75	19786	9286.417	18348.58	0.67	0.14	0.034
ILMN_3167333	mmu-miR-20b	1182.333	1137.167	1574.333	815.3333	2208.917	2436	1329.583	1679.417	893.75	1599.167	648.1667	1094.833	1.58	0.46	0.424
ILMN_3167371	mmu-miR-21	25463.42	23384.17	27087.58	24500.92	25891.08	24957.08	27525.75	25891.08	25463.42	20911.25	25891.08	23985.08	1.02	0.04	0.786
ILMN_3169096	mmu-miR-21*	230.1667	1154.917	849.1667	628.6667	576.5	489.4167	1034.583	603.1667	256.3333	1009.083	242.5833	361.75	1.63	0.47	0.770
ILMN_3167774	mmu-miR-210	12656	9739.083	11632.25	12095.75	13665.33	11469	4243.5	7904.5	9184.083	6369.833	9871.417	9739.083	1.66	0.29	0.014
ILMN_3168266	mmu-miR-211	318.6667	203.5833	458.75	361.75	383.1667	324.8333	544.25	6237.917	293.6667	483.6667	280.1667	393.6667	0.85	0.23	0.351
ILMN_3167761	mmu-miR-212	12497.5	5646.75	9438.917	7820.25	8873.167	8736.833	12251	11632.25	9004.417	12251	7190.917	9985.333	0.88	0.11	0.264
ILMN_3167046	mmu-miR-214	14851.75	10089.58	15395	13133.08	12811.67	10822.92	14252.67	10822.92	13760.83	14851.75	14851.75	9633	0.99	0.05	0.789
ILMN_3167234	mmu-miR-215	1137.167	1278.083	1854.583	1189.333	6093.417	1173.75	1854.583	1599.167	683.8333	2006.667	628.6667	1018.333	2.59	1.46	0.437
ILMN_3167177	mmu-miR-216b	421.6667	216.8333	453.5	324.8333	329.0833	332.0833	524.1667	515.6667	351.4167	683.8333	393.6667	461.25	0.76	0.13	0.091
ILMN_3169109	mmu-miR-218-2*	383.1667	254.4167	483.6667	277.5833	290.5833	329.0833	567.8333	648.1667	344.75	489.4167	307.8333	339.1667	0.83	0.15	0.201
ILMN_3167523	mmu-miR-219	567.8333	372	763.8333	550.0833	497.0833	515.6667	937.1667	731.5833	426.25	964.4167	383.1667	559	0.95	0.21	0.375

Table B2. -Continued

Illumia_ID	NAME	LCA1	LCA2	LCA3	LCA4	LCA5	LCA6	RCA1	RCA2	RCA3	RCA4	RCA4	RCA6	LCA/RCA		
		signal	signal	signal	signal	signal	signal	signal	signal	signal	signal	signal	signal	ratio	SEM	p-value
ILMN_3167773	mmu-miR-22	2162.667	14561.83	2983.667	5752.583	5925.5	6988.917	4992.583	9438.917	12251	849.1667	11156.33	11156.33	1.69	1.03	0.455
ILMN_3167681	mmu-miR-221	1854.583	366.1667	312.75	2281.917	1450.5	2480.25	1746.167	3074	3903.917	3804.083	5925.5	3655.333	0.46	0.16	0.023
ILMN_3167963	mmu-miR-222	9346.417	11743.58	7064.083	11156.33	10089.58	9004.417	4075.75	7190.917	8816.583	9985.333	9346.417	7820.25	1.35	0.22	0.141
ILMN_3166979	mmu-miR-223	15807.75	24957.08	21350.83	23985.08	24500.92	26179.5	11283.75	11743.58	11632.25	3254.25	9985.333	883.3333	7.47	4.52	0.005
ILMN_3167997	mmu-miR-23b	20911.25	18895.42	22751.92	21755.67	21350.83	20911.25	25891.08	24957.08	24957.08	22194.33	24957.08	24500.92	0.86	0.03	0.008
ILMN_3168211	mmu-miR-24	26179.5	27087.58	25463.42	26650.33	26650.33	26650.33	26179.5	26650.33	25891.08	26650.33	25463.42	25891.08	1.01	0.01	0.232
ILMN_3169098	mmu-miR-24-2*	5302.583	12497.5	5985.583	6873.917	8095.417	8653.917	3970.25	4585.5	6434.583	8221.333	5302.583	3970.25	1.59	0.30	0.136
ILMN_3168476	mmu-miR-25	25891.08	25891.08	27525.75	26179.5	26179.5	25891.08	18348.58	26179.5	24500.92	26179.5	23985.08	22751.92	1.13	0.06	0.074
ILMN_3168005	mmu-miR-26a	15100.5	13133.08	13665.33	17161.5	13760.83	14561.83	17845.75	19786	18348.58	17505.17	22751.92	21755.67	0.75	0.06	0.011
ILMN_3167374	mmu-miR-26b	8394.833	4379.5	209.75	5371.667	3204.833	6791.75	12497.5	10534.83	10822.92	6534	11896.83	8461.333	0.50	0.13	0.018
ILMN_3168323	mmu-miR-27a	24500.92	24500.92	24500.92	24957.08	23985.08	25463.42	23384.17	25463.42	26179.5	25891.08	24500.92	26650.33	0.97	0.02	0.139
ILMN_3169102	mmu-miR-27a*	304.25	329.0833	773	524.1667	515.6667	533.5	1182.333	1480.333	304.25	827.8333	245	369.25	1.20	0.40	0.416
ILMN_3168409	mmu-miR-27b	11048.17	9985.333	4877.833	11743.58	9438.917	9438.917	2784.583	13760.83	12936.67	10684.58	13364.42	15807.75	1.25	0.55	0.420
ILMN_3169055	mmu-miR-27b*	3850	3903.917	6434.583	594	7611	238.3333	471.5	290.5833	2947.25	7508.083	5868	4131.917	4.20	2.22	0.903
ILMN_3168514	mmu-miR-291a-3p	1599.167	1891.5	1800.25	1351.583	1599.167	1294.083	1599.167	1891.5	1278.083	2606.083	1117.667	1214.667	1.07	0.14	0.918
ILMN_3167737	mmu-miR-293	2784.583	3532.167	3532.167	2606.083	2699.75	2754.917	3730.333	3119.333	1912.583	3730.333	1828.917	2120.25	1.20	0.18	0.601
ILMN_3169076	mmu-miR-293*	477.1667	283.8333	603.1667	461.25	458.75	497.0833	979.5	763.8333	3204.833	1214.667	497.0833	874.25	0.49	0.10	0.088
ILMN_3167957	mmu-miR-294	320.5	211.1667	467.4167	312.75	332.0833	274.9167	272	405.3333	274.9167	383.1667	166.4167	151.9167	1.34	0.24	0.504
ILMN_3169078	mmu-miR-295*	1189.333	2067.5	3204.833	1154.917	1070.583	5587.833	1800.25	1308.5	620.6667	7561.333	676.3333	950.5833	2.50	0.98	0.888
ILMN_3168154	mmu-miR-297a	4243.5	5427.667	4556.833	3776.083	4031.417	3389.167	4131.917	3776.083	2824.917	4288.5	3655.333	2659.417	1.22	0.11	0.117
ILMN_3167645	mmu-miR-297b-5p	286.8333	178.0833	268.5833	221.3333	197.5833	194.8333	200.6667	245	194.8333	351.4167	194.8333	209.75	1.02	0.13	0.817
ILMN_3168963	mmu-miR-297c*,mr	4075.75	175	5259.667	222.9167	937.1667	5693.167	9184.083	214.6667	6791.75	8461.333	3119.333	222.9167	4.65	4.18	0.355
ILMN_3168928	mmu-miR-299	431.5833	863.9167	1703.417	1294.083	1308.5	1202.583	1943.917	1182.333	436.5833	1506.5	1009.083	613.3333	1.50	0.54	0.963
ILMN_3169100	mmu-miR-29a*	1278.083	1294.083	1828.917	1202.583	1154.917	1214.667	1679.417	1429.75	671.25	1655.25	695.1667	1034.583	1.33	0.31	0.612
ILMN_3167643	mmu-miR-29c	874.25	4777.167	1189.333	754.6667	849.1667	723	8653.917	6434.583	1599.167	1408.083	613.3333	7508.083	0.60	0.20	0.104
ILMN_3168040	mmu-miR-302c	836.25	594	918.5	613.3333	467.4167	586.0833	918.5	1137.167	544.25	620.6667	172.8333	351.4167	1.41	0.32	0.757
ILMN_3167455	mmu-miR-30a	11896.83	20911.25	6695.167	9346.417	10684.58	11896.83	11632.25	8536.417	15100.5	12497.5	13665.33	10534.83	1.10	0.29	0.976
ILMN_3167448	mmu-miR-30b	13133.08	21350.83	14851.75	13760.83	16401	13133.08	16401	16716.83	17845.75	11743.58	18348.58	13665.33	0.99	0.08	0.795
ILMN_3169085	mmu-miR-30c-2*	2365.333	2912.75	3074	2227.667	2162.667	2317.417	3389.167	2659.417	1351.583	3204.833	1189.333	1891.5	1.30	0.26	0.626
ILMN_3167711	mmu-miR-30e*	4313.5	5071.25	6237.917	7416.333	3074	3532.167	5985.583	6369.833	7111.083	8005.833	6873.917	5198.25	0.74	0.07	0.016
ILMN_3167828	mmu-miR-31*	298.8333	497.0833	1429.75	990.3333	893.75	1048.917	1614.25	1070.583	329.0833	1480.333	256.3333	387.8333	1.98	0.72	0.993
ILMN_3167403	mmu-miR-320	12811.67	12095.75	16401	15395	15395	17505.17	9286.417	14851.75	17505.17	18348.58	21755.67	25463.42	0.89	0.10	0.136
ILMN_3167956	mmu-miR-323-3p	950.5833	874.25	1329.583	863.9167	648.1667	671.25	1018.333	849.1667	489.4167	1070.583	620.6667	849.1667	1.22	0.30	0.663
ILMN_3168413	mmu-miR-324-3p	9286.417	14252.67	12497.5	12811.67	14252.67	14252.67	6534	7611	10223.75	5071.25	10534.83	6237.917	1.78	0.22	0.004
ILMN_3167905	mmu-miR-326	17505.17	12656	13962.67	15100.5	16716.83	16209.25	9438.917	8394.833	12811.67	16401	12811.67	13962.67	1.31	0.14	0.065
ILMN_3168198	mmu-miR-328	21755.67	22751.92	23384.17	22751.92	22751.92	22751.92	16716.83	21755.67	23384.17	23384.17	21350.83	22194.33	1.07	0.05	0.193
ILMN_3168522	mmu-miR-329	489.4167	1614.25	1048.917	1679.417	695.1667	990.3333	1244.667	567.8333	2120.25	836.25	1854.583	458.75	1.38	0.44	0.828
ILMN_3167996	mmu-miR-335-5p	918.5	1182.333	1154.917	1094.833	1117.667	1154.917	1214.667	1703.417	1202.583	2120.25	964.4167	964.4167	0.88	0.11	0.231
ILMN_3168934	mmu-miR-337-5p	3594	4585.5	4031.417	3254.25	3361.167	3204.833	4313.5	3730.333	2754.917	4209.083	3163.833	2784.583	1.09	0.10	0.637
ILMN_3167344	mmu-miR-338-3p	1538.583	9004.417	6175.917	918.5	5693.167	1070.583	613.3333	715.25	410.75	893.75	4243.5	806.8333	5.64	2.61	0.102
ILMN_3168936	mmu-miR-339-3p	723	4131.917	1655.25	4585.5	1137.167	5071.25	1828.917	3970.25	2436	1368.417	342	594	2.89	1.25	0.274
ILMN_3168301	mmu-miR-339-5p	7416.333	6873.917	5302.583	6175.917	3970.25	8816.583	661.5	4992.583	2404.333	5868	2067.5	6093.417	3.20	1.61	0.027
ILMN_3166998	mmu-miR-340-3p	827.8333	683.8333	1070.583	586.0833	3655.333	436.5833	559	661.5	515.6667	1048.917	4075.75	5302.583	1.02	0.28	0.368
ILMN_3168866	mmu-miR-340-5p	191.4167	1018.333	230.1667	188.8333	178.0833	200.6667	286.8333	241.1667	164	369.25	267.3333	383.1667	1.33	0.59	0.756
ILMN_3167123	mmu-miR-341:9.1	2281.917	3026	2867	2048.417	1854.583	1655.25	2730.417	2208.917	1294.083	2867	1891.5	1776	1.17	0.23	0.673
ILMN_3168165	mmu-miR-342-3p	8095.417	12251	5752.583	11469	13364.42	9871.417	2912.75	2699.75	8461.333	2480.25	7277.917	6434.583	2.67	0.66	0.038
ILMN_3167891	mmu-miR-344	2659.417	2317.417	8095.417	5925.5	3443.417	7561.333	8461.333	8816.583	3804.083	6434.583	5150.25	8653.917	0.86	0.28	0.293
ILMN_3168939	mmu-miR-345-3p	1294.083	1390.25	5493.5	1506.5	883.3333	1094.833	1776	1574.333	849.1667	1968.583	2606.083	5427.667	1.56	0.99	0.737
ILMN_3168128	mmu-miR-345-5p	1891.5	2404.333	5071.25	4739.917	2730.417	3318.75	443.0833	3655.333	1828.917	1308.5	1408.083	2730.417	2.41	0.57	0.095
ILMN_3167734	mmu-miR-346	19786	2559.167	14252.67	8873.167	8310.833	11156.33	12936.67	12656	9286.417	17845.75	8873.167	16401	0.90	0.22	0.488
ILMN_3168429	mmu-miR-34a	355.8333	436.5833	3163.833	3804.083	671.25	344.75	594	5587.833	2699.75	5302.583	1655.25	550.0833	0.60	0.15	0.185
ILMN_3168929	mmu-miR-34b-3p	280.1667	893.75	256.3333	214.6667	5587.833	594	203.5833	272	259.8333	421.6667	200.6667	265.1667	6.04	4.38	0.292
ILMN_3168326	mmu-miR-350	307.8333	290.5833	355.8333	351.4167	312.75	2983.667	410.75	4877.833	4647.833	567.8333	773	524.1667	1.27	0.89	0.330
ILMN_3168444	mmu-miR-369-3p	185.3333	220.4167	661.5	515.6667	524.1667	467.4167	964.4167	489.4167	232.5833	628.6667	180.9167	307.8333	1.45	0.48	0.843
ILMN_3168318	mmu-miR-374	324.8333	304.25	342	298.8333	272	4131.917	483.6667	4486.667	5587.833	554.5	6988.917	467.4167	1.70	1.43	0.235
ILMN_3167229	mmu-miR-375	586.0833	1214.667	3026	5646.75	1182.333	5150.25	2162.667	4712.75	4556.833	1891.5	1943.917	683.8333	2.05	1.17	0.918
ILMN_3168505	mmu-miR-376a	815.3333	443.0833	836.25	603.1667	567.8333	567.8333	10089.58	576.5	5493.5	815.3333	344.75	533.5	0.74	0.24	0.200
ILMN_3167566	mmu-miR-376b	893.75	2784.583	990.3333	883.3333	1094.833	863.9167	1117.667	1009.083	3730.333	1614.25	783.8333	918.5	1.12	0.36	0.665
ILMN_3167443	mmu-miR-379	1263.167	836.25	1506.5	1117.667	1034.583	893.75	1408.083	1390.25	836.25	2048.417	893.75	1294.083	0.95	0.19	0.416
ILMN_3167239	mmu-miR-382	6695.167	7561.333	188.8333	8461.333	8394.833	9633	7713.917	1173.75	5798.167	9739.083	10089.58	8221.333	1.70	0.96	0.861
ILMN_3169113	mmu-miR-382*	461.25	161.3333	263.1667	220.4167	185.3333	209.75	274.9167	263.1667	197.5833	277.5833	1329.583	272	0.89	0.22	0.388
ILMN_3168062	mmu-miR-411*:9.1	5493.5	2606.083	2784.583	1943.917	2120.25	2067.5	2947.25	2365.333	1368.417	3163.833	1244.667	2067.5	1.39	0.23	0.276
ILMN_3167373	mmu-miR-423-3p	12095.75	16209.25	13364.42	12497.5	14851.75	12656	5646.75	6093.417	7416.333	11048.17	8461.333	6695.167	1.90	0.20	0.003
ILMN_3168947	mmu-miR-425	471.5	510.9167	1614.25	1182.333	990.3333	1137.167	2120.25	1408.083	3532.167	1635.083	334.9167	695.1667	1.06	0.43	0.201
ILMN_3168193	mmu-miR-433*	232.5833	198.9167	497.0833	366.1667	344.75	334.9167	533.5	366.1667	172.8333	461.25	148.5833	218.6667	1.42	0.41	0.905
ILMN_3168954	mmu-miR-450a-3p	533.5	277.5833	550.0833	387.8333	355.8333	342	283.8333	393.6667	318.6667	783.8333	241.1667	414.6667	1.18	0.24	0.986
ILMN_3167614	mmu-miR-451	8310.833	13665.33	503.4167	1776	372	6434.583	1202.583	18895.42	11743.58	10534.83	6237.917	8536.417	1.44	1.10	0.158
ILMN_3167131	mmu-miR-455	245	483.6667	329.0833	342	318.6667	286.8333	6695.167	436.5833	286.8333	524.1667	298.8333	431.5833	0.78	0.17	0.346
ILMN_3167714	mmu-miR-455*	1202.583	1094.833	1599.167	1048.917	979.5	1018.333	1429.75	1368.417	723	1776	827.8333	1244.667	1.07	0.24	0.761
ILMN_3168948	mmu-miR-463	267.3333	221.3333	533.5	383.1667	351.4167	366.1667	676.3333	458.75	245	515.6667	318.6667	355.8333	0.99	0.26	0.484
ILMN_3167236	mmu-miR-465a-3p,	754.6667	773	1538.583	964.4167	806.8333	874.25	1308.5	937.1667	467.4167	950.5833	274.9167	410.75	1.80	0.47	0.380
ILMN_3168989	mmu-miR-465c-5p	731.5833	576.5	1202.583	1538.583	715.25	918.5	1506.5	1189.333	594	1450.5	567.8333	1048.917	1.03	0.24	0.615
ILMN_3167875	mmu-miR-466a-3p,	1329.583	1450.5	2281.917	1450.5	3492.75	1263.167	1635.083	1746.167	4585.5	2404.333	6093.417	5925.5	0.59	0.09	0.043
ILMN_3168949	mmu-miR-466a-5p	3289.5	3850	3361.167	2436	2436	2227.667	3204.833	2867	1679.417	3289.5	2006.667	2162.667	1.23	0.18	0.312
ILMN_3168991	mmu-miR-466c-5p	1943.917	1968.583	298.8333	234.75	1429.75	559	4379.5	344.75	277.5833	4739.917	2699.75	256.3333	1.67	0.86	0.296
ILMN_3169037	mmu-miR-466f	4209.083	4647.833	4379.5	3163.833	4817.25	4347.25	4031.417	3594	2048.417	3970.25	3419.333	2227.667	1.44	0.21	0.085
ILMN_3168994	mmu-miR-466f-3p	4817.25	5198.25	7277.917	10223.75	7416.333	8536.417	14561.83	12811.67	4031.417	10089.58	9438.917	10684.58	0.86	0.22	0.187
ILMN_3168993	mmu-miR-466f-5p	648.1667	431.5833	815.3333	554.5	483.6667	510.9167	763.8333	754.6667	458.75	874.25	372	483.6667	1.03	0.19	0.701
ILMN_3168996	mmu-miR-466h	11283.75	8736.833	372	4992.583	8816.583	7611	4647.833	361.75	3655.333	2784.583	7611	4434.333	5.22	3.80	0.130
ILMN_3169027	mmu-miR-466i	5259.667	1635.083	8736.833	12251	8005.833	9985.333	14851.75	14252.67	5925.5	5111.333	7416.333	11632.25	1.05	0.34	0.503
ILMN_3169023	mmu-miR-466l	458.75	312.75	510.9167	405.3333	405.3333	361.75	497.0833	695.1667	461.25	1018.333	489.4167	723	0.70	0.12	0.070
ILMN_3168950	mmu-miR-467a	1912.583	2480.25	2162.667	1408.083	1189.333	1538.583	3361.167	2227.667	1329.583	2436	1214.667	1800.25	0.95	0.16	0.451
ILMN_3169022	mmu-miR-467e	863.9167	613.3333	1034.583	2480.25	594	648.1667	1009.083	1244.667	628.6667	990.3333	421.6667	372	1.44	0.29	0.407
ILMN_3169039	mmu-miR-467f	2606.083	4075.75	6746.5	6791.75	7508.083	6237.917	8221.333	5150.25	2227.667	6873.917	2404.333	4288.5	1.62	0.48	0.643
ILMN_3169048	mmu-miR-467h	2048.417	2006.667	2659.417	1655.25	1480.333	1480.333	2227.667	1968.583	1094.833	2559.167	1018.333	1703.417	1.22	0.26	0.725
ILMN_3168457	mmu-miR-484	15395	16716.83	17161.5	16209.25	17505.17	18895.42	8536.417	12936.67	13962.67	17161.5	12497.5	12656	1.36	0.12	0.017
ILMN_3167240	mmu-miR-486	22194.33	23985.08	24957.08	22194.33	22194.33	23384.17	24500.92	24500.92	23985.08	23985.08	19786	19786	1.03	0.04	0.698
ILMN_3167805	mmu-miR-487b	222.9167	293.6667	648.1667	483.6667	447.5833	447.5833	723	383.1667	175	405.3333	127.0833	234.75	1.90	0.58	0.583
ILMN_3168506	mmu-miR-489	4777.167	5532	5198.25	4712.75	5371.667	4739.917	4947.75	4434.333	3419.333	4817.25	4777.167	3318.75	1.21	0.09	0.066
ILMN_3167583	mmu-miR-490	366.1667	324.8333	559	458.75	559	754.6667	1137.167	893.75	550.0833	1244.667	232.5833	320.5	1.14	0.41	0.362
ILMN_3167553	mmu-miR-491	369.25	265.1667	447.5833	339.1667	265.1667	256.3333	351.4167	254.4167	180.9167	379.75	265.1667	241.1667	1.25	0.25	0.365

Table B2. -Continued

Illumia_ID	NAME	LCA1	LCA2	LCA3	LCA4	LCA5	LCA6	RCA1	RCA2	RCA3	RCA4	RCA4	RCA6	LCA/RCA		
		signal	signal	signal	signal	signal	signal	signal	signal	signal	signal	signal	signal	ratio	SEM	p-value
ILMN_3168999	mmu-miR-493	259.8333	170.9167	366.1667	283.8333	254.4167	298.8333	393.6667	351.4167	198.9167	918.5	254.4167	232.5833	0.93	0.23	0.349
ILMN_3168446	mmu-miR-494	550.0833	369.25	950.5833	620.6667	603.1667	661.5	2208.917	1154.917	815.3333	1351.583	908.8333	1182.333	0.57	0.13	0.046
ILMN_3169000	mmu-miR-504	23985.08	4992.583	8394.833	2317.417	6913.75	4817.25	11743.58	2784.583	1614.25	5925.5	2281.917	8736.833	2.17	0.73	0.284
ILMN_3169017	mmu-miR-511	1351.583	2824.917	4131.917	3532.167	3730.333	2912.75	5198.25	3361.167	1154.917	3655.333	990.3333	1655.25	1.86	0.61	0.707
ILMN_3168686	mmu-miR-532-3p	908.8333	477.1667	1278.083	908.8333	731.5833	849.1667	2436	1329.583	754.6667	1854.583	1034.583	1506.5	0.70	0.21	0.077
ILMN_3167658	mmu-miR-540-3p	676.3333	393.6667	5925.5	426.25	387.8333	372	603.1667	497.0833	361.75	5798.167	2867	489.4167	3.21	2.64	0.794
ILMN_3167074	mmu-miR-542-3p	3254.25	4031.417	3492.75	2559.167	2281.917	2162.667	3289.5	2824.917	1703.417	3443.417	2559.167	2281.917	1.17	0.20	0.526
ILMN_3167043	mmu-miR-546	990.3333	676.3333	1018.333	731.5833	620.6667	5985.583	908.8333	806.8333	1480.333	1189.333	379.75	4347.25	1.04	0.16	0.654
ILMN_3168117	mmu-miR-547	179.0833	143.6667	259.8333	227	216.8333	241.1667	426.25	329.0833	227	372	290.5833	268.5833	0.71	0.11	0.052
ILMN_3167513	mmu-miR-551b:9.1	188.8333	159.4167	245	241.1667	248	234.75	267.3333	372	298.8333	426.25	283.8333	245	0.73	0.08	0.037
ILMN_3169004	mmu-miR-574-3p	17845.75	18348.58	18895.42	18895.42	18348.58	17845.75	13962.67	13962.67	16401	15100.5	15395	14851.75	1.23	0.02	0.000
ILMN_3169003	mmu-miR-574-5p	5693.167	1538.583	4075.75	4777.167	5752.583	5427.667	7820.25	7111.083	6913.75	7064.083	7351.417	8310.833	0.61	0.08	0.004
ILMN_3169020	mmu-miR-582-5p	1450.5	1263.167	1968.583	1390.25	1278.083	1390.25	2559.167	1854.583	950.5833	2365.333	849.1667	1368.417	1.07	0.25	0.582
ILMN_3167257	mmu-miR-592	5427.667	5798.167	4947.75	4313.5	4877.833	4031.417	4585.5	4131.917	3492.75	4556.833	4947.75	3389.167	1.19	0.08	0.073
ILMN_3167379	mmu-miR-615-3p	5752.583	6534	5150.25	4556.833	5259.667	4647.833	4877.833	4556.833	4131.917	4947.75	4992.583	3594	1.19	0.07	0.058
ILMN_3168964	mmu-miR-615-5p	277.5833	524.1667	567.8333	695.1667	613.3333	773	268.5833	265.1667	170.9167	221.3333	175	267.3333	2.64	0.39	0.006
ILMN_3167305	mmu-miR-652	9438.917	10223.75	8461.333	9633	11156.33	8461.333	1351.583	7713.917	8095.417	7904.5	8816.583	10089.58	2.11	0.98	0.154
ILMN_3168475	mmu-miR-654-3p	7713.917	783.8333	1117.667	1968.583	6369.833	4434.333	3804.083	5071.25	7351.417	2520.75	4131.917	5798.167	0.90	0.31	0.532
ILMN_3169006	mmu-miR-654-5p	783.8333	603.1667	1214.667	783.8333	754.6667	806.8333	1263.167	1117.667	554.5	6791.75	477.1667	661.5	1.04	0.31	0.378
ILMN_3167968	mmu-miR-667	3804.083	4947.75	1776	4947.75	1655.25	4712.75	4712.75	221.3333	471.5	410.75	5427.667	5371.667	6.69	3.61	0.550
ILMN_3167115	mmu-miR-669b	1703.417	232.5833	554.5	436.5833	426.25	3443.417	671.25	447.5833	1655.25	503.4167	159.4167	263.1667	3.34	1.99	0.431
ILMN_3166951	mmu-miR-669c	3730.333	2659.417	4712.75	7713.917	4288.5	2699.75	7064.083	8095.417	7904.5	6746.5	10822.92	2520.75	0.68	0.14	0.063
ILMN_3169035	mmu-miR-669h-3p	256.3333	188.8333	421.6667	355.8333	307.8333	307.8333	436.5833	342	238.3333	477.1667	216.8333	334.9167	1.00	0.20	0.586
ILMN_3168279	mmu-miR-676	5646.75	6623.167	5111.333	4347.25	5071.25	5493.5	5371.667	4347.25	3594	4877.833	4434.333	2983.667	1.31	0.14	0.071
ILMN_3167520	mmu-miR-679	3532.167	3655.333	3443.417	2659.417	2317.417	2365.333	3850	3289.5	2365.333	3361.167	2912.75	2559.167	1.00	0.10	0.833
ILMN_3168277	mmu-miR-681	1244.667	754.6667	1294.083	950.5833	773	964.4167	874.25	1094.833	731.5833	1679.417	524.1667	990.3333	1.15	0.20	0.944
ILMN_3167156	mmu-miR-690	11469	13962.67	12811.67	13962.67	16209.25	13962.67	15807.75	16401	14561.83	16716.83	11632.25	12251	0.97	0.10	0.566
ILMN_3166942	mmu-miR-691	443.0833	234.75	489.4167	393.6667	324.8333	426.25	773	723	483.6667	676.3333	443.0833	715.25	0.64	0.09	0.016
ILMN_3168503	mmu-miR-692	263.1667	150.1667	286.8333	274.9167	286.8333	283.8333	383.1667	453.5	369.25	594	324.8333	554.5	0.61	0.09	0.013
ILMN_3168422	mmu-miR-693-5p	361.75	259.8333	334.9167	265.1667	238.3333	221.3333	277.5833	200.6667	153.75	268.5833	179.0833	203.5833	1.36	0.17	0.053
ILMN_3167541	mmu-miR-694	1574.333	2162.667	2754.917	1912.583	1776	1854.583	3163.833	2436	1308.5	2983.667	1263.167	1429.75	1.14	0.24	0.849
ILMN_3167754	mmu-miR-700	7064.083	6913.75	8873.167	5493.5	6791.75	203.5833	256.3333	4947.75	4739.917	318.6667	4817.25	2754.917	8.26	4.67	0.080
ILMN_3167918	mmu-miR-701	806.8333	533.5	883.3333	683.8333	544.25	554.5	950.5833	827.8333	533.5	1294.083	533.5	827.8333	0.89	0.17	0.279
ILMN_3167248	mmu-miR-703	351.4167	242.5833	443.0833	372	339.1667	369.25	230.1667	238.3333	218.6667	332.0833	150.1667	230.1667	1.59	0.20	0.018
ILMN_3168285	mmu-miR-706	4739.917	141	5371.667	5259.667	4556.833	2867	22751.92	15100.5	9346.417	431.5833	7508.083	11048.17	2.31	1.98	0.089
ILMN_3167086	mmu-miR-707	3318.75	1506.5	2404.333	1635.083	1506.5	1599.167	2867	2120.25	1137.167	3074	1182.333	1943.917	1.10	0.23	0.884
ILMN_3168249	mmu-miR-708	22751.92	10534.83	21755.67	21350.83	20911.25	22194.33	24957.08	23985.08	22194.33	24500.92	17161.5	18895.42	0.93	0.11	0.463
ILMN_3168185	mmu-miR-708*	329.0833	197.5833	339.1667	263.1667	234.75	227	245	236.5833	193	334.9167	150.9167	221.3333	1.22	0.16	0.354
ILMN_3167605	mmu-miR-709	10822.92	12936.67	15807.75	13364.42	14561.83	13364.42	6175.917	11283.75	11048.17	12936.67	11283.75	12936.67	1.28	0.11	0.026
ILMN_3167133	mmu-miR-712*	236.5833	238.3333	369.25	307.8333	298.8333	290.5833	421.6667	379.75	250.75	510.9167	224.5833	329.0833	0.91	0.16	0.312
ILMN_3167549	mmu-miR-719	10428.17	2699.75	3119.333	2365.333	2784.583	2404.333	3119.333	2730.417	2208.917	3492.75	1351.583	2404.333	1.58	0.40	0.303
ILMN_3167188	mmu-miR-720	24957.08	25463.42	22194.33	23384.17	24957.08	21350.83	23985.08	20911.25	19786	22751.92	22194.33	17161.5	1.13	0.04	0.011
ILMN_3169121	mmu-miR-742*	7351.417	4434.333	9346.417	7561.333	7064.083	5925.5	9739.083	3850	5071.25	9633	3254.25	4947.75	1.32	0.23	0.486
ILMN_3167180	mmu-miR-744	16209.25	11632.25	16716.83	16401	15807.75	15395	10534.83	11469	11896.83	14252.67	10428.17	13364.42	1.30	0.09	0.014
ILMN_3167621	mmu-miR-758	2006.667	849.1667	1480.333	937.1667	723	950.5833	1574.333	1278.083	603.1667	1746.167	544.25	1117.667	1.18	0.29	0.958
ILMN_3168961	mmu-miR-760	937.1667	361.75	937.1667	1800.25	2067.5	695.1667	2281.917	2162.667	613.3333	3532.167	754.6667	1070.583	1.00	0.40	0.291
ILMN_3168003	mmu-miR-761	4288.5	2947.25	3318.75	3594	5646.75	6534	10822.92	5798.167	990.3333	2730.417	3361.167	3289.5	1.54	0.44	0.946
ILMN_3167967	mmu-miR-762	2867	3361.167	7111.083	3204.833	836.25	2784.583	6237.917	4777.167	7064.083	3850	3804.083	1173.75	0.93	0.31	0.202
ILMN_3168100	mmu-miR-763	211.1667	1800.25	267.3333	6988.917	10223.75	3074	7561.333	2983.667	7277.917	10822.92	236.5833	4585.5	7.53	7.14	0.514
ILMN_3168106	mmu-miR-764-5p	453.5	1329.583	586.0833	836.25	11469	4992.583	11156.33	10428.17	5752.583	5493.5	4347.25	7351.417	0.62	0.41	0.169
ILMN_3168388	mmu-miR-7a	4585.5	298.8333	683.8333	2983.667	2006.667	458.75	6913.75	3419.333	5427.667	4434.333	5985.583	4739.917	0.33	0.11	0.001
ILMN_3169112	mmu-miR-7a*	21350.83	3074	9871.417	2730.417	6534	8221.333	5587.833	5493.5	3119.333	7416.333	5111.333	6791.75	1.73	0.58	0.357
ILMN_3168519	mmu-miR-7b	763.8333	515.6667	964.4167	661.5	586.0833	620.6667	863.9167	950.5833	567.8333	1278.083	436.5833	648.1667	0.99	0.19	0.519
ILMN_3169012	mmu-miR-872	234.75	151.9167	290.5833	293.6667	263.1667	263.1667	387.8333	232.5833	236.5833	329.0833	286.8333	324.8333	0.85	0.09	0.133
ILMN_3169124	mmu-miR-872*	715.25	8095.417	2559.167	5693.167	268.5833	431.5833	431.5833	3903.917	379.75	447.5833	3389.167	4712.75	3.89	2.03	0.655
ILMN_3169013	mmu-miR-873	1614.25	1655.25	2520.75	1429.75	1390.25	1351.583	7277.917	1912.583	1173.75	2699.75	1048.917	1679.417	0.98	0.28	0.377
ILMN_3169014	mmu-miR-875-3p	594	4313.5	6988.917	9004.417	4647.833	8394.833	11048.17	9633	166.4167	11632.25	193	3074	11.68	7.15	0.919
ILMN_3169016	mmu-miR-877	3119.333	1034.583	211.1667	6237.917	5532	613.3333	250.75	209.75	477.1667	216.8333	5259.667	197.5833	8.46	4.43	0.143
ILMN_3169011	mmu-miR-878-5p	334.9167	250.75	379.75	304.25	280.1667	268.5833	342	267.3333	188.8333	320.5	176.75	170.9167	1.34	0.18	0.154
ILMN_3168968	mmu-miR-879	483.6667	241.1667	318.6667	332.0833	256.3333	236.5833	227	256.3333	222.9167	355.8333	214.6667	200.6667	1.30	0.18	0.183
ILMN_3169123	mmu-miR-881*	1828.917	274.9167	515.6667	447.5833	361.75	355.8333	503.4167	524.1667	387.8333	9004.417	405.3333	576.5	1.17	0.52	0.429
ILMN_3168975	mmu-miR-883b-3p	387.8333	256.3333	671.25	489.4167	461.25	387.8333	586.0833	414.6667	263.1667	613.3333	268.5833	318.6667	1.26	0.31	0.758
ILMN_3168974	mmu-miR-883b-5p	372	227	361.75	256.3333	221.3333	242.5833	334.9167	293.6667	230.1667	286.8333	250.75	280.1667	1.02	0.12	0.981
ILMN_3166986	mmu-miR-92a	18895.42	19786	20911.25	20911.25	21755.67	21755.67	21755.67	23384.17	20911.25	21755.67	17505.17	16716.83	1.04	0.08	0.830
ILMN_3169103	mmu-miR-92a*	178.0833	176.75	236.5833	267.3333	379.75	272	628.6667	544.25	383.1667	471.5	165.5833	242.5833	0.87	0.31	0.187
ILMN_3169007	mmu-miR-92b	7111.083	8461.333	10089.58	7064.083	7904.5	4486.667	232.5833	4243.5	3289.5	6913.75	3903.917	194.8333	10.29	5.32	0.007
ILMN_3168517	mmu-miR-93	10684.58	10684.58	8653.917	9286.417	10428.17	12497.5	7351.417	2520.75	7561.333	3594	7820.25	6369.833	2.12	0.47	0.008
ILMN_3169104	mmu-miR-93*	2208.917	7713.917	6913.75	2947.25	8461.333	3026	2317.417	1351.583	5111.333	1943.917	4585.5	1154.917	2.33	0.71	0.047
ILMN_3168174	mmu-miR-96	1968.583	2227.667	2912.75	2120.25	1968.583	1776	3074	2067.5	1182.333	2754.917	1390.25	1614.25	1.24	0.27	0.728
ILMN_3168262	mmu-miR-99b	17161.5	22194.33	16209.25	17845.75	18895.42	18348.58	15100.5	12095.75	14252.67	15807.75	14561.83	14561.83	1.30	0.11	0.025
ILMN_3169129	solexa-1127-427	9871.417	15100.5	12095.75	7611	9985.333	9739.083	7611	5371.667	1746.167	453.5	4739.917	5868	5.26	2.45	0.005
ILMN_3169130	solexa-1201-400	1018.333	1480.333	1635.083	544.25	1408.083	3492.75	1294.083	1800.25	806.8333	1429.75	248	544.25	2.69	1.09	0.358
ILMN_3169134	solexa-1416-339_2	241.1667	185.3333	324.8333	286.8333	259.8333	254.4167	405.3333	312.75	248	458.75	272	2699.75	0.70	0.17	0.285
ILMN_3169138	solexa-200-2167	5925.5	7904.5	4288.5	5985.583	3804.083	5532	280.1667	250.75	5198.25	211.1667	1450.5	3361.167	14.35	5.83	0.032
ILMN_3169140	solexa-201-2163	156.75	164	242.5833	238.3333	232.5833	248	205.1667	332.0833	312.75	393.6667	277.5833	248	0.75	0.07	0.031
ILMN_3168343	solexa-2054-231	467.4167	222.9167	383.1667	318.6667	320.5	320.5	754.6667	483.6667	307.8333	695.1667	339.1667	497.0833	0.73	0.13	0.056
ILMN_3169146	solexa-27-9416	27525.75	26650.33	23985.08	25891.08	25463.42	24500.92	21350.83	22751.92	22751.92	24957.08	23384.17	23384.17	1.11	0.04	0.029
ILMN_3169147	solexa-284-1594	12251	11283.75	11469	11896.83	12656	12811.67	5259.667	5302.583	6237.917	6695.167	6369.833	9346.417	1.91	0.13	0.000
ILMN_3169149	solexa-3024-155	964.4167	883.3333	1094.833	773	874.25	715.25	990.3333	1263.167	883.3333	1828.917	763.8333	836.25	0.89	0.12	0.316
ILMN_3169150	solexa-3062-153	10223.75	12811.67	11896.83	8095.417	9004.417	12251	4434.333	4647.833	8873.167	6623.167	9004.417	12497.5	1.60	0.30	0.078
ILMN_3169151	solexa-308-1456	16716.83	21755.67	11743.58	13665.33	13962.67	13665.33	3655.333	9004.417	8736.833	11896.83	8394.833	7561.333	2.16	0.51	0.016
ILMN_3167558	solexa-4153-111	497.0833	731.5833	1450.5	1018.333	918.5	827.8333	1480.333	990.3333	372	1202.583	594	586.0833	1.46	0.52	0.902
ILMN_3169158	solexa-5560-82	3074	4817.25	4777.167	6623.167	7561.333	3903.917	8310.833	9184.083	4877.833	6988.917	7111.083	10428.17	0.71	0.13	0.082
ILMN_3169159	solexa-5593-81	1173.75	964.4167	1408.083	893.75	11743.58	5798.167	10428.17	5868	5868	13133.08	3850	9184.083	0.71	0.48	0.179
ILMN_3169160	solexa-564-789	290.5833	224.5833	576.5	414.6667	393.6667	421.6667	783.8333	554.5	324.8333	763.8333	351.4167	503.4167	0.84	0.22	0.221
ILMN_3169162	solexa-897-515	544.25	453.5	715.25	533.5	950.5833	477.1667	836.25	4075.75	827.8333	883.3333	3289.5	453.5	0.60	0.14	0.130
ILMN_3168513	mmu-let-7c	10089.58	4486.667	34.91667	7351.417	2983.667	1968.583	3903.917	3492.75	11156.33	9871.417	9739.083	6873.917	0.87	0.39	0.277
ILMN_3167189	mmu-let-7f	9004.417	2208.917	5587.833	8005.833	4209.083	6623.167	10223.75	5693.167	8221.333	102.9167	7064.083	7277.917	13.54	12.85	0.788
ILMN_3169082	mmu-miR-106b*	2730.417	6791.75	471.5	2784.583	3903.917	7713.917	26.08333	10223.75	4075.75	5587.833	2947.25	4486.667	18.17	17.30	0.718
ILMN_3167552	mmu-miR-10a	220.4167	426.25	205.1667	205.1667	156.75	172.8333	178.0833	410.75	165.5833	272	661.5	3204.833	0.76	0.21	0.293
ILMN_3167670	mmu-miR-125a-5p	7190.917	7351.417	3655.333	4877.833	4347.25	5752.583	5693.167	51.91667	1800.25	5427.667	8653.917	11469	24.47	23.43	0.995

Table B2. -Continued

Illumia_ID	NAME	LCA1	LCA2	LCA3	LCA4	LCA5	LCA6	RCA1	RCA2	RCA3	RCA4	RCA4	RCA6	LCA/RCA		
		signal	signal	signal	signal	signal	signal	signal	signal	signal	signal	signal	signal	ratio	SEM	p-value
ILMN_3167031	mmu-miR-127	11156.33	9871.417	9184.083	12936.67	11632.25	7190.917	39.08333	2480.25	7713.917	8873.167	11048.17	7190.917	49.02	47.29	0.070
ILMN_3168302	mmu-miR-140*	6746.5	5302.583	10428.17	9985.333	7713.917	8310.833	8873.167	9985.333	9871.417	32.16667	11469	12095.75	52.36	51.61	0.787
ILMN_3167703	mmu-miR-150	3492.75	3389.167	4243.5	1854.583	2606.083	2281.917	1390.25	5646.75	6746.5	41.83333	5532	5985.583	8.15	7.24	0.282
ILMN_3168346	mmu-miR-152	2404.333	5752.583	36.58333	8653.917	8736.833	6093.417	5925.5	13133.08	11469	7277.917	11743.58	14252.67	0.53	0.16	0.034
ILMN_3169092	mmu-miR-15a*	151.9167	194.8333	222.9167	180.9167	180.9167	191.4167	254.4167	156.75	964.4167	234.75	122.5	3119.333	0.73	0.23	0.249
ILMN_3169106	mmu-miR-19a*	142.5833	153.75	426.25	344.75	334.9167	318.6667	620.6667	421.6667	203.5833	559	234.75	344.75	0.94	0.29	0.342
ILMN_3169107	mmu-miR-28*	4379.5	7277.917	3730.333	42.83333	5798.167	5259.667	5150.25	431.5833	5150.25	10223.75	5693.167	1450.5	3.85	2.65	0.914
ILMN_3168927	mmu-miR-296-3p	150.9167	628.6667	8005.833	4288.5	421.6667	10428.17	731.5833	298.8333	863.9167	436.5833	723	143.6667	15.76	11.50	0.118
ILMN_3167035	mmu-miR-29a	5371.667	8653.917	29.91667	7904.5	6695.167	7064.083	5868	3318.75	9985.333	5532	9633	10822.92	1.05	0.36	0.501
ILMN_3168172	mmu-miR-29b	7277.917	3594	69.75	1244.667	4313.5	3655.333	8095.417	8310.833	3026	6093.417	8736.833	8005.833	0.42	0.12	0.002
ILMN_3167729	mmu-miR-30c	9633	10428.17	36.83333	9438.917	7351.417	11743.58	13760.83	17505.17	13364.42	12811.67	13962.67	13760.83	0.57	0.12	0.014
ILMN_3167224	mmu-miR-30d	1094.833	4739.917	52.33333	3074	5150.25	4288.5	4777.167	6175.917	4947.75	5693.167	8536.417	3254.25	0.58	0.19	0.032
ILMN_3166969	mmu-miR-324-5p	1655.25	5150.25	1182.333	2006.667	1679.417	471.5	94.83334	1635.083	1018.333	220.4167	1173.75	3026	5.41	2.74	0.363
ILMN_3168985	mmu-miR-327	218.6667	130.5833	277.5833	250.75	218.6667	410.75	1173.75	863.9167	559	648.1667	458.75	815.3333	0.37	0.07	0.007
ILMN_3167584	mmu-miR-351	203.5833	191.4167	2048.417	6434.583	3254.25	8005.833	3776.083	683.8333	114.8333	324.8333	671.25	159.4167	15.51	7.77	0.219
ILMN_3168131	mmu-miR-453	194.8333	134	332.0833	218.6667	211.1667	224.5833	2699.75	426.25	290.5833	254.4167	205.1667	277.5833	0.70	0.17	0.300
ILMN_3169041	mmu-miR-466j	164	131.4167	224.5833	200.6667	200.6667	245	332.0833	280.1667	241.1667	387.8333	197.5833	224.5833	0.75	0.12	0.085
ILMN_3168479	mmu-miR-760:9.1	2480.25	79.08334	6873.917	4434.333	863.9167	2947.25	7904.5	5752.583	1574.333	8394.833	1800.25	7904.5	1.01	0.67	0.192
ILMN_3168958	mmu-miR-770-5p	8873.167	11896.83	12251	7277.917	7190.917	8095.417	87.91666	3532.167	4313.5	7111.083	6913.75	3730.333	18.56	16.48	0.029
ILMN_3169058	mmu-miR-99b*	4712.75	1943.917	70.75	471.5	3532.167	937.1667	2480.25	471.5	1009.083	4777.167	1679.417	1574.333	1.48	0.64	0.959
ILMN_3169142	solexa-239-1823	312.75	467.4167	214.6667	431.5833	198.9167	161.3333	187.1667	467.4167	138.0833	227	120.5	893.75	1.33	0.26	0.782
ILMN_3169152	solexa-3253-144	6988.917	4288.5	4347.25	6746.5	95.16666	3776.083	2520.75	198.9167	6534	8816.583	453.5	6988.917	4.42	3.45	0.933
ILMN_3167574	mmu-miR-106b	405.3333	9286.417	307.8333	3655.333	6175.917	3730.333	161.3333	1450.5	6695.167	156.75	1308.5	2606.083	6.41	3.51	0.392
ILMN_3169051	mmu-miR-1198	5532	9438.917	8221.333	5587.833	3850	7820.25	31.16667	56	8536.417	1094.833	6791.75	2867	59.24	36.01	0.109
ILMN_3169052	mmu-miR-1199	176.75	122.5	179.0833	150.1667	4585.5	176.75	344.75	216.8333	242.5833	205.1667	304.25	198.9167	3.08	2.40	0.415
ILMN_3168303	mmu-miR-124	214.6667	150.9167	304.25	236.5833	242.5833	185.3333	151.9167	197.5833	2317.417	263.1667	146.6667	118.75	1.07	0.24	0.405
ILMN_3168012	mmu-miR-142-3p	227	405.3333	227	179.0833	175	164	156.75	188.8333	150.9167	230.1667	369.25	187.1667	1.20	0.25	0.793
ILMN_3168980	mmu-miR-147	436.5833	236.5833	414.6667	242.5833	241.1667	267.3333	304.25	3163.833	1244.667	304.25	112.75	132.6667	1.13	0.35	0.301
ILMN_3169054	mmu-miR-15b*	524.1667	2867	6534	3903.917	8536.417	2120.25	179.0833	4739.917	5532	142.5833	5198.25	3804.083	5.72	4.35	0.443
ILMN_3167223	mmu-miR-28	4877.833	8310.833	9739.083	4209.083	11048.17	6369.833	72	11896.83	12095.75	80	10684.58	9438.917	20.60	12.67	0.976
ILMN_3169077	mmu-miR-294*	110.1667	107.75	3850	5427.667	164	3419.333	447.5833	324.8333	178.0833	7351.417	203.5833	3443.417	4.12	3.50	0.813
ILMN_3168935	mmu-miR-338-5p	3776.083	1599.167	6623.167	165.5833	155.5	178.0833	236.5833	242.5833	156.75	4031.417	2436	119.25	11.07	6.71	0.594
ILMN_3167006	mmu-miR-378	8653.917	6746.5	2824.917	6534	4739.917	48.58333	5071.25	55.25	6623.167	3776.083	5798.167	5150.25	21.13	20.20	0.795
ILMN_3168946	mmu-miR-409-5p	97.5	267.3333	283.8333	7190.917	230.1667	280.1667	510.9167	274.9167	112.75	209.75	3074	5259.667	6.35	5.60	0.916
ILMN_3167988	mmu-miR-411	3970.25	8816.583	85.58334	73.91666	1614.25	2048.417	1094.833	559	6093.417	265.1667	4031.417	286.8333	4.54	2.51	0.734
ILMN_3169005	mmu-miR-590-5p	117.6667	193	10534.83	410.75	414.6667	393.6667	695.1667	320.5	129.1667	307.8333	101	185.3333	14.98	13.33	0.368
ILMN_3168959	mmu-miR-666-3p	143.6667	166.4167	293.6667	245	250.75	259.8333	477.1667	283.8333	134.5833	366.1667	111.1667	175	1.25	0.35	0.706
ILMN_3168270	mmu-miR-674*	554.5	200.6667	3776.083	32.16667	550.0833	41.08333	1368.417	1202.583	1048.917	5985.583	937.1667	2824.917	0.80	0.57	0.295
ILMN_3167814	mmu-miR-678	193	136.6667	216.8333	158.1667	146.6667	216.8333	312.75	268.5833	191.4167	236.5833	151.9167	274.9167	0.78	0.10	0.061
ILMN_3167999	mmu-miR-712	9739.083	7064.083	10822.92	11283.75	11283.75	11283.75	43.16667	40.83333	3970.25	533.5	2120.25	8816.583	71.52	41.08	0.001
ILMN_3167710	mmu-miR-759	172.8333	447.5833	194.8333	161.3333	5111.333	4379.5	169	180.9167	150.1667	4486.667	198.9167	4992.583	5.23	4.11	0.970
ILMN_3169153	solexa-403-1161	683.8333	1202.583	150.9167	3289.5	1244.667	1368.417	4817.25	2947.25	4777.167	129.1667	4379.5	6746.5	4.42	4.21	0.092
ILMN_3169155	solexa-447-1003	3903.917	5693.167	1244.667	1070.583	1009.083	218.6667	2365.333	41.41667	1189.333	35.83333	2824.917	366.1667	28.50	22.30	0.355
ILMN_3168955	mmu-miR-1224	153.75	128.1667	200.6667	170.9167	172.8333	197.5833	197.5833	178.0833	139.6667	191.4167	136.6667	180.9167	1.03	0.12	0.997
ILMN_3169061	mmu-miR-125b*	197.5833	695.1667	241.1667	175	188.8333	2006.667	170.9167	334.9167	280.1667	101	145.8333	148.5833	3.44	2.02	0.253
ILMN_3166992	mmu-miR-139-5p	4486.667	5493.5	4739.917	4131.917	267.3333	628.6667	60.16667	59.33333	3163.833	68.5	2520.75	3492.75	38.21	17.33	0.287
ILMN_3168045	mmu-miR-17*	7561.333	5587.833	9004.417	5868	7111.083	10223.75	6434.583	194.8333	8653.917	54.33333	5587.833	44.16667	61.94	37.88	0.046
ILMN_3168226	mmu-miR-23a	8816.583	503.4167	2365.333	88.58334	88.58334	1635.083	8816.583	7820.25	8005.833	105.9167	8221.333	3419.333	0.45	0.17	0.051
ILMN_3167837	mmu-miR-31	2520.75	2281.917	38.58333	874.25	2754.917	2730.417	35.75	3204.833	6988.917	40.83333	4486.667	1854.583	15.79	11.46	0.535
ILMN_3168180	mmu-miR-378*	4947.75	2048.417	52.16667	49.08333	1202.583	3119.333	3254.25	76.58334	908.8333	7820.25	4288.5	2480.25	4.98	4.36	0.451
ILMN_3168410	mmu-miR-425*	4434.333	5868	827.8333	8736.833	227	1800.25	99.91666	117.6667	661.5	119.25	3492.75	6913.75	28.18	12.99	0.462
ILMN_3168006	mmu-miR-434-5p	90.41666	6175.917	3254.25	141	5302.583	7904.5	77.25	82.33334	1429.75	9286.417	6434.583	5071.25	13.48	12.31	0.971
ILMN_3168995	mmu-miR-466g	5198.25	342	8536.417	146.6667	135.5833	134	6623.167	142.5833	125.5833	979.5	3026	3532.167	11.90	11.22	0.995
ILMN_3167437	mmu-miR-497	122.5	815.3333	1390.25	806.8333	3318.75	33.75	2659.417	31.58333	1408.083	4075.75	5646.75	2365.333	4.61	4.24	0.057
ILMN_3169021	mmu-miR-582-3p	136.6667	129.8333	250.75	194.8333	187.1667	211.1667	307.8333	203.5833	118.75	241.1667	96.08334	166.4167	1.20	0.28	0.936
ILMN_3168011	mmu-miR-672	7508.083	5371.667	6791.75	70	68.16666	4075.75	8394.833	81.25	8394.833	2824.917	7561.333	5111.333	11.44	10.94	0.437
ILMN_3168259	mmu-miR-682	26.41667	34.25	431.5833	1614.25	1263.167	2659.417	3443.417	2048.417	158.1667	29.08333	230.1667	1308.5	10.96	8.95	0.822
ILMN_3168374	mmu-miR-693-3p	209.75	134.5833	234.75	166.4167	150.9167	5111.333	218.6667	175	130.5833	232.5833	211.1667	191.4167	5.28	4.29	0.371
ILMN_3167961	mmu-miR-764-3p	31.16667	28.08333	1912.583	1009.083	1828.917	683.8333	4347.25	2754.917	715.25	3419.333	33.75	1202.583	9.62	8.92	0.288
ILMN_3168976	mmu-miR-874	1429.75	2730.417	71.16666	5071.25	1538.583	815.3333	6791.75	81.58334	2983.667	85.58334	918.5	1635.083	15.86	10.21	0.931
ILMN_3169131	solexa-1278-371	379.75	2436	1263.167	4243.5	43.83333	250.75	53.5	4209.083	1635.083	5371.667	5071.25	53.5	2.32	1.18	0.172
ILMN_3169156	solexa-4983-92	89.66666	990.3333	169	164	129.1667	1943.917	366.1667	259.8333	5371.667	134.5833	426.25	7713.917	0.98	0.59	0.188
ILMN_3169161	solexa-622-718	8005.833	9633	10684.58	9184.083	4131.917	5302.583	159.4167	94.25	7611	1263.167	8095.417	75.08334	38.71	17.34	0.057
ILMN_3168724	mmu-let-7i*	515.6667	2120.25	2480.25	3730.333	827.8333	205.1667	122.5	70	1263.167	64.16666	105.9167	161.3333	17.28	9.29	0.056
ILMN_3168105	mmu-miR-148a	131.4167	5259.667	7561.333	7111.083	102.9167	4313.5	87.66666	620.6667	5693.167	123.6667	6534	4556.833	11.63	9.26	0.572
ILMN_3167626	mmu-miR-199b*	42.83333	6988.917	544.25	4379.5	4486.667	10684.58	7111.083	46.91667	10684.58	41.08333	5752.583	58.5	73.17	34.05	0.870
ILMN_3167002	mmu-miR-200c	1776	3204.833	8310.833	2754.917	5198.25	2824.917	100.4167	65.25	2730.417	65.25	2784.583	56.91667	27.26	9.17	0.003
ILMN_3168487	mmu-miR-203	1368.417	5111.333	129.1667	3492.75	117.6667	3594	8005.833	161.3333	4209.083	188.8333	149.1667	2208.917	8.80	5.43	0.922
ILMN_3168933	mmu-miR-330	120.5	2520.75	159.4167	159.4167	143.6667	135.5833	158.1667	218.6667	185.3333	256.3333	185.3333	155.5	2.57	1.79	0.416
ILMN_3167081	mmu-miR-330*	6791.75	3730.333	4992.583	5150.25	2520.75	3804.083	76	90.16666	1506.5	120.5	107.75	1828.917	33.71	13.25	0.003
ILMN_3169081	mmu-miR-34c*	138.0833	113.8333	187.1667	156.75	205.1667	230.1667	263.1667	222.9167	211.1667	290.5833	101.25	101	1.13	0.33	0.605
ILMN_3167244	mmu-miR-410	155.5	114.1667	170.9167	143.6667	120.5	158.1667	320.5	166.4167	155.5	218.6667	131.4167	211.1667	0.77	0.09	0.076
ILMN_3167599	mmu-miR-467b	274.9167	125.5833	191.4167	216.8333	166.4167	125.5833	142.5833	179.0833	145.8333	283.8333	169	193	1.06	0.20	0.951
ILMN_3168236	mmu-miR-483*	169	105	185.3333	176.75	158.1667	149.1667	138.0833	158.1667	132.6667	222.9167	155.5	227	0.96	0.13	0.505
ILMN_3168520	mmu-miR-668	6175.917	7190.917	7904.5	2404.333	34.91667	5646.75	33.75	40.08333	5259.667	11283.75	6175.917	71.16666	73.91	36.14	0.716
ILMN_3167536	mmu-miR-669a	3163.833	38.08333	2730.417	39.08333	41.41667	46.5	6988.917	3254.25	443.0833	2067.5	1429.75	754.6667	1.12	1.01	0.156
ILMN_3168059	mmu-miR-674	1408.083	87.91666	2317.417	2867	3163.833	4556.833	97.5	38.58333	5646.75	39.08333	1776	2912.75	15.64	11.74	0.491
ILMN_3167422	mmu-miR-98	141	114.8333	150.1667	3443.417	139.6667	351.4167	4739.917	2006.667	169	214.6667	586.0833	179.0833	3.20	2.58	0.598
ILMN_3168463	mmu-let-7e	5868	40.75	3804.083	33.75	222.9167	35.5	38.16667	248	3389.167	42.33333	1574.333	2317.417	26.00	25.55	0.744
ILMN_3168941	mmu-miR-139-3p	187.1667	248	180.9167	148.5833	149.1667	179.0833	185.3333	187.1667	151.9167	238.3333	92.08334	100.4167	1.26	0.17	0.402
ILMN_3169099	mmu-miR-26b*	2947.25	763.8333	6093.417	33	30	30.41667	194.8333	32	4817.25	30.08333	1614.25	676.3333	6.90	4.15	0.527
ILMN_3168356	mmu-miR-290-5p	83.58334	205.1667	221.3333	169	165.5833	166.4167	241.1667	134.5833	93.16666	164	117.6667	108.5833	1.37	0.27	0.555
ILMN_3167226	mmu-miR-296-5p	6623.167	7611	4647.833	79.75	5868	222.9167	41.08333	5925.5	53.5	60.16667	2365.333	40.25	43.12	27.34	0.048
ILMN_3169084	mmu-miR-30c-1*	2699.75	4556.833	4434.333	3970.25	3289.5	62.91667	57.41667	49.08333	54.33333	72.16666	2048.417	2436	46.35	15.95	0.078
ILMN_3168146	mmu-miR-434-3p	119.25	661.5	105.9167	421.6667	142.5833	1746.167	98	2317.417	2281.917	121.5	2162.667	3903.917	0.92	0.54	0.040
ILMN_3167221	mmu-miR-485	6237.917	3163.833	37.83333	197.5833	33.25	7351.417	32.41667	3389.167	2784.583	32.75	2208.917	35.75	67.51	41.64	0.454
ILMN_3167912	mmu-miR-501-3p	272	1703.417	2606.083	2067.5	533.5	54.33333	41.66667	42.75	93.5	4347.25	471.5	41.08333	12.86	6.87	0.609
ILMN_3169046	mmu-miR-669e	170.9167	550.0833	4209.083	3026	7277.917	3289.5	30	30.41667	31.25	26.75	715.25	32	64.09	24.03	0.029
ILMN_3167514	mmu-miR-671-5p	112.75	90.41666	127.0833	1703.417	2559.167	121.5	131.4167	3026	121.5	4712.75	191.4167	165.5833	2.73	2.13	0.502
ILMN_3168056	mmu-miR-673-5p	3204.833	3443.417	7351.417	139.6667	63.5	71.16666	550.0833	50.5	4712.75	7713.917	114.8333	42.75	12.97	11.08	0.917
ILMN_3167095	mmu-miR-770-3p	1154.917	950.5833	42.58333	6913.75	52.33333	48.33333	7416.333	62.91667	4434.333	10428.17	44.83333	4777.167	2.85	2.46	0.048

Table B2. -Continued

Illumia_ID	NAME	LCA1	LCA2	LCA3	LCA4	LCA5	LCA6	RCA1	RCA2	RCA3	RCA4	RCA4	RCA6	LCA/RCA		
		signal	signal	signal	signal	signal	signal	signal	signal	signal	signal	signal	signal	ratio	SEM	p-value
ILMN_3169128	solexa-110-3896	94.25	115.9167	238.3333	203.5833	193	1189.333	324.8333	234.75	111.1667	267.3333	90.16666	124.9167	2.56	1.43	0.478
ILMN_3169133	solexa-1328-360	4992.583	1429.75	38.83333	35.75	220.4167	1429.75	105.9167	2606.083	39	44.75	515.6667	7064.083	8.35	7.76	0.797
ILMN_3169137	solexa-1837-257	7820.25	4877.833	30.75	503.4167	1368.417	30.08333	30.41667	51.08333	918.5	3903.917	874.25	130.5833	59.09	42.53	0.424
ILMN_3167725	solexa-4179-110	3443.417	72.16666	43.66667	41.41667	4992.583	43.5	5111.333	8221.333	36.83333	8536.417	3318.75	8873.167	0.56	0.27	0.082
ILMN_3168578	solexa-5306-86	42.33333	30	31.25	40.83333	1048.917	908.8333	9004.417	7416.333	268.5833	2947.25	40.08333	4647.833	4.42	4.35	0.068
ILMN_3167894	mmu-miR-146b	102.9167	3776.083	4585.5	5302.583	2912.75	1828.917	106.6667	123.6667	110.1667	179.0833	128.1667	125.5833	23.34	5.78	0.012
ILMN_3167522	mmu-miR-154	92.08334	5925.5	112.75	1173.75	2947.25	150.1667	119.25	105	7190.917	2162.667	9184.083	123.6667	9.88	9.31	0.497
ILMN_3169093	mmu-miR-16*	118.75	318.6667	3419.333	3119.333	98.66666	1912.583	216.8333	477.1667	101.25	129.8333	72	109.3333	12.98	5.82	0.101
ILMN_3167698	mmu-miR-184	254.4167	123.6667	193	193	124.9167	127.0833	172.8333	165.5833	136.6667	185.3333	161.3333	178.0833	1.03	0.14	0.910
ILMN_3167167	mmu-miR-190	158.1667	118.75	172.8333	172.8333	134	156.75	132.6667	170.9167	148.5833	198.9167	130.5833	220.4167	0.94	0.09	0.389
ILMN_3169097	mmu-miR-22*	96.08334	139.6667	93.5	85.58334	94.83334	1278.083	141	2559.167	1070.583	131.4167	1599.167	1329.583	0.42	0.16	0.091
ILMN_3168515	mmu-miR-224	49.58333	3119.333	54.83333	2520.75	48.16667	1408.083	46.83333	41.08333	1854.583	51.58333	3594	236.5833	21.97	13.28	0.834
ILMN_3169101	mmu-miR-29c*	111.1667	937.1667	153.75	129.8333	2480.25	143.6667	165.5833	191.4167	874.25	937.1667	3970.25	238.3333	1.18	0.75	0.257
ILMN_3168938	mmu-miR-342-5p	28.5	1189.333	6369.833	29.66667	4947.75	4585.5	31.75	6695.167	32.41667	28.33333	28.83333	2947.25	61.96	38.74	0.505
ILMN_3167820	mmu-miR-409-3p	43.33333	723	5868	671.25	683.8333	32.75	28.83333	32.75	1034.583	28.5	31.25	1599.167	12.45	4.57	0.357
ILMN_3167973	mmu-miR-433	54.33333	489.4167	1891.5	55.25	1703.417	59.16667	54.25	63.5	497.0833	4585.5	950.5833	59	2.55	1.15	0.722
ILMN_3167845	mmu-miR-677	238.3333	68.16666	198.9167	39	1329.583	883.3333	48.16667	50.58333	267.3333	723	51.25	49.91667	8.46	4.41	0.401
ILMN_3166950	mmu-miR-697	224.5833	187.1667	254.4167	187.1667	161.3333	1450.5	130.5833	135.5833	99.91666	125.5833	94.83334	110.1667	3.67	1.91	0.219
ILMN_3167032	mmu-miR-699	5587.833	4209.083	123.6667	2912.75	4777.167	1506.5	150.9167	114.8333	72.58334	107.75	1137.167	94.25	20.43	6.37	0.014
ILMN_3169125	mmu-miR-877*	4031.417	70.25	83	77.25	75.33334	101	5532	5111.333	1891.5	4131.917	91.16666	1263.167	0.29	0.16	0.033
ILMN_3169143	solexa-2402-197	70.75	214.6667	103.9167	4031.417	3594	3163.833	117.6667	115.9167	221.3333	117.6667	1506.5	70.33334	14.09	8.20	0.092
ILMN_3168320	mmu-miR-1	30.58333	31.58333	30.83333	33.25	31.25	524.1667	9985.333	6791.75	2162.667	35.5	2983.667	31.25	2.96	2.77	0.085
ILMN_3169063	mmu-miR-136*	216.8333	4347.25	7416.333	53.75	179.0833	46.08333	42.75	42.33333	39.58333	43.33333	1480.333	42.83333	49.59	32.10	0.254
ILMN_3168426	mmu-miR-148b	47.83333	1574.333	45.66667	52.16667	45.66667	151.9167	70	1828.917	6175.917	52.91667	6746.5	1278.083	0.44	0.18	0.126
ILMN_3167158	mmu-miR-30a*	221.3333	93.5	129.8333	191.4167	129.8333	111.1667	153.75	139.6667	2606.083	550.0833	1202.583	141	0.57	0.21	0.166
ILMN_3168986	mmu-miR-343	175	149.1667	220.4167	155.5	145.8333	175	176.75	176.75	109.3333	111.1667	75.33334	91.5	1.52	0.21	0.083
ILMN_3167743	mmu-miR-34c	3389.167	34.91667	132.6667	40.08333	2227.667	40.08333	43.33333	42.58333	176.75	5646.75	815.3333	36.58333	13.94	12.86	0.907
ILMN_3168962	mmu-miR-423-5p	1800.25	138.0833	40.75	979.5	38.08333	39	40.08333	4288.5	234.75	62.91667	41.08333	4379.5	10.27	7.37	0.390
ILMN_3168997	mmu-miR-467c	31.75	3970.25	27.75	29.33333	30.41667	3850	38.58333	31.75	4243.5	33.75	332.0833	3163.833	21.34	20.74	0.989
ILMN_3167642	mmu-miR-499	31.83333	30.58333	32.08333	8394.833	6434.583	5868	31.25	30	5985.583	32.58333	110.1667	5532	53.19	41.96	0.503
ILMN_3167017	mmu-miR-500	1214.667	46.83333	56.91667	4486.667	964.4167	1679.417	50.58333	42.83333	38.83333	4379.5	47.58333	45.75	14.10	6.18	0.073
ILMN_3167887	mmu-miR-543	27.75	169	203.5833	48.33333	27.16667	30	461.25	1214.667	28.83333	38.08333	467.4167	28.5	1.61	1.11	0.175
ILMN_3166970	mmu-miR-743a	57.75	49.91667	75.33334	76	62.58333	118.75	3594	224.5833	220.4167	159.4167	218.6667	342	0.28	0.06	0.258
ILMN_3168973	mmu-miR-883a-3p	80.75	92.08334	165.5833	145.8333	134.5833	150.9167	248	164	105	203.5833	115.9167	150.9167	0.89	0.18	0.321
ILMN_3168940	mmu-miR-101b	68.5	1009.083	65.25	2699.75	67.58334	62.58333	70.75	86.58334	414.6667	81.25	259.8333	103.9167	7.81	5.40	0.335
ILMN_3168979	mmu-miR-105	95.16666	908.8333	136.6667	120.5	101.25	130.5833	220.4167	151.9167	96.75	170.9167	118.75	156.75	1.70	0.87	0.505
ILMN_3169028	mmu-miR-1-2-as	135.5833	108.5833	145.8333	138.0833	141	114.8333	125.5833	134	131.4167	242.5833	188.8333	259.8333	0.79	0.11	0.115
ILMN_3167434	mmu-miR-15a	87.66666	142.5833	101.25	118.75	176.75	101.25	101	103.9167	339.1667	194.8333	227	120.5	0.79	0.14	0.186
ILMN_3167279	mmu-miR-302b	129.1667	112.75	134.5833	111.8333	100.4167	115.9167	242.5833	128.1667	141	103.9167	129.1667	620.6667	0.73	0.13	0.231
ILMN_3168138	mmu-miR-30e	52.5	332.0833	59.58333	54.33333	57.41667	69.75	467.4167	60.16667	431.5833	65.83334	46.83333	254.4167	1.35	0.85	0.321
ILMN_3169009	mmu-miR-466d-3p	35.75	33.83333	1368.417	1574.333	36.58333	33.83333	36.16667	5532	31.33333	40.25	2754.917	37.33333	14.12	8.65	0.458
ILMN_3168957	mmu-miR-671-3p	88.58334	414.6667	87.66666	57.75	5985.583	70.25	55.75	7277.917	60.16667	68.16666	2480.25	39.58333	1.36	0.33	0.710
ILMN_3168248	mmu-miR-696	56.83333	53.5	3903.917	69.25	3419.333	3254.25	114.8333	98	2067.5	88.41666	87.66666	93.16666	12.94	7.62	0.095
ILMN_3167384	solexa-783-586	36.83333	66.83334	272	1034.583	32.16667	34.75	33.16667	32.16667	53.16667	34.66667	503.4167	731.5833	6.38	4.76	0.953
ILMN_3167276	mmu-miR-10b	2067.5	36.58333	35.58333	34.91667	1891.5	32.41667	34.75	3804.083	30.58333	38.58333	35.58333	33.25	19.28	11.74	0.982
ILMN_3169044	mmu-miR-1193	2824.917	806.8333	59.16667	59	61.08333	4877.833	67.75	64.58334	59.58333	84.16666	72.16666	54.25	24.44	14.60	0.151
ILMN_3168025	mmu-miR-134	94.83334	339.1667	138.0833	123.6667	111.8333	120.5	139.6667	4379.5	79.08334	102.1667	2227.667	107.75	0.81	0.27	0.204
ILMN_3167495	mmu-miR-207	2227.667	101	124.9167	105	5493.5	119.25	143.6667	146.6667	113.8333	136.6667	124.9167	142.5833	10.48	7.11	0.230
ILMN_3167457	mmu-miR-24-1*	61.08333	320.5	28.08333	29.16667	26.41667	29.08333	30.83333	28.5	28.5	5198.25	27.16667	1390.25	2.54	1.77	0.283
ILMN_3168984	mmu-miR-297c	37.41667	62.91667	39.58333	36.33333	37.16667	37.83333	49.58333	4817.25	695.1667	43.5	36.58333	205.1667	0.48	0.18	0.281
ILMN_3167369	mmu-miR-300	74.33334	64.16666	130.5833	94.83334	89.66666	102.1667	58.5	121.5	143.6667	145.8333	134.5833	250.75	0.74	0.13	0.080
ILMN_3169080	mmu-miR-302a*	148.5833	111.8333	164	127.0833	114.8333	139.6667	164	122.5	102.9167	134	119.25	102.1667	1.12	0.12	0.463
ILMN_3166938	mmu-miR-322	39.33333	1912.583	40.08333	3318.75	34.66667	38.08333	36.58333	39.58333	39.08333	42.75	1968.583	47.58333	21.48	13.66	0.500
ILMN_3167611	mmu-miR-331-3p	283.8333	124.9167	50.08333	47.58333	47.58333	45.08333	44.58333	44.16667	2480.25	51.91667	731.5833	47.25	1.86	0.99	0.310
ILMN_3168943	mmu-miR-362-3p	125.5833	155.5	122.5	114.1667	103.9167	122.5	123.6667	118.75	200.6667	193	806.8333	127.0833	0.77	0.17	0.284
ILMN_3168420	mmu-miR-429	91.16666	129.1667	151.9167	150.9167	151.9167	169	238.3333	141	101	176.75	90.41666	114.8333	1.13	0.20	0.929
ILMN_3167050	mmu-miR-452	121.5	105.9167	142.5833	131.4167	138.0833	107.75	148.5833	169	135.5833	259.8333	164	139.6667	0.77	0.08	0.065
ILMN_3166991	mmu-miR-469	83	80	158.1667	132.6667	125.5833	141	211.1667	145.8333	95.16666	224.5833	96.75	145.8333	0.91	0.20	0.323
ILMN_3169001	mmu-miR-509-5p	86.58334	70.75	90.41666	91.16666	84.16666	84.83334	111.8333	129.8333	134	172.8333	123.6667	164	0.62	0.04	0.002
ILMN_3168199	mmu-miR-532-5p	33.83333	827.8333	41.08333	41.08333	4243.5	44.83333	47.25	6746.5	36.58333	37.16667	56.83333	36.16667	13.16	12.30	0.836
ILMN_3167846	mmu-miR-665	51.58333	280.1667	89.16666	82	2048.417	91.16666	129.8333	85.58334	1776	81.58334	54.33333	72.58334	7.28	6.10	0.883
ILMN_3167909	mmu-miR-714	1679.417	1048.917	60.83333	49.75	44.75	50.5	56	6913.75	57.41667	48.33333	54.83333	72.16666	5.62	4.87	0.534
ILMN_3167900	mmu-miR-715	70.33334	1117.667	54.25	56	65.25	83.58334	3026	227	58.5	52.33333	51.58333	50.5	1.64	0.69	0.563
ILMN_3168397	mmu-miR-801:9.1	5071.25	6369.833	56.83333	56.83333	443.0833	82	79.75	62.58333	51.08333	47.83333	46.91667	45.33333	29.82	17.48	0.158
ILMN_3167809	mmu-miR-99a	32.41667	50.58333	34.66667	33.75	209.75	30.25	30.08333	4313.5	31.41667	34.25	30.58333	447.5833	1.68	1.05	0.338
ILMN_3169154	solexa-4327-106	31.33333	32.41667	33.75	84.41666	31.16667	165.5833	32	36.58333	32.75	9438.917	33.25	4243.5	0.65	0.20	0.213
ILMN_3169157	solexa-5067-90	30.75	165.5833	31.16667	2824.917	1912.583	31.41667	34.66667	33.16667	31.75	30.83333	30.41667	34.41667	27.05	16.32	0.171
ILMN_3169088	mmu-let-7c-2*,mmu	44.16667	44.83333	42.33333	38.58333	41.08333	44.16667	3419.333	44.83333	3361.167	55.25	44.58333	46.5	0.60	0.19	0.173
ILMN_3169091	mmu-let-7f*	102.1667	96.75	143.6667	135.5833	132.6667	148.5833	191.4167	172.8333	124.9167	200.6667	114.1667	135.5833	0.86	0.12	0.215
ILMN_3167353	mmu-miR-107	98	73.16666	91.5	153.75	77.25	132.6667	108.5833	113.8333	117.6667	153.75	883.3333	136.6667	0.73	0.14	0.313
ILMN_3167547	mmu-miR-122	159.4167	96.08334	149.1667	121.5	115.9167	105.9167	109.3333	131.4167	120.5	175	103.9167	146.6667	0.99	0.13	0.724
ILMN_3168921	mmu-miR-125a-3p	883.3333	69.25	29.5	27.83333	763.8333	29.5	27.75	27.83333	26.41667	26.41667	30.75	26.41667	10.41	5.75	0.161
ILMN_3169083	mmu-miR-130b*	73.16666	59.16667	73.91666	3850	62.33333	111.8333	88.58334	84.16666	510.9167	86.58334	49.58333	56.83333	8.23	7.25	0.426
ILMN_3167823	mmu-miR-135a	265.1667	73.91666	99.91666	98.66666	87.66666	102.9167	121.5	106.6667	98	161.3333	102.1667	158.1667	1.00	0.24	0.920
ILMN_3169111	mmu-miR-138*	93.5	119.25	146.6667	149.1667	150.1667	159.4167	71.16666	76	69.25	84.41666	65.25	66.16666	1.91	0.18	0.002
ILMN_3169064	mmu-miR-141*	34.25	148.5833	32.41667	29.91667	31.58333	30.75	29.91667	30.83333	216.8333	33.66667	32.41667	35.5	1.47	0.68	0.775
ILMN_3168509	mmu-miR-142-5p	109.3333	93.16666	161.3333	124.9167	106.6667	129.1667	149.1667	120.5	90.41666	148.5833	108.5833	169	0.98	0.16	0.576
ILMN_3168361	mmu-miR-181a-1*	29.16667	3289.5	30	30.08333	1635.083	29.75	29.5	30.58333	30	29.66667	102.9167	30.58333	21.24	17.43	0.208
ILMN_3168494	mmu-miR-181d	75.08334	74.33334	84.41666	93.5	90.16666	112.75	193	149.1667	111.8333	150.9167	132.6667	153.75	0.61	0.06	0.006
ILMN_3167529	mmu-miR-183	65.83334	63.91667	64.58334	151.9167	128.1667	65.25	259.8333	73.5	62.58333	70	58.16667	66.83334	1.25	0.32	0.841
ILMN_3168371	mmu-miR-202-3p	76	88.58334	96.75	99.91666	98	95.16666	81.25	124.9167	127.0833	149.1667	125.5833	96.75	0.81	0.05	0.021
ILMN_3167355	mmu-miR-216a	129.8333	87.66666	155.5	198.9167	136.6667	117.6667	372	136.6667	84.16666	115.9167	73.91666	86.58334	1.29	0.27	0.893
ILMN_3168380	mmu-miR-218	44.83333	42.58333	46.83333	42.75	43.33333	45.33333	47.58333	5985.583	40.25	51.08333	5371.667	44.58333	0.66	0.21	0.175
ILMN_3167913	mmu-miR-299*	89.16666	90.16666	110.1667	112.75	113.8333	103.9167	113.8333	138.0833	128.1667	166.4167	153.75	129.8333	0.75	0.03	0.002
ILMN_3168116	mmu-miR-301a	56	383.1667	77.75	90.41666	59	69.25	91.5	91.5	1943.917	83	78.25	92.08334	1.24	0.61	0.434
ILMN_3169057	mmu-miR-30b*	60.83333	54.33333	72.16666	64.58334	69.75	76	3532.167	80.75	773	83.58334	56.41667	59.83333	0.68	0.22	0.272
ILMN_3168944	mmu-miR-335-3p	32.08333	31.41667	863.9167	38	32.41667	35.83333	39.33333	39	3074	36.16667	39.33333	39	0.78	0.11	0.358
ILMN_3168937	mmu-miR-341	33.5	32.58333	33.25	33.66667	2659.417	36.33333	4209.083	38.41667	34.41667	35	35.75	37.41667	13.02	12.27	0.782
ILMN_3168288	mmu-miR-34b-5p	103.9167	103.9167	156.75	134	112.75	145.8333	188.8333	6873.917	2912.75	180.9167	105	138.0833	0.58	0.19	0.212
ILMN_3167215	mmu-miR-370	29.66667	89.66666	26.08333	26.41667	489.4167	27.41667	29.33333	26.41667	27.16667	280.1667	26.08333	26.75	4.21	2.95	0.652
ILMN_3167419	mmu-miR-376a*	80	81.25	87.91666	89.66666	81.58334	91.5	135.5833	1614.25	88.58334	98.66666	113.8333	112.75	0.68	0.14	0.324

Table B2. -Continued

Illumia_ID	NAME	LCA1	LCA2	LCA3	LCA4	LCA5	LCA6	RCA1	RCA2	RCA3	RCA4	RCA4	RCA6	LCA/RCA		
		signal	signal	signal	signal	signal	signal	signal	signal	signal	signal	signal	signal	ratio	SEM	p-value
ILMN_3167098	mmu-miR-380-3p	2436	35.08333	37.41667	37.33333	661.5	34.91667	35	34.75	35.58333	43.16667	38.16667	41.08333	15.12	11.22	0.257
ILMN_3168071	mmu-miR-450b-3p	84.16666	91.5	117.6667	114.8333	105	105	129.1667	150.9167	122.5	169	129.8333	134	0.75	0.05	0.008
ILMN_3166954	mmu-miR-465a-5p	161.3333	85.58334	131.4167	102.1667	99.91666	124.9167	155.5	127.0833	94.83334	158.1667	143.6667	117.6667	0.92	0.12	0.357
ILMN_3169126	mmu-miR-467e*	93.16666	97.5	93.16666	100.4167	96.08334	87.66666	90.41666	101.25	105.9167	178.0833	142.5833	214.6667	0.75	0.10	0.086
ILMN_3167334	mmu-miR-485*	52.91667	671.25	53.16667	142.5833	56.41667	62.33333	64.16666	57.41667	49.58333	53.75	57.41667	62.33333	3.04	1.75	0.303
ILMN_3167922	mmu-miR-541	30.08333	29.66667	30.41667	30.83333	33	29.16667	4288.5	29.75	30.08333	29.16667	554.5	30	0.68	0.21	0.305
ILMN_3167888	mmu-miR-666-5p	166.4167	120.5	135.5833	110.1667	93.16666	75.08334	65.83334	5427.667	62.91667	80.75	111.8333	113.8333	1.26	0.39	0.378
ILMN_3168126	mmu-miR-685	41.08333	57.41667	48.83333	46.5	46.83333	51.08333	683.8333	45.33333	54.25	55.75	60.83333	4313.5	0.64	0.20	0.292
ILMN_3166949	mmu-miR-805	29.08333	28.83333	31.16667	59.83333	29.5	979.5	30.58333	28.83333	27.83333	30.41667	1094.833	29.33333	6.41	5.40	0.959
ILMN_3168967	mmu-miR-871	145.8333	91.16666	120.5	109.3333	153.75	6175.917	115.9167	111.1667	107.75	143.6667	93.16666	96.08334	11.65	10.53	0.359
ILMN_3168970	mmu-miR-881	69.75	71.16666	111.1667	101	102.1667	106.6667	112.75	6623.167	80.75	101.25	64.16666	3850	0.77	0.27	0.195
ILMN_3167447	mmu-miR-9	29.75	379.75	30.25	1746.167	29.16667	31.83333	30.25	29.91667	29.5	31.41667	29.08333	30.25	12.06	8.91	0.273
ILMN_3169145	solexa-2564-185	43.16667	351.4167	46.25	1599.167	54.33333	47.58333	52.33333	57.75	96.08334	69.25	79.08334	77.25	5.30	3.67	0.314
ILMN_3167808	mmu-miR-101a	36.58333	33.25	34.25	31.83333	31.41667	32.58333	3318.75	34.41667	35.75	33.5	33.75	33.66667	0.80	0.16	0.362
ILMN_3169059	mmu-miR-101a*	72.16666	60.83333	119.25	78.25	60.83333	57.75	221.3333	44.58333	56	70.25	38.08333	56.33333	1.26	0.25	0.843
ILMN_3169036	mmu-miR-1188	35.58333	33.16667	43.5	32.41667	32.58333	1614.25	50.5	56.83333	56.33333	46.91667	84.83334	115.9167	2.84	2.22	0.406
ILMN_3169045	mmu-miR-1194	51.91667	62.58333	134	129.1667	121.5	136.6667	209.75	94.83334	52.91667	130.5833	56	80	1.38	0.37	0.959
ILMN_3169050	mmu-miR-1196	43.5	27.41667	29.08333	30.58333	32.08333	34.66667	29.16667	31.25	33.66667	33.83333	461.25	36.83333	0.86	0.19	0.364
ILMN_3168942	mmu-miR-125b-3p	503.4167	77.25	100.4167	90.16666	85.58334	96.75	136.6667	108.5833	87.91666	124.9167	99.91666	111.8333	1.33	0.47	0.495
ILMN_3169062	mmu-miR-127*	82.33334	37.16667	49.58333	45.08333	44.16667	1329.583	56.91667	52.33333	43.66667	59.33333	45.33333	52.91667	5.03	4.02	0.363
ILMN_3167099	mmu-miR-130b	115.9167	127.0833	175	113.8333	109.3333	134.5833	89.16666	148.5833	102.1667	150.1667	93.5	89.66666	1.22	0.15	0.352
ILMN_3166936	mmu-miR-135a*	30.83333	29.5	31.33333	30.41667	4712.75	28.08333	33	31.41667	30.58333	29.33333	34.41667	30.08333	23.63	22.66	0.364
ILMN_3166940	mmu-miR-137	128.1667	95.16666	128.1667	136.6667	122.5	108.5833	107.75	111.8333	106.6667	146.6667	141	129.1667	0.98	0.07	0.641
ILMN_3169066	mmu-miR-150*	40.83333	45.75	76	87.91666	73.91666	80	128.1667	908.8333	46.83333	53.5	42.58333	50.16667	1.16	0.31	0.390
ILMN_3166999	mmu-miR-153	31.58333	36.33333	41.41667	37.83333	36.58333	31.16667	31.33333	33.83333	34.25	497.0833	34.75	32.08333	0.90	0.17	0.376
ILMN_3166946	mmu-miR-155	73.91666	56.33333	79.08334	67.75	67.75	65.83334	76.58334	89.16666	75.33334	111.8333	2659.417	87.66666	0.67	0.15	0.344
ILMN_3168073	mmu-miR-186	90.16666	70.33334	94.83334	80.75	75.08334	79.75	84.16666	112.75	88.41666	99.91666	139.6667	106.6667	0.81	0.09	0.093
ILMN_3168837	mmu-miR-190b	149.1667	102.9167	92.08334	91.5	94.25	87.91666	70.33334	78.25	76	118.75	65.83334	64.16666	1.37	0.18	0.141
ILMN_3167801	mmu-miR-200a	52.33333	54.83333	7190.917	41.83333	40.75	39.33333	35.58333	34.91667	33.5	36.83333	35.5	33.75	36.86	35.56	0.359
ILMN_3167217	mmu-miR-201	101.25	76	94.25	92.08334	83	93.16666	134	211.1667	98.66666	95.16666	59	65.25	0.98	0.17	0.441
ILMN_3167196	mmu-miR-204	47.58333	38.83333	46.5	42.33333	39.33333	43.16667	43.66667	40.25	46.08333	39	414.6667	43.33333	0.87	0.16	0.372
ILMN_3167091	mmu-miR-205	2120.25	58.5	61.08333	58.5	60.16667	52.16667	46.25	54.33333	52.5	53.16667	51.08333	59.33333	8.54	7.46	0.358
ILMN_3168019	mmu-miR-206	30.25	29.33333	26.41667	26.08333	26.08333	28.33333	6873.917	28.33333	28.33333	28.08333	27.75	28.08333	0.81	0.16	0.363
ILMN_3167762	mmu-miR-214*	50.08333	544.25	46.91667	51.25	47.58333	48.16667	47.83333	49.75	50.08333	50.16667	52.33333	51.08333	2.63	1.66	0.371
ILMN_3167296	mmu-miR-217	113.8333	83.58334	118.75	128.1667	101	98.66666	124.9167	114.1667	103.9167	132.6667	121.5	149.1667	0.87	0.07	0.122
ILMN_3168926	mmu-miR-290-3p	6093.417	42.75	47.58333	44.16667	42.83333	41.83333	45.08333	45.75	43.83333	49.08333	44.75	49.08333	23.31	22.37	0.364
ILMN_3169056	mmu-miR-29b*	32.41667	57.75	32.16667	32.75	33.5	31.33333	34.25	33.66667	65.83334	32.41667	32.41667	1408.083	0.87	0.23	0.360
ILMN_3167235	mmu-miR-302c*	72.58334	50.5	62.91667	62.33333	57.75	63.5	361.75	62.33333	78.25	66.83334	61.08333	68.5	0.77	0.12	0.295
ILMN_3167931	mmu-miR-322*	66.16666	179.0833	66.83334	62.91667	61.75	67.58334	60.83333	77.75	70.25	82	68.16666	83	1.14	0.24	0.599
ILMN_3168931	mmu-miR-323-5p	73.5	410.75	53.5	54.33333	54.33333	54.33333	48.33333	48.83333	42.83333	61.08333	52.91667	50.08333	2.36	1.21	0.316
ILMN_3168391	mmu-miR-361	43.83333	38.41667	41.83333	44.75	41.83333	43.33333	51.91667	48.16667	45.33333	44.16667	1154.917	42.58333	0.77	0.15	0.354
ILMN_3166955	mmu-miR-369-5p	53.75	45.66667	53.75	56.41667	56.91667	59.58333	75.08334	67.58334	54.83333	63.5	59.16667	2006.667	0.71	0.15	0.349
ILMN_3167597	mmu-miR-374*	38.41667	33	38.16667	38.83333	38.41667	47.58333	45.33333	41.66667	36.58333	248	32.58333	34.25	0.90	0.17	0.378
ILMN_3168438	mmu-miR-376b*	79.75	67.75	88.58334	73.16666	69.25	77.25	84.83334	98.66666	74.33334	75.33334	263.1667	90.41666	0.82	0.13	0.278
ILMN_3169116	mmu-miR-376c*	2983.667	52.33333	74.33334	65.25	73.5	89.66666	96.75	109.3333	94.25	33.75	57.75	61.08333	6.13	4.95	0.364
ILMN_3168477	mmu-miR-381	52.16667	98.66666	52.5	52.33333	46.25	50.08333	51.08333	54.25	265.1667	76.58334	70.33334	84.16666	0.83	0.23	0.302
ILMN_3168945	mmu-miR-384-5p	77.75	82	80.75	86.58334	80.75	81.58334	89.66666	102.9167	89.66666	127.0833	98	150.1667	0.77	0.05	0.030
ILMN_3168473	mmu-miR-412:9.1	29.33333	29.75	28.33333	28.5	30.58333	30.41667	31.58333	32.41667	30.41667	30	135.5833	28.83333	0.83	0.12	0.330
ILMN_3168987	mmu-miR-421	58.16667	56	2436	49.58333	44.83333	46.91667	49.08333	56.41667	51.91667	54.25	50.58333	51.91667	8.63	7.66	0.365
ILMN_3169010	mmu-miR-449b	46.83333	43.83333	48.16667	48.58333	47.25	3361.167	63.5	59	48.83333	56.91667	54.33333	54.33333	11.01	10.17	0.371
ILMN_3168990	mmu-miR-466b-5p	45.08333	43.33333	62.58333	48.83333	39.58333	73.91666	51.58333	40.75	52.16667	45.33333	45.75	4209.083	0.85	0.17	0.364
ILMN_3168992	mmu-miR-466e-5p	79.08334	81.58334	105	103.9167	111.1667	138.0833	134.5833	143.6667	129.8333	155.5	86.58334	99.91666	0.88	0.15	0.271
ILMN_3167338	mmu-miR-467a*,mi	33.25	1368.417	31.41667	31.58333	31.33333	35.58333	32.75	32.58333	34.91667	31.33333	46.5	30.75	7.79	6.84	0.368
ILMN_3168998	mmu-miR-467d	46.91667	101.25	50.16667	47.83333	49.75	55.75	2824.917	59.16667	47.58333	60.83333	41.83333	49.58333	0.98	0.23	0.372
ILMN_3168437	mmu-miR-468	39	41.08333	47.58333	723	43.66667	53.5	54.33333	53.5	49.91667	52.5	55.75	47.58333	3.02	2.15	0.393
ILMN_3167114	mmu-miR-470	5111.333	49.08333	73.16666	63.91667	54.83333	58.5	68.16666	72	59.33333	70.75	66.16666	67.75	13.25	12.35	0.367
ILMN_3168526	mmu-miR-501-5p	27.16667	27.83333	29.75	26.75	28.33333	28.5	26.41667	30.08333	979.5	31.58333	28.5	28.5	0.80	0.16	0.360
ILMN_3167147	mmu-miR-503	127.0833	102.1667	4486.667	122.5	105.9167	97.5	101.25	119.25	115.9167	165.5833	109.3333	98.66666	7.25	6.29	0.368
ILMN_3169002	mmu-miR-509-3p	56.33333	49.75	59.33333	56.91667	53.5	66.16666	90.16666	95.16666	89.16666	93.5	134	84.83334	0.60	0.05	0.005
ILMN_3168953	mmu-miR-540-5p	2754.917	28.33333	31.75	30.41667	29.91667	26.41667	28.5	29.33333	26.75	27.16667	27.41667	27.16667	17.00	15.93	0.361
ILMN_3169019	mmu-miR-598	205.1667	117.6667	102.1667	111.1667	89.16666	85.58334	59.83333	88.41666	84.83334	135.5833	82.33334	79.75	1.49	0.39	0.269
ILMN_3169026	mmu-miR-669d	62.91667	54.25	61.75	59.16667	49.91667	53.75	5302.583	61.08333	62.33333	59	68.5	70.75	0.73	0.15	0.359
ILMN_3169032	mmu-miR-669f	36.33333	35	36.33333	35.08333	36.33333	39.08333	39	37.41667	123.6667	40.75	38	38.41667	0.83	0.11	0.297
ILMN_3169034	mmu-miR-669h-5p	60.16667	52.16667	72.58334	64.16666	65.83334	72.16666	379.75	82	61.08333	73.16666	62.33333	69.25	0.83	0.15	0.332
ILMN_3169031	mmu-miR-669j	91.5	421.6667	91.16666	81.58334	90.41666	79.08334	95.16666	105.9167	82.33334	138.0833	95.16666	93.5	1.41	0.52	0.496
ILMN_3169024	mmu-miR-669k	55.25	47.58333	58.16667	48.16667	51.25	49.58333	56.33333	628.6667	43.33333	49.91667	46.08333	46.83333	0.92	0.18	0.382
ILMN_3167810	mmu-miR-670	100.4167	98	108.5833	108.5833	123.6667	146.6667	166.4167	185.3333	142.5833	187.1667	87.91666	95.16666	0.90	0.18	0.277
ILMN_3168960	mmu-miR-673-3p	51.25	46.91667	59.83333	50.5	48.33333	44.58333	44.75	47.58333	3318.75	47.58333	44.16667	41.66667	0.90	0.18	0.366
ILMN_3167012	mmu-miR-675-5p	1390.25	47.58333	63.5	59.33333	68.5	66.83334	66.16666	79.08334	70.75	50.58333	50.5	54.83333	4.38	3.33	0.363
ILMN_3167632	mmu-miR-680	34.91667	32	320.5	33.83333	34.41667	35	36.58333	38	36.16667	37.83333	31.58333	33.83333	2.28	1.32	0.378
ILMN_3168521	mmu-miR-686	81.58334	75.33334	89.66666	75.08334	66.83334	75.33334	80	71.16666	66.16666	88.58334	4209.083	88.41666	0.86	0.18	0.364
ILMN_3168002	mmu-miR-688	27.83333	27.75	27.83333	27.41667	28.5	26.75	5493.5	27.16667	29.66667	27.83333	26.41667	26.08333	0.84	0.17	0.363
ILMN_3168037	mmu-miR-702	130.5833	2365.333	115.9167	93.16666	82.33334	84.16666	75.33334	90.41666	77.75	87.66666	70.75	82	5.44	4.15	0.338
ILMN_3167181	mmu-miR-711	150.1667	84.41666	125.5833	119.25	97.5	93.5	80.75	97.5	100.4167	114.1667	94.25	122.5	1.14	0.16	0.502
ILMN_3168148	mmu-miR-713	50.16667	45.33333	49.91667	4647.833	46.08333	50.58333	52.5	54.33333	48.16667	56	48.58333	51.25	14.63	13.67	0.365
ILMN_3168502	mmu-miR-718	134.5833	110.1667	178.0833	125.5833	118.75	129.8333	175	155.5	114.1667	151.9167	91.5	131.4167	1.02	0.14	0.838
ILMN_3168403	mmu-miR-721	114.8333	109.3333	107.75	106.6667	110.1667	109.3333	815.3333	101	97.5	108.5833	100.4167	128.1667	0.88	0.15	0.369
ILMN_3167851	mmu-miR-741	67.58334	52.5	5532	56.33333	56.83333	51.91667	54.83333	59.83333	44.16667	44.83333	39.08333	37.83333	21.91	20.67	0.359
ILMN_3169119	mmu-miR-744*	339.1667	69.75	90.16666	81.25	79.08334	73.5	72.58334	73.91666	63.5	82.33334	64.58334	74.33334	1.71	0.60	0.300
ILMN_3168977	mmu-miR-876-5p	54.83333	44.75	45.08333	1828.917	43.5	44.75	43.83333	41.83333	42.25	46.08333	45.08333	49.75	7.49	6.44	0.360
ILMN_3169135	solexa-173-2522	62.33333	1070.583	50.5	46.08333	45.75	45.66667	50.08333	46.83333	47.83333	45.08333	42.33333	46.08333	4.71	3.63	0.354
ILMN_3169141	solexa-2307-205	124.9167	111.1667	141	134.5833	119.25	153.75	180.9167	150.1667	119.25	139.6667	88.58334	88.58334	1.11	0.16	0.881

APPENDIX C

miRNA expression profiles in response to OS and LS in HUVEC

Table C1. miRNA expression profiles in HUVEC exposed to OS or LS for 1 day.

	LS1	LS2	LS3	OS1	OS2	OS3	OS/LS		
Reporter Name	Signal	Signal	Signal	Signal	Signal	Signal	ratio	SEM	p-value
hsa-miR-663	1,517	2,341	1,816	5,999	7,515	9,565	4.14	0.60	4.72E-03
hsa-miR-151-3p	2,274	2,122	2,035	1,595	1,430	1,403	0.69	0.01	5.36E-03
hsa-miR-320a	7,461	8,651	6,688	3,882	4,032	3,265	0.49	0.02	5.54E-03
hsa-miR-320c	6,884	8,587	6,438	3,606	3,696	3,033	0.48	0.03	6.02E-03
hsa-miR-320d	5,010	6,266	4,530	2,482	2,478	2,014	0.45	0.03	6.31E-03
hsa-miR-1275	818	973	668	1,798	1,524	1,415	1.96	0.20	1.46E-02
hsa-miR-320b	5,505	7,860	5,729	2,698	2,864	2,771	0.45	0.04	1.89E-02
hsa-miR-191	2,982	3,037	3,175	2,755	2,553	2,766	0.88	0.02	2.67E-02
hsa-miR-1469	2,437	4,343	4,032	7,278	11,308	15,663	3.16	0.38	2.87E-02
hsa-miR-638	2,255	4,588	3,310	7,095	11,709	16,326	3.54	0.72	3.07E-02
hsa-miR-195	4,623	3,895	3,875	3,037	3,081	2,402	0.69	0.05	3.20E-02
hsa-miR-149*	93	221	135	307	1,043	1,216	5.66	1.71	4.64E-02
hsa-miR-27b	3,660	5,044	5,259	2,111	2,086	3,358	0.54	0.07	4.82E-02
hsa-miR-15b	5,555	3,835	4,768	8,904	7,629	6,082	1.62	0.21	5.63E-02
hsa-miR-31	5,173	5,108	4,660	3,765	2,792	3,587	0.68	0.07	5.69E-02
hsa-miR-27a	7,423	10,343	9,756	4,803	4,445	7,317	0.61	0.09	6.69E-02
hsa-miR-187*	32	65	42	113	482	509	7.73	2.50	6.93E-02
hsa-miR-20b	1,545	1,211	1,511	1,923	1,648	2,078	1.33	0.04	7.23E-02
hsa-miR-1915	434	1,578	921	1,706	4,768	6,013	4.49	1.05	7.42E-02
hsa-miR-24	6,731	8,185	8,268	6,016	5,770	6,768	0.81	0.05	7.48E-02
hsa-miR-22	897	1,584	1,293	605	540	921	0.58	0.12	8.08E-02
hsa-miR-1308	1,824	1,128	1,299	2,948	2,369	1,749	1.69	0.22	9.29E-02
hsa-miR-425	501	474	515	439	346	410	0.80	0.04	9.45E-02
hsa-miR-494	280	350	419	601	404	640	1.61	0.29	9.66E-02
hsa-miR-130b	664	608	701	558	377	465	0.71	0.07	9.86E-02
hsa-miR-139-5p	487	406	343	113	123	103	0.28	0.02	7.63E-03
hsa-miR-192	61	86	62	29	17	33	0.40	0.10	2.26E-02
hsa-miR-125a-3p	62	61	58	40	29	32	0.56	0.05	2.32E-02
hsa-miR-424*	73	80	86	107	109	105	1.34	0.07	2.64E-02
hsa-miR-194	33	53	39	14	23	21	0.46	0.04	3.33E-02
hsa-miR-421	72	52	73	163	114	104	1.96	0.27	3.42E-02
hsa-miR-939	21	32	11	48	89	64	3.59	1.09	4.28E-02
hsa-miR-1231	41	37	22	58	177	138	4.14	1.44	4.95E-02
hsa-miR-625	288	170	170	128	66	86	0.45	0.03	5.20E-02
hsa-miR-671-5p	33	30	24	51	37	57	1.73	0.35	5.23E-02
hsa-miR-379*	24	20	14	33	40	29	1.82	0.23	5.72E-02
hsa-miR-217	289	230	251	360	327	300	1.29	0.07	6.03E-02
hsa-miR-197	229	207	195	117	159	105	0.61	0.08	6.14E-02
hsa-miR-181a*	17	15	21	25	23	33	1.53	0.05	6.75E-02
hsa-miR-933	16	23	17	34	23	34	1.69	0.35	7.19E-02
hsa-miR-484	156	210	160	115	89	139	0.68	0.13	7.20E-02
hsa-miR-193a-3p	22	29	33	18	15	22	0.66	0.09	7.33E-02
hsa-miR-1908	23	29	19	46	112	188	5.25	2.41	7.92E-02
hsa-miR-22*	60	88	78	42	56	55	0.68	0.02	8.00E-02
hsa-miR-498	14	15	16	22	41	52	2.47	0.49	8.38E-02
hsa-miR-140-3p	142	168	220	105	117	117	0.66	0.06	8.39E-02
hsa-miR-411*	29	29	52	71	82	59	2.10	0.50	8.90E-02
hsa-miR-25*	21	19	10	49	31	26	2.17	0.29	8.99E-02
hsa-miR-532-5p	84	102	102	81	60	80	0.78	0.11	1.06E-01
hsa-miR-20a	5,077	4,091	4,671	6,449	4,934	6,296	1.27	0.04	1.07E-01
hsa-miR-487a	20	19	22	36	23	35	1.53	0.15	1.10E-01
hsa-miR-720	394	535	317	287	229	268	0.67	0.13	1.17E-01
hsa-miR-28-3p	109	146	112	97	103	77	0.76	0.07	1.21E-01
hsa-miR-1268	113	195	102	227	262	198	1.76	0.21	1.27E-01
hsa-miR-574-3p	507	659	395	428	288	329	0.71	0.13	1.28E-01
hsa-miR-127-3p	361	462	522	303	354	372	0.77	0.04	1.29E-01
hsa-miR-125a-5p	8,505	9,514	9,904	6,236	8,524	7,065	0.78	0.06	1.31E-01
hsa-miR-185	936	663	765	659	647	522	0.79	0.09	1.36E-01
hsa-miR-150*	13	32	23	37	66	31	2.09	0.43	1.40E-01
hsa-miR-181a-2*	33	39	58	66	50	83	1.58	0.23	1.44E-01
hsa-miR-337-3p	21	32	29	30	57	41	1.56	0.12	1.45E-01
hsa-miR-16	7,076	6,516	8,955	9,117	9,376	9,288	1.25	0.12	1.50E-01
hsa-miR-106a	3,874	3,525	3,904	5,342	3,924	5,524	1.30	0.10	1.51E-01
hsa-miR-99b	2,275	3,013	2,928	2,116	1,983	2,508	0.81	0.08	1.54E-01
hsa-miR-654-3p	18	22	41	44	34	77	1.96	0.28	1.56E-01
hsa-miR-1826	17,885	17,103	14,214	11,560	15,947	10,539	0.77	0.08	1.59E-01
hsa-miR-766	70	41	48	47	32	32	0.70	0.04	1.75E-01
hsa-miR-1301	44	49	29	31	27	24	0.71	0.08	1.76E-01
hsa-miR-25	3,803	3,156	3,885	4,033	4,158	4,200	1.15	0.08	1.77E-01
hsa-miR-602	34	32	12	37	67	39	2.13	0.60	1.80E-01
hsa-miR-17	4,117	3,506	4,002	5,266	3,978	5,682	1.28	0.08	1.81E-01
hsa-miR-299-5p	113	99	131	127	138	142	1.20	0.10	1.81E-01
hsa-miR-361-3p	32	61	41	33	28	27	0.71	0.17	1.90E-01
hsa-miR-18b	122	92	117	179	116	138	1.30	0.09	1.93E-01
hsa-miR-328	20	34	24	18	18	20	0.75	0.11	1.95E-01
hsa-miR-500*	30	40	42	33	23	31	0.81	0.15	1.96E-01
hsa-miR-23a*	161	196	124	116	119	131	0.79	0.14	2.00E-01
hsa-miR-30d	795	949	877	711	556	824	0.81	0.11	2.00E-01
hsa-miR-874	27	22	21	33	23	36	1.31	0.19	2.02E-01
hsa-miR-146a	52	87	59	111	86	73	1.45	0.35	2.08E-01
hsa-miR-450a	8	17	20	17	33	23	1.77	0.31	2.11E-01

Table C1.-Continued

Reporter Name	LS1 Signal	LS2 Signal	LS3 Signal	OS1 Signal	OS2 Signal	OS3 Signal	OS/LS ratio	SEM	p-value
hsa-miR-222	9,269	16,795	11,386	7,589	7,071	11,501	0.75	0.17	2.25E-01
hsa-miR-30a	1,074	1,500	1,338	860	567	1,253	0.70	0.17	2.33E-01
hsa-miR-24-2*	50	79	64	56	38	53	0.81	0.19	2.35E-01
hsa-miR-125b	10,627	12,660	12,225	9,950	11,006	11,236	0.91	0.02	2.35E-01
hsa-miR-126*	117	103	54	162	216	89	1.71	0.21	2.39E-01
hsa-miR-224	641	825	649	679	597	524	0.86	0.10	2.47E-01
hsa-miR-130b*	27	20	29	28	30	32	1.22	0.13	2.51E-01
hsa-miR-214	3,201	2,231	2,152	2,427	1,910	1,499	0.77	0.05	2.55E-01
hsa-miR-769-5p	39	21	29	22	17	26	0.76	0.10	2.57E-01
hsa-miR-218	60	42	53	47	46	28	0.80	0.16	2.63E-01
hsa-miR-148b	34	57	65	56	68	86	1.39	0.13	2.66E-01
hsa-miR-365	188	191	245	199	276	288	1.23	0.12	2.66E-01
hsa-miR-150	46	100	50	58	35	33	0.76	0.27	2.75E-01
hsa-miR-378	25	48	28	26	21	24	0.78	0.18	2.79E-01
hsa-miR-1281	67	61	47	56	87	77	1.30	0.24	2.79E-01
hsa-miR-886-3p	157	284	32	61	65	17	0.38	0.09	2.81E-01
hsa-miR-30a*	391	277	325	315	286	216	0.83	0.11	2.81E-01
hsa-miR-454	229	129	187	304	290	169	1.49	0.40	2.82E-01
hsa-miR-34a	564	715	819	499	579	667	0.84	0.02	2.83E-01
hsa-miR-744*	36	23	26	28	13	21	0.72	0.08	2.83E-01
hsa-miR-29c	285	383	381	159	216	376	0.70	0.14	2.86E-01
hsa-miR-628-3p	24	23	25	45	34	22	1.39	0.28	2.92E-01
hsa-miR-765	38	27	32	30	27	16	0.77	0.14	2.96E-01
hsa-miR-374b	402	228	279	426	904	302	2.04	0.97	2.99E-01
hsa-miR-503	203	170	205	181	186	156	0.91	0.10	3.01E-01
hsa-miR-29b	38	61	67	28	30	61	0.71	0.12	3.02E-01
hsa-miR-27b*	46	33	47	39	37	30	0.86	0.14	3.02E-01
hsa-miR-23a	15,614	23,487	19,827	16,137	13,293	18,962	0.85	0.14	3.05E-01
hsa-miR-629*	32	29	28	35	18	16	0.75	0.16	3.08E-01
hsa-miR-23b	13,685	20,676	18,711	13,222	11,963	17,791	0.83	0.13	3.08E-01
hsa-miR-625*	96	41	51	61	32	29	0.66	0.07	3.17E-01
hsa-miR-497	62	93	120	75	68	61	0.82	0.21	3.19E-01
hsa-miR-936	58	73	19	52	12	15	0.61	0.23	3.22E-01
hsa-miR-425*	25	29	36	28	24	26	0.88	0.12	3.32E-01
hsa-miR-487b	257	274	319	345	275	325	1.12	0.11	3.35E-01
hsa-miR-10a*	25	30	33	39	30	32	1.16	0.19	3.40E-01
hsa-miR-30e	75	187	151	60	64	146	0.70	0.19	3.43E-01
hsa-miR-193a-5p	1,798	1,144	1,101	1,068	1,303	795	0.82	0.16	3.44E-01
hsa-miR-181c	77	115	67	80	62	63	0.84	0.15	3.50E-01
hsa-miR-629	137	93	99	115	84	72	0.82	0.05	3.51E-01
hsa-miR-7	212	56	58	257	266	73	2.41	1.17	3.60E-01
hsa-miR-181a	1,390	1,971	2,092	1,400	1,424	1,778	0.86	0.08	3.61E-01
hsa-miR-93	970	815	997	1,120	881	1,104	1.11	0.02	3.61E-01
hsa-miR-18a	379	235	326	473	306	369	1.23	0.05	3.65E-01
hsa-miR-199a-3p	1,678	1,266	1,092	1,435	970	913	0.82	0.03	3.67E-01
hsa-miR-29b-1*	59	44	24	71	61	40	1.40	0.12	3.68E-01
hsa-let-7i	19,285	16,065	16,742	18,472	14,269	14,366	0.90	0.03	3.77E-01
hsa-miR-1246	12,056	10,558	6,525	18,662	14,974	7,816	1.39	0.10	3.89E-01
hsa-miR-221	6,172	10,480	8,676	5,501	5,937	9,005	0.83	0.14	3.96E-01
hsa-miR-1260	41	25	45	27	29	32	0.85	0.16	3.96E-01
hsa-miR-744	55	52	66	63	56	70	1.10	0.03	4.14E-01
hsa-miR-151-5p	7,912	6,436	6,962	6,727	7,223	5,539	0.92	0.10	4.24E-01
hsa-let-7f	19,347	14,963	17,414	20,380	19,884	16,336	1.11	0.12	4.40E-01
hsa-miR-1180	104	86	83	89	90	71	0.92	0.07	4.48E-01
hsa-miR-566	17	29	11	37	17	21	1.57	0.49	4.49E-01
hsa-miR-106b*	35	45	32	53	43	34	1.17	0.17	4.50E-01
hsa-miR-654-5p	21	26	23	41	23	23	1.27	0.32	4.62E-01
hsa-miR-424	122	250	344	222	252	493	1.42	0.23	4.72E-01
hsa-miR-30e*	76	77	89	62	92	62	0.91	0.15	4.74E-01
hsa-miR-376a	44	86	78	73	64	137	1.38	0.32	4.76E-01
hsa-miR-21	29,666	26,154	27,238	32,577	27,914	27,329	1.06	0.03	4.77E-01
hsa-miR-126	28,962	29,268	33,123	35,613	30,945	30,022	1.06	0.09	4.80E-01
hsa-miR-28-5p	850	727	676	656	830	555	0.91	0.12	4.82E-01
hsa-miR-199a-5p	33	68	56	71	44	77	1.39	0.43	4.85E-01
hsa-miR-130a	155	153	236	150	145	175	0.88	0.07	4.87E-01
hsa-miR-1280	1,525	1,282	775	1,481	1,354	1,257	1.22	0.20	5.01E-01
hsa-miR-370	22	44	11	43	27	26	1.66	0.54	5.04E-01
hsa-miR-886-5p	277	272	140	222	209	116	0.80	0.02	5.17E-01
hsa-miR-543	7	18	15	15	10	37	1.70	0.58	5.18E-01
hsa-miR-411	25	47	59	55	45	52	1.33	0.41	5.21E-01
hsa-miR-1237	29	25	13	35	21	23	1.30	0.29	5.22E-01
hsa-let-7d*	47	79	65	55	53	58	0.91	0.15	5.35E-01
hsa-miR-584	1,168	592	534	873	564	357	0.79	0.08	5.38E-01
hsa-miR-323-3p	16	36	31	33	35	28	1.33	0.41	5.39E-01
hsa-miR-361-5p	1,697	1,360	1,664	1,802	2,076	1,373	1.14	0.21	5.40E-01
hsa-miR-92b	5,776	4,289	3,864	6,101	5,564	4,019	1.13	0.08	5.48E-01
hsa-miR-885-5p	33	8	15	13	8	15	0.79	0.20	5.57E-01
hsa-let-7a	21,479	16,868	19,903	23,795	21,538	17,607	1.09	0.11	5.58E-01
hsa-miR-339-3p	20	35	19	36	25	23	1.24	0.31	5.78E-01
hsa-miR-92a	13,469	10,821	10,233	13,768	12,135	10,900	1.07	0.03	5.80E-01
hsa-miR-433	51	63	69	52	61	57	0.95	0.06	5.89E-01
hsa-miR-134	290	215	242	305	282	221	1.09	0.12	6.06E-01

Table C1.-Continued

Reporter Name	LS1 Signal	LS2 Signal	LS3 Signal	OS1 Signal	OS2 Signal	OS3 Signal	OS/LS ratio	SEM	p-value
hsa-miR-34a*	12	33	20	16	14	21	0.93	0.27	6.15E-01
hsa-miR-26a	11,092	10,103	10,212	10,494	11,419	10,274	1.03	0.05	6.16E-01
hsa-miR-409-3p	91	88	69	171	152	46	1.42	0.38	6.16E-01
hsa-miR-1228	40	17	20	30	31	24	1.26	0.31	6.18E-01
hsa-miR-107	2,060	2,286	2,733	2,216	2,042	2,428	0.95	0.06	6.22E-01
hsa-miR-377	14	36	14	37	13	29	1.69	0.67	6.23E-01
hsa-miR-15a	383	265	532	361	449	489	1.18	0.25	6.24E-01
hsa-miR-193b*	28	33	35	32	35	23	0.95	0.14	6.29E-01
hsa-miR-362-5p	28	49	55	36	45	34	0.93	0.20	6.51E-01
hsa-miR-16-2*	20	15	28	23	15	42	1.20	0.16	6.56E-01
hsa-miR-574-5p	1,762	751	857	1,668	1,390	805	1.25	0.30	6.61E-01
hsa-miR-19b	620	1,413	1,169	1,100	840	1,791	1.30	0.36	6.63E-01
hsa-miR-1238	36	31	13	33	21	12	0.82	0.08	6.69E-01
hsa-miR-98	1,195	558	615	958	1,517	497	1.44	0.64	6.71E-01
hsa-miR-181b	1,991	2,679	3,100	1,363	2,439	3,257	0.88	0.11	6.72E-01
hsa-miR-100	5,797	7,017	7,061	6,739	5,899	8,652	1.08	0.12	6.74E-01
hsa-let-7d	17,011	12,680	15,595	16,862	17,131	13,616	1.07	0.14	6.79E-01
hsa-let-7b	12,004	7,659	9,605	9,634	10,684	6,566	0.96	0.22	6.81E-01
hsa-miR-132	183	92	116	120	116	105	0.94	0.17	6.82E-01
hsa-miR-1290	28	42	20	38	49	20	1.18	0.11	6.85E-01
hsa-miR-329	62	87	75	85	58	103	1.14	0.24	6.99E-01
hsa-miR-101	22	39	33	37	40	25	1.15	0.27	7.10E-01
hsa-miR-106b	918	741	822	1,012	737	858	1.05	0.03	7.12E-01
hsa-miR-30b	926	1,166	1,788	940	1,525	1,892	1.13	0.09	7.14E-01
hsa-miR-940	72	55	28	80	58	36	1.16	0.07	7.19E-01
hsa-miR-1249	39	34	20	32	32	19	0.91	0.04	7.32E-01
hsa-miR-923	5,326	5,726	7,457	10,697	4,445	6,586	1.22	0.39	7.34E-01
hsa-miR-181d	38	74	324	49	122	398	1.39	0.13	7.41E-01
hsa-miR-345	47	86	87	69	80	79	1.11	0.18	7.52E-01
hsa-miR-381	15	38	31	22	19	30	0.98	0.29	7.53E-01
hsa-miR-19a	16	26	30	18	24	40	1.12	0.13	7.54E-01
hsa-miR-423-5p	2,948	1,979	2,443	2,397	2,913	1,661	0.99	0.24	7.55E-01
hsa-miR-10a	2,297	1,751	1,775	1,908	2,309	1,362	0.97	0.17	7.66E-01
hsa-miR-663b	16	33	10	19	12	16	1.06	0.38	7.74E-01
hsa-miR-128	952	727	860	936	820	700	0.97	0.09	7.85E-01
hsa-miR-505*	167	111	165	149	180	93	1.02	0.31	7.90E-01
hsa-miR-376c	218	392	313	251	177	456	1.02	0.30	7.93E-01
hsa-miR-660	44	39	37	51	31	35	0.97	0.10	7.95E-01
hsa-miR-26b	2,180	1,465	1,817	1,513	2,448	1,298	1.03	0.32	7.96E-01
hsa-miR-485-3p	92	89	112	76	111	125	1.06	0.13	8.20E-01
hsa-miR-455-3p	535	476	704	634	528	591	1.04	0.10	8.25E-01
hsa-miR-483-5p	80	77	101	76	123	56	1.03	0.30	8.31E-01
hsa-miR-155	11,663	7,176	7,277	10,337	10,064	6,762	1.07	0.17	8.34E-01
hsa-miR-379	538	285	342	528	425	279	1.10	0.20	8.38E-01
hsa-miR-216a	202	262	393	240	227	466	1.08	0.11	8.39E-01
hsa-miR-505	24	56	84	30	32	87	0.95	0.19	8.53E-01
hsa-miR-29a	6,250	6,847	6,780	6,484	4,895	8,303	0.99	0.15	8.56E-01
hsa-miR-154	36	51	59	39	47	53	0.97	0.06	8.58E-01
hsa-miR-431	19	38	31	24	27	30	0.99	0.17	8.60E-01
hsa-miR-30c-2*	29	39	35	36	39	30	1.04	0.12	8.67E-01
hsa-miR-452	22	29	25	35	24	21	1.08	0.26	8.71E-01
hsa-miR-502-3p	18	40	25	32	23	29	1.17	0.36	8.75E-01
hsa-miR-10b	5,136	4,093	4,494	4,442	6,069	3,790	1.06	0.21	8.80E-01
hsa-miR-342-3p	133	210	299	143	230	297	1.05	0.03	8.82E-01
hsa-miR-30c	2,717	3,063	3,990	2,662	3,464	3,869	1.03	0.05	8.90E-01
hsa-let-7c	17,157	12,264	14,951	16,100	16,261	12,720	1.04	0.15	8.90E-01
hsa-miR-324-3p	23	38	19	25	26	23	1.00	0.16	8.94E-01
hsa-miR-877	257	116	168	183	236	100	1.12	0.46	9.00E-01
hsa-let-7e	13,546	9,652	12,884	11,007	14,448	9,993	1.03	0.23	9.07E-01
hsa-miR-342-5p	27	41	34	45	47	20	1.13	0.31	9.08E-01
hsa-miR-296-5p	36	26	23	31	32	20	0.99	0.13	9.10E-01
hsa-let-7g	11,998	8,480	10,620	10,724	10,519	9,184	1.00	0.12	9.12E-01
hsa-miR-1307	70	95	100	72	91	106	1.02	0.03	9.13E-01
hsa-miR-382	459	248	278	384	379	238	1.07	0.23	9.15E-01
hsa-miR-1304	32	18	25	23	28	22	1.04	0.25	9.29E-01
hsa-miR-1229	41	13	18	22	24	16	1.10	0.39	9.29E-01
hsa-miR-7-1*	28	22	23	42	12	26	1.05	0.27	9.38E-01
hsa-miR-331-3p	69	114	113	86	86	114	1.01	0.14	9.42E-01
hsa-miR-186	32	95	85	47	44	137	1.18	0.36	9.54E-01
hsa-miR-221*	33	56	36	43	42	35	1.01	0.16	9.58E-01
hsa-miR-103	2,330	2,417	3,067	2,567	2,402	2,846	1.01	0.05	9.61E-01
hsa-miR-1234	43	22	19	30	27	24	1.04	0.17	9.68E-01
hsa-miR-324-5p	55	90	98	76	64	96	1.03	0.20	9.71E-01
hsa-miR-495	321	441	431	434	358	388	1.02	0.17	9.75E-01
hsa-miR-1913	33	26	22	37	28	17	1.00	0.11	9.75E-01
hsa-miR-137	63	58	84	52	86	68	1.04	0.22	9.77E-01
hsa-miR-337-5p	19	28	34	24	25	30	1.01	0.13	9.81E-01
hsa-miR-99a	1,330	2,381	2,249	1,516	1,828	2,615	1.02	0.13	9.83E-01
hsa-miR-432	595	314	357	469	589	246	1.12	0.38	9.85E-01
hsa-miR-206	13	17	100	12	16	115	1.02	0.07	9.86E-01
hsa-miR-152	74	71	67	81	79	54	1.01	0.10	9.90E-01